Synthesis, Characterization, and Molecular Docking Studies of Homoleptic and Heteroleptic Zinc(II), Copper(II), Nickel(II) Complexes of Semicarbazone and Thiosemicarbazone Derivative Ligands for Biological Applications

Fekadu Muleta Gudeta

A PhD Dissertation Submitted to the Department of Applied Chemistry
School of Applied Natural Sciences

Presented in Partial Fulfillment for the Requirements of the Degree of Doctor of Philosophy in Applied Chemistry (Bioinorganic Chemistry)

Office of Postgraduate Studies
Adama Science and Technology University

April, 2023
Adama, Ethiopia

Synthesis, Characterization, and Molecular Docking Studies of Homoleptic and Heteroleptic Zinc(II), Copper(II), Nickel(II) Complexes of Semicarbazone and Thiosemicarbazone Derivative Ligands for Biological Applications

By

Fekadu Muleta Gudeta

Main Supervisor:
Prof. Tegene Desalegn

Co- Supervisor:
Dr. Taye Beyene Demissie (Associate Professor)

A PhD Dissertation Submitted to the Department of Applied Chemistry
School of Applied Natural Sciences

Presented in Partial Fulfillment of the Requirements for the Degree of Doctor of Philosophy in Applied Chemistry (Bioinorganic Chemistry)

Office of Postgraduate Studies
Adama Science and Technology University

April, 2023
Adama, Ethiopia

DECLARATION

I hereby declare that this dissertation entitled **"Synthesis, Characterization, and Molecular Docking Studies of Homoleptic and Heteroleptic Zinc(II), Copper(II), Nickel(II) Complexes of Semicarbazone and Thiosemicarbazone Derivative Ligands for Biological Applications"** is my original work. It has never been submitted for the award of any academic degree, diploma or certificate in any other university. All sources of materials used for this dissertation have been duly acknowledged through appropriate list of references.

Fekadu Muleta	_____	_____
Name of student	**Signature**	**Date**

RECOMMENDATION

We, the supervisors of this dissertation, hereby certify that we have read and revised the dissertation entitled "**Synthesis, Characterization, and Molecular Docking Studies of Homoleptic and Heteroleptic Zinc(II), Copper(II), Nickel(II) Complexes of Semicarbazone and Thiosemicarbazone Derivative Ligands for Biological Applications**" prepared under our guidance by **Fekadu Muleta** and submitted in partial fulfillment of the requirements for the degree of Doctor of Philosophy in Applied Chemistry (**Bioinorganic Chemistry)**. Therefore, we recommend the submission of the dissertation to the department for further review and defense.

Prof. Tegene Desalegn	_____	_____
Main Supervisor	Signature	Date
Dr. Taye Beyene (PhD, Assoc. Prof.)	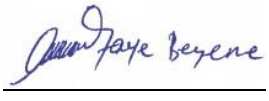	_____
Co-supervisor	Signature	Date

APPROVAL PAGE

We hereby certify that the recommendations and suggestions made by the board of examiners are appropriately incorporated into the final version of the dissertation entitled "**Synthesis, Characterization, and Molecular Docking Studies of Homoleptic and Heteroleptic, Zinc(II), Copper(II), Nickel(II) Complexes of Semicarbazone and Thiosemicarbazone Derivative Ligands for Biological Applications**" by **Fekadu Muleta Gudeta**.

Prof. Tegene Desalegn
Main Supervisor Signature Date

Dr. Taye Beyene (PhD, Assoc. Prof.)
Co-supervisor Signature Date

We, the undersigned, members of the Board of Examiners of the open defense of the dissertation by **Fekadu Muleta Gudeta**, have read and evaluated the dissertation entitled "**Synthesis, Characterization, and Molecular Docking Studies of Homoleptic and Heteroleptic Zinc(II), Copper(II), Nickel(II) Complexes of Semicarbazone and Thiosemicarbazone Derivative Ligands for Biological Applications**" and examined the candidate during the open defense. This is, therefore, to certify that the dissertation is accepted for partial fulfillment of the requirements of the degree of Doctor of Philosophy in **Bioinorganic Chemistry.**

Chairperson Signature Date

Internal Examiner Signature Date

External Examiner 1 Signature Date

External Examiner 2 Signature Date

Finally, approval and acceptance of the dissertation is contingent upon submission of its final copy to the Office of Postgraduate Studies (OPGS) through the candidate's Department Graduate Council (DGC) and School Graduate Committee (SGC).

Department Head Signature Date

School Dean Signature Date

Office of Postgraduate Studies, Dean Signature Date

ACKNOWLEDGEMENTS

In the beginning, thanks to God for all the blessing in my studying and all my life, I submit my feelings of gratitude to God at the outset.

I owe my advisors, Prof. Tegene Desalegn and Dr. Taye Beyene, my deepest appreciation and love for welcoming me and favorably directing and supervising my dissertation work. I am grateful for their politeness and the follow-up, advice, comments, assistance, and personal attention they provided throughout my worked. Both Prof. Tegene Desalegn and Dr. Taye Beyene have my utmost respect and love.

In addition to my advisors, I would like to thank Dr. Rajalakshmanan Eswaramoorthy, Dr. Hadgu Hailekiros, Dr. Eneyew Amare, and Dr. H.C. Ananda Murthy for their helpful criticism in the processes my dissertation work progressed. I would also like to express my gratitude to Dr. H.C. Ananda Murthy for supporting me in the characterization of samples using SEM-EDX in overseas.

I also want to express my gratitude to my lab colleagues Mr. Aklilu Guale, Mr. Teshale Assefa, Mr. Temesgen Bailu, and Mr. Mamaru Bitew, as well as the lab technicians Mr. Guta Amenu, Mr. Lemi, and Ms. Bontu Tiki, for sharing their ideas, comments, materials, and suggestions with me while we were working in the lab.

Additionally, I would like to thank Adama Science and Technology University for giving me the opportunity to pursue a PhD study as well as Wolaita Sodo University for the financial support and sponsorship. Moreover, I want to thank the Department of Applied Chemistry, School of Applied Natural Science for its unreserved and sustained support during my study.

Finally, I would like to thank my parents, brothers, and sisters for supporting me on this journey. I also owe my brother, Mr. Alemayehu Sileshi, a debt of gratitude for helping me to transport the chemicals from abroad that were essential for my work. A special thank you to my wife and boys for bearing with me and putting up with any difficulties they may have experienced while I was away for my PhD study.

TABLE OF CONTENTS

CONTENTS **PAGE**

LIST OF TABLES

LIST OF FIGURES

LIST OF SCHEMES

LIST OF APPENDIXES

ACRONYMS AND ABBREVIATION

ADMET	Absorption, Distribution, Metabolism, Excretion and Toxicity
AMR	Antimicrobial Resistance
ANOVA	Analysis of Variance
DMF	Dimethylformamide
DMSO	Dimethylsulfoxide
DNA	Deoxyribose nucleic acid
DPPH	1-1-diphenyl 2-picryl hydrazyl
DTA	Differential Thermogravimetric analysis
FTIR	Fourier Transform Infrared
HOMO	Highest Occupied Molecular Orbital
LMCT	Ligand to Metal charge transfer
LUMO	Lowest unoccupied molecular orbital
MDR	Multi-drug resistances
MIC	Minimum inhibitory concentration
MLCT	Metal to Ligand charge transfer
MRSA	Methicillin-resistant Staphylococcus aureus
NMR	Nuclear magnetic resonance
OPA	Ortho-Phthalaldehyde
PD	Pharmacodynamics
PDA	Potato-dextrose agar (Potato-dextrose agar)
PK	Pharmacokinetics
RNA	Ribonucleic acid
ROS	Reactive Oxygen Species
SEM-EDX	Scanning Electron Microscopy- Energy Dispersive X-Ray
TGA	Thermal gravimetric analysis
TLC	Thin layer chromatography
TPSA	Topological polar surface area
WHO	World Health Organization
XRD	X-ray diffraction

ABSTRACT

The importance of semicarbazone and thiosemicarbazone organic compounds and their metal complexes as pharmaceutical, medicinal, antibacterial, antioxidant, and antifungal targets has recently become an area of research in both bioinorganic and medicinal chemistry. In this study, the semicarbazone and thiosemicarbazone derivative organic ligands and their metal complexes having a plethora of potentially exciting bioactivities and coordination chemistry were synthesized, characterized and their biological activities were evaluated. Specifically, the ***Zn(II)****,* ***Cu(II),*** *and* ***Ni(II)*** *complexes of bidentate ON (****L1****),* ***Zn(II)****,and* ***Cu(II)) complexes of*** *SN (****L2****), and tridentate ONN (****L3*** *and* ***L4****) ligands have been prepared. The compounds were characterized with various methods such as* ^{1}*H-NMR,* ^{13}*C-NMR, FT-IR, UV-Vis, and mass spectroscopies, conductometer, SEM-EDX, XRD, TGA/DTA techniques. The synthesized ligands and their metal complexes were screened for their antibacterial activity against two Gram-negative (Escherichia coli and Pseudomonas aeruginosa and two Gram- positive (Staphylococcus aureus and Streptococcus pyogenes) bacteria strains using disc diffusion method. The compounds were also evaluated for their antioxidant activity by DPPH assay. On the bases of spectroscopic studies the structure and the molecular formula of the synthesized compounds were proposed. The antimicrobial activity result showed the best activities were achieved by* $[Zn(L2)_2]$ *complex* ***4*** *(15.44 ± 0.31 mm) against Pseudomonas aeruginosa****),*** $[Cu(L2)_2]$ *complex* ***5*** *(14.00 ± 0.20 mm) against Streptococcus pyogenes,* $[Zn(L3)_2].2H_2O$ *complex* ***6*** *(16.22 ± 0.27 mm) against Staphylococcus aureus,* $[Cu(L3)_2].3H_2O$ *complex* ***7*** *(18.66 ± 0.34 mm) against Staphylococcus aureus bacteria pathogens compared to trimethoprim with a mean inhibition zone of 18.70 ± 0.47 mm to 21.48 ± 0.46 mm diameter. Also, the antioxidant potential result showed that complexes;* $[Ni(L1)_2Cl]$ ***(3)****,* $[Ni(L3)_2].3H_2O$ ***(8),*** $[Cu(L2)_2]$ ***(5)****,* $[Cu(L3)_2].3H_2O$ ***(7)*** *and* $[Zn(L2)_2]$ ***(4)*** *exhibited good antioxidant activity with percentage scavenging potentials of 85.76, 81.43, 78.55, 78.45 and 76.78% at 100 μg/mL respectively compared with standard ascorbic acid 89.74%. The in silico analysis results were also in good agreement with the in vitro experimental results. Thus, this study revealed that the coordination of metal ions with bioactive organic ligands could serve as candidate in metal based drug development for biological applications.*

Keywords: *Dehydrozingerone, Semicarbazone, Thiosemicarbazone, Metal Complex, Molecular Docking, Bioactivity*

1. INTRODUCTION

1.1. Background of the study

The synthesis of metal complexes involving transition metals and organic ligands has become a focal area of current researches due to their enhanced and various biological activities. The introduction of metal ion and binding components into a biological system for the treatment of different types of diseases is one of the main subdivisions in the field of modern bioinorganic and medicinal chemistry. Many biologically active compounds used as drugs possess enhanced pharmacological and cytotoxic potentials when administered in the form of metal-based compounds (Mittapally, Taranum, & Parveen, 2018). Metal-based compounds for antibacterial activity have novel modes of action to treatment bacterial infections with resistance to conventional antibiotics. The organic ligands, semicarbazone, and thiosemicarbazone derivative-based metal complexes are important and relevant compounds being studied in recent researches with impactful contributions to the scientific world (Bakir, Lawrence, Ferhat, & Conry, 2017; DS; Martins et al., 2014).

Semicarbazones are organic compounds with the structure $R_1R_2C=N-NH-(C=O)-NR_3R_4$, which are obtained by aldol condensation through refluxing of semicarbazide hydrochloride with suitable aldehydes or ketones functional groups. Thiosemicarbazones are derivatives of semicarbazones that contain sulfur atoms in place of oxygen of the carbonyl functional group. Both are formed when ammonia-containing compounds (nucleophiles) such as semicarbazide or thiosemicarbazide are added to the carbonyl group (-C=O) of aldehyde or ketones, yields an imine (-C=N-) containing derivatives. This imine group is the main influential functional group making semicarbazone and thiosemicarbazones moieties to be biologically active compounds (More, Joshi, Mishra, & Khanna, 2019a). Interestingly, semicarbazone and thiosemicarbazone are important organic compounds that can act as special ligands in coordination chemistry, possessing a variety of coordination modes or variable binding sites with metals resulting in their stable complexes. The coordination mode is influenced by the number and type of substituent (R- groups) (More, Joshi, Mishra, & Khanna, 2019b). That is due to the active donor atoms or sites of the ligand varying depending upon the nature of substituent groups. Semicarbazones and thiosemicarbazones can coordinate with metals as neutral molecules or after undergo deprotonation as anionic ligands, which makes them as

versatile ligands adopting a variety of coordination modes (More et al., 2019b). They exhibit better selectivity, can form macrocyclic ligands, and they possess the ability to produce new and unique complexes with enhanced biological activities (Adhikari et al., 2019). The aromatic substituent on semicarbazone and thiosemicarbazone skeletons can further enhance the delocalization of electron charge density (Dhabale, Shah, Tiwari, & Patani, 2022; Mosa, Ibrahim, & Aldhlmani, 2013). They behave as chelating ligands upon coordination with a metal center; the delocalization of electrons is further increased through the metal chelate rings. This is an important part of their bioactivity. The coordination possibilities are further increased if the substituent has additional heteroatoms as donor atoms (Reena & Prathapachandra Kurup, 2011).

Most of the semicarbazones, and thiosemicarbazones derivative compounds show a wide range of biological activities, such as antiviral, antibacterial, fungicidal, antiparasitic (Bahojb Noruzi et al., 2020), and antioxidant activities (Simons, Walsh, Maillard, & Russell, 2000). However, the development of microbial resistance to their activity reduces their effectiveness greatly and affects them as a choice as potent drug candidates (Choudhary, Sharma, Nagar, Mohsin, & Meena, 2011). Research reports indicate that the semicarbazone and thiosemicarbazone compounds synthesized and used as antimicrobial activity shows only one way of action mechanism (M. Singh, Gangwar, Nath, & Singh, 2016), as a result, microbial can easily able to develop resistant against their bioactivity (Pelosi, 2010).

The synthesis and use of complex compounds of essential transition metal ions with one or more than one type of bioactive organic ligands derived from both natural product constituents and synthetic derivatives can be used as a new strategy to enhance the biological activities of the organic ligands to tackle and minimize the alarmingly increasing microbial resistance to common antibiotics. This could be attributed to the fact that metal-bearing compounds display a significantly enhanced bioactivities as compared to the free organic ligands (Choudhary et al., 2011). The biological properties of organic ligands are often enhanced by coordination with the metal ion. This might be explained in terms of mode of action of the metal complexes towards microbes. The first one could be associated with lipophilicity, which controls the rate of entry of active compounds into the cell, is modified due to coordination. The other mechanism of action involves binding to metal *in vivo* or the

metal complex may be a vehicle for activation of the ligand as the cytotoxic agent (Polo-Ceron, 2019). This is mostly related to Tweedy's chelation theory according to which chelation reduces the polarity of the metal atom because of the partial sharing of its positive charge with the ligand, which favors permeation of the complexes through the lipid layer of the bacteria cell membrane. Other factors such as solubility, conductivity, and dipole moment which are affected by the presence of metal ions may also be possible reasons for increasing the biological activities of the metal complexes as compared to the corresponding free ligand. Moreover, coordination of ligands to metal centers may lead to a significant reduction in drug resistance (Randall, 2013).

Several reported antibiotics require coordination to metal ions to function properly. These include bleomycin, streptonigrin, bacitracin, and albomycin which all depend on coordinated metal ions to maintain proper structure and biological function (Randall, 2013). The term ‘metalloantibiotic’ has been coined to describe such metal ion-dependent antibiotics and they are known to exert their bioactivities through interactions with a variety of biomolecules including DNA, RNA, proteins, lipids, and receptors. These metalloantibiotics are well known to exhibit antibacterial capability. Metal ions are electron deficient, whereas most biological molecules such as proteins and DNA are electron-rich. The attraction of these opposing charges leads to a general tendency for metal ions to bind and interact with biological molecules (Hossain, Zakaria, & Kudrat-E-Zahan, 2018).

Thus, bioactive organic ligand combinations with metals have proven to be an essential feature of antimicrobial treatment due to significant advantages such as metals can increase activity through the use of compounds with synergistic or additive activity (Montelongo-Peralta, León-Buitimea, Palma-Nicolás, Gonzalez-Christen, & Morones-Ramírez, 2019), impede drug resistance (Rizzotto, 2012a), decrease required doses, reducing both cost and the chances of toxic side effects (Farrell, 2012), and increase the spectrum of activity (Claudel, Schwarte, & Fromm, 2020).

The ortho-Phthalaldehyde (OPA) is an aromatic dialdehyde organic compound that has shown antimicrobial activity (Simons et al., 2000). However, both gram-positive and gram-negative bacteria species develop resistance to its activity (Simons et al., 2000). It can react

with primary amine-containing compounds (Cabrera-Martinez, Setlow, & Setlow, 2002; Simões et al., 2007). Therefore it can react with semicarbazides /thiosemicarbazides, which are primary amine-containing compounds to form the semicarbazone and thiosemicarbazone derivatives.Thus, in this aspect, the synthesis of semicarbazone and thiosemicarbazone derivative ligands from natural product origin (dehydrozingerone) and synthetic origin (ortho-phthalaldehyde) for their homoleptic and heteroleptic metal complex formation were purposely targeted.

In addition, it is well known that natural product-based medicine plays a central role in medicinal aspects. Hence, it becomes important to focus on natural constituents of traditionally used medicinal plants as a base for developing new bioactive derivative organic ligands. Thus, the dehydrozingerone and zingerone, which are natural product constituents of traditional medicinal plants, present in the rhizomes of ginger (*Zingiber officinale*) structurally similar to the vanillin ketone group were used in traditional medicinal applications (Hampannavar, Karpoormath, Palkar, & Shaikh, 2016; Yogosawa et al., 2012). These constituents of ginger show bioactivities like antibacterial (Burmudžija et al., 2017; Kubra, Bettadaiah, Murthy, & Rao, 2014), antioxidant (Kuo et al., 2005), antitumor (Motohashi et al., 1998), and antifungal (Hampannavar et al., 2016; Yamano et al., 2023) activities. But these constituents alone cannot have the potential to overcome the drug-resistant microorganisms currently developing. Thus, to increase their bioactivities, homoleptic and heteroleptic metal complexes of both synthetic origin and natural product derivatives of semicarbazone and thiosemicarbazone ligands were our new strategies to develop enhanced bioactive compounds to reduce drug-resistant microbial pathogens, which have not been reported yet.

In addition, the *in-silico* pharmacokinetics (PK) and pharmacodynamics (PD) which play a crucial role in drug development (Awasthi, Lohani, Singh, Singh, & Jaggi, 2014; Daina, Michielin, & Zoete, 2017) were done for the synthesized compounds. The evaluation of pharmacological parameters such as drug-likeness, ADME, and toxicity are of paramount significance in the selection or identifying lead compounds (Daina et al., 2017). Recently, *in-silico* methods that include molecular docking analysis and online ADMET predictions (Swiss ADME, Pro-Tox II, and OSIRIS property explorer) are being employed in the process

of identifying the potential bioactive molecules (Priyanka Banerjee, Eckert, Schrey, & Preissner, 2018; Garg, Tadesse, & Eswaramoorthy, 2021; Matta & Gillespie, 2002; Süleymanoğlu, Kubaşık, & Direkel, 2021; Oleg Trott & Olson, 2010). These had been performed to determine the 3D structure of the ligands and complexes to correlate both the experimental values with the theoretical value for the analysis of drug-likeness of the newly synthesized ligands and their metal complexes.

Thus, herein the synthesis, antimicrobial, antioxidant, antifungal, *in*-silico molecular docking analysis, and drug-likeness studies of novel homoleptic and heteroleptic Cu(II), Zn(II), and Ni(II) complexes involving the new ligands were studied and reported. The aim was to explore their potency as novel bactericidal, antioxidant, and antifungal agents generated due to the presence of different natural product-based and synthetic origin derivatives of bioactive ligands hybrid through coordination by essential metal ions.

1.2. Statement of the problem

The scientific community is highly struggling to keep up with the pace at which microbial infections are evading antibiotics through the development of mechanisms for drug resistance. Research shows that more than 3 million people die annually from bacteria-related infections and it has been predicted that resistant infections will cause 10 million deaths per year by 2050, making antibiotic-resistant infections more deadly than cancer according to a 2019 report from WHO.

Despite this growing risk, few antibiotics with a novel mode of action are being produced, leading to a lack of antibiotics that can effectively treat bacterial infections with AMR. Thus**,** the growing concern regarding drug-resistant microbial strains and biofilm-associated infections, calls for the development of additional enhanced bactericidal chemicals. Penicillin was originally effective for Gram-positive bacteria such as *S. aureus*. But resistance is developed by penicillin-resistant *S. aureus*, which produces the penicillin-hydrolyzing enzyme penicillinase. Similarly, different microbial species now a day develop resistance towards many commonly used bactericidal chemicals; the WHO has called on nations to develop national strategies plan on how to minimize the development of antimicrobial resistance through the development of new novel antibiotics holding variable mechanism of

action. According to previous reports, there were only a few antibiotic drug candidates in clinical trials. Hence there is a substantial need for the development of potent antimicrobial agents. Some antibiotics in clinical use are Tigecycline, carbapenems, and aminoglycosides which are old antibiotics, and Ceftolozane, ceftazidime, meropenem, and eravacycline are new antibiotics that are commonly in use while microbial resistance is a big issue on their effectiveness and futurity. Therefore, vast research on pharmaceuticals is necessary to develop a new therapeutic approach to discover promising and effective antibiotic drugs possessing novel modes of biological activities.

The chemistry of semicarbazones and thiosemicarbazones derivatives has been receiving considerable attention nowadays primarily due to their potential biological activities. Even though there are several semicarbazone and thiosemicarbazone organic ligands reported with different biological activities, there were limited previous studies reported particularly on the natural product-based derivatives of semicarbazone and thiosemicarbazone ligands and their metal complexes. Hence, we were encouraged to synthesize new ligands from natural product-based semicarbazone and thiosemicarbazone derivatives and their homoleptic and heteroleptic transition metal complexes and evaluate their bioactivity potentials. The metal can be employed as a vehicle for the activation of the ligand as the cytotoxic agent (Hossain, Islam, & Nuruzzaman).

This highlights a great need for a continued search for more bioactive compounds which can be easily synthesized and possess enhanced bioactivity for antioxidants, antifungals, and are more effective antimicrobials against those drug-resistant disease-causing microbial.

1.3. Objectives of the study

1.3.1. General objectives

The overall objective of this study was to synthesize, characterize, and *in* silico molecular docking studies of homoleptic (Zn(II), Cu(II), and Ni(II)) and heteroleptic (Zn(II), Cu(II)) complexes of natural product-based derivatives of new semicarbazone and thiosemicarbazone ligands and evaluation of their biological applications.

1.3.2. Specific objectives

The specific objectives of this study were:

- To synthesize semicarbazone and thiosemicarbazone derivative organic ligands from natural product constituents of ginger (dehydrozingerone), vanillin, and ortho-phthalaldehyde (OPA).
- To synthesize homoleptic Zn(II), Cu(II), and Ni(II) complexes of dehydrozingerone-semicarbazone and thiosemicarbazone organic ligands.
- To synthesize homoleptic Zn(II), Cu(II), and Ni(II) complexes of (1E)-1,4-bis(4-hydroxy-3-methoxy benzylidene) semicarbazone ligand using the standard protocol.
- To synthesize heteroleptic Zn(II), and Cu(II) complexes of ortho-phthalaldehyde (OPA)-semicarbazone and dehydrozingerone-semicarbazone ligands using the standard protocol.
- To determine the physical properties (melting point, solubility, and molar conductivity) of the newly synthesized compounds.
- To characterize the ligands and their complexes with spectroscopic methods such as UV-Vis, FT-IR, ^{1}H NMR, ^{13}C-NMR, and Mass Spectroscopies, and also with SEM-EDX, and XRD techniques.
- To investigate the thermal stability of the complexes by using thermogravimetric analysis (TGA) methods.
- To evaluate the antioxidant activities of the ligands and the synthesized metal complexes using DPPH assay techniques.
- To evaluate antifungal activities against *Aspergillums fumigates* and *Candida albicans* fungi species by the disc diffusion method.
- To evaluate the *in vitro* antibacterial activities against two Gram-positive (*Staphylococcus aureus ATCC 25923* and *Streptococcus pyogenes ATCC 19615*) and two gram-negative (*Escherichia coli ATCC 25922* and *Pseudomonas aeruginosa ATCC 27853*) bacterial strains of the prepared compounds and compare them with standard drugs using disc diffusion method.
- To study the *In-silico* molecular docking analysis of the synthesized ligands and their transition metal complexes.

1.4. Significance of the study

Despite the fact that a large amount of information is available on the synthesis and biological activities of organic semicarbazone and thiosemicarbazone derivatives, the challenge of increasing drug-resistant microbial strains has remained global concern. The treatment of bacterial infections is becoming more difficult because of a decline in the current arsenal of useful antibiotics, the raising of antibiotic resistance, and the slow rate of new drug development (Randall, 2013). In recent years, metal-based drug developments derived from nitrogen, oxygen, and sulfur-containing ligands are a new area of research to overcome drug-resistant microbial pathogens (Canpolat & Kaya, 2004). Some metal-complex-based medicines may be safe and effective for the treatment of microbial infection. Thus, the synthesized semicarbazone and thiosemicarbazone derivatives of synthetic origin (OPA) and natural product constituent of ginger (dehydrozingerone) ligands namely:- [4-(4–hydroxy-3-methoxyphenyl)but–3-en-2-one]semicarbazone (**L1**), (4-(4–hydroxy-3-methoxyphenyl)but–3-en-2-one)thiosemicarbazone(**L2**),(*1E*)-1,4-bis(4-hydroxy-3-methoxybenzylidene semicarbazone ligand (**L3**), and OPA-bis(semicarbazone) (**L4**) to improve their metal chelating ability and promote a synergetic biological effect of their resulting complexes. Hence, we synthesized novel Zn(II), Cu(II), and Ni(II) complexes as homoleptic and heteroleptic complexes from the ligands and evaluated their antibacterial, antifungal, and free radical scavenging (antioxidant) activities. Accordingly, the result obtained shows that there is a potential to design metal complexes as candidate for drug development for multidrug resistant microbial strains and improved antioxidant activities.

In addition, the *in* silico (molecular docking) studies were done to support the experimental results. Thus, this study shows the green light on the effectiveness of metal complexes of natural product-based semicarbazone and thiosemicarbazone derivative ligands for applications as effective bioactive drug agents.

1.5. Beneficiaries

This study helps researchers to get reliable information on natural product-based derivatives of semicarbazone, thiosemicarbazone ligands, and their metal complexes as a baseline for further investigations. In addition, research institutions academia, pharmaceuticals, local communities that are working on natural products and their metal complexes for medications

could use the data to strengthen their believe in using ginger products as a source for medications, and researchers interested in coordination chemistry and their biological applications and related studies could be the primary beneficiaries of this study.

1.6. Expected outcomes

Currently, researchers gave great attention to microbial-causing infectious diseases for the reason of the increase in drug-resistant and newly developed pathogens spreading throughout the world. Even if there are some commercial antibiotic drugs, it is not easy to overcome drug-resistant microbial till present. Thus, this study was planned to synthesize copper(II), zinc(II), and nickel(II) based homoleptic and heteroleptic complexes of semicarbazone and thiosemicarbazone, derivatives of natural product constituents as ligands and evaluated their performance for biological application with a focus on expected enhanced antimicrobial, antioxidant and antifungal activities. The outcome shows that the targeted metal complexes of semicarbazone and thiosemicarbazone derivatives were effective against selected gram-negative and gram-positive bacterial strains as well as radical scavenging and antifungal activity phenomenon. Furthermore, this study confirmed that there is a potential in the design and synthesis of homoleptic and heteroleptic metal complexes of natural product derivatives of semicarbazone and thiosemicarbazone-based drug development. The results of the study were also published on internationally reputable Scopus, and web of science indexed journals as a plat form to communicate the finding to scientific community.

2. LITERATURE REVIEW

2.1. The chemistry of semicarbazone and thiosemicarbazone compounds

Semicarbazones and thiosemicarbazones are a class of organic compounds obtained by condensation of semicarbazides/thiosemicarbazides with suitable aldehydes or ketones functional groups respectively. Semicarbazone is a derivative of semicarbazide which contains an additional ketone functional group and thiosemicarbazone is a derivative of semicarbazone which contain a sulfur atom in place of oxygen (Scheme 1).

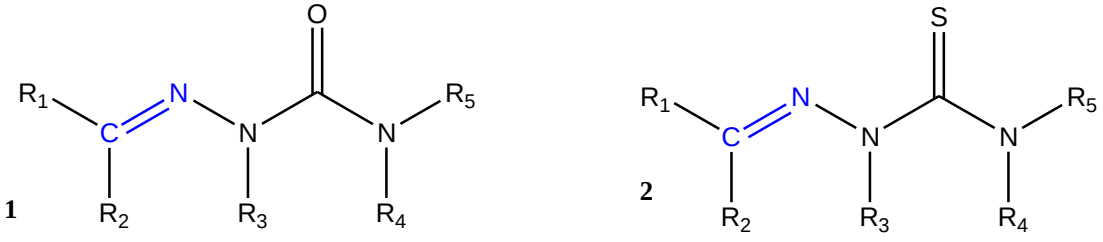

Semicarbazone Thiosemicarbazone

Scheme 1. General structures of semicarbazone **(1)** and thiosemicarbazone **(2)** derivatives

Both semicarbazone and thiosemicarbazone can be synthesized by condensation reactions between primary amines and aldehyde or ketone functional groups (More et al., 2019b; Sankar, Jose, Nithya, & Meeran). The semicarbazone is formed when ammonia-containing compounds (nucleophiles) such as semicarbazide are added to the carbonyl group (-C=O) of aldehyde or ketones forming an imine (-C=N-) containing derivatives (Scheme 2)

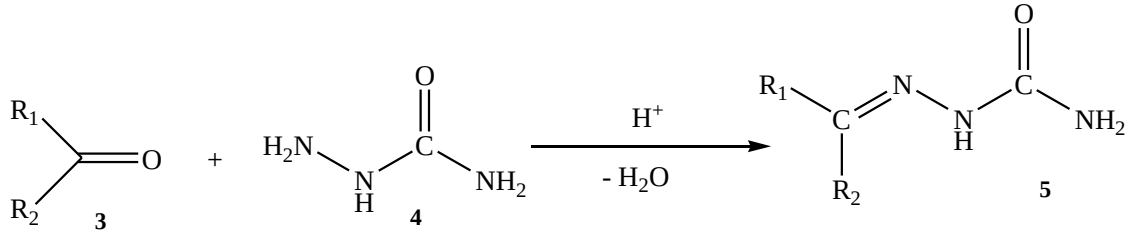

Aldehyde / ketone Semicarbazide Semicarbazone derivative

Scheme 2. Synthesis route of semicarbazone derivatives

Similarly, thiosemicarbazone is an organic compound synthesized from the reaction between thiosemicarbazide with aldehyde/ketone functional groups through a condensation reaction mechanism (Scheme 3). Thiosemicarbazones show thione-thiol tautomeric structure due to the presence of the NH-C=S and N=C-SH groups with delocalized thiamine vibration.

They exist as thione in solid form but as an equilibrium combination of thione and thiol in solution (Emam, Bondock, & Aldaloa, 2023).

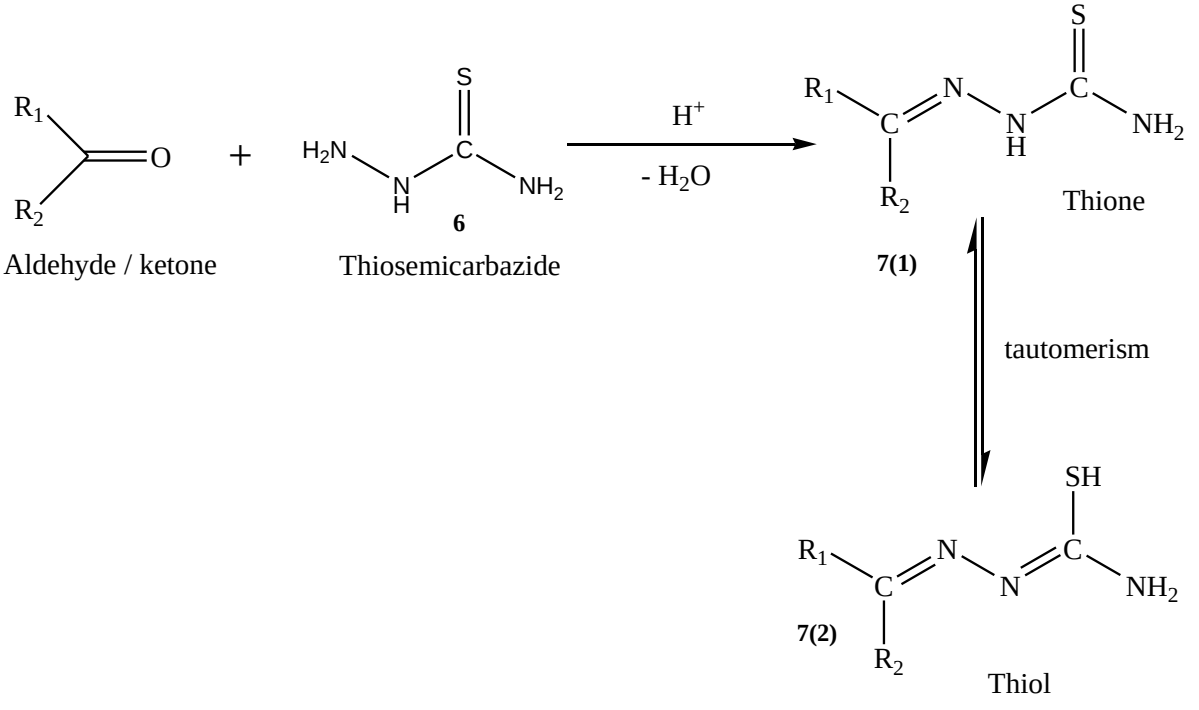

Scheme 3. Synthesis route of thiosemicarbazone derivatives; where: $R_{1,}$ R_2 = alkyl, aryl or H.

Thiosemicarbazone can adopt different possible coordination modes. In most cases, thiosemicarbazone coordinates as bidentate ligands via azomethine nitrogen and thione/thiolato sulfur. It can act as an ionic ligand by deprotonating thiol sulfur and coordinating with metals.

Numerous studies have established that semicarbazide reacts with aldehydes and ketones through a typical acid catalysis reaction. According to further research, the rate-determining step in the synthesis of semicarbazone at neutral pH is the acid-catalyzed dehydration of the carbinolamine addition product, while the reaction is nucleophilically attacked by semicarbazide on the carbonyl atom at more acidic circumstances (Cordes & Jencks, 1962a). The general reaction mechanism of semicarbazone and thiosemicarbazone formation is shown by scheme 4.

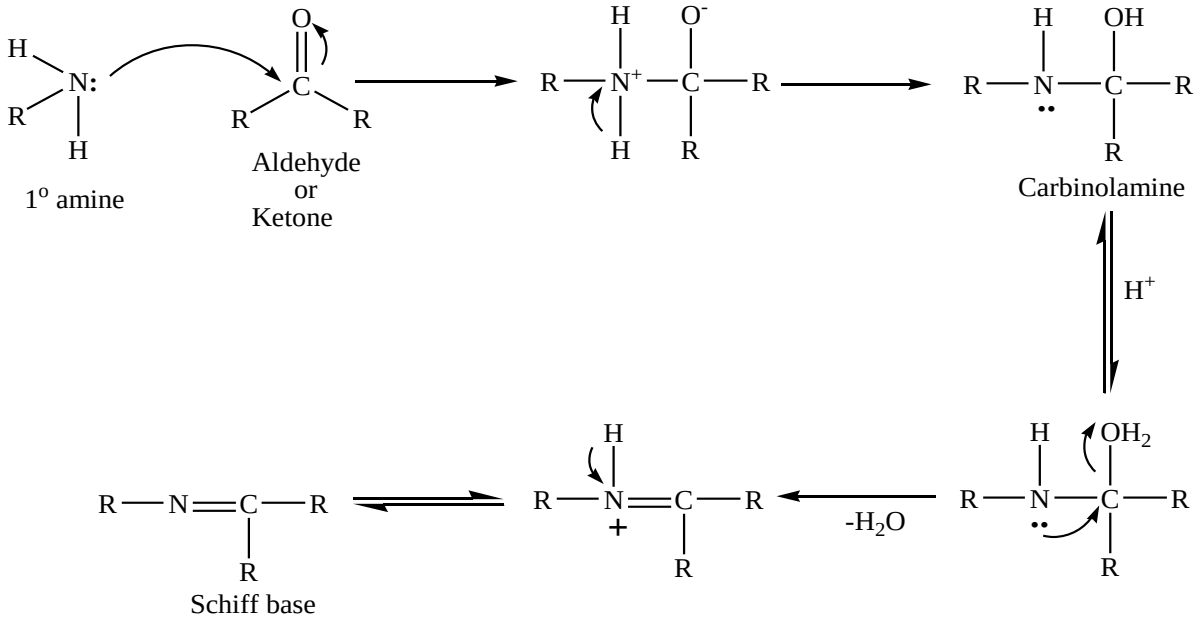

Scheme 4. Mechanism of Schiff base formation (Cordes & Jencks, 1962b)

2.2. Coordination modes of semicarbazones and thiosemicarbazone with transition metals

Interestingly, semicarbazone and thiosemicarbazone show a variety of coordination modes with transition metals. The coordination mode is influenced by the number and type of substituent. They hold several hetero atoms acting as electron donors while coordinating with metals (More et al., 2019b). They are considered as special ligands in coordination chemistry due to their better coordination tendency, form more stable complexes, better selectivity, can form macrocyclic ligands, and ability to produce some new and unique complexes with enhanced biological activities (Adhikari et al., 2019; Reena & Prathapachandra Kurup, 2011). The aromatic substituent on the semicarbazone skeleton can further enhance the delocalization of electron charge density. These classes of compounds usually react with metallic cations giving complexes in which the semicarbazone behaves as chelating ligands upon coordination to a metal center; the delocalization is further increased through the metal chelate rings (Reena & Prathapachandra Kurup, 2011). The coordination possibilities are further increased if the substituent has additional donor atoms. Based on the type of substituents on the semicarbazone skeleton, the coordination mode of the ligands can be

either: CNO, NO, and ONN for semicarbazone derivatives and ONS, NS, and SNN for thiosemicarbazone derivatives (Dhabale et al., 2022). The different coordination mode of substituted benzaldehyde semicarbazone is given in the Figure 1 below.

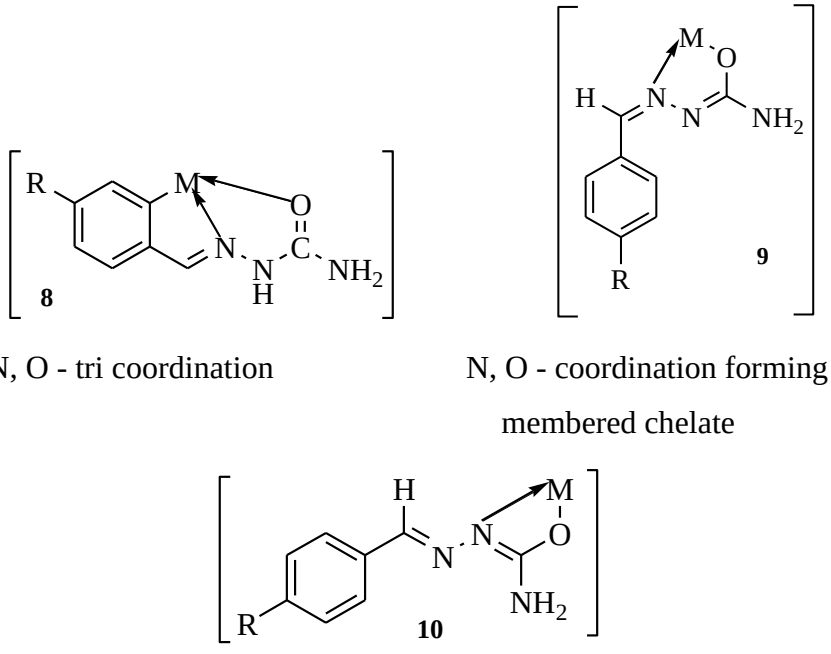

C, N, O - tri coordination

N, O - coordination forming five membered chelate

Four member chelate formation N, O – donor

Figure 1. Coordination modes of substituted benzaldehyde semicarbazone derivatives with Metals (Dhabale et al., 2022)

2.3. Semicarbazone and thiosemicarbazone derivatives based metal complexes

2.3.1. Zinc(II) complexes

Zinc is one of the essential transition metals found though out human body. It is the most abundant transition metal in the brain after iron. The importance of Zn^{2+} ions in metalloenzymes and metal-based medicines has been highlighted by numerous studies Stanić et al., 2010). There are two distinct mechanisms account for their antibacterial activity: (i) a direct interaction with microbial membranes leading to membrane destabilization and enhanced permeability (Stanić et al., 2010); (ii) an interaction with nucleic acids and deactivation of enzymes of the respiratory system (Fang, Chen, Xu, Yang, & Hildebrand, 2006). Together, these two mechanisms cause cell death.

In searching the literature, there are many zinc complexes synthesized and reported, but only few drugs used in the treatment of diseases such as Alzheimer's disease,(Di Vaira et al., 2004), antimicrobial (Kasuga et al., 2003), anticonvulsant (d'Angelo et al., 2008; Morgant et al., 2008), anti-inflammatory, antidiabetic or antitumor activities (Sakurai, Kojima, Yoshikawa, Kawabe, & Yasui, 2002).

Most of the Zn(II) complexes of semicarbazone and thiosemicarbazone ligands reported are showing tetrahedral as well as octahedral geometrical arrangements (Gobara, 2017). The ligands are known to be bidentate or tridentate in their coordination mode. The ethyl acetoacetate semicarbazone and thiosemicarbazone are found to be tridentate in their Zn(II) complex in which the third coordinating center is provided by the acetyl carbonyl group. The discovery of Zn(II) complexes of thiosemicarbazones gave promising antimicrobial activities. The zinc(II) complexes of picolinaldehyde-*S*-methyl-and-*S*-benzylthiosemicarbazones which were active in comparison to their metal-free ligands were reported (Figure 2) (Kizilcikli et al., 2007). Zinc(II) complex with the ligand (1H-imidazole-2-carboxaldehyde) thiosemicarbazone is recently reported as a candidate for antimicrobial and antioxidant agents (Gobara, 2017).

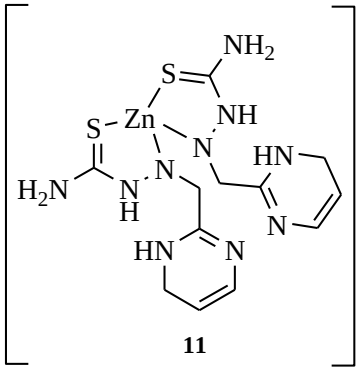

11

Figure 2. The structure of Zn(II) complex, $[Zn(C_6H_7N_5S)_2]$ of thiosemicarbazone derivative

Zinc(II) complexes of carboxylates were reported with good antibacterial activity; a strong inhibitive effect on *E. coli* and *S. aureus* (Markesbery, 1997). In the search for zinc(II) complexes of known antimicrobial drugs strong antibacterial activity has been achieved. The various nitrogen-donor ligands have been studied and the complexes were found more potent than the drugs alone (M. Patel, Chhasatia, & Parmar, 2010). In addition, zinc(II) complexes of salicylaldimine were found to be active against *S. aureus* (Kaczmarek, Jastrząb, Hołderna-Kędzia, & Radecka-Paryzek, 2009). The Zinc(II) complexes of sulfa-drugs, such as

sulfadiazine and sulfamerazine also reported to be effective as antifungal agents against *Aspergillus* and *Candida* spp (Rizzotto, 2012a). The Zinc(II) complexes with amino acids have been also developed with antimicrobial activity. The zinc complex of pyrithione is a good example of an agent of antibacterial and antifungal activity (Figure 3). In the form of bis(N-oxopyridine-2-thionato) zinc(II) the drug inhibits the membrane transport processes by blocking the proton pump in fungi (Barnett, Kretschmar, & Hartman, 1977).

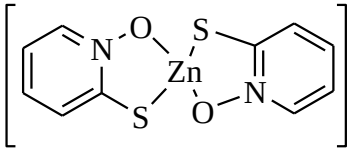

12

Figure 3. Structure of zinc pyrithione

There are also reports of novel Zn(II) complexes of heterocyclic Schiff base ligands showing promising antimicrobial and antifungal agents (Figure 4 (13 and 14)) (Yamgar et al., 2014).

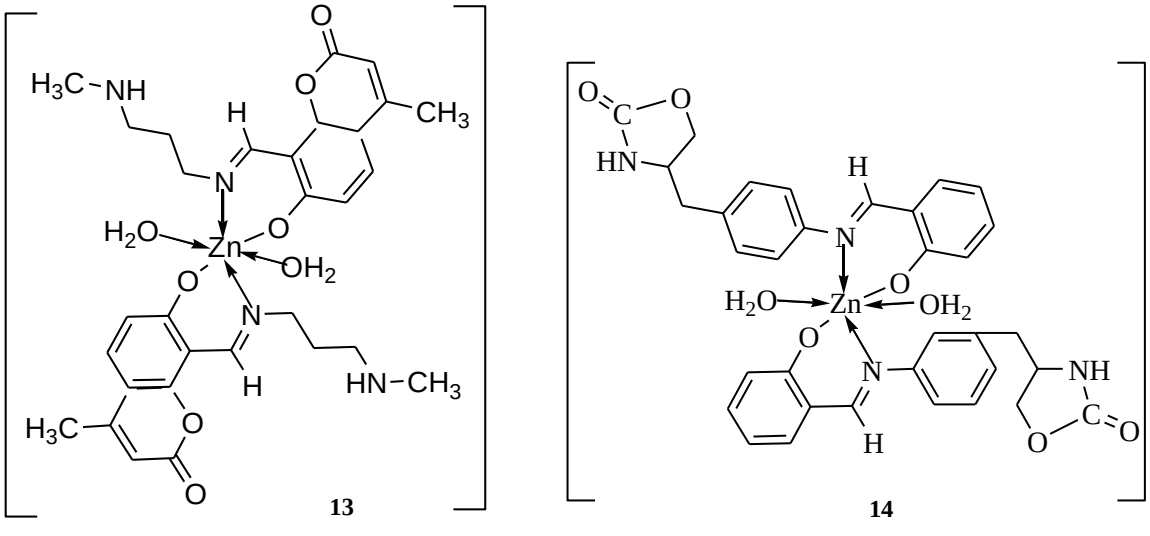

Figure 4. Zn (II) complexes ($[Zn(L)_2(H_2O)_2]$ with profound antibacterial activities

2.3.2. Copper(II) complexes

Most attention has been given to copper because it is an essential transition element for life. Copper is an essential component of a biological system, in which many chemicals need it to function properly. The coordination chemistry of copper has provoked the interest of numerous researchers due to its well-informed biological characteristics. There has been an interest in the medical uses of copper, as a complexing ion of known biologically active

ligands and drugs. Some copper (II) complexes based on Schiff-bases have been successfully synthesized and used as models in biological systems (Aghatabay et al., 2007). Mainly as: an antimicrobial (Suksrichavalit, Prachayasittikul, Nantasenamat, Isarankura-Na-Ayudhya, & Prachayasittikul, 2009), antioxidant, catalytic (Soroceanu & Bargan, 2022), anti-inflammatory (Kovala-Demertzi, 2000; Pederson & Aust, 1973; Rainsford, Brune, & Whitehouse, 1977) activities. It has been reported that copper(II) complexes of thiosemicarbazone-based derivatives showed antimicrobial activities (Rosu et al., 2010) (Kulkarni, Revankar, Kirasur, & Hugar, 2012; Shikha Parmar & Kumar, 2009; S Parmar & Kumar, 2010; Rodríguez-Argüelles, López-Silva, Sanmartín, Pelagatti, & Zani, 2005).The thiosemicarbazone derivative of copper(II) has good activity in the killing of *S. aureus*, *Salmonella Typhimurium*, and *Klebsiella pneumonia* after 6 h of incubation (Lobana et al., 2020). Copper(II) complexes of semicarbazones and thiosemicarbazones with a different coordination mode through, O, N, and S donor atoms have been synthesized and evaluated for antimicrobial, antifungal, and antioxidant activities showing promising potential (Figure 5)

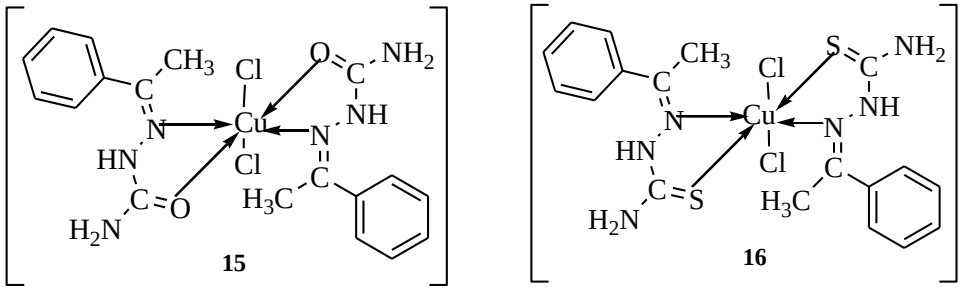

Figure 5. Cu(II) complexes with semicarbazone (**15**) and thiosemicarbazone ligands (**16**) (Where X = Cl^{-}) (Hossain, Zakaria, Kudrat-E-Zahan, & Zaman, 2017)

In many pieces of research, the antimicrobial, antioxidant, anti-inflammatory, and anticancer activities of copper(II) complexes have been investigated and reported. The commonly used antibacterial drugs have been used as ligands and form stable copper complexes. It was reported that the antimicrobial activity against *Mycobacterium smegmatis* bacteria species, the copper complex when compared to free ciprofloxacin, a bacterial gyrase inhibitor, increased three times (Patole et al., 2003). This might be due to assisted diffusion of the drug through the cell membranes by the existence of the copper metal, probably by an increase in the lipophilicity of the drug (Jiménez-Garrido et al., 2005). The potential against

Streptococcus aureus can also happen by the slow release of the ligands inside the bacterial cell. This was due to the intercellular reduction of Cu(II) into Cu(I) which can activate oxygen which is toxic for bacteria (Bottari et al., 2000).

Moreover, the copper(II) complexes of sulfacetamide, (N-[4-(aminofenil) sulfonil] acetamide), sulfanilamide, and sulfisoxazole have been reported to show promising antibacterial, antifungal, and antioxidant activity results (Blasco, Perelló, Latorre, Borrás, & Garciá-Granda, 1996; Kremer et al., 2006). The copper(II) complexes of benzimidazoles have shown strong antibacterial activity against *Staphylococcus Epidermidis* and also against fungi (Arjmand, Mohani, & Ahmad, 2005; Tavman, Boz, Seher Birteksöz, & Cinarli, 2010). The enhancement of antimalarial activity by copper coordination to ligands is commonly due to the reduction of Cu(II) to Cu(I) (Gokhale et al., 2003). Copper coordination of derivatives of salicylate has been one of the most often synthesized compounds in the search for biologically active compounds (Figure 6).

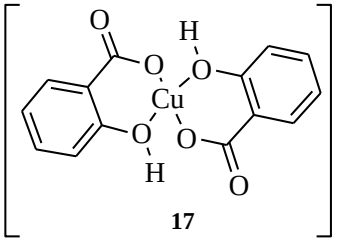

17

Figure 6. Structure of copper(II) salicylate derivative

Tetragonal distorted octahedral complexes of formula $[Cu(HTSC)_2X_2]$ (X = Cl,) were reported in the case of 4-benzylamidothiosemicarbazone and l-(α)-furyl-4 benzylamidosemicarbazone (Guillot et al., 1977). Cu(II) complexes with semicarbazone and thiosemicarbazone-based ligands: 2-formyl pyridine semicarbazone, 2-formyl pyridine thiosemicarbazone, 5-methyl-2-formyl pyridine semicarbazone, 5-methyl-2-formyl pyridine thiosemicarbazone were reported as the best candidates of bioactive synthetic metal complexes (Chandra, Raizada, & Verma, 2012). Also, Cu(II) complexes (Figure 7) with salicylaldehyde semicarbazone and thiosemicarbazone (Scheme 5 and 6) were reported to be showed greatest bioactive potential than their respective organic ligands (Ba, At, & Mg, 2018).

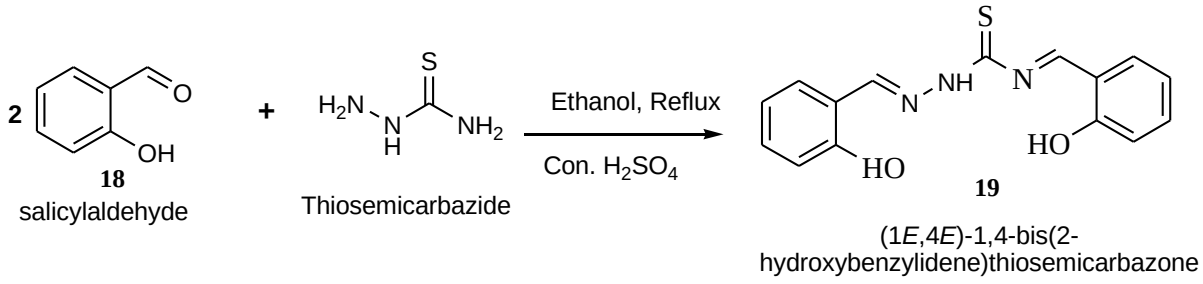

Scheme 5. Synthesis of (1E, 4E)-1,4-bis(2-hydroxybenzylidene)thiosemicarbazone

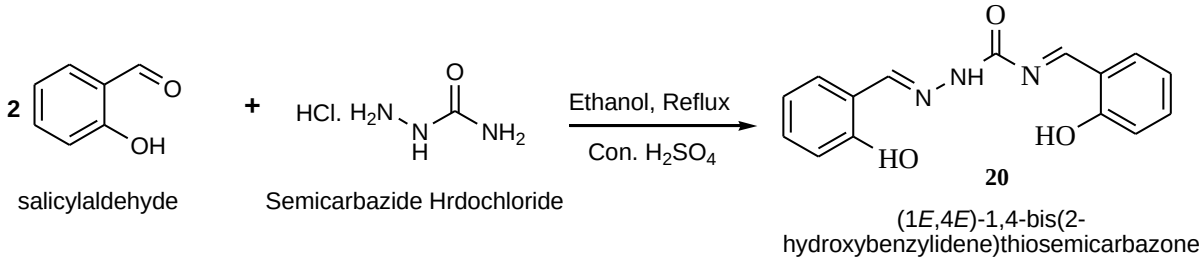

Scheme 6. Synthesis of (1E, 4E)-1,4-bis(2-hydroxybenzylidene)semicarbazone

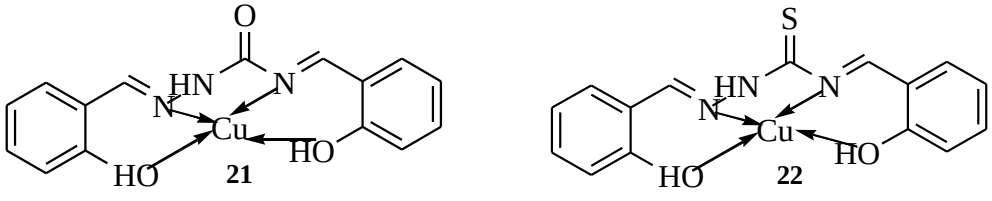

Figure 7. Cu(II) complexes of semicarbazone, $[C_{15}H_{11}CuN_3O_3]$ (**21**) and thiosemicarbazone $[C_{15}H_{11}CuN_3O_2S]$ complex (**22**).

The synthesis of Cu(II) complexes of 3-Methoxysalicylaldehyde semicarbazone and thiosemicarbazone were also reported and showed remarkable antibacterial and antifungal activities (Jayanthi et al., 2017; More et al., 2019b) (Figure 8). The Cu(II) complexes are found to have higher microbial activity than the constituent ligands.

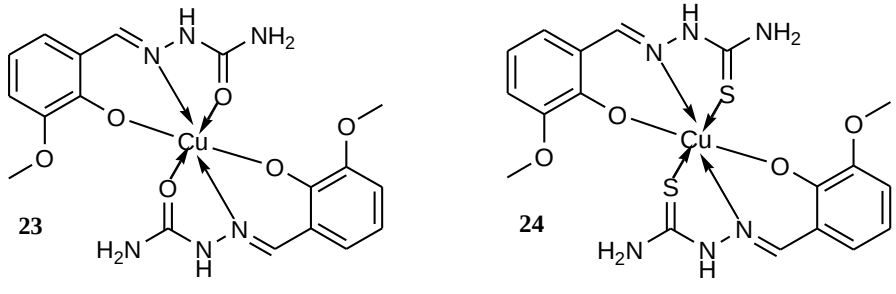

Figure 8. Structure of 3-Methoxysalicylaldehyde semicarbazone (**23**) and thiosemicarbazone (**24**) Cu(II) complexes

2.3.3. Nickel(II) complexes

Nickel like copper and zinc has specific functions in the biological system (S. Kumar & Trivedi, 2016). Our RNA and DNA include nickel, which is used in conjunction with nucleic acids to carry out certain tasks such as in RNA structural stabilization, glucose-degrading or glucose-using enzymes activation. Nickel plays a crucial role in the synthesis of red blood cells [Wilfred, 2013]. According to previous studies labile four, five, and six coordinated nickel(II) complexes with semicarbazone and thiosemicarbazone ligands exhibit antibacterial activities. The six coordinated Ni(II) complexes of semicarbazone and thiosemicarbazones have been also reported as compounds that have both antibacterial and antifungal activities (Chandra & Tyagi, 2008) (Figure 9).

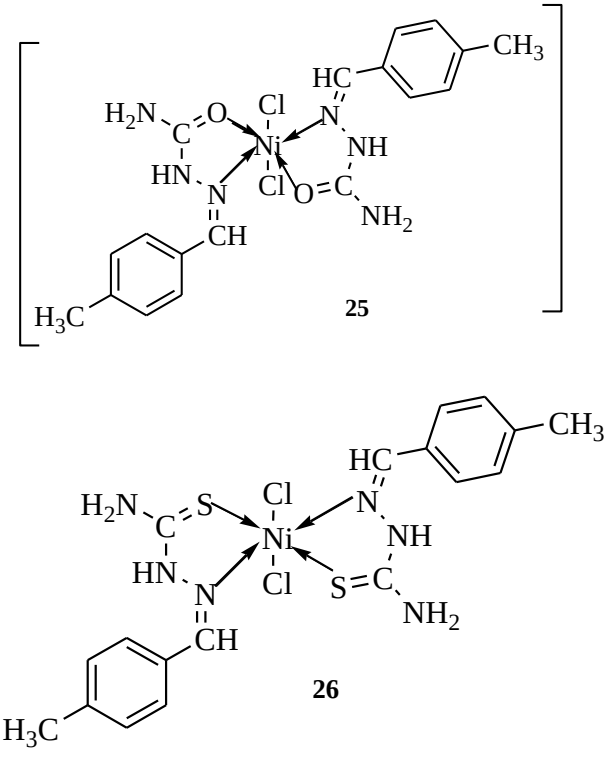

Figure 9. Ni(II) complexes of semicarbazone (25) and thiosemicarbazone (26) ligands (Tyagi, 2008)

2.4. Biological activities of semicarbazones, thiosemicarbazones, and their metal complexes

Semicarbazone and thiosemicarbazone are presents a wide range of bioactivities, and their chemistry and pharmacological applications have been investigated. Most of the semicarbazone and thiosemicarbazone synthesized and used as antimicrobial activity showed only one way of action mechanism (M. Singh et al., 2016), as a result, microbial can easily able to develop resistant against their bioactivity (Pelosi, 2010). Thus, the biological properties of semicarbazones/thiosemicarbazones are often related to metal ion coordination. Firstly, lipophilicity, which controls the rate of entry into the cell, is modified by coordination. Also, the metal complex can be more bioactive than the free ligand (Babamale, Lawal, Rajee, & Oloyede, 2016). The mechanism of action can involve binding to a metal *in vivo* or the metal complex may be a vehicle for the activation of the ligand as the cytotoxic agent (Babamale, Lawal, Oloyede, & Rajee, 2016). Several related semicarbazone and thiosemicarbazone copper complexes have been found to be active in cell destruction, as well as in the inhibition of DNA synthesis of microorganism (Babamale, Lawal, Oloyede, et al., 2016). Generally, coordination may lead to a significant reduction in drug resistance. The biological activities of semicarbazones are mainly characterized by the existence of an imine group **–N=CH-**, which helps to clarify the mechanism of transamination and racemization reaction in a biological system (Mahmoud, Deghadi, & Mohamed, 2018). It exhibits antibacterial, antiviral, and antifungal effects in its biological properties. They can work as models for biologically important species. N-(Salicylidene)-2-hydroxyaniline (Figure 10) is active against *Mycobacterium tuberculosis* but drug-resistance was developed latter (Da Silva et al., 2011).

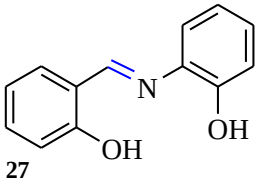

27

Figure 10. N-(Salicylidene)-2-hydroxyaniline as the bioactive compound

Semicarbazone metal complexes of Cu(II) and Ni(II) derived from 4-chlorobenzylidene-2-aminothiazole and 2-nitrobenzylidene-2-aminothiazole were synthesized (Hossain et al.; some & Benzothiazole; Udoisang, Johnson, & Efiong, 2019). And screened against the

Gram-positive bacteria; *Staphylococcus aureus* and Gram-negative bacteria; *Escherichia coli* and fungi *Aspergillus Niger* and *Candida albicans*. The antimicrobial data showed that the metal complexes were biologically more active compared to the free ligand against all pathogenic species but both the ligands and their complexes needed further investigation or modification to have a high potential to overcome drug-resistant microbial (Al-Amiery, Kadhum, & Mohamad, 2012; Mittapally et al., 2018). Other new class of copper (II) complexes with newly synthesized ligands 2-acetylbenzofuran semicarbazone and thiosemicarbazone were studied as an important antioxidant, and antibacterial agents in the biological system (Al-Amiery, Al-Majedy, Ibrahim, & Al-Tamimi, 2012; Piri, Moradi-Shoeili, & Assoud, 2017). The metal complexes show higher antioxidant, antibacterial activities, and radical scavenging potency. Copper(II) complexes derived from 2-acetyl benzofuran thiosemicarbazone show remarkable antioxidant and antibacterial activities (Goel, Chandra, & Dwivedi, 2016). All the metal complexes have a potent antimicrobial activity.

Krishna et al. synthesized new heterocyclic 3-acetyl-2,5-dimethylthiophene-semicarbazone, and thiosemicarbazone, and formed their complexes by reacting with zinc, copper, and nickel metals in a 1:2 molar ratio (Figure 11). The complexes showed the highest antibacterial and antioxidant activates serving as drug candidates clinically.

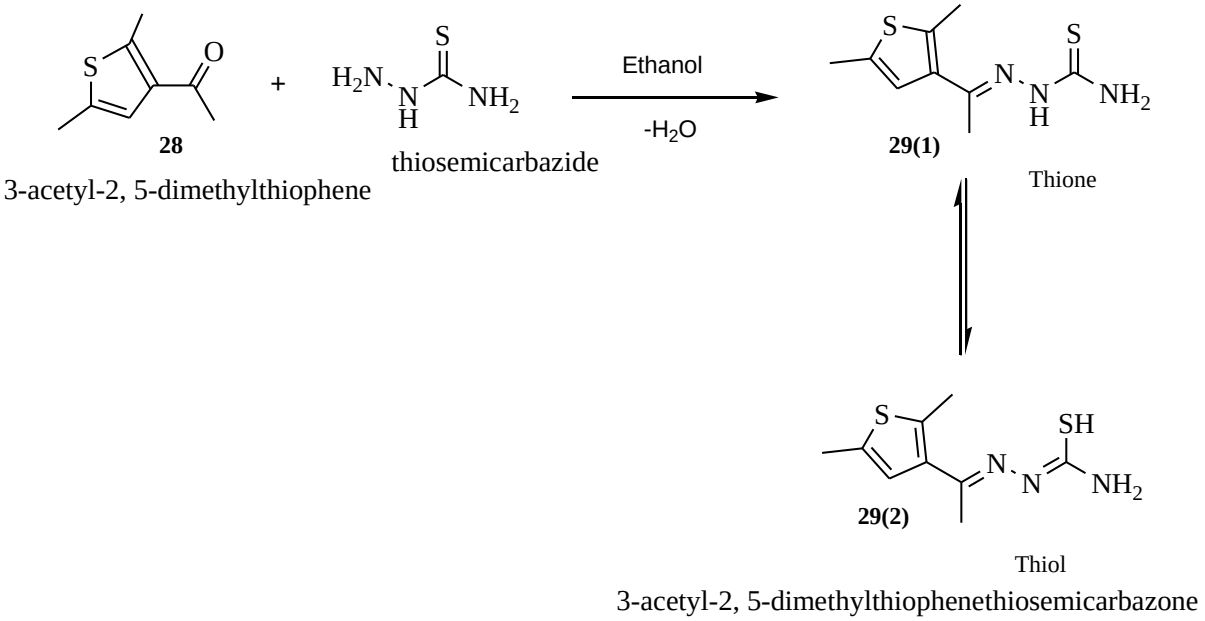

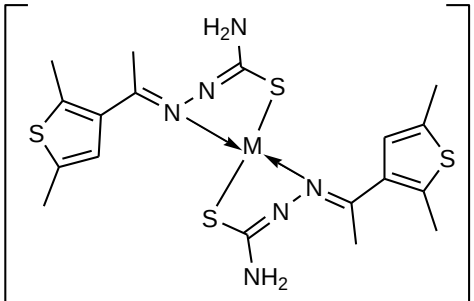

30

Figure 11. Synthesis of 3-acetyl-2,5-dimethylthiophenethiosemicarbazone ligand and structure of its corresponding complexes (Krishna et al,2016)

2.5. Biochemistry of Cu(II), Zn(II), and Ni(II) metal ions

The use of transition metal complexes as therapeutic compounds has become more and more pronounced. Many biologically active compounds used as drugs possess modified pharmacological and cytotoxic potentials when administered in the form of metal-based compounds (Mittapally et al., 2018). Various metal ions potentially and commonly used are copper, nickel, and zinc because they can form low molecular weight complexes and as a result, proven to be more beneficial against many diseases (as antimicrobial, anti-inflammatory, antioxidant, and anticancer) in their complex form (Hossain et al., 2018). Several commonly used antibiotics are known to require coordinated metal ions to function properly (Randall, 2013). Biologically applicable metal complexes have several requests in terms of their synthetic design. First, a biologically active metal complex should have a high thermodynamic stability to transport the metal or the ligand to the target or active site. Second, the metal-to-ligand bonding should be hydrolytically stable. The rate with which the metal undergoes ligation or de-ligation reactions is of great importance. Also, the molecular weight of the metal complex is a basic criterion. The compounds of low molecular weight with a neutral charge and some extent water solubility are soluble in most mediums and may move through biological membranes by passive diffusion (Medici, Peana, & Zoroddu, 2018).

Copper complexes show antimicrobial activity both in either Cu(I) and Cu(II) oxidation states, but Cu(II) is the most utilized. This is because copper with an oxidation state of two

(Cu(II)) is mostly stable in biological systems and plays a crucial role in living organisms. Cu(II) is a structural component of different enzymes such as superoxide dismutase, ascorbate oxidase, cytochrome c oxidase, ceruloplasmin, and laccase and amine oxidases. Several metabolically important molecules with catalytic activity, transfer process, oxygen transfer, needs incorporating transition metal ions into their active sites. In this aspect, copper is one of the most important transition metals being more biocompatible, eliminate the risk for toxicity which is the main drawback for other metal ions with biomedical importance. Nowadays, Cu(II) complexes of mixed ligands such as phenthrolines with amino acids, polypyridyl ligands and antibiotic molecules, were synthesized in order to enhance the activity of the drug itself (Medici et al., 2018). The link of 1,10-phenanthroline together with antibiotics increases the stability of the Cu(II)-antibiotic complex, as in the case of lomefloxacin. Studies on four coordinated complexes against *E. coli* strains revealed that the free antibiotic and its copper derivative have the same activity, while their cell intake route appeared to be completely different, which is common to other Cu(II)-antibiotic compounds. Thus, copper complexes of antibiotics commonly possess higher activities with respect to the free drugs and could be used in antimicrobial therapies due to their difference in cellular intake and mechanisms of action (Medici et al., 2018). Copper (II) complexes also can act as an antioxidant. Free radicals occur during metabolic process or naturally in the body and can react with biomolecules causing damage on our cell walls, reacting with genetic material, and leading to the happening of varies health problems and diseases. As an antioxidant, the Cu^{2+} ion itself at the required part of the body can scavenges or neutralize free radicals and may reduce some of the damage they cause (Osredkar & Sustar, 2011).

Zinc ions are also effective antimicrobial agents even at low concentrations. Gastroenteritis is strongly reduced by the assimilation of zinc and this effect could be due to the direct antimicrobial action of the zinc ions in the gastrointestinal tract (Osredkar & Sustar, 2011). The investigation of complexes of Zinc with semicarbazone and thiosemicarbazones gave promising results as well. Zinc resembles other transition metals in the formation of stable complexes with O, N, and S-donor ligands. A noticeable selective activity was seen by zinc (II) complexes of picolinaldehyde-S-methyl- and -S-benzylthiosemicarbazones which were active in comparison to their metal-free ligands. Moreover, there zinc (II) complexes of salicylaldimine were found active against *S. aureus* (Buczkowska, 2011). Drug combinations

with metals like Cu, Zn, and Ni have proven to be an essential feature of antimicrobial treatment due to a number of important considerations such as metals can increase activity through the use of compounds with synergistic or additive activity (Montelongo-Peralta et al., 2019), thwart drug resistance (Rizzotto, 2012a, 2012b), decrease required doses, reducing the chances of toxic side effects (Farrell, 2012), increase the spectrum of activity (Farrell, 2012).

2.6. Mechanisms of action of antibiotics and microbial resistance to antibiotics

The mechanism of action of antibiotic agents can be grouped based on the function that is affected by the agents, these includes inhibition of the cell wall synthesis, inhibition of nucleic acid function and synthesis, inhibition of ribosome function, cell membrane function and inhibition of folate metabolism (Figure 12) (Chohan, Sumrra, Youssoufi, & Hadda, 2010).

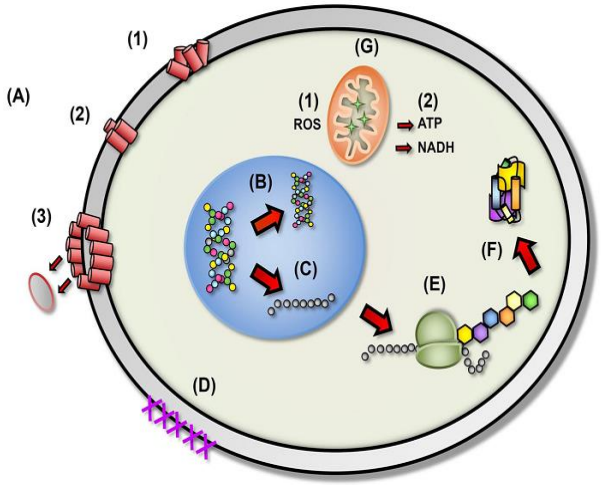

Figure 12. The proposed mechanistic modes of action for antimicrobial agents in microbial cells (Chohan et al., 2010)

(A) Disruption of cell membrane integrity: (1) random insertion into the membrane, (2) alignment of hydrophobic sequences, and (3) removal of membrane sections and formation of pores. (B) Inhibition of DNA synthesis. (C) Blocking of RNA synthesis. (D) Inhibition of enzymes necessary for linking cell wall structural proteins. (E) Inhibition of ribosomal function and protein synthesis. (F) Blocking of chaperone proteins necessary for proper

folding of proteins. (G) Targeting of mitochondria: - (1) inhibition of cellular respiration and induction of ROS formation and (2) disruption of mitochondrial cell membrane integrity and efflux of ATP and NADH (Peters, Shirtliff, & Jabra-Rizk, 2010).

The classical mechanism of action of cationic antimicrobials is the disruption of the anionic bacterial cell membrane (G. Wang, 2014). This way, bacterial destruction occurs through the interaction between the electrostatic forces of positively charged amino acid components of the cell membrane and the negatively charged cell surface (Guilhelmelli et al., 2013). Bacterial cell membranes are rich in negatively charged phospholipids, such as cardiolipin (CL), phosphatidylglycerol (PG), and phosphatidylserine (PS); these are stabilized by divalent metal cations such as Mg^{2+} and Ca^{2+} (Guilhelmelli et al., 2013). Gram-negative bacteria have an additional lipopolysaccharide-rich outer membrane, which stands as a barrier to the cytoplasmic membrane.

On the other hand, human cells are rich in neutral phospholipids, such as phosphatidylcholine (PC), phosphatidylethanolamine (PE), and sphingomyelin (SM). This difference in membrane composition between humans and bacteria makes the cationic antimicrobial highly selective against bacteria (Guilhelmelli et al., 2013). In humans, interaction with them is even less likely because of the presence of cholesterol, which affects the fluidity of phospholipids in the membrane and increases its stability (M Amerikova, 2019; Meri Amerikova, Pencheva El-Tibi, Maslarska, Bozhanov, & Tachkov, 2019). Even though, antimicrobials are the most successful forms of therapy in medicine, the efficiency of antimicrobials is conceded by an increasing number of antibiotic resistance pathogens. Antimicrobial resistance can be explained in either of two ways. (i) intrinsic resistance in which microorganisms naturally do not possess target sites for the antimicrobials and the antimicrobial does not affect them and (ii) acquired resistance in which a naturally susceptible microorganism acquires a mechanism to not be affected by the antimicrobial (Acar & Rostel, 2001; Holmes et al., 2016). Mechanisms of acquired resistance include the formation of an enzyme that deactivates the antimicrobial agent, post- transcriptional or post-translation modification of the antimicrobial agent's target, reduced uptake to the antimicrobial agent, and active efflux of the antimicrobial agent (Figure 13)**.**

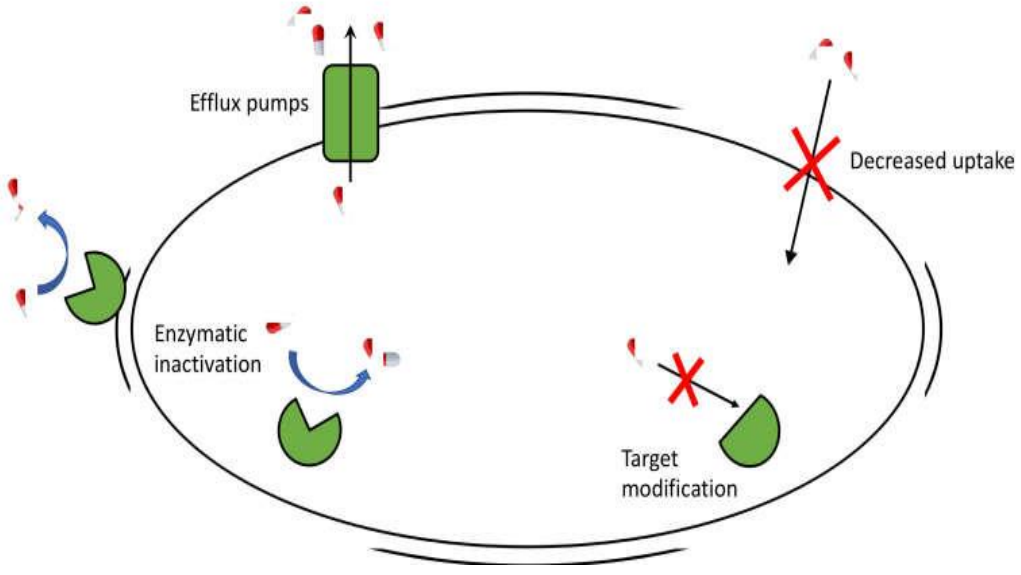

Figure 13. Representation of different mechanisms of antibiotic resistance

2.7. Development of antimicrobial agents to overcome drug-resistance

Improvements in the mode of action of antimicrobial agents have continued to achieve higher antimicrobial spectrum and activity. Penicillin was originally effective for Gram-positive microorganisms such as *S. aureus*. Later, penicillin-resistant *S. aureus* developed which produces the penicillin-hydrolyzing enzyme penicillinase. To address the resistance methicillin was developed (Brown & Wright, 2016; Viganor et al., 2017). On the other hand, attempts to expand the antimicrobial spectrum yielded ampicillin, which is also effective for Gram-negative *Enterobacteriaceae*, and piperacillin, which is effective even for *Pseudomonasaeruginosa* but latter resistance, was developed. In most cases, antimicrobial agents formerly effective are no longer useful. *S. aureus* is the resistant bacterium most familiar in the clinical setting (Bolhuis & Aldrich-Wright, 2014). This bacterium rapidly acquired resistance to sulfonamides when they were in use. Penicillin was initially effective for this microorganism, but resistant strains that produce penicillinase increased latter on. Therefore, penicillinase-stable methicillin was developed. However, as early as the following year methicillin-resistant *S. aureus* (MRSA) was isolated again (Saga & Yamaguchi, 2009). In general, the capacity of microorganisms to acquire resistance to antimicrobial agents has exceeded our imagination.

2.8. The action of metal complex compounds to overcome drug-resistant microorganisms

Recently, metal complexes become an extremely versatile and reliable tool for the development of improved medicinal compounds. Certainly, it is possible to adjust the chemical properties of metal complexes by controlling the coordinated metal center oxidation number and choosing the most appropriate bioactive organic ligands for biological applications. But the challenge in the discovery of innovative and improved metal-based drugs largely depends on the development of innovative and enriched ligands for the functional metal atom (Болатчиев, Батурин, & Базиков, 2018). Metal complexes have provided unique modes of action: ligand exchange or release at the target site, ROS generation, redox activation, and catalytic generation of toxic species or depletion of essential substrates of the microorganisms (Simons et al., 2000). Such mechanisms are not possible to achieve with purely organic compounds (Frei et al., 2020a). Metal ions play a major role in the actions of synthetic and natural metallo-antibiotics and are involved in specific interactions of these antibiotics with proteins, nucleic acids, membranes, and other biomolecules including DNA, RNA, proteins, receptors, and lipids. DNA offers an interesting, target for potential antimicrobials, and this is an approach currently attracting significant attention. Many Cu(II), and Zn(II) complexes containing phenyl ligands have been reported to interact and cleave DNA, with the phenyl ligands increasing the intercalative properties of the complexes (Bolhuis & Aldrich-Wright, 2014). Several research have been reported on the antibacterial activity of ternary metal (II)-phenyl complexes (metal = Cu^{2+}, Ni^{2+}, Zn^{2+}, Co^{2+}, Mn^{2+}) containing known antibiotics. However, still there is a development of antimicrobial resistance by microbial (Cabrera-Martinez et al., 2002).

2.9. Structure and biochemistry of *Ortho*-Phthalaldehyde (OPA) and natural constituents of Ginger (dehydrozingerone)

2.9.1. *O*-Phthalaldehyde or *ortho*-phthalaldehyde (OPA)

Ortho - Phthalaldehyde (OPA) is the latest aromatic dialdehyde organic compound (Figure 14) active towards microbial pathogens (Simons et al., 2000). But immediately both gram-

positive and gram-negative bacteria pathogens develop resistance to its activity (Simons et al., 2000). The two aldehyde functional groups that exist on OPA have been proposed to have an effective bactericidal character. However, microorganisms that have acquired resistance to OPA have yet to happen (Cabrera - Martinez et al., 2002). The physical parameters of OPA were determined to be odorless, stable, effective over a wide 3 - 9 pH range, and non-irritant to the eyes and nasal passages (Simões et al., 2007).

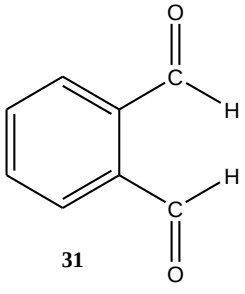

31

Figure 14. Structure of *ortho*-phthalaldehyde (OPA)

OPA is also an important compound used in a very sensitive fluorescent reagent for analyzing amines or sulfhydryls in solution, notably contained in proteins, amino acids, and peptides by capillary electrophoresis and chromatography. OPA is so reactive towards primary amine-containing compounds. It reacts with thiols in presence of an amine such as n-propylamine or 2-aminoethanol (Cabrera-Martinez et al., 2002). OPA reacts with histidine through the formation of Van der Waals interaction which arises from π-π stacking of the two aromatic components, in OPA and imidazole in histidine. To date, very few papers have been published about its antimicrobial activity (Cabrera-Martinez et al., 2002; Simões et al., 2007). Little is known about the bactericidal action of OPA, only a postulated mechanism is explained about its toxic effects on microbial. It can react strongly with amino groups in proteins and amino acids, and is believed to pass through the outer cell membranes in bacteria (Russell, 2003; Weckesser & Jügrens, 1988). Some reports demonstrated that OPA shows bactericidal activity even at low concentrations against *Escherichia coli*, *Pseudomonas aeruginosa*, and *Staphylococcus aureus* bacteria species (Gopal et al., 2015). However, OPA-resistant Mycobacterium *chelonae* strains have been identified as causing high levels of resistance which are believed to be associated with the arabinogalactan/ arabinomannan portion of the cell wall. From the reported data on bactericidal activity of OPA, why microbial develop resistance on it can be explained by two proposed factors that could account for it. First, aromatic aldehydes such as OPA, are less reactive than aliphatic

aldehydes in nucleophilic addition reactions (the nucleophile is the amine group); do to this, the reaction of OPA with amine-containing moiety would be expected to be less efficient. The second, more influential factor is due to the steric restrictions of OPA. Thus, further synthetic or structural development is needed to overcome this microbial resistance issues (Philippe, Verdu, Morère-Le Paven, Limami, & Planchet, 2019).

2.9.2. Components of Ginger (dehydrozingerone and zingerone)

Ginger (*Zingiber officinale*) is a medicinal plant that has been widely used all over the world, since ancient times, for a wide array of unrelated illnesses including pain, cramps, rheumatism, injures, painful throats, muscular aches, vomiting, hypertension, indigestion, fever, antimicrobial, antifungal and infectious diseases (Rehman & Gohar, 2022). Ginger has direct anti-microbial activity and thus can be used in the treatment of bacterial infections. Different research reports have shown that it shows a variety of biological activities such as antifungal, anti-inflammatory, antiviral, antimicrobial, antioxidant, and antitumor. Dehydrozingerone is one of the main chemical constituents of the medicinal plants ginger which are characterized by different antimicrobial activities (Teles et al., 2019). The aromatic constituent of Ginger includes; Dehydrozingerone, zingerone, and bisabolene, while the pungent constituents are known as gingerols and shogaols as shown in figure 15 and 16 bellows. Dehdrozingerone is present as a major stable component in ginger. It is a member of Methoxyphenol family and its related derivatives. They have a basic phenolic ring with a methoxy group attached to a benzene ring. Dehydrozingerone is known to have potent pharmacological activities (Teles et al., 2019). Dehydrozingerone is primarily present in dry ginger**,** but cooking or drying also converts gingerol (another component in ginger) into dehydrozingerone (Baliga et al., 2012; Jesudoss, Santiago, Venkatachalam, & Subramanian, 2017). It is also recognized as being an efficient free radical scavenger (Ahmad et al., 2015). Experimental data showed that the content of dehydrozingerone is low in fresh ginger while on drying and roasting the amount increase significantly (Prasad & Tyagi, 2015).

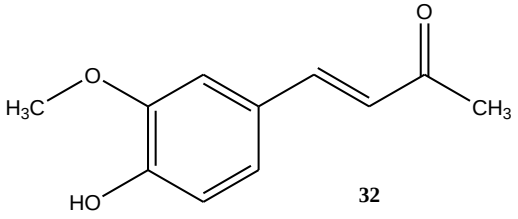

32

Figure 15. Chemical structure of dehydrozingerone

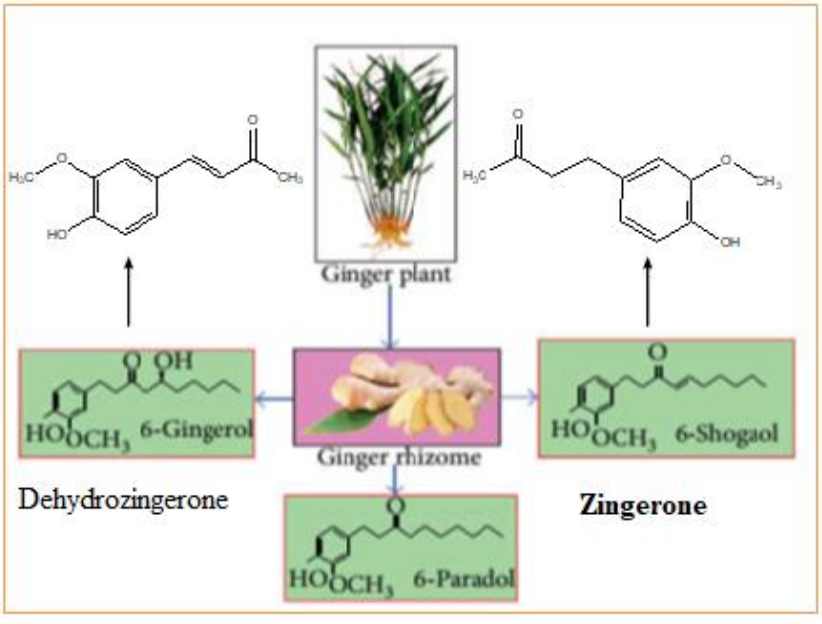

Figure 16. Ginger, ginger rhizome with its major active components (Prasad & Tyagi, 2015)

2.10. Biological Application of Transition Metal Complexes

2.10.1. Antimicrobial Activity of Transition Metal Complexes

Treatment of infection diseases caused by microbial remains an issue and challenging problem due to the combined effects of factors such as emerging infectious diseases and the growing number of multi-drug resistant microbial pathogens (Kalaichelvan & Maleckid; Vijayan et al., 2015). Microbial infections are one of the leading diseases which are caused millions of deaths reported every year because of the lack of effective antimicrobial therapy due to microbial resistance towards conventional antibiotics (Frieri, Kumar, & Boutin, 2017; C. Ghosh, Sarkar, Issa, & Haldar, 2019). As mentioned above semicarbazones, thiosemicarbazones, and their derivatives are an important class of organic ligands which can be synthesized from different sources of aldehyde and ketone groups possessing a wide range of biological activities. So that, the issue of antimicrobial resistance against commonly used antibiotics are becoming critical and a worldwide problem. The bacteria, methicillin-resistant *Staphylococcus aureus* (MRSA) and vancomycin resistant *Enterococcus faecium* (VREF), are resistant to the clinically used antibiotics such as methicillin and vancomycin (S.-X. Zhang et al.,2016). Considering the high rising of drug-resistant microbial, developing another strategy to fight against bacterial infections is therefore urgently needed. Therefore,

searching for a novel and an effective antimicrobial agent is important to overcome this problem. Accordingly, metal complexes of semicarbazone and thiosemicarbazone-derived organic ligands and metal complexes showed good antibacterial activity against *Escherichia coli*, *Pseudomonas aeruginosa*, and *Staphylococcus pyogenes* (Shakir, Hanif, Alam, & Younus, 2016).

Therefore, it has been found interesting to study the structural property and biological activity of metal complexes containing the semicarbazone and thiosemicarbazone moieties. According to the results of studies on copper(II), nickel(II), and zinc(II) complexes containing ONNO(S) donor atoms of semicarbazone and thiosemicarbazone organic ligands the complexes have shown the highest zone of inhibition against all the tested strains (Kargar, Adabi Ardakani, Munawar, Ashfaq, & Tahir, 2021; Kargar, Ardakani, Tahir, Ashfaq, & Munawar, 2021). The results of previously reported studies indicated that all metal complexes have higher antimicrobial activities than the parent ligand. This higher activity of the metal complexes may be due to the mechanism of action of metal ions on the bacteria cell membrane (Surati & Sathe, 2016). Metal coordinated organic ligands bear polar and nonpolar properties together; making them suitable for permeation to the cells and tissues (Nair, Arish, & Joseyphus, 2012). Furthermore, chelation may enhance or raise the biochemical potential of bioactive organic molecules (Surati & Sathe, 2016). The character of the metal ion coordinated to the organic ligand may have its role in increasing the lipophilic character of the central metal ion, because of the partial sharing of its positive charge with the donor groups and possible π-electron delocalization over the chelate ring. This makes the permeation of metal complexes compounds through the lipid layer of the cell membrane easier. The increase in lipophilicity of the ligand up on metal coordination may contribute to its simplistic transport into the bacterial cell which blocks the metal binding sites in the enzyme of microorganisms (Mandewale, Kokate, Thorat, Sawant, & Yamgar, 2019; Mandewale et al., 2018)

2.10.2. Antioxidant activities of transition metal (Zn, Cu, and Ni) complexes

Free radicals are atoms or molecules that have unpaired electrons and are unstable molecules unavoidably produced in biological systems during regular metabolism. These unstable molecules have a great capability of interacting with biomolecules such as proteins, lipids,

and DNA in health human cells through electron sharing with them and are known to cause various degenerative disorders, like mutagenesis, carcinogenesis, cardiovascular disturbances, and so on (Phaniendra, Jestadi, & Periyasamy, 2015; Valko, Rhodes, Moncol, Izakovic, & Mazur, 2006). Therefore, the intake of antioxidants is mandatory to protect biomolecules from damage caused by free radicals. Antioxidants are substances that can prevent and stabilizing the damage caused by free radicals by providing electrons. Antioxidants turn free radicals into waste as by-products, which can be removed from the body. Thus, the intake of antioxidants as synthetic drugs is known to lower the risk of several diseases caused due to free radicals (Lobo, Patil, Phatak, & Chandra, 2010; Nimse & Pal, 2015; Sen & Chakraborty, 2011). In biological systems, antioxidants prevent oxidative damage by acting as scavengers to reactive oxygen species (ROS) (Sen & Chakraborty, 2011). Vitamin C and vitamin E are well-known non-enzymatic antioxidants within normal cells that interact directly with radicals such as hydroxyl and peroxyl intermediates and help to minimize the consequences of lipid peroxidation in membranes. But natural antioxidants have their own merits and drawbacks such as a lack of water solubility and regular antioxidant activity. Most natural antioxidants are lipid-soluble with a lower absorption capacity, such as vitamin E. Many synthetic antioxidants that have been developed recently exhibit good antioxidant properties (J. Kumar, Kumar, Sati, & Hota, 2020). Hence synthetic antioxidants are widely used because they are effective and cheaper than natural antioxidants. The search for metal-based derived antioxidants has received much attention and effort to develop compounds having a high capacity in scavenging free radicals to overcome various disorders and diseases associated with oxidative damage, caused by ROS. Recently, several semicarbazone and thiosemicarbazones Schiff base have been investigated as effective scavengers of ROS, acting as antioxidants. Although semicarbazone and thiosemicarbazone derivative compounds were synthesized and have shown antioxidant activities, scientific information on their metal complexes as antioxidant properties of natural product-based derivatives is scarce. Therefore, the assessment of such properties remains an interesting and useful task to find promising sources of natural product-based derivatives of semicarbazone and thiosemicarbazone-metal complexes as antioxidants.

The method known as the DPPH (1, 1-Diphenyl-2-Picrylhydrazyl) assay was developed by Blois (1958) with the viewpoint to determine the antioxidant activity using a stable free

radical α, α-diphenyl-β-picrylhydrazyl (DPP). The method is aimed at determining the level at which antioxidants can scavenge DPPH. The unpaired electron of a nitrogen atom in DPPH is reduced by receiving a hydrogen atom from antioxidants to the corresponding hydrazine. DPPH is characterized as a stable free radical under the delocalization of the spare electron over the molecule (Scheme 7), so that the molecules do not dimerize, like most other free radicals. The delocalization also gives rise to the deep violet color, with absorption in methanol solution at around 517 nm. On mixing DPPH solution with a substance that can donate a hydrogen atom, it gives rise to the reduced form with the loss of violet color or DPPH produces violet/purple color in solution. This fades to shades of yellow color in the presence of antioxidants (Rahman, Islam, Biswas, & Khurshid Alam, 2015; Sinha & Dixit, 2022). DPPH shows a strong absorption band at 517 nm due to its odd electron and the solution appears a deep violet color, the absorption vanishes as the electron pairs off and the resulting decolonization is stoichiometric with respect to the number of electrons taken up. DPPH method is a rapid, easy, inexpensive, and widely used method to determine the activity of compounds to act as free radical scavengers or hydrogen donors, and to evaluate antioxidant activity. It is a valid accurate, easy, and economic method to evaluate the radical scavenging activity of newly synthesized compounds (O. A. El-Gammal, Mohamed, Rezk, & El-Bindary, 2021; El Jemli et al., 2016). When a solution of DPPH in its radical form is mixed with a proton-donating substance such as antioxidants, the radicals are scavenged, and DPPH=H is formed with a concomitant decrease in absorbance (Contreras-Guzmán & Strong III, 1982; Sánchez-Moreno, 2002). Antioxidants react with free radicals by different reaction mechanisms such as single electron transfer, hydrogen atom transfer, or the combination of both mechanisms (Choudhary et al., 2011;Kobayashi, Otsuka, & Shimada, 2021).

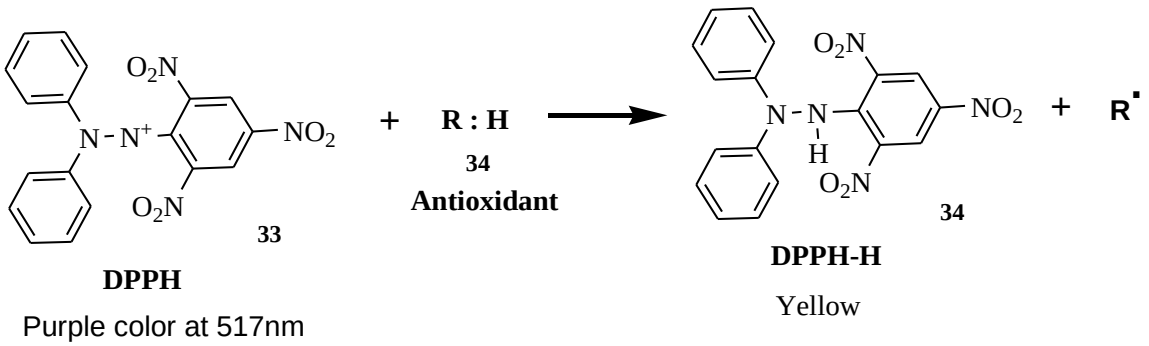

Scheme 7. Reaction mechanism of DPPH with antioxidants (Bondet, Brand-Williams, & Berset, 1997; Santos-Sánchez, Salas-Coronado, Villanueva-Cañongo, & Hernández-Carlos, 2019).

When the antioxidant substance scavenges the DPPH radical, the absorbance becomes decrease, which is proportional to the concentration of radicals that are being scavenged (Liang & Kitts, 2014). The measurements are done using a UV-Visible spectrophotometer at room temperature and the free radical scavenging potential is expressed as the percentage of DPPH radical scavenge (equation 1).

$$\text{DPPH scavenged (\%)} = \frac{\textbf{Absorbance of control} - \textbf{Absorbance of sample}}{\textbf{Absorbance of control}} \times 100 \quad \ldots\ldots\ldots\ldots\ldots (1)$$

2.11. Molecular docking and *In-silico* drug-likeness predictions

Pharmacokinetics (PK) and pharmacodynamics (PD) play a crucial role in drug development (Awasthi et al., 2014; DeLano, 2002). The evaluation of pharmacological parameters such as drug-likeness, ADME, and Toxicity is paramount in identifying lead compounds (DeLano, 2002). Recently, *in-silico* methods that include molecular docking analysis and online ADMET predictions (SwissADME, Pro-Tox II, and OSIRIS property explorer) facilitate the process of identifying the potential bioactive molecule (P Banerjee & Eckert, 2018; Garg et al., 2021; O Trott & Olson, 2009).

2.11.1. Molecular docking

Molecular docking has now become a novel approach for the screening of synthetic bioactive compounds in drug discovery in recent years. Computer-assisted drug design is an area that is rapidly growing and has resulted in many successes. Many big pharmaceutical industries, academic resources, and research personnel are using the tools for new drug development.

It is one of the most frequently used methods in structure-based drug design, due to its ability to predict the binding-conformation of compounds to the appropriate target binding site protein (Khan, Ahemad, Chuah, Naidu, & Htar, 2020). It validates the molecular mechanisms for ligands at the active site of a protein. The molecular docking approach can be used to model the interaction between a molecule and a protein which allows us to characterize the behavior of small molecules in the binding site of target proteins as well as to elucidate fundamental biochemical processes (Meng, 2011). Molecular docking assists in the process of computer-aided drug designing by considering every possible conformation of the protein and targeted molecules (Meng, 2011). Molecular docking techniques aim to predict the best matching binding mode of a ligand to a macromolecular partner. Ligand binding to

macromolecules plays a key role in medicine as a guiding mechanism in biological processes. The binding of drugs to proteins and DNA has led to vast structural studies using both experimental and theoretical methods.

Because DNA plays a major role in the replication and transcription of the cell, it has been considered to be a major target for antibiotics, antiviral and anticancer drugs (Francis, Gas, Daugeron, Bravo, & Seraphin, 2012). DNA-binding drugs are common for different diseases such as bacterial, viral, and fungal infections (Baeuerle & Baichwal, 1997). The different modes of drug binding to DNA include intercalation between adjacent base pairs, and intrusion into the minor groove and the major groove (Chaires, 2006). Intercalation and minor-groove binding are the predominant DNA-binding modes of small molecules (Mišković, Bujak, Baus Lončar, & Glavaš-Obrovac, 2013). This computer-simulated ligand binding method of screening bioactive compounds is a powerful technique for investigating intermolecular interactions for rational drug design. The information gained from the docking result can be used to suggest the binding energy, free energy, and stability of complexes. The crucial advantage of molecular docking tools is that it requires less investment in resources and time in comparison to *in vivo* lab studies and important to support the *in vitro* biological studies.

3. MATERIALS AND METHODS

3.1. Chemicals and Reagents

The chemicals and reagents used during this study were Semicarbazide hydrochloride ($CH_5N_3O.HCl$) 99%, thiosemicarbazide (CH_5N_3S) 99%, glacial acetic acid (CH_3COOH) 99.5%, *ortho* - phthalaldehyde (OPA) ($C_8H_6O_2$) 99%, sodium acetate (CH_3COONa) 99.99%, dehydrozingerone ($C_{11}H_{12}O_3$) 99.9%, Vanillin ($C_8H_8O_3$) 99.9%, acetone (C_3H_6O) 99.5%, sodium hydroxide (NaOH) 97%, metal salts ($ZnCl_2$ 99.9%, $CuCl_2.2H_2O$ 99% and $NiCl_2.6H_2O$ 98%), dimethyl sulfoxide (DMSO) 99.99%, sodium hydroxide (NaOH) and concentrated H_2SO_4 were obtained from Alchem Pvt. Ltd., Addis Ababa. Calcium carbide (CaC_2), and the organic solvents ethanol (CH_3CH_2OH), methanol (CH_3OH), diethyl ether ($C_4H_{10}O$), ethyl acetate, chloroform, and hydrochloric acid (HCl), were used. L-Ascorbic acid and 2,2-diphenyl-1-picrylhydrazyl (DPPH) were used for the biological activity test. All chemicals and reagents, including salts and solvents, were of analytical grade and used without further purification. De-ionized water was used for solution preparations.

3.2. Instruments and apparatus

The basic instruments used for this study and their function and application were: an electro-thermal Stuart SMP^3 (UK) to determine the melting point determination of the newly prepared compounds, thin layer chromatography (TLC) (Co.KG, Germany) was used to check the progress of reaction and the purity of the prepared compounds. The spots were detected using a UV lamp. The absorbance of the compounds was scanned in the UV- Vis range of 200.0 – 800.0 nm under the Abs Test Model using Chem LAB UV Spectrometer (SM-1600 Spectrophotometer, Germany) at the Department of Biology, Adama Science and Technology University, Ethiopia. Elemental analysis was done using CHN analyzer (PerkinElmer@2400series II) at Department of Biomaterials, Saveetha Dental College and Hospitals, Saveetha Institute of Medical and Technical Sciences, Saveetha University, India. Elemental composition analysis oxygen, chlorine, and metals in the complexes and surface morphology were done by using energy dispersive x-ray spectroscopy (EDX) together with scanning electron microscopy (SEM) (CARL ZE 155, OXFORD instrument's EDX) at Multimedia University, Malaysia. A Perkin Elmer FTIR spectrophotometer in the wavelength range of 400–4000 cm^{-1}), Model No BX, was used to record FTIR spectral data using KBr

discs at the Department of Chemistry Addis Ababa University. A Bruker Avance 400 MHz NMR spectrometer was used to acquire the NMR spectral data in DMSO-d_6 as a solvent and chemical shifts (δ) were reported in ppm and the coupling constants (J) are reported in Hertz which were done at the Department of Chemistry Addis Ababa University Ethiopia, LC-MS (model LCMS-8030, mass range *m/z* 10 to 2000, sensitivity ESI positive: 1 pg reserpine, S/N > 3,000:1 (RMS), resolution R < 0.7 FWHM) at the University of the Witwatersrand, PO Wits, Johannesburg 2050, South Africa, XRD data were obtained using Philips X-pert pro diffractometer, PW 1830 (X-ray tube target: Cu-Kα(λ=1.5406 nm) at the Institute of Chemical Engineering, Jimma University, Ethiopia. Thermogravimetric analysis (TGA) was performed under N_2-atmosphere with the SHIMADZU's DTG-60H thermal analyzer which is a TG-DTA-DSC instrument used to measure mass loss vs temperature and the scanning were carried out up to 1500 K through a heating rate of 10.0 deg/min at Department of Chemical Engineering, Bahir Dar University.

3.3. Synthesis of semicarbazone and thiosemicarbazone derivative ligand

The ligands were synthesized according to the reported procedures (Mishra, Pandeya, Pannecouque, Witvrouw, & De Clercq, 2002; Mukhametzhanova, Shtrykova, Kuksenok, & Filimonov, 2014) by condensation through the reflux method.

3.3.1. Synthesis of [4-(4-hydroxy-3-methoxyphenyl)but-3-en-2-one]semicarbazone (L1)

Semicarbazide hydrochloride (0.01 mol, 1.12 g) and CH_3COONa (0.01 mol, 0.82 g) were dissolved in 25 mL of distilled water in a round bottom flask. The contents were warmed in an oil bath until a clear homogeneous solution was formed to release semicarbazide from its salt form. To the homogeneous solution, dehydrozingerone or (4-(4-hydroxy-3-methoxyphenyl)but-3-en-2-one) (0.01 mol,1.92 g) in ethanol (25 mL) was slowly added and heated to reflux in the temperature range of 65 - 70 °C. A dropwise catalytic quantity of HCl (five drops) was slowly added while heating in an oil bath under reflux for four hours (Witvrouw, & De Clercq, 2002). The progress of the reaction and formation of the product were monitored using thin-layer chromatography (TLC). Finally, the product was cooled on ice, filtered, re-dissolved, and crystallized from ethanol to eliminate unreacted species and dried under vacuum desiccator, where brown colored solid was obtained.

3.3.2. Synthesis of [4-(4-hydroxy-3-methoxyphenyl)but-3-en-2-one]thiosemicarbazone ligand (L2)

The dehydrozingerone thiosemicarbazone ligand was prepared using a reported procedure with minor modifications (Belicchi Ferrari, Capacchi, & Biscegile, 2001; Oladimeji & Valan, 2020). A warm ethanol solution (25 mL) of thiosemicarbazide (0.91 g, 0.01 mol) was mixed with an ethanol solution (25 mL) of dehydrozingerone (1.92 g, 0.01 mol) with a 0.5 mL of acetic acid while stirring continuously. The contents were refluxed in the 65-70 °C temperature range for four hours. The progress of the reaction completion and product formation were monitored using TLC. The resulting product was cooled to form a precipitate, which was filtered with Wattman No 1 filter paper, washed with cold methanol to remove unreacted amine and ketone, and then dried using $CaCl_2$ as a drying agent in a vacuum desiccator where a yellowish crystal were obtained.

3.3.3. Synthesis of (1E)-1,4-bis(4-hydroxy-3-methoxybenzylidene)semicarbazone ligand (L3)

The ligand (**L3**), (1E)-1,4-bis(4-hydroxy-3-methoxybenzylidene)semicarbazone was synthesized by adopting previously reported procedures (Hossain et al., 2017) with minor modifications to provide good yield. Accordingly, Vanillin (0.02 mol, 3.04 g) **was** dissolved in absolute ethanol (25 mL) was added slowly to a constant stirring solution of semicarbazide hydrochloride (0.01 mol, 1.12 g) and sodium acetate (0.01 mol, 0.82 g) in 50 mL hot ethanol in a two necked round bottom flask with 5 mL of concentrated H_2SO_4 (Hossain et al., 2017). The mixture was refluxed in the temperature range of 70 - 75 ^oC for six hours. The reaction progress was checked by TLC in a ethyl acetate and methanol mixture in the ratio of 7:3 by volume. An orange product was obtained after cooling, and it was filtered, washed with ethanol and diethyl ether, and dried using $CaCl_2$ as a drying agent in a vacuum desiccator. The product obtained was gray colored powder.

3.3.4. Synthesis of *o*-phthalaldehyde disemicarbazone ligand (L4)

The semicarbazone was prepared using a reported procedure (Goel et al., 2016). Semicarbazide hydrochloride (0.01 mol, 1.11 g) was dissolved in 30 mL ethanol and was mixed with 30 mL ethanolic solution of *ortho*-phthalaldehyde (0.005 mol, 0.670 g) together with CH_3COONa (0.01 mol, 0.82 g). The semicarbazide was generated from semicarbazide

hydrochlorides by CH_3COONa. The CH_3COOH produced during the reaction progress protonates the C = O functional group of *ortho* – phthalaldehyde (OPA), which eases the nucleophilic reaction of carbon. The clear solution formed was continuously stirred under reflux in the temperature range of 65 - 70 °C for two hours. The completion and product formation were monitored and confirmed by TLC in a ethyl acetate and methanol mixture in the ratio of 9:1 by volume. The product obtained was filtered using small micro-sized filter paper, washed repeatedly with warm water, and finally dried in a vacuum desiccator over $CaCl_2$.

3.4. Synthesis of homoleptic transition metal complexes

The homoleptic zinc(II), copper(II), and nickel(II) complexes (**1-8**) were synthesized by reacting the ligand **L1, L2,** and **L3** with the metals chloride salts as per the modified reported methods (Siji, Kumar, Suma, & Kurup, 2010). The homoleptic complexes **1-3** where synthesized from **L1**, complexes **4** and **5** from **L2,** and complexes **6-8** where from **L3** ligands.

3.4.1. Synthesis of Zinc(II) complex of L1 (1)

A warm ethanol solution (25 mL) of $ZnCl_2$ (1 mmol, 0.136 g) was mixed with an ethanol solution (25 mL) of (**L1**) (2 mmol, 0.50 g) by 1:2 molar ratio. The mixture was stirred while refluxing the mixture for five hours in the temperature range of 70 - 75 °C till color change. The pH was adjusted at around 7 by 5% NaOH drop wise addition while stirring the mixture for another 30 minute. The completion of the reaction and product formation were checked by TLC in a ethyl acetate and methanol mixture in the ratio of 5:5 by volume. After TLC result confirmed the completion of the reaction, the mixture was allowed to cool at room temperature. Then, the product was separated, filtered, and thoroughly cleaned first with warm water and methanol and dried under vacuum desiccators over anhydrous $CaCl_2$ (Naz et al., 2020). The product obtained was then stored in a vial for characterization and biological applications.

3.4.2. Synthesis of Copper (II) complex of L1 (2)

$CuCl_2 \cdot 2H_2O$ salt (0.17 g, 1 mmol) was dissolved in 25 mL warm absolute ethanol and was added to a solution of **L1** (0.50 g, 2 mmol) which was dissolved in 25 mL of absolute ethanol in 1:2 mole ratio. A few drops of sodium hydroxide (5 % NaOH) were added to adjust the pH to be around 7. The mixture was heated under reflux in an oil bath for four hours between 70

- 75 ^{o}C till color change occurred (Naz et al., 2020). The reaction completion and product formation were checked by TLC in a ethyl acetate and methanol mixture in the ratio of 7:3 by volume. After the TLC indicated the formation and completion of the reaction, the reaction mixture containing red precipitate was allowed to cool to room temperature. The solution was filtered, washed with ethanol, and left to dry under vacuum desiccators over anhydrous $CaCl_2$.

3.4.3. Synthesis of Nickel(II) complex of L1 (3)

$NiCl_2.6H_2O$ (0.24 g, 1 mmol) was dissolved in 20 mL warm absolute ethanol was added dropwise to the solution of 0.50 g (2 mmol) of **L1** dissolved in 25 mL of absolute ethanol under constant stirring. A few drops of 5 % NaOH were added to adjust the pH to be around 7. The mixture was heated under reflux in an oil bath for three hours in the temperature range of 70 - 75 ^{o}C till color change occurred (Jirjees et al.; Ramachandran, Raja, Bhuvanesh, & Natarajan, 2013). After TLC results showed a single spot indicating the completion of the reaction, it was allowed to cool to room temperature and filtered off, washed with ice-cold methanol, and dried at room temperature. The brown powder product was obtained and left to dry overnight in a vacuum desiccator over $CaCl_2$.

3.4.4. Synthesis of Zinc(II) complex of L2 (4)

An ethanolic solution (25 mL) of $ZnCl_2$ (1 mmol, 0.136 g) was mixed with a warm ethanolic solution (25 ml) of (4-(4-hydroxy-3-methoxyphenyl)but-3-en-2-one) thiosemicarbazone **(L2)** (2 mmol, 0.53 g). A few drops of sodium hydroxide (5 % NaOH) were added to adjust the pH to be around 7. The contents were refluxed for five hours between 70 - 75 °C. After TLC results indicated the completion of the reaction, the mixture was allowed to cool to room temperature (Ejidike, Bamigboye, & Clayton, 2021). Then after, the white precipitate formed was filtered and washed with ethanol to remove unreacted species. Finally, the solution was left to dry in a vacuum desiccator over $CaCl_2$.

3.4.5. Synthesis of Copper(II) complex of L2 (5)

$CuCl_2.2H_2O$ salt (0.170 g, 1mmol) was dissolved in 25 mL of warm absolute ethanol with stirring was added to a solution containing (4-(4-hydroxy-3-methoxyphenyl)but-3-en-2-one) thiosemicarbazone (0.53 g, 2 mmol) (L2) in 25 mL of absolute ethanol. The pH of the mixture was adjusted around 7 by drop wise addition of 5% NaOH. The mixture was refluxed for three hours in the temperature range of 70 - 75 ^{o}C (Dwivedi, 2013). After TLC results

indicated the completion of the reaction, the brown solid precipitate obtained was filtered, washed with ethanol, left to dry in a desiccator.

3.4.6. Synthesis of Zinc(II) complex of L3 (6)

Hot ethanolic solution (20 mL) of $ZnCl_2$ (1 mmol, 0.136 g) was mixed with a hot ethanolic solution (20 mL) of (1E)-1,4-bis(4-hydroxy-3-methoxybenzylidene)semicarbazone ligand (**L3**) (2 mmol, 0.687 g) in 1:2 mole ratio. The mixture was treated with 5% NaOH solution to adjust the pH around 7 range (Goel, Chandra, & Dwivedi, 2013; Jirjees et al.). The mixture was refluxed for four and half an hour in the temperature range of 70 - 75 ^{0}C under a water bath. On cooling a precipitates was formed and was filtered, washed with ethanol, and diethyl ether, and dried in vacuum desiccators over anhydrous $CaCl_2$. The purity of the product was checked by thin-layer chromatography (TLC).

3.4.7. Synthesis of Copper(II) complex of L3 (7)

The ligand (**L3**) (2 mmol, 0.687 g) (20 mL) was dissolved in methanol (20 mL) in a 250 mL two-neck round bottom flask. After a half an hour of stirring, a methanol solution (20 mL) of $CuCl_2.2H_2O$ (1 mmol, 0.17 g) was added drop wise to the flask by 1:2 mole ratio (Ramachandran et al., 2013). Under constant stirring, a drop of 5% sodium hydroxide solution was added to the mixture. The reaction mixture was refluxed for five hours in the temperature range of 70 - 75 ^{o}C. Progress of the reaction was monitored by TLC and after the completion, the reaction was cooled to room temperature and then washed using ice-cold methanol to remove unreacted metal ions and ligand and then dried in a vacuum over anhydrous calcium chloride in a desiccator. Then the brown powder product obtained after drying was kept in a vial for further analysis and applications.

3.4.8. Synthesis of Nickel (II) complex of L3 (8)

To a 20 mL of methanolic solution of (1E)-1,4-bis(4-hydroxy-3-methoxybenzylidene) semicarbazone ligand (**L3**) (2 mmol, 0.687 g), 20 mL of warm methanol solution of nickel chloride, $NiCl_2.6H_2O$ (1 mmol, 0.24 g) was added dropwise under constant stirring by 1:2 mole ratio. Then after, a drop of sodium hydroxide (5% NaOH) was added under the constant string at room temperature to adjust the pH to be around 7 and refluxed for three hours between 70 - 75 ^{o}C under a water bath. The reaction progress was monitored by using TLC and after TLC showed a single spot confirming the completion of the reaction, the mixture was allowed to cool to room temperature overnight (Uddin et al., 2020). The resulting

reaction mixture was filtered, and washed with ice-cold methanol to remove unreacted species, where a gray powder was obtained.

3.5. Synthesis of heteroleptic Zn(II) and Cu(II) complexes from L1 and L4 ligands

The heteroleptic complexes of metal ions were synthesized according to the reported procedure with modification (Ejidike, Bamigboye, & Clayton, 2021; Ejidike, Bamigboye, Fadare, Adetunji, & Obaleye, 2022; Uddin et al., 2020).

3.5.1. Synthesis of heteroleptic Zn(II) complex (9), of L1 and L4

$ZnCl_2$ (1 mmol, 0.136 g) was dissolved in ethanol (20 mL). Then, by stirring magnetically with heating in an oil bath, 30 mL ethanol solution containing dehydrozingerone semicarbazone (**L1**) (1 mmol, 0.250 g) and *ortho*-phthalaldehyde disemicarbazone (**L4**) (1 mmol, 0.190 g) prepared separately were added together to the metal solution by 1:1:1 mole ratio. Then, the mixture of the metal salt solution and ligand solution was refluxed in the temperature range of 70 -75 °C for five hours under water bath until the color change observed. Then pH was adjusted around 7 by dropwise addition of 5% of NaOH solution with further stirring for 30 minutes. The progress of the reaction was monitored with TLC and after completion of the reaction; the mixture was cooled to room temperature. The reaction mixture was filtered then washed repeatedly using cold absolute methanol to remove unreacted metal ion and ligand. Finally the solid product obtained was recrystallized from ethanol and dried in vacuum desiccators over anhydrous $CaCl_2$ (Bamigboye, Ejidike, Awolope, Obaleye, & Ejimofor, 2021; Sarker, Hossen, Haque, Zamir, & Asraf, 2020). The dried, milky colored powder product was preserved in a clean vial for further analysis and use.

3.5.2. Synthesis of heteroleptic copper(II) complex (10), ML1L4 type

To a 20 mL ethanol solution of $CuCl_2.2H_2O$ (1 mmol, 0.17g), a mixture of 20 mL ethanol solution of [4-(4-hydroxy-3-methoxyphenyl)but-3-en-2-one]semicarbazone (**L1**) (1 mmol, 0.25 g) and 20 Ml solution of *O*-phthalaldehyde disemicarbazone (**L4**) (1 mmol, 0.19 g) ligands were added in 1:1:1 mole ratio while continuous stirring. Then, the reaction mixture was refluxed for five hours between 70 - 75 °C till the color of the reaction mixture was changed. Then pH of the reaction mixture was raised to around 7 by adding 5% NaOH

solution drop wise with constant stirring. Stirring was continued for another half an hour. The contents were cooled and the solid product of the mixed ligand complex was filtered, washed thoroughly first with ethanol, and finally dried under vacuum desiccators over anhydrous $CaCl_2$ (Pr Shirode, Agrawal, Jain, & Yeole, 2015). The reddish powdered product was obtained and kept in an airtight vial for further analysis.

3.6. Methods of Characterization of the ligands and their homoleptic and heteroleptic metal complexes

Several methods, conventional and modern, are available for the characterization of ligands and their complex compounds. The synthesized ligands and their corresponding metal complexes were distinctly colored and characterized by using physical and spectroscopic techniques.

3.6.1. Electronic spectral analysis of metal complexes

Electronic spectroscopy is the measurement of the wavelength and intensity of absorption of near ultraviolet and visible light by a sample. UV-Vis spectroscopy is usually applied to organic molecules and inorganic ions or complexes. The absorption of UV or visible radiation corresponds to the excitation of outer electrons. Coordination compounds can undergo one of three different forms of electronic transition. Many inorganic species show ligand-to-metal charge transfer (LMCT) transition and metal-to-ligand charge transfer (MLCT) transition (not as common as (LMCT). Electron transition probability in ligand field transition (d-d transition) is determined by the spin selection rule and the orbital (Laporte) selection rule (Jirjees et al.; Perkampus, 2013). The UV visible electronic spectra (200 – 800 nm) were recorded by UV-Vis-1800 series (Shimadzu) double beam spectrophotometer using DMSO solvent.

3.6.2. Molar conductivity

The molar conductivity values of the synthesized complexes in dimethyl sulfoxide solution (10^{-3} M) at room temperature were measured by direct reading using an electrical conductometer (AD8000). To know the oxidation number and stereochemistry of the central metal ion in coordination complexes, molar conductivity values are used in conjunction with electronic spectra (Greenfield, Julve, & Doyle, 2019).

3.6.3. Melting point determination

Thomas Hoover melting point device was used to determine the melting points of the synthesized compounds using the capillary tube method. The melting point of the synthesized organic ligands and their complexes were determined by introducing required amount of sample into a capillary tube, attached to the stem of a thermometer centered in a heating bath. The bath was heated slowly, and the temperatures at which melting begins and complete was recorded where the average melting point was calculated and recorded.

3.6.4. Infrared spectra analysis

FT-IR studies were conducted to determine the functional group present in the ligands and the metal complexes (Jirjees et al.; Mantsch & Chapman, 1996). In this study, the Infrared spectra were recorded on the Perkin Elmer model FTIR type 1650 spectrophotometer in the wave-number region of 4000 - 400 cm^{-1}. The spectra of the 10 mg solid samples were recorded as KBr pellets. The position of bands provides significant indications regarding the bonding sites of the ligand molecules when forming complexes with metal.

3.6.5. NMR spectra analysis

NMR spectroscopy enables us to record differences in magnetic properties of the various magnetic nuclei present and to deduce in large measure the position of these nuclei within the molecule. We can deduce how many different kinds of the chemical environment are there in the molecules and also which atom is present in neighboring groups (Dreyer, 1965).

^{13}C NMR spectra (A Bruker Avance 400 MHz NMR spectrometer): ^{13}C NMR spectra of the ligands were recorded in dry DMSO-d_6. All the ligands are non-hygroscopic, stable at room temperature, partially soluble in water, ethanol, and methanol but completely soluble in DMSO-d_6.

^{1}H NMR Spectra: The proton NMR spectra enable us to know different chemical and magnetic environments corresponding to a proton in molecules. The ^{1}H NMR spectra of the ligand were recorded in DMSO-d_6 solution. To obtain the ^{1}H NMR spectra for the complexes formed, 5 mg of samples were used. The NMR spectra obtained were able to provide detailed information about the chemical environment and structure of the ligands synthesized. The chemical shifts were recorded using tetramethylsilane (TMS) as an internal standard for ^{1}H NMR spectra analysis.

3.6.6. X-ray diffraction analysis

The particle nature of the complexes was studied using powder X-ray diffractometer (XRD), (Philips X-pert pro diffractometer, PW 1830 with Cu Kα radiation). The powder X-ray diffraction (PXRD) patterns of the synthesized metal complexes (**1 – 10**) were recorded using 80 mg of dried powdered samples. The data was recorded at 2θ ranging from 10 to 80.00° at lambda (λ) value at 1.54 A°.

3.6.7. Mass spectra analysis

The mass spectroscopic (MS) studies were performed in search of the molecular weights of the newly synthesized complexes. It enables us to know relative molecular masses with very high accuracy, from which exact molecular formulas can be deduced.(Duckworth, Barber, & Venkatasubramanian, 1986).

3.6.8. Thermogravimetric analyses

Thermogravimetric analysis (TGA) provides useful information about the thermal stability, thermal decomposition stages and fragmented parts of complexes. In addition, TGA analysis can verify the presence or absence of coordinated or lattice water molecules in complexes and comparison of the thermal stability of the ligands and their respective complexes. Thermal analyses of the synthesized metal complexes were recorded under N_2-atmosphere (20 mL/min) using a 10 mg dried sample using the SHIMADZU's DTG-60H thermal analyzer. The weight losses were recorded between 25 – 1200 °C with a heating rate of 10 ^{o}C/min.

3.7. The *In-silico* studies of the ligands and their transition metal complexes

3.7.1. *In-silico* molecular docking methodology

Recently, *in-silico* methods that include molecular docking analysis and online ADMET predictions (SwissADME, Pro-Tox II, and OSIRIS property explorer) facilitate the process of identifying the potential molecule (P Banerjee & Eckert, 2018; Garg et al., 2021; O Trott & Olson, 2009).

3.7.1.1. Preparation of ligands

The 2D structures of all synthesized compounds were drawn and each structure was analyzed using ChemDraw 16.0. The selected molecules were treated quantum mechanically by applying the DFT method using the Gaussian 09 program suite at the Becke-3-Lee-YangPar (B3LYP) level combined with the standard 6-31G (d,p) basis set. During the optimization procedure, all the parameters were set to obtain a stable structure with minimum energy. The global minimum energy of the title compound was determined from the structure optimization procedure. The 3D coordinates (.PDB) of each molecule were obtained through an optimized structure.

3.7.1.2. Preparation of macromolecules

The crystal structure of receptor molecules *S. aureus* Gyrase (PDB ID 2XCT) was downloaded from the protein data bank. The protein preparation was done using the reported standard protocol by removing the co-crystallized ligand, selected water molecules, and cofactors, the target protein file was prepared by leaving the associated residue with protein by using Auto Preparation of target protein file Auto Dock 4.2.6 (MGL tools 1.5.6).

3.7.1.3. AutoDock Vina analysis

Graphical user interface program Auto Dock 4.2.6 was used to set the grid box for docking simulations. The grid was set so that it surrounds the region of interest in the macromolecule. The docking algorithm provided with AutoDock Vina was used to search for the best-docked conformation between ligand and protein. During the docking process, a maximum of nine conformers were considered for each ligand. The conformations with the most favorable (least) free binding energy were selected for analyzing the interactions between the target receptor and ligands by Discovery studio visualizer and PyMOL. AutoDock Vina with the standard protocol used to dock the protein S. aureus Gyrase (PDB ID 2XCT) and synthesized ligands into the active site of proteins (O Trott & Olson, 2009),

3.7.1.4. *In-silico* pharmacokinetics and toxicity

Drug-likeness is a prediction that determines whether a particular pharmacological agent has properties consistent with being an orally active drug. The chemical structure of the compounds was converted to their canonical simplified molecular input line entry system (SMILE) and submitted to the SwissADME tool to estimate *in-silico* pharmacokinetic

parameters. SwissADME predictor provides information on the number of hydrogen donors, hydrogen acceptors and rotatable bonds, and the total polar surface area of a compound (P Banerjee & Eckert, 2018; Garg et al., 2021). The analyses of the compounds were compared with that of Trimethoprim drugs.

3.8. Methods of studying biological activities

The ligands and their metal complexes were tested for their antimicrobial activities, at the Department of Biology, School of Natural Science, Adama Science and Technology University.

3.8.1. Antibacterial activity analysis of the ligands and their complexes

The newly synthesized compounds was screened for their in vitro antibacterial activity against microbial strains of two Gram-positive bacteria (*Staphylococcus aureus* ATCC 25923 *and Streptococcus pyogenes ATCC 19615)* and two Gram-negative Bacteria (*Escherichia coli, ATCC 25922* and *Pseudomonas aeruginosa ATCC 27853*) at 100 and 200 μg/Ml concentratiosns by the zone of inhibition (disc diffusion method) using Trimethoprim as standard drugs (Manandhar, Luitel, & Dahal, 2019). The medium was prepared from molten nutrient agar (NA). The test compounds were dissolved in DMSO. Twenty-five milliliters of nutrient agar (NA) were placed in a petri dish. After solidification, the test bacteria were spread over the medium using a sprinter. The disc of Watman no 1 filter paper (blank paper disk with a diameter of 6 mm) saturated with the test compounds (at 100 and 200 μg/mL concentrations) were placed at equidistant placed from the center in the incubated petri dish (Balouiri, Sadiki, & Ibnsouda, 2016). Filter paper discs treated with DMSO severed as control and Trimethoprim was used as the standard drug. The Petri dishes were kept in the refrigerator for 24 hours for pre-diffusion and then incubated for 72 hours at 37 ^{o}C and the inhibition zone around each disk was measured with slipping calipers of the Clinical Laboratory Standers (Aliyu & Mohammed, 2009; Manandhar et al., 2019). The zone of inhibition was calculated in millimeters and compared with standard drugs. The % inhibition will be calculated by using the formula of equation 2 (O. A. El-Gammal et al., 2021).

$$\text{Inhibition zone (\%)} = \frac{(C-T)}{C} \, x \, 100 \qquad \ldots\ldots \qquad \mathbf{(2)}$$

where C = colony diameter (mm) of the control, T = colony diameter (mm) of the test plat.

3.8.2. Antioxidant activity test of the ligands and their metal complexes by the DPPH free radical scavenging activity assay

DPPH (2, 2-diphenyl-1-picrylhydrazyl) is the most common method that is widely used method of the antioxidant potential evaluation due to its ease, speed, and sensitivity. DPPH is a stable free radical that can abstract hydrogen from any molecule having the capacity to donate such an atom, leading to bleaching of the strong absorption at 517 nm. The reaction can, therefore, be conveniently used to examine the radical scavenging ability of the prospective molecule (S. Dutta, Padhye, Priyadarsini, & Newton, 2005). The scavenging reaction between (DPPH) and an antioxidant (H-A) can be written as:

$$\underset{\text{(Purple)}}{\text{(DPPH)}} + \text{(H-A)} \longrightarrow \underset{\text{(Yellow)}}{\text{DPPH-H}} + \text{(A)}$$

When antioxidants react with DPPH it is reduced to the DPPH-H and consequently, the absorbance changed from the DPPH radical to the DPPH-H form. The degree of change in color indicates the scavenging potential of the antioxidant compounds in terms of hydrogen-donating ability (El-Ghorab, Nauman, Anjum, Hussain, & Nadeem, 2010). The antioxidant activities of the synthesized semicarbazone and thiosemicarbazone derivative ligands and their homoleptic and heteroleptic metal complexes were evaluated using the DPPH free radical scavenging assay (S. Dutta et al., 2005). 200 µl of test sample solution (100 µg/mL) was added to 4 mL of 100 µM methanolic DPPH. After vortexing, the mixture was incubated for 20 minutes at room temperature and the absorbance at 517 nm was measured by using a spectrophotometer. Ascorbic acid (100 µg/mL) was used as standard. A blank was prepared without adding a standard or test compound. The lower absorbance of the reaction mixture indicates the higher free radical scavenging activity. The capability to scavenge the DPPH radical was calculated using the following equation (equation 3) (Singhal et al., 2011).

$$\text{DPPH scavenging activity (\%)} = \frac{\text{A control} - \text{A test}}{\text{A control}} \; x \; 100 \quad \ldots\ldots\ldots\ldots\ldots\ldots\ldots\ldots\ldots\ldots \; (3)$$

Where: A control is the absorbance of the control (without compound)

A test is an absorbance in the presence of the test compounds.

The antioxidant activity of the newly synthesized ligands and their homoleptic and heteroleptic ligand complexes were determined by comparing them with standard ascorbic acid. The IC_{50} parameter, which represents the concentration of the material in question

necessary to inhibit 50% of free radicals, was determined. Thus, a lower IC_{50} value indicates a greater ability to neutralize free radicals (Hazra, Biswas, & Mandal, 2008).

3.8.3. Antifungal activity screening

The antifungal activity of the synthesized ligands and their complexes were evaluated against *Aspergillums fumigates* and *Candida albicans* fungi species by the disc diffusion method (Sridhar, Duggirala, & Puchchakayala, 2014). Petri dishes were sterilized in a hot air oven at 180 ºC for 30 minutes and the Sterilized Potato-dextrose *agar (PDA)* medium was cooled to room temperature. 20 mL of the Potato-dextrose *agar (PDA)* was poured into Petri dishes and then allowed to solidify at room temperature. Then with a sterile cork borer 8 mm well was formed. 60 µL inoculums were poured into a petri dish and spreading was done with a sterilized L- shaped rod. 30 µl of 25, 50, and 100 mg/mL samples were transferred into the wells and the fungal culture Petri dishes were put into a refrigerator for diffusion and then transferred into an incubator for incubation at 27 °C for 72 hours. Fluconazole was used as the positive control 5 mg/mL and DMSO as a negative control to compare the antifungal effect. Then zone of inhibition was measured, in mm, after three days and the inhibition zone was calculated for each compound. All the procedures were done in triplicate and the mean values were taken. The growth inhibition percentage diameter was calculated using equation 4 (Abbas, Ahmad, Barkat, & Aslam, 2017).

$$\text{Percentage inhibition} = \frac{(C-T)}{(C)}\ x\ 100 \quad \ldots\ldots\ldots\ldots\ldots\ldots\ldots\ldots\ldots\ldots\ldots (4)$$

Where; C = diameter of the fungus colony in the control plates after three days and

T = diameter of the fungus colony in the tested plates at the same period

3.9. Statistical analyses

All the antibacterial, antifungal, and antioxidant data analyses generated by triplicate measurements were reported as mean plus standard deviation. The data were grouped and statistically evaluated with SPSS 16.0 software. The hypothesis testing method ANOVA followed by the 'least significant difference' test was used. A value of $P < 0.05$ was considered to indicate statistical significance. All results were expressed as mean ± Standard error m`ean (S.E.M) (Hesamian, 2016; D. K. Lee, In, & Lee, 2015).

4. RESULTS AND DISCUSSION

4.1. Synthesis of ligands and their homoleptic and heteroleptic metal complexes

The synthesis of semicarbazone and thiosemicarbazone derivative ligands and their homoleptic and heteroleptic complexes were successfully done following the established procedure presented in sections 3.3 and 3.4 respectively with the necessary reaction conditions. The semicarbazide used as the starting materials for the synthesis of the ligands exists as stable form in semicarbazide hydrochloride, which can be released from its salt form when the reagent CH_3COONa was added in the synthesis process. The acetic acid (CH_3COOH) produced during the reaction, protonates the carbonyl oxygen of dehydrozingerone and *ortho*-phthalaldehyde and activates the C = O carbon favorable to nucleophilic reaction. Then, the semicarbazone and thiosemicarbazone derivative ligands were synthesized by reaction of the amine group of semicarbazide/thiosemicarbazide with ketone and aldehyde functional group forming imine (-C = N-) containing derivatives as indicated in the general reaction mechanisms described by Schemes 8 - 11. The semicarbazone derivative ligands, [4-(4-hydroxy-3-methoxyphenyl)but-3-en-2-one] semicarbazone (**L1)** and (4-(4-hydroxy-3-methoxyphenyl)but-3-en-2-one)thiosemicarbazone (**L2)** were derived from Ginger (traditional medicinal plant) composed of a compound dehydrozingerone and the third ligand, (1E)-1,4-bis(4-hydroxy-3-methoxybenzylidene) semicarbazone (**L3**) was prepared from vanillin (major fragmented part of dehydrozingerone) in good yields as shown in Table 1. The homoleptic metal complexes (**1-8**) were synthesized in a 1:2 metal ion to ligand (**M: 2L**) mole ratio from their corresponding ligands. The other ligand *ortho*-phthalaldehyde-disemicarbazone (**L4**) was synthesized from the starting raw material *ortho*-phthaldehyde which is the latest synthetic bioactive compound (Simons et al., 2000). Then, the heteroleptic metal complexes (complex **9** and **10**) were synthesized from **L1** and **L4** in 1:1:1 ligands to metal ion (L1: M: L4) mole ratio.

The overall physicochemical properties and stoichiometry proposed for the compounds were presented in Table 1. The analytical data of the structure of the ligands and their complexes are in good agreement with the proposed empirical formula.

Table 1. Physicochemical properties of ligands and their metal compounds

Compound	Empirical Formula	Mwt.	Color	Yield (%)	Melting point (°C)	Conductivity (Λ_m)($\eta^{-1}cm^2\ mol^{-1}$)
L1	$C_{12}H_{15}N_3O_3$	249.28	Brown	78	171.5	-
L2	$C_{12}H_{15}N_3O_2S$	265.35	Yellow	71	119	-
L3	$C_{17}H_{17}N_3O_5$	343.34	Orange	85	179	-
L4	$C_{10}H_{12}N_6O_2$	248.24	Cloudy	75	241	-
$[Zn(L1)_2(Cl)_2]$ **(1)**	$C_{24}H_{30}N_6O_6\ ZnCl_2$	634.95	Green	69	285-290	16
$[Cu(L1)_2(Cl)_2]$ (**2**)	$C_{24}H_{30}N_6O_6\ CuCl_2$	633.06	Red	62	250-260	18
$[Ni(L1)_2Cl]$ **(3)**	$C_{24}H_{30}N_6O_6NiCl$	592.68	Brown	58	255-265	6,8
$[Zn(L2)_2]$ (**4**)	$C_{24}H_{30}N_6O_4S_2\ Zn$	596.09	Milky	62	>300	12.4
$[Cu(L2)_2$ (**5**)	$C_{24}H_{30}N_6O_4S_2Cu$	593.89	Brown	57	>300	14
$[Zn(L3)_2].2H_2O$ (**6**)	$C_{34}H_{36}ZnN_6O_{12}$	784.17	Milky	56	>298	4.5
$[Cu(L3)_2].3H_2O$ **(7)**	$C_{34}H_{38}CuN_6O_{13}$	801.18	Brown	62	270-278	14.8
$[Ni(L3)_2].4H_2O$ **(8)**	$C_{34}H_{40}NiN_6O_{14}$	814.17	Gray	68	>300	9.6
[Zn(L1)(L4)] (**9**)	$C_{22}H_{25}ZnN_9O_5$	560.86	Milky	58.5	>300	5.4
[Cu(L1)(L4)] (**10**)	$C_{22}H_{25}CuN_9O_5$	558.13	Red	54	>300	16.4

Note: **L1** = ligand 1**, L2** = ligand 2**, L3** = ligand 3 and **L4** = ligand 4

Solubility tests of all the synthesized ligands and complexes were done to determine the suitable solvents that could be utilized for recrystallization, spectroscopic measurements, and bioactivity evaluations. As shown in Table 2, the synthesized ligands and their complexes exhibited from low to high solubility in common organic solvents. The **L1** and **L4** were soluble in organic polar solvents, such as methanol, ethanol, and chloroform but partially soluble in water, while **L2** and **L3** had lesser solubility in these solvents at room temperature. **L3** was partially soluble in chloroform and highly soluble in dimethyl sulfoxide (DMSO).

The homoleptic zinc (II), copper (II), and nickel (II) complexes synthesized from **L1**, **L2**, and **L3** were not soluble in common polar solvents such as water, ethanol, and methanol while the heteroleptic copper (II) and zinc (II) complexes synthesized from **L1** and **L4** were partially soluble in the aforementioned solvents. But all the synthesized ligands and complexes were completely soluble in DMSO. The solubility test showed that the solid compounds are all insoluble in water confirming that they are non-polar compounds which is the favorable properties for penetration into nonpolar bacterial cell membrane as one mechanism of action. The compounds were stored for months without any significant changes in their appearance.

Table 2. The solubility test of the ligands (**L1 - L4**) and their metal complexes (**1-10**)

Compounds	Solubility				
	H_2O	**EtOH**	**MeOH**	**$CHCl_3$**	**DMSO**
L1	+	++	++	++	+++
L2	-	+	+	+	+++
L3	+	+	+	-	+++
L4	+	++	++	++	+++
Complex **1**	-	-	-	+	+++
Complex **2**	-	+	+	++	+++
Complex **3**	-	-	+	-	+++
Complex **4**	-	-	+	++	+++
Complex **5**	-	-	+	+	+++
Complex **6**	-	-	+	+	+++
Complex **7**	-	-	+	++	+++
Complex **8**	-	+	+	+	+
Complex **9**	-	++	+	+	++
Complex **10**	-	++	+	+	++

Note:- insoluble, + partially soluble, ++ soluble, +++ highly soluble

The overall synthesis of the ligands and their respective metal complexes were described by the reaction mechanisms which were represented by the schemes 8 - 18.

4.1.1. Ligand 1 (L1)

The [4-(4-hydroxy-3-methoxyphenyl)but-3-en-2-one]semicarbazone (**L1**) ligand was synthesized by reacting the amine group of semicarbazide with ketone (C=O) functional group of dehydrozingerone in methanol solution forming imine (-C=N-) containing derivative as indicated by the mechanism in scheme 8. The semicarbazide base released from semicarbazide hydrochloride when the reagent sodium acetate (CH_3COONa) in the presence of HCl was introduced during the time of synthesis process. The formed acetic acid is able to protonate the oxygen of carbonyl carbon of dehydrozingerone to activate the C=O carbon for nucleophilic attack (Holm, Everett Jr, & Chakravorty, 1966).

The proposed synthesis route and reaction mechanism steps of the **L1** ligand are presented in scheme 8.

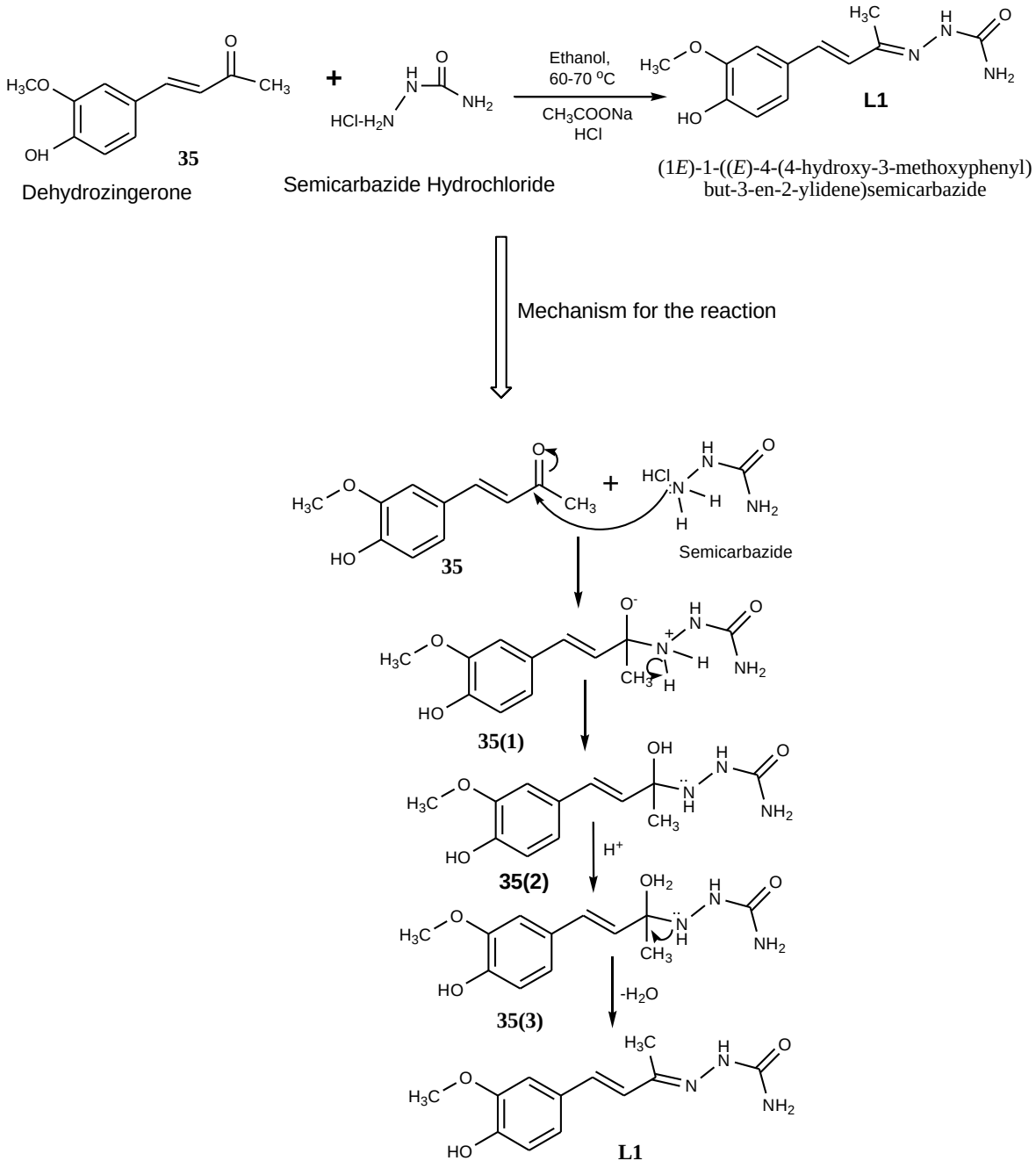

Scheme 8. Synthesis route and reaction mechanism of [4-(4-hydroxy-3- methoxyphenyl)but-3-en-2-one]semicarbazone (**L1**) (Proulx et al., 2011).

The ligand **(L1)**: $\mathbf{C_{12}H_{15}N_3O_3}$; Yield 78%; brown powder; melting point = 170 - 172 °C; *R*f = 0.68 (EtOAc: methanol = 9:1); UV–Vis λ_{max} (MeOH): 209, 333 nm; Elemental analysis: Calculated (%); C, 57.81; H, 6.07; N, 16.92. Found %; C, 57.70; H, 5.82; N, 16.73. FT-IR (υ cm^{-1}, KBr (pellet)): 3578 ν(O-H str.), 3485 - 3204 ν(N-H str.), 2929 ν(aromatic C-H str.),

2852 ν(aliphatic C-H str.), 1696 ν(C= O str.), 1592 ν(imine C = N str.), 1521 ν(aromatic C=C str.), 1437 ν(phenolic O-H bend), 1256 ν(asymmetric C-O-C str.), 1027 ν(symmetric N-N str.) (Figure 17); ^{1}H NMR (400 MHz, DMSO-d_6), δ/ppm: 9.35 (s, 1H, N–NH), 9.28 (s, 1H, O–H), 6.93 (d, *J* = 16.6 Hz, 1H, Ph–HC = CH-), 6.71 (d, *J* = 16.6 Hz, 1H, Ph–HC = CH-), 7.11 (s, 1H, ArH), 6.75–6.83 (d, 2H, ArH), 6.44 (s, 2H, NH_2), 3.80 (s, 3H, OCH_3), 2.01 (s, 3H, CH_3) (Appendix 1); ^{13}C NMR (101 MHz, DMSO–d_6) δC = 157.7 (C-12), 148.29 (C-11), 147.46 (C-10), 146.67 (C-9) 132.23 (C-8), 128.59 (C-7), 127.01 (C-6), 120.85 (C-5), 116.07 (C-4), 110.22 (C-3), 55.97 (C-2), 11.97 (C-1) (Appendix 2); ^{13}C-Dept (101 MHz, DMSO–d_6) δC = 132.24 (C-8), 127.01 (C-7), 120.26 (C-5), 116.10 (C-4), 110.24 (C-3), 55.99 (C-2), 11.98 (C-1) (Appendix 3).

4.1.2. Ligand 2 (L2)

The (4-(4-hydroxy-3-methoxyphenyl)but-3-en-2-one)thiosemicarbazone ligand (**L2**) was prepared by reacting one mole of dihydrozingerone with equivalent mole amounts of thiosemicarbazide. Thiosemicarbazones are a class of organic compounds obtained experimentally by condensation of thiosemicarbazide with aldehydes or ketones functional group (Fathy et al., 2022). Accordingly, the ligand (**L2**) was synthesized in high yield via the addition of amine group of thiosemicarbazide with ketone (C=O) functional group of dehydrozingerone forming imine (-C=N-) containing derivative as indicated by the reaction mechanism in scheme 9.

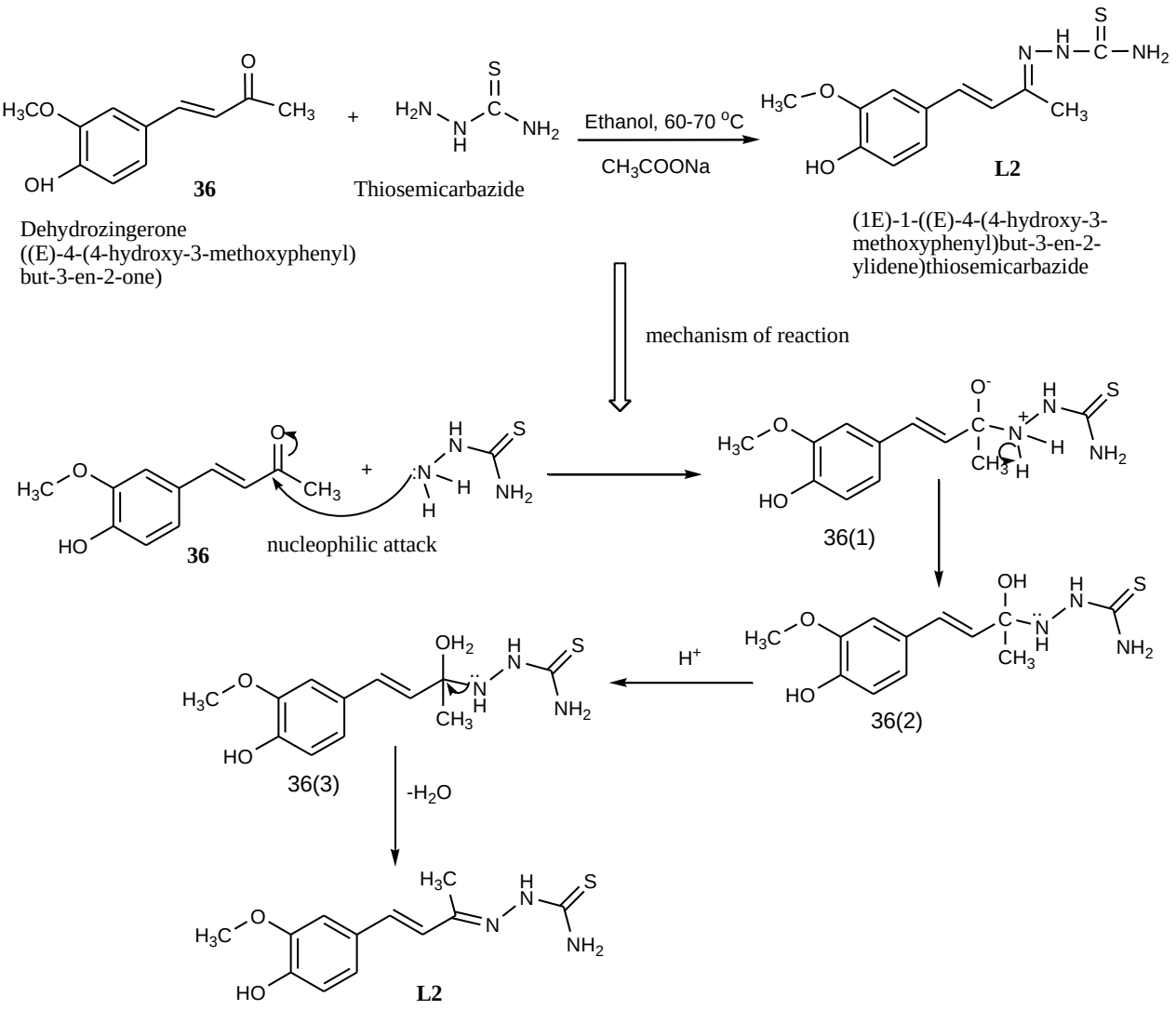

Scheme 9. Synthesis and reaction mechanism of (4-(4-hydroxy-3-methoxyphenyl) but-3-en-2-one)thiosemicarbazone (L2)

Ligand **(L2)**: $C_{12}H_{15}N_3O_2S$; yellowish-orange powder; Yield: 71 %; melting point: 118 - 120 ^{o}C, *R*f = 0.34 (EtOAc: methanol = 9:1), Elemental analysis: Calculated (%); C, 54.27; H, 5.65; N, 15.82. Found %; C, 53.91; H, 5.54; N, 16.10. UV-Vis λ_{max} (MeOH): 350 nm ($n\rightarrow\pi^*$) (Appendix 16); FT-IR (υ cm^{-1}, KBr (pellet)): 3451 ν(O-H str.), 3309.8 ν(N-H str.), 2929 ν(aromatic C-H str.), 2852 ν(aliphatic C-H str.), 1745 ν(aromaticity), 1611 ν(C=N str.), 1513 ν(aromatic C=C str.), 1273 ν(C=S str.), 1016 ν(symmetric N-N str.) (Figure 9); ^{1}H NMR (400 MHz, DMSO-d_6) δ/ppm, 10.20 (s, 1H,NH), 9.35 (s, 1H, OH), 8.21 (s, 1H, ArH), 7.77 (d, *J* = 16.6 Hz, 1H, Ph-**H**C=CH-), 7.13 (d, *J* = 16.6 Hz, 1H, Ph-HC=C**H**-), 6.99 (d, *J* = 8.1 Hz, 1H, ArH), 6.78 (d, *J* = 8.1 Hz, 1H, ArH), 6.72 (s, 2H, NH_2), 3.82 (s, 3H, OCH_3), 2.11 (s, 3H, CH_3); ^{13}C NMR (101 MHz, DMSO-d_6) δc = 178.89 (C-12), 149.94 (C-11), 148.31 (C-10),

148.25 (C-9), 134.65 (C-8), 128.31 (C-7), 126.35 (C-6), 121.26 (C-5), 116.10 (C-4), 110.38 (C-3), 55.99 (C-2), 12.61 (C-1); ^{13}C-Dept (101 MHz, DMSO-d_6) δ_C = 134.65 (C-8), 126.35 (C-7), 121.26 (C-5), 116.10 (C-4), 110.39 (C-3), 56.00 (C-2), 12.61 (C-1) (Appendix 4-6).

4.1.3. Ligand 3 (L3)

The synthesis of vanillin based semicarbazone ligand (L3) was achieved with good yield and relatively with high purity. The synthesis scheme and proposed mechanisms of the (**L3**) are presented in scheme 10.

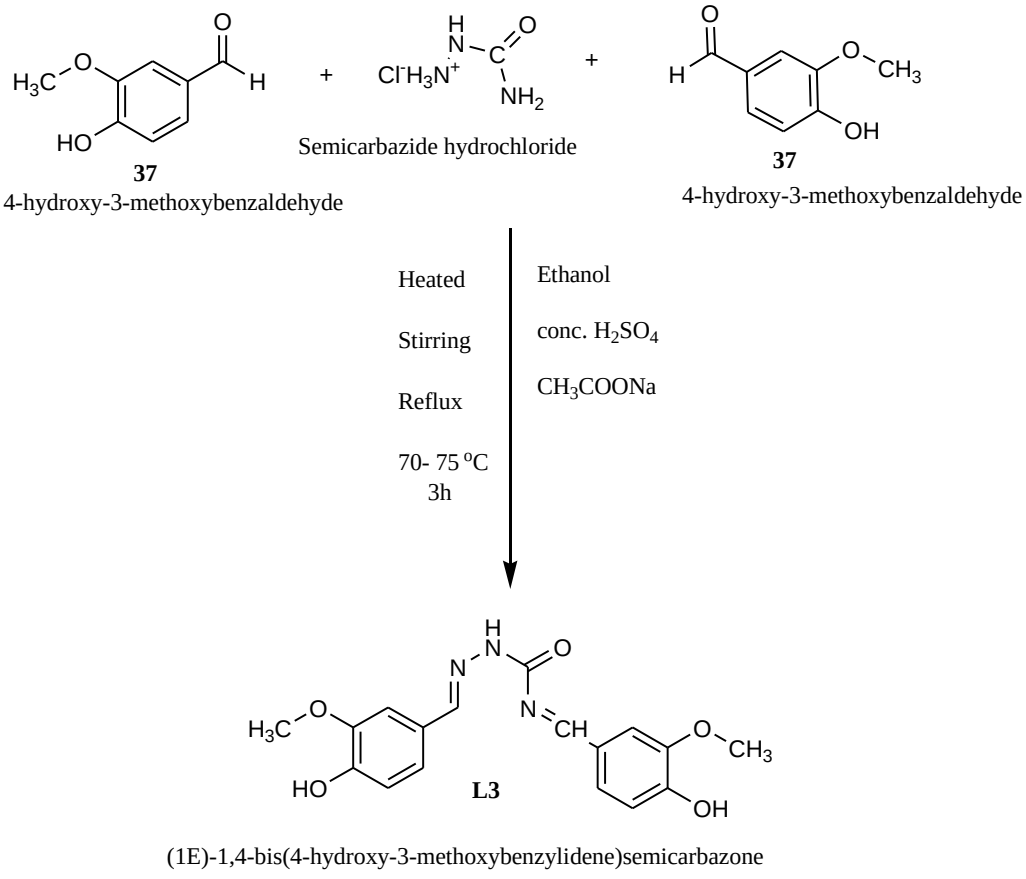

Scheme 10. Synthesis pathway of (1E)-1,4-bis(4-hydroxy-3-methoxybenzylidene) semicarbazide ligand (L3)

Ligand (**L3**), $C_{17}H_{17}N_3O_5$: Yield: 85%, orange powder, melting point = 178 - 180 °C, Rf = 0.6 (EtOAc: methanol = 9:1). Elemental analysis of $C_{17}H_{17}N_3O_5$ (Mwt. = 343.34 g/mol): Calc. %; C = 59.47; N = 12.24, O = 23.30, H = 4.99. UV-Vis λ_{max} (DMSO): 294 nm ($\pi \rightarrow \pi^*$) & 318 nm ($n \rightarrow \pi^*$) (Appendix 19). FTIR (υ cm^{-1}, KBr (pellet)): 3447 υ(O-H str.), 3293 υ(N-H str.), 3069 υ(arom C-H str.), 2929 υ(aliph C-H str.), 1643 ν(C=O str.), 1593 ν(C=N str.), 1506 ν(arom C=C str.), 1033 ν(C-N str.) (Figure 24). ^{1}H NMR (DMSO-d_6, ppm, 400 MHz); δ = 10.08 (H_7), 8.59 (H_6), 7.74 (H_5), 7.38 (H_4), 6.97 (H_3), 6.78 (H_2) and 3.83 (H_1)

(Appendix 5). ^{13}C NMR (ppm, 101 MHz, DMSO-d_6) δ_c = 157.48 (C-8), 150.42 (C-7), 140.46 (C-6), 126.75 (C-5), 121.54 (C-4), 115.65 (C-3), 109.39 (C-2) and 56.13 (C-1) and ^{13}C-Dept-135 (ppm, DMSO-d_6, 101 MHz) δ_c = 140.47 (C-6), 121.54 (C-4), 115.65 (C-3), 109.40 (C-2) and 56.14 (C-10 (Appendix 6 and **7**).

4.1.4. Ligand (L4)

The ortho-phthaladehyde-disemicarbazone ligand (**L4**) was synthesized by reacting one mole of ortho-phthaladehyde (OPA) with two moles of semicarbazide. The two moles of semicarbazide react with the two aldehyde functional groups through the condensation process by the fact that semicarbazones are organic compounds obtained experimentally by condensation of semicarbazide with aldehydes or ketones functional group. The two aldehydes (dialdehyde) functional groups that exist on OPA are so sensitive to react with primary amine containing groups (Cabrera-Martinez et al., 2002). The schematic representation for the synthesis of the (**L4**) is presented in scheme 11.

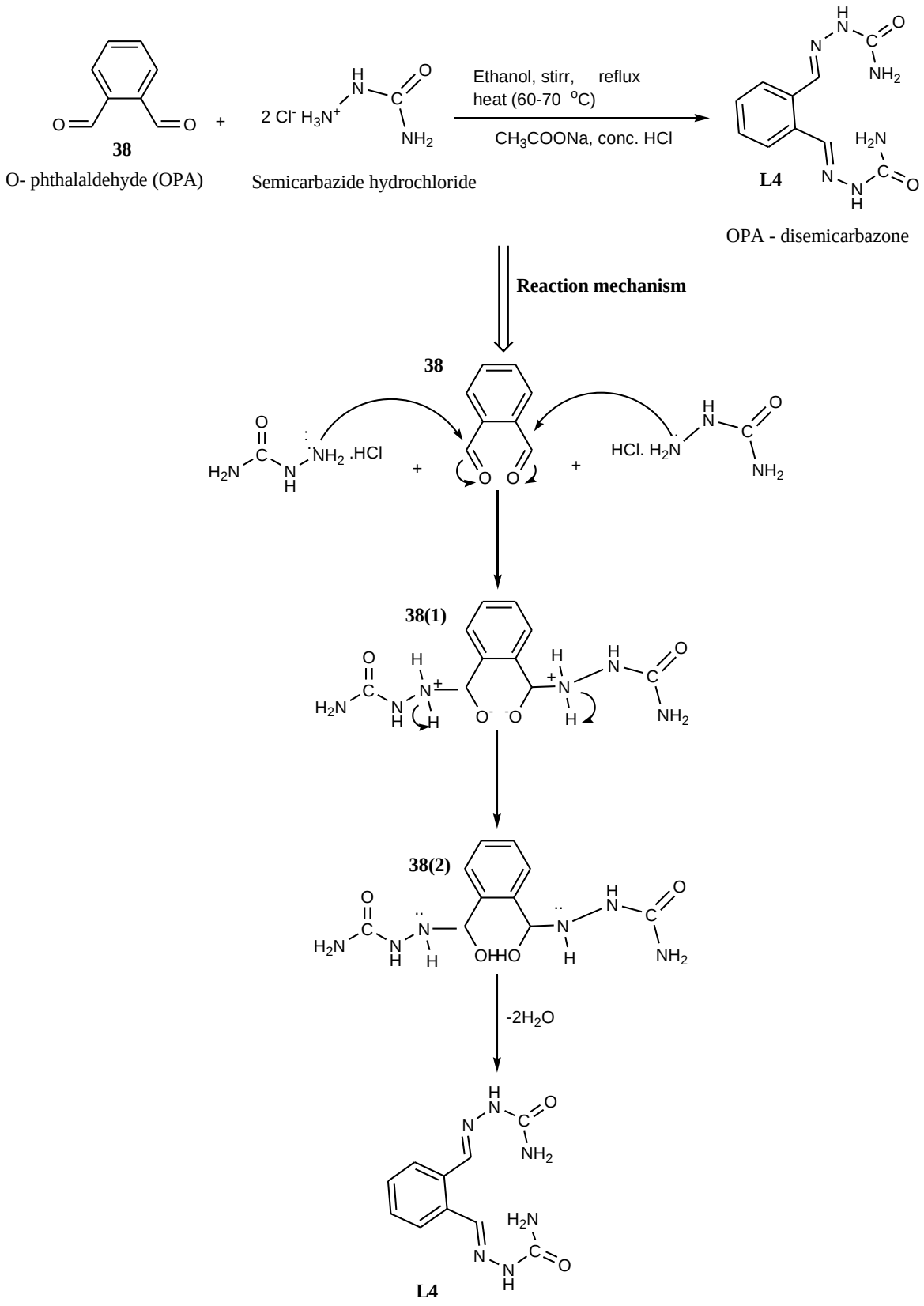

Scheme 11. Synthesis pathway of ortho-phtatahaldehydedisemicarbazide ligand (**L4**)

The ligand **(L4)**; $C_{10}H_{12}N_6O_2$: Yield: 75 %, cloudy powder, melting point = 240 - 242 °C, Rf = 0.41 (EtOAc: methanol = 7:3). Elemental analysis for $C_{10}H_{12}N_6O_2$ (Mwt. = 248.24 g/mol), Calc. %; C = 48.38; H = 4.87, N = 33.83, found; C = 47.86, H = 4.64, N = 34.02. UV–Vis λ_{max} (DMSO):282 & 314.5 (Appendix 22). FT-IR (υ cm^{-1}, KBr (pellet)): 3372 υ(1^o N-H str.), 3203.4 υ(N-H str.), 3055.4 υ(arom C-H str.), 2921 υ(aliph C-H str.), 1688.5 ν(C=O str.), 1583 ν(C=N str.), 1505.4 ν(arom C=C str.), 1088.6 ν(C-N str.) (Figure 28). ^{1}H NMR (DMSO-d_6, ppm, 400 MHz); δ = 10.42 (s, 2H, H_5), 8.33 (d, *J* = 8.6 Hz, 2H, H_4), 7.87 (dd, 8.6, 9.4 Hz, 2H, H_3), 7.37 (s, 2H, H_2), 6.50 (s, 4H, H_1) (Appendix 10). ^{13}C NMR (ppm, 101 MHz, DMSO-d_6) δ_c = 157.2 (C-5), 138.8 (C-4), 132.4(C-3), 129.3 (C-2), 128.3(C-1). ^{13}C-Dept-135 (ppm, DMSO-d_6, 101 MHz) δ_c = 138.9 (C-4), 129.3 (C-2), 128.3 (C-1) (Appendix 11).

4.1.5. Complex 1

The Zn(II) complex of [4-(4-hydroxy-3-methoxyphenyl)but-3-en-2-one]semicarbazone ligand (**L1**) was prepared according to the procedure indicated in chapter three. The scheme of the synthesis of complex **1** is shown in scheme 12.

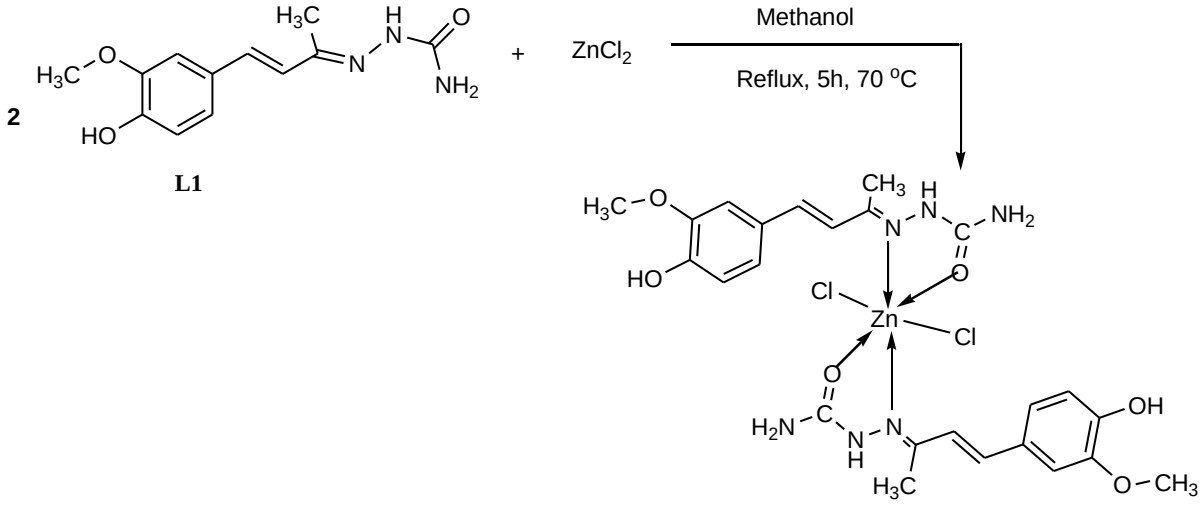

Scheme 12. Proposed synthesis pathway and structure of complex **1**

Zinc (II) complex; $[Zn(L1)_2(Cl)_2]$. Yield: 68%; greenish-white powder, mp. 285 - 290 ^{o}C, Elemental composition: Calc. %; C, 45.36; H, 4.72; N, 13.23. Found %; C, 45.18; H, 4.33; N, 13.15; FT-IR (υ cm^{-1}, KBr (pellet)): 3378 υ(O-H str.), 3267-3155 υ(N-H str.), 2929 υ(aromatic C-H str.), 2852 υ(aliphatic C-H str.), 1653 υ(C=O str.), 1583 υ(C=N str.), 1506 υ(Ar-C=C str.), 1425 υ(phenolic O-H bend.), 1278 υ(asymmetry C-O-C str.), 1028 υ(symmetry N-N str.), 538 υ(M-N str.), 443 υ(M-O str.) (Figure 18). M/z = 634.11

$[C_{24}H_{30}N_6O_6ZnCl_2]^+$ (Appendix 26). UV-Vis λ_{max} (DMSO): 234, 266, and 332 nm (Appendix 13). TGA mass loss 11 % (225 - 280 °C, 1st step, calc.2 × Cl = 71 g) and 36.6% (280 - 449 °C, 2nd step, calc. one dehydrozingerone = 191.12 g and 36.7% (450 - 730 °C), 3rd step, loss of another **L1** moiety) (Figure 41 and 42). Molar conductance (λ) = 16 $\Omega^{-1}cm^2mol^{-1}$.

4.1.6. Complex 2

The Cu(II) complex of L1 was obtained by a reaction between $CuCl_2.2H_2O$ and L1 in a 1:2 mole ratio respectively**.** The schematic representation for the synthesis of complex 2 is presented in scheme 13.

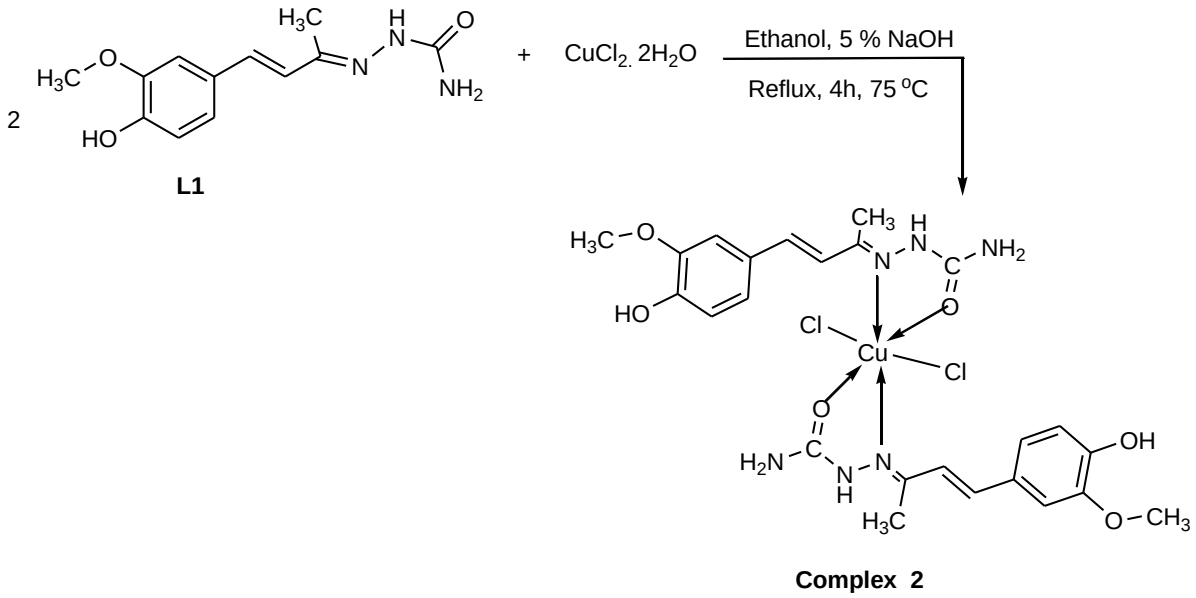

Scheme 13. Proposed synthesis pathway and structures of complex **2**

Copper complex (**2**); $[Cu(L_1)_2(Cl)_2]$. Yield: 62 %; reddish powder, mp. = 250-260 °C; Elemental analysis, Calc. %; C, 45.50; H, 4.74; N, 13.26. Found %; C, 45.23; H, 4.71; N, 13.19; FT-IR (υ cm^{-1}, KBr (pellet)): 3335 υ(O-H str.), 2929 υ(aromatic C–H str.), 2852 υ(aliphatic C–H str.), 1668 υ(C=O str.), 1583 υ(C=N str.), 1505 υ(aromatic C=C str.), 1460 υ(phenolic O-H bend.), 1251 υ(asy C-O-C str.), 1043 υ(sym N-N str.), 546 υ(M-N), 409 υ(M-O) (Figure 19). M/z = 631.96 $[C_{24}H_{30}Cl_2CuN_6O_6]$ (Appendix 27). UV-Vis λ_{max} (DMSO): 211nm, 264 nm and 333 nm (Appendix 14); TGA mass loss 11 % (160 - 252 °C, 1st step, calc. 2 × Cl = 71 g) and 36.7 % (253 - 87 °C, 2 step, loss of $C_{12}H_{15}N_3O_2$) moiety, mass loss of 39% (495-714 °C, 3rd step , loss of one L1) (Figure 43); molar conductance (λ_m) =18 $\Omega^{-1}cm^2mol^{-1}$.

4.1.7. Complex 3

The reaction of semicarbazone ligand **L1** with $NiCl_2.6H_2O$ results in the formation of $[Ni(L_1)_2Cl]$ complex. The schematic representation for the synthesis of this complex is presented in scheme 14.

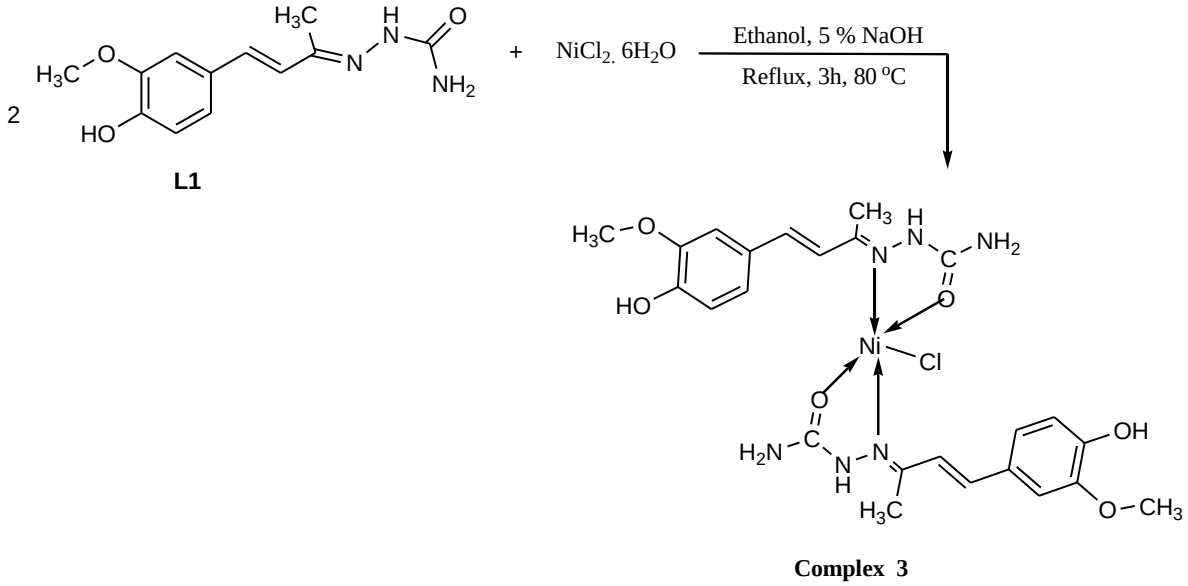

Scheme 14. Proposed synthesis pathway and structure of complex 3

Complex **3** has a proposed chemical formula $[Ni(L_1)_2Cl]$, which is brown colored powder-crystal type solid. Yield: 58 %, mp. 255 - 265 ^oC; Elemental analysis, Calc. %; C, 48.64; H, 5.10; N, 14.18. Found %; C, 48.38; H, 4.91; N, 14.16; FT-IR (υ cm^{-1}, KBr (pellet)): 3578 υ(O-H str.), 3127-3155 υ(N-H str.), 2929 υ(aromatic C-H str.), 2852 υ(aliphatic C-H str.), 1660 υ(C=O str.), 1582 υ(C=N str.), 1505 υ(Ar-C=C str.), 1405 υ(phenolic O-H bend.), 1250 υ(asymmetry C-O-C str.), 1050 υ(symmetry N-N str.), 503 υ(M-N), 390 υ(M-O) (Figure 20). M/z = 591.14 $[C_{24}H_{30}ClN_6]^+$ (Mwt = 592.68 g/mol) (appendix 28). UV-Vis: λ_{max} (DMSO) = 275 nm, and 370 nm. TGA mass loss 5.9 % (130 - 256 °C), 1st step, calc.1 × Cl = 35.37g) and 52 % (260 - 760 °C), 2nd step, calc. one dehydrozingerone part = 191.12 g). Molar conductance (λ) = 6.8 $ɲ^{-1}cm^2mol^{-1}$.

4.1.8. Complex 4

The zinc (II) complex of **L2** was synthesized in 1:2 ratio of zinc chloride salt ($ZnCl_2$) to ligand **L2** as presented in Scheme 15. The synthesis was done by mixing both reagents in ethanol and allowed to undergo a reaction through the refluxing process.

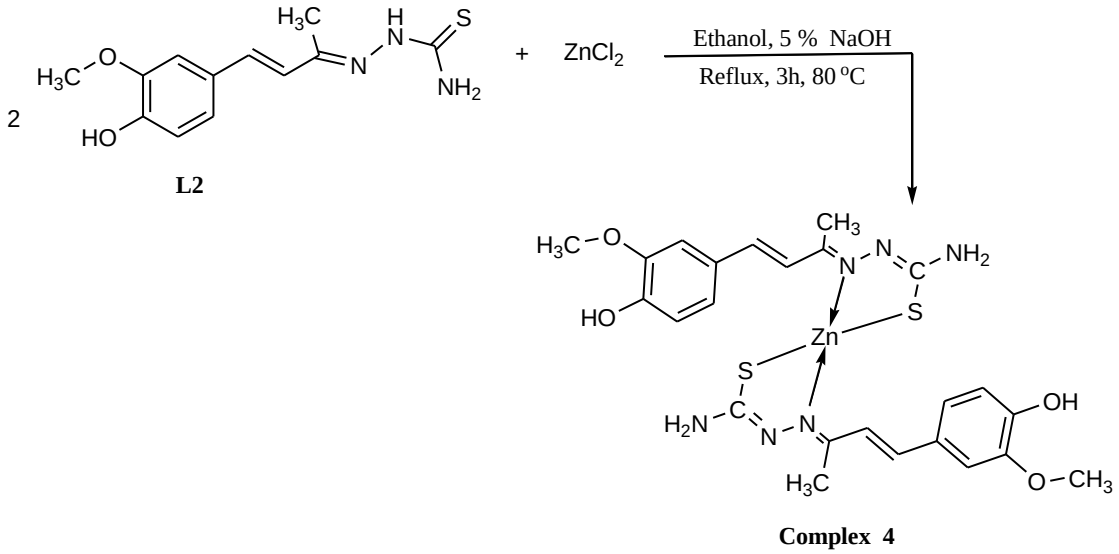

Scheme 15. Proposed synthesis and structure of **[Zn(L2)$_2$]** complex **4**

Complex **4** has a formula of [Zn(L_2)$_2$] which is a white powdered solid. Yield: 62%, mp. > 300 ^{o}C, Elemental compositions of Calc. %; C, 48.32; H, 5.03; N, 14.09, found %; C, 47.98; H, 4.87; N, 13.86, FT-IR (υ cm^{-1}, KBr (pellet)): 3354 υ(O-H str.), 3273, 3185 υ(N-H str.), 2929 υ(aromatic C-H str.), 2838 υ(aliphatic C-H str.), 1627 υ(C=N str.), 1529 υ(aromatic C=C str.), 1413 υ(phenolic O-H bend.), 1364 υ(asy C-O-C str.), 1245 υ(C-S str.), 1023 υ(sym N-N str.), 566 υ(M-N), 434 υ(M-S) (Figure 22). M/z = 598.09 $[C_{24}H_{28}N_6O_4S_2Zn]^+$ (Appendix 29). UV-Vis λ_{max} (DMSO): 415 nm. TGA mass loss 32.05% (261.7 - 380 ^{o}C, 1 step, calc.1 × DZ = 191.34 g) and 56.8% (634 -764.7 ^{o}C, 1 x DZ + thiol = 339.76 g); molar conductance (λ_m) = 12.4 $\Omega^{-1}cm^2mol^{-1}$.

4.1.9. Complex 5

Complex **5** was synthesized in absolute ethanol in the ratio of $CuCl_2.2H_2O$ to ligand (**L2**) by 1:2 mole ratios after three hours of stirring through refluxing technique between 70 ^{o}C - 75 ^{o}C temperatures. The schematic representation for the synthesis of the complex is presented in scheme 16.

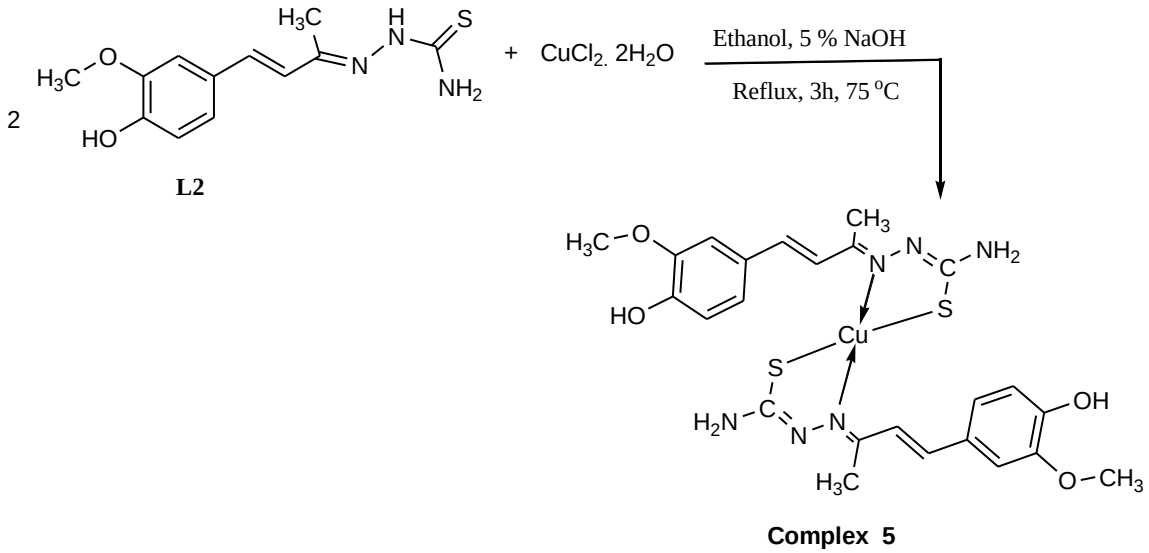

Scheme 16. Proposed synthesis pathway and structure of complex **5**

The synthesized copper(II) complex (**5**) has a molecular formula of $[Cu(L_2)_2]$, brown powder with a yield of 57 %, and starts to decompose above 300 ^oC temperature. Elemental composition: Calc. %; C, 45.70; H, 5.39; N, 13.33 and found %; C, 45.68; H, 5.27; N, 13.08. FT-IR (υ cm^{-1}, KBr (pellet)): 3413 υ(O-H str.), 3240, 3155 υ(N-H str.), 3037, 2928 υ(aromatic C–H str.), 1589 υ(C=N str.), 1521 υ(aromatic C=C str.), 1413 υ(phenolic O-H bend.), 1265 υ(C-S str.), 1029 υ(sym N-N str.), 533 υ(M-N str.), 420 υ(M-S str.) (Figure 23). M/z = 593.11 $[C_{24}H_{28}CuN_6O_4S_2]^+$ (Appendix 30). UV-Vis: λ_{max} (DMSO) = 408 nm, 452 nm and 511 nm (Appendix 18); TGA mass loss 39.5 % (230 - 343 ^oC, 1st step, corresponds to a loss of L1) and 39.5 % (470 - 736 ^oC, 2nd step, calc. 1 x DZ= 192.21 g or loss of the other coordinated L2 molecule) (Figure 48); molar conductance (λ_m) = 14.5 $\Omega^{-1}cm^2mol^{-1}$.

4.1.10. Complexes 6, 7 and 8

The overall synthesis of the complexes of zinc (II), copper (II), and nickel (II) metals with the ligand L3 followed the same procedure. The metal salts were reacted with L3 in a 1:2 mole ratio and the products obtained were very pure in good yield. The schematic representations of the synthesis of complexes **6, 7,** and **8** were shown in scheme 17.

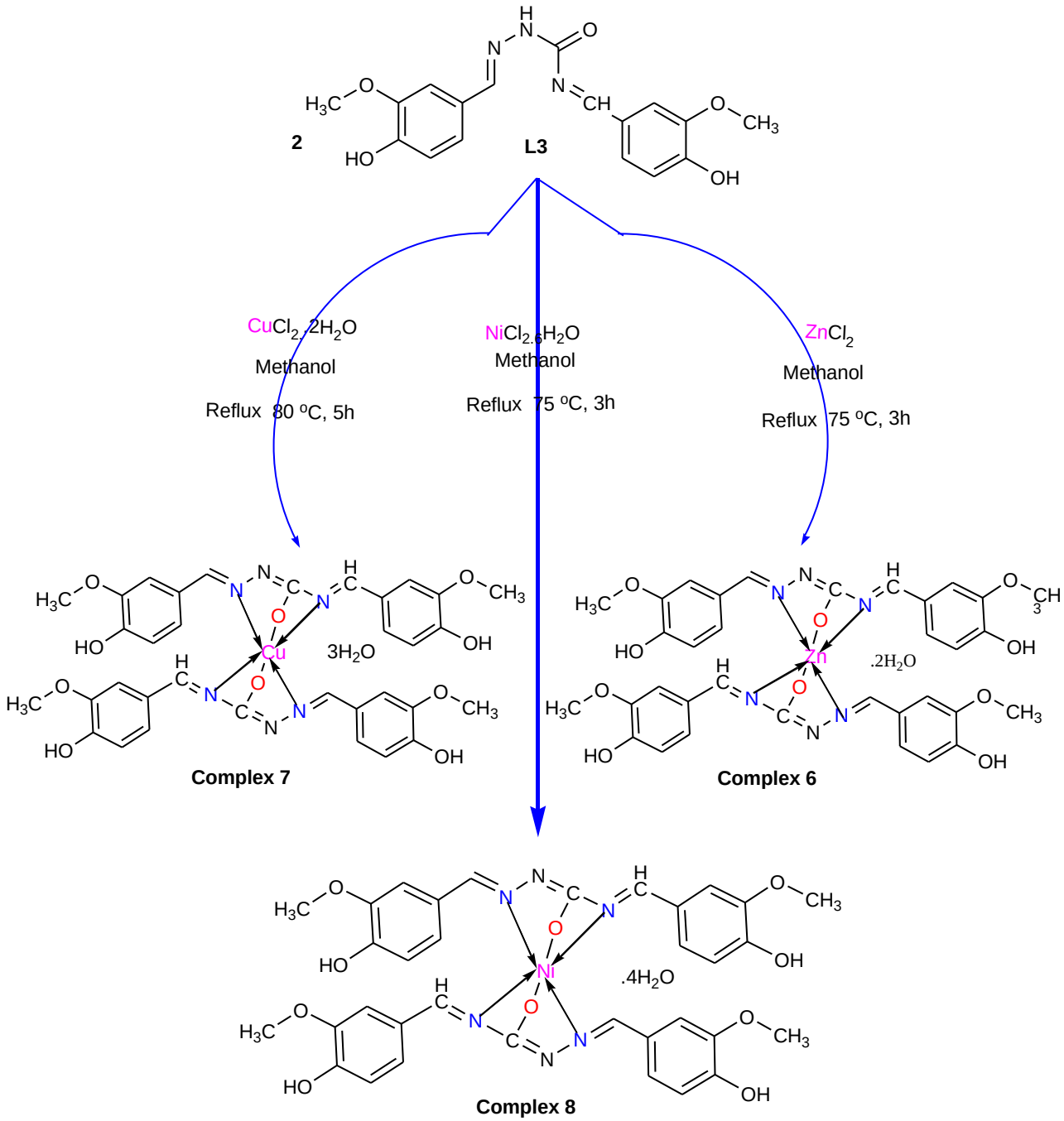

Scheme 17. Synthesis route and structures of complexes 6, 7 and 8

The synthesized complex **6** was proposed to have molecular formula $[Zn(L3)_2].2H_2O$, a white powdered with a Yield: 56 % which is decomposed at a temperature above 298 ^oC. The elemental analysis of the complex showed the formula $C_{34}H_{36}N_6O_{12}Zn$ (Mwt. = 784.17 g/mol) has the composition of Calc. %: C = 52.03, H = 4.59, O = 24.48, N = 10.71, Zn = 8.03, found %: C = 51.88, H= 4.26, O = 24.34, N = 10.28, Zn = 8.02. UV-Vis λ_{max} (DMSO): 335 nm (L→M) (Appendix 20). FT-IR (υ cm^{-1}, KBr (pellet)): 3447 υ(O-H), 3067 υ(arom C-H), 2929 υ(alph C-H), 1582 υ(C=N), 612 υ(M-N), 551 υ(M-O) (Figure 26). M/z = 784.17

($[C_{34}H_{36}ZnN_6O_{12}]^+$) (Appendix 29). TGA mass loss 6.7 % (60 - 120 °C, 1st step, loss of H_2O molecule), 3.81 % (190 - 274 °C, 2nd, loss of ($C_{17}H_{16}N_3O_4$), and 36.8 % (calc. 1 x $C_{16}H_{14}N_3O_3$) (Figures 50 and 51), Molar conductance (λ_m) = 4.5 $\Omega^{-1}cm^2mol^{-1}$.

Complex **7** has a molecular formula of $[Cu(L3)_2].3H_2O$; brown powder form and yield: 59 % with a melting point of more than 300 ^oC. The complex is soluble in common solvents such as methanol, chloroform, and DMSO. Elemental composition for $C_{34}H_{38}CuN_6O_{13}$ (Mwt. = 801.18 g/mol) calc. %: C = 50.92, H = 4.64, N = 10.48, O = 25.86, Cu = 8.01; found %: C = 50.76, H = 4.36, O = 25.48, N = 10.34, Cu = 7.96. UV-Vis λ_{max} (DMSO): 265 nm, and 330 nm (L→M). FT-IR (υ cm^{-1}, KBr (pellet)): 3447 υ(O-H str.), 3069 υ(arom C-H str.), 2929 υ(alph C-H str.), 1582 υ(C=N str.), 560 υ(M-N str.), 470 υ(M-O str.) (Figure 26). M/z = 801.18 ($[C_{34}H_{38}CuN_6O_{13}]$)$^+$ (Appendix 31). TGA mass losses: 6.8% (62 - 165 °C, 1st step, calc. 3× H_2O = 54.04 g), and 3.9% (166-172, 2nd step loss of CH_3O^+ and 30.8 % (273 - 533 °C, 3rd, loss of $2(C_7H_7O_2)$. Molar conductance (λ_m) = 14.8 $\Omega^{-1}cm^2mol^{-1}$.

Complex 8 with proposed molecular formula of $[NiL_3].4H_2O$; a Gray-colored powder with a good yield: 68% and melting point temperature of more than 300 ^oC. Elemental composition for $C_{34}H_{40}NiN_6O_{14}$ (Mwt. = 814.2 g/mol), calc. %: C = 50.18, H = 4.72, O = 27.77, N = 10.11, Ni = 7.02, and found %: C = 50.17, H = 4.61, O = 27.66, N = 10.04, Ni = 7.01. UV-Vis λ_{max} (DMSO) = 275 nm and 306 nm (Appendix 22). FT-IR (υ cm^{-1}, KBr (pellet)): 3447 υ(O-H str.), 3011 υ(arom C-H str.), 2852 υ(alph C-H str.), 1582 υ(C=N str.), 548 υ(M-N str.), 493 υ(M-O str.) (Figure 3). m/e- = 814.20 g/mol ($[C_{34}H_{40}NiN_6O_{14}]^+$) (Appendix 33). TGA mass loss 6.8 % (60 – 160 °C, 1st step, loss of H_2O molecules), 20.95 % (250 - 347 °C, 2nd step, loss of $C_8H_8O_2$ and CH_3O = 136.052 g & CH_3O = 31.0814 g and 30.8 % (347 – 590 °C, 3rd step, loss of $2C_7H_7O_2$) (Figure 58). Molar conductance (λ_m) = 9.6 $\Omega^{-1}cm^2mol^{-1}$.

4.1.11. Complexes 9 and 10

The heteroleptic complex compounds of copper (II) complex **9** and zinc (II) complex **10** with the two semicarbazone derivative ligands: [4-(4-hydroxy-3- methoxyphenyl)but-3-en-2-one]semicarbazone (**L1**) and ortho-phtaladehyde disemicarbazone (**L4**) have been synthesized in 1:1:1 (L1:M: L4) mole ratio in absolute ethanol solution. The general schematic representation for the synthesis of complex 9 and 10 are shown in scheme 18.

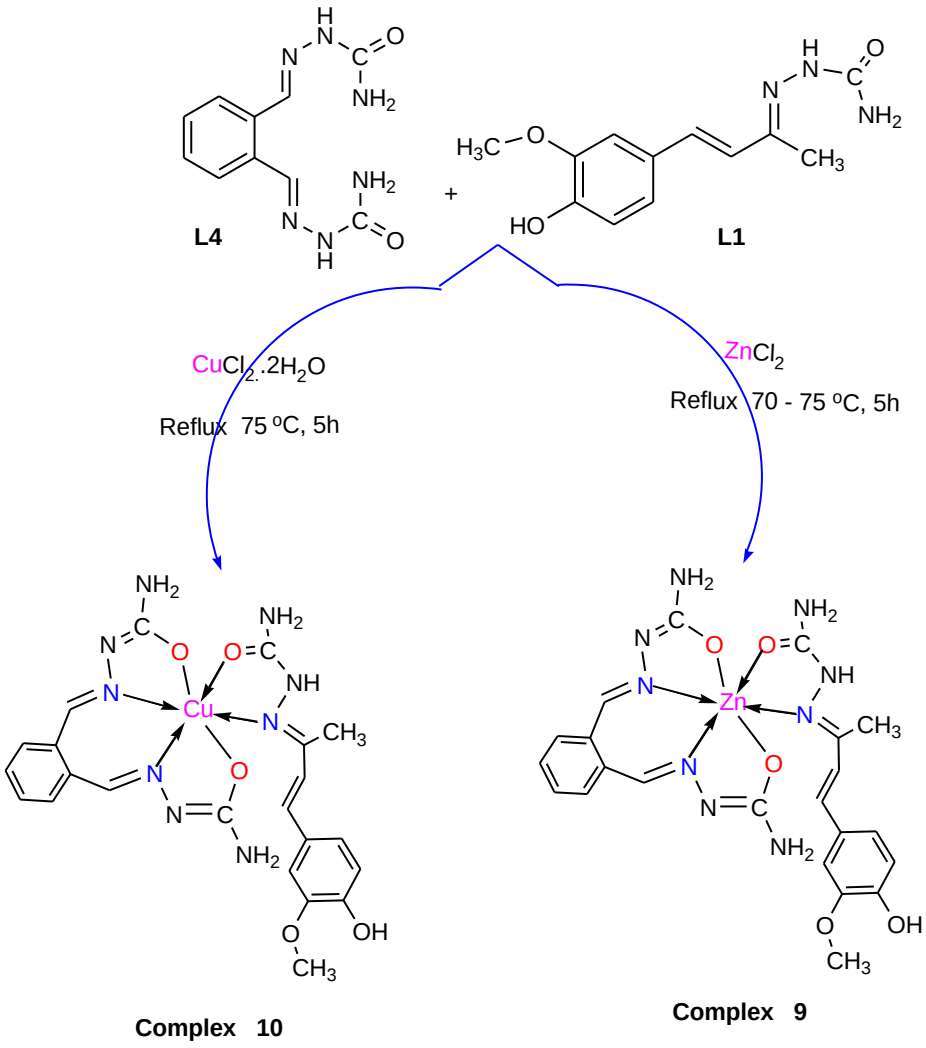

Scheme 18. Proposed synthesis pathway and structures of complex **9** and **10**

The obtained heteroleptic zinc complex **9** has a molecular formula of [Zn(L1)(L4)]; white powdered, yield: 58.5%; melting point > 300 ^{o}C. It is soluble in solvents such as ethanol, methanol, chloroform, and DMSO. Elemental compositions for $C_{22}H_{25}N_9O_5Zn$ (Mwt. = 560.88 g/mol) calc. %: C = 47.11, H = 4.49, O = 14.26, N = 22.48, Zn = 11.23, found %: C = 46.78, H = 4.26, O = 14.20, N = 22.18, Zn = 11.21. UV-Vis: λ_{max} (DMSO) = 340 nm (L→M) (Appendix 24). FT-IR (υ cm^{-1}, KBr (pellet)): 3376 υ(O-H str.), 3267, 3155 υ(N-H str.), 2920 υ(arom C-H str.), 2844 υ(alph C-H str.), 1652 υ(C=O str.), 1530 υ(C=N str.), 1505 υ(arom C=C str.), 538 υ(M-N str.), 443 υ(M-O str.) (Figure 29). M/z = 559.1034 ($[C_{22}H_{25}N_9O_5Zn]^+$). TGA mass loss of 34.2 % (207.1 – 394.1 °C, 1st step, calc.1 × $C_{14}H_{10}O_3$ = 191.8 g), 38.3 % (397.4 - 738.9 °C, 2nd, 214.8 g fragmented part of L_1. Molar conductance (λ_m) = 5.4 Ω^{-1}cm^{2}mol^{-1}.

Complex **10** has a molecular formula of [Cu(L_1)(L_4)]; brownish colored powder, yield: 54.6 %; has melting point above 300 ^oC and is soluble in solvents: ethanol, methanol, chloroform, and DMSO. Elemental composition for $C_{22}H_{25}N_9O_5Cu$ (Mwt. = 558.13 g/mol) calculated %: C = 47.03, H = 4.50, O = 14.33, N = 22.55, Cu = 11.06, found %: C = 46.86, H = 4.23, O = 14. 21, N = 21.98. Cu = 11.04. UV-Vis λ_{max} (DMSO) = 262 nm, 362 nm, and 354 nm (Appendix 25). FT-IR (υ cm^{-1}, KBr (pellet)): 3404 υ(O-H str.), 3267, 3146 υ(N-H str.), 2926 υ(arom C-H str.), 2851 υ(alph C-H str.), 1602 υ(C=O str.), 1524 υ(C=N str.), 1504 υ(arom C=C str.), 1361 υ(asy C-O-C str.), 1023 υ(sym N-N str.), 538 υ(M-N str.), 448 υ(M-O str.) (Figure 3). M/z = 558.06 ($[C_{22}H_{25}N_9CuO_5]^+$). (TGA mass loss 44.5% (225.2- 313°C, 1st step, calc.1 × $C_{10}H_{12}N_6O_2$ = 248.8 g), 5.6 % (387.3 - 413.9 °C, 2nd, CH_3 + NH_2 = 31.3 g) and 21.8 % (497.4 - 586.8 °C, 3rd step, 1 x $C_7H_7O_2$ = 122.9 g). Molar conductance (λ_m) = 16.4 $\Omega^{-1}cm^2mol^{-1}$.

4.2. Characterization of the synthesized ligands and the metal complexes

4.2.1. NMR spectral analysis of the synthesized ligands

The ^{1}H NMR, ^{13}C-NMR, and ^{13}C-DEPT-135 spectrum data, which provides precise information regarding the positional elucidation and number of proton and carbon atoms were used to unambiguously confirm the structures of the synthesized compounds. The chemical shifts were recorded using tetramethylsilane (TMS) as an internal standard for the NMR spectra analysis.

4.2.1.1. ^{1}H-NMR and ^{13}C-NMR spectra analysis of L1 and L2

The ^{1}H NMR spectrum of **L1** shows signal protons at 2.01 and 3.89 ppm which were attributed to protons of the -CH_3 (H_1) attached to imine carbon and -OCH_3 (H_2) of the methoxy group protons respectively (Appendix 1). The NH_2 group protons (H_3) due to carbothioamide exhibited a signal found at 6.44 ppm. Also, signal protons observed at 6.93 and 6.71 ppm was assigned to protons (H_4 and H_7) of the ethylene group. However, signals for protons in the aromatic ring (H_8, H_6, and H_5) appeared at 7.11, 6.83, and 6.75 ppm respectively. The hydroxyl proton (OH) (H_9) of the phenyl ring appeared at 9.28 ppm and the signal at 9.35 ppm assignable to the proton bonded to nitrogen (NH) (H_{10}) (Festus, Okafor, & Ekennia, 2019) as indicated in Appendix 1. Thus, the data matches with the structure proposed for the ligand.

Additional evidence for the real structure of the prepared ligand **L1** was confirmed by the ^{13}C NMR and ^{13}C - DEPT-135 spectrum data which provides exact information regarding carbon atoms' position in the proposed structures (Appendixes 2 and 3). The ^{13}C-NMR spectral (Appendix 2) of **L1** showed signals at 157.7 ppm assigned to a carbon of C-12 (C=O) group and the signal of C-11 (C=N) was located at 148.29 ppm. The signals of aromatic carbons (C-9 and C-10) attached with methoxy and hydroxyl (-OH) groups were indicated at 147.46 and 146.67 ppm respectively. The carbon signals of ethylene (C-7 and C-8) were located at 128.59 and 132.23 ppm respectively (Andres et al., 2020; Bisceglie et al., 2020; Bisceglie et al., 2018). Also, signals at 127.01, 120.85, 116.07, and 110.22 ppm were for aromatic carbons C-6, C-5, C-4, and C-3, and the signals for methoxy and methyl carbons C-2 and C-1 were indicated at 55.97 and 11.97 ppm, which were fitted with the expected structure (Appendix 2).

The ^{13}C-dept-135 spectra also showed that there is no CH_2 group shown because no spectra were shown down. But the -CH and CH_3 groups were indicated on the ^{13}C- NMR spectra were also exactly shown on the ^{13}C-dept spectra (-CH_3 indicated at 11.98 (C-1) and 55.98 (C-2) and -CH indicated at 110.24 (C-3), 116.08 (C-4), 120.86 (C-5), 127.01 (C-7) & 132.24 (C-8)). The other spectrum shown on ^{13}C-NMR spectra but not appeared on ^{13}C- dept-135 spectra are the quaternary carbons indicated at signals 127.01 (C-6), 147.46 (C-10), 148.29 (C-11), 146.67 (C-9) and 157.70 (C-12) (Appendix 3).

Similarly, the proton NMR spectra of **L2** showed a signal at 10.20 ppm assignable to the proton bonded to nitrogen (N-H) (H_9). The proton bonded in the hydroxyl (O-H) (H_{10}) of the phenyl appeared as a singlet at 9.35 ppm. The three protons (H_3, H_4, H_5) in the benzene ring was resonate between the chemical shift values 6.72–7.13 ppm. The other signal protons located at 2.11 and 3.83 ppm were ascribed to the -CH_3 (H_1) and -OCH_3 (H_2) bonded protons respectively (Appendix 4).

The carbon skeleton of dehydrozingerone thiosemicarbazone (**L2**) ligand was analyzed using the ^{13}C-NMR spectrum as shown in Appendix 5. The Carbon of the C=S (C-12) group was shown by the signal at 178.89 ppm and the signals of aromatic carbons C- 10 and C-11 attached to hydroxyl (-OH) and methoxy group were observed at 148.28 and 149.94 ppm respectively. While the signals of ethylene C-7 and C-8 carbons were located at 134.65 and

128.31 ppm respectively. The other carbon signal of the C=N (C-9) was found at 147.87 ppm (L. V. Kumar & Nath, 2019). The carbon of the methyl C-1 (CH_3) group bonded with the imine carbon was indicated at 12.61 ppm and that of carbon in the methoxy C-2 (-OCH_3) group was founded at 55.99 ppm. The carbon atoms in the aromatic ring, C-3, C-4, C-5, and C-6 resonated at 110.38, 116.10, 121.26, and 126.35 ppm respectively.

The ^{13}C-dept-135 spectra of L2 also showed, that there is no CH_2 group shown because no spectra were shown down. But the -CH and CH_3 groups were indicated on the ^{13}C- NMR spectra were also exactly shown on the ^{13}C-dept spectra (-CH_3 indicated at 12.61(C-1) and 55.99 (C-2) and -CH indicated at 110.39 (C-3), 116.10 (C-4), 121.26 (C-5), 126.35(C-7) & 134.65 (C-8)). The other spectrum shown on ^{13}C-NMR spectra but not appeared on ^{13}C- dept-135 spectra are the quaternary carbons indicated at signals 126.35 (C-6), 148.28 (C-10), 149.94 (C-11), 147.87 (C-9) and 178.89 (C-12) (Appendix 6).

4.2.1.2. ^{1}H NMR and ^{13}C-NMR spectral analysis of L3

The ^{1}H NMR spectra of **L3** showed a single signal located at 3.83 ppm, which is allocated to protons found on the methoxy group (OCH_3) represented by H_1. The other signals protons located at 6.78, 6.97 and, 7.38 ppm are assigned to the aromatic protons indicated by H_2, and H_3 which are shown by doublet peaks and H_4 by singlet peaks respectively. Also, the proton signal found at 7.74 ppm is for the proton of the hydroxyl (OH) group bound to the aromatic ring (H_5) while the proton signals observed at 8.59 and 10.08 ppm are due to the protons appeared on (NH) (H_6) and imine carbon (-CH=N-) (H_7) respectively as shown in appendix **7**. Thus, the overall protons signal locations matched exactly with the proposed structure for the synthesized ligand (**L3**).

Further, the conformation for the formation of **L3** was checked by analyzing the ^{13}C-NMR and Dept-135 spectrum, which gave information about the nature of carbon atoms that exist in the proposed structure (Appendix 8 and 9). The ^{13}C NMR spectra of the ligand (L3) indicate carbon signals at 157.48 ppm assigned to a carbon (C-8) of carbonyl (C=O) group and the carbon signal of C=N (C-6) existed at 140.46 ppm, which is additional information for the real formation of semicarbazone ligand, **L3**. The carbon signals of the benzene ring C-2, C-3, C-4, C-5, and C-7 were observed at 109.39, 115.65, 121.54, 126.75, and 150.42 ppm respectively. Furthermore, carbon signals at 56.13 ppm were for the methoxy (-OCH_3) group represented by C-1 (Appendix 8).

The ^{13}C -Dept-135 spectra data also indicated that there is no secondary carbon (-CH_2) group found in the proposed structure. This is because no peak in Appendix 9 showed a down peak. But the CH_3 and CH groups which were shown in ^{13}C-NMR also showed on Dept-135 spectra which were found at 56.14 (C-1), 109.40 (C-2), 115.65 (C-3), 121.54 (C-4) and 140.47 (C-6) ppm. The rest spectra which were shown on ^{13}C-NMR but not observed on Dept-135 spectra are the quaternary carbons located at signals 126.75 (C-5), 150.42 (C-7), and 157.48 (C-8) ppm as shown by Appendix 9, which were best correlate with the proposed structure for the ligand.

4.2.1.3. NMR spectra analysis of L4

Proton signals around 6.5 and 7.37 ppm in the proton NMR spectra of **L4** were assigned to NH_2 (H_1) and NH (H_2) protons, respectively. The CH (H_3) and (H_4) protons were also detected at 7.87 and 8.33 ppm, respectively. The signal around 10.43 ppm validates the N=CH (H_5) proton, indicating that the ligand (L4) was perfectly synthesized (Appendix 10).

In ^{13}C NMR graph of **L4** showed a signal at 157 ppm allotted to a carbonyl of the amide (-NC=O) (C-5) group and the signal for carbon in (C=N) (C-4) was located at 138.86 ppm. The remaining signals are seen at 128.3, 129.3, and 132.4 ppm (C-1, C-2, and C-3) were assigned to aromatic carbon signals, which perfectly match the expected structure (Appendix 11).

4.2.2. FTIR spectra analysis

The FTIR spectral information is another tool used to allocate the vibrational frequencies that confirm the important functional groups that exist in the newly prepared compounds. The important FTIR bands and assignments of the main functional groups of the synthesized ligands: [4-(4-hydroxy-3-methoxyphenyl)but-3-en-2-one]semicarbazone(**L1**), [4-(4-hydroxy-3-methoxyphenyl)but-3-en-2-one]thiosemicarbazone(**L2**),(1E)-1,4-bis(4-hydroxy-3-methoxybenzylidene)semicarbazide ligand (**L3**) and their homoleptic and heteroleptic copper(II), zinc(II) and nickel (II) complexes data were displayed in table 3 and 4 below and the spectra graphs were presented in Figures 17 - 30. The spectra of the ligands were compared to the spectra of their complexes to analyze changes that occurred during complexation to confirm complex formation.

4.2.2.1. FTIR Spectra of L1 and its metal complexes

In the FTIR spectra of **L1**, the characteristic and diagnostic peaks were observed in 3578 - 448 cm $^{-1}$ (Figure 17). The O-H bond stretching band was found at 3578 cm^{-1} (Noblía et al., 2005). The bands at 3485–3204 cm^{-1} were assigned to (N-H) stretching (Sajjad Hussain Sumrra et al., 2014). The characteristic aromatic C-H stretching bands appeared around 2929 cm^{-1}. Also, the aliphatic C-H stretching band was found at 2852 cm^{-1}. The carbonyl stretching bond was indicated by a band at 1696 cm^{-1} (C=O) and the imine (C=N) bond, υ(C=N) was found at 1592 cm^{-1}, hence giving a clue of condensation product, with best confirmation for the exact formation of the [4-(4-hydroxy-3- methoxyphenyl)but-3-en-2-one]semicarbazone ligand **(L1)**. The stretching of the aromatic C=C bond was seen at 1521 cm^{-1}. Furthermore, the band located at 1437 cm^{-1} was allotted to phenolic O–H bending while the aromatic alkyl ether had shown two characteristic peaks; asymmetric C-O-C stretch at 1256 cm^{-1} and symmetric stretch at 1027 cm^{-1} (Lu et al., 2018).

The formation of complexes and binding sites of ligands were confirmed by comparing the FTIR spectra bands of the ligand with the metals. The carbonyl (C=O) and imine (C=N) stretching frequencies were found at 1696 cm^{-1} and 1592 cm^{-1}, respectively for the **L1** ligand (Jirjees et al.; Sajjad Hussain Sumrra et al., 2014). But for the Zn(II), Cu(II), and Ni(II), the ν(C = O) stretching was observed at 1653 cm^{-1}, 1668 cm$^{-1,}$ and 1660 cm^{-1} respectively, showing a shift to lower by 43 cm^{-1}, 28 cm^{-1}, and 36 cm^{-1} respectively. This is the confirmation of the coordination of **L1** with the metal through the oxygen binding site which is in agreement with the literature reports of how coordination of the metals with donor atom lowers the bond strength with the other atoms (Alias, Kassum, & Shakir, 2014; Tyagi, Chandra, Saraswat, & Yadav, 2015). The FTIR bands of imine group (C = N) stretching bands were located at 1583 cm^{-1} for both Zn(II) complex (1) and Cu(II) complex (2) and 1582 cm^{-1} for Ni(II) complex (**3**), showing a decrease of the vibration frequencies by 9 cm $^{-1}$ and 10 cm^{-1} respectively, confirming coordination of L1 ligands through the nitrogen atom with the metals (El-Sonbati, Diab, Morgan, Abou-Dobara, & El-Ghettany, 2020; Jirjees et al.; Sajjad H Sumrra & Chohan, 2012). Additionally, the new weak bands appeared between 538 - 546 cm^{-1} and 398 – 443 cm^{-1} corresponding to υ(M-N) and υ(M-O), respectively (Ferraro, 2012). This means that, the appearance of the new bands in their metal complexes at 538–546 and 398 – 443 cm^{-1} which were assigned to *ν*(M-N) and *ν*(M-O) vibrations (Hanif & Chohan, 2013), respectively, and these bands were absent in their free ligands (Figures 18, 19 and 20).

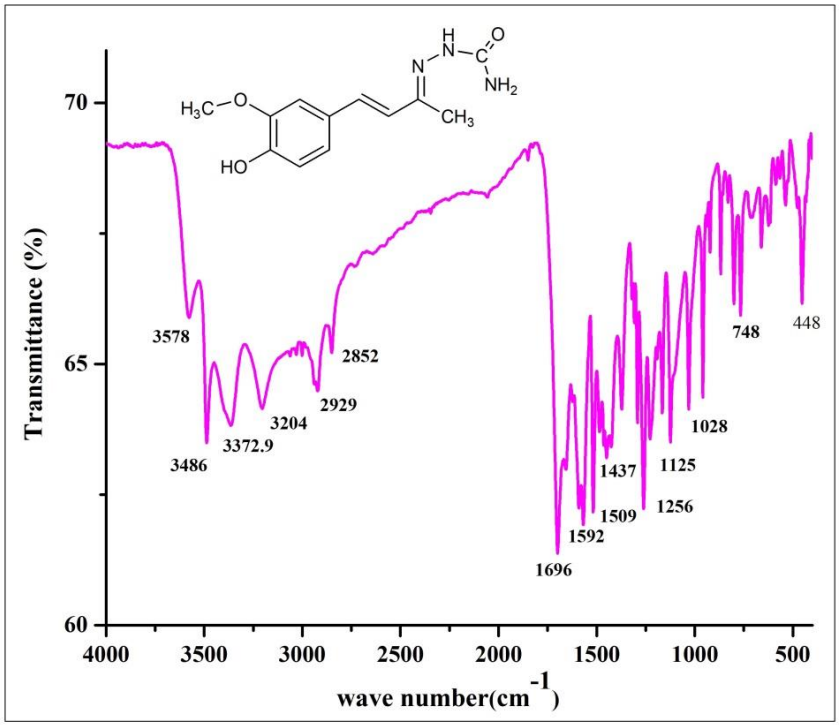

Figure 17. FTIR spectrum of ligand (L1)

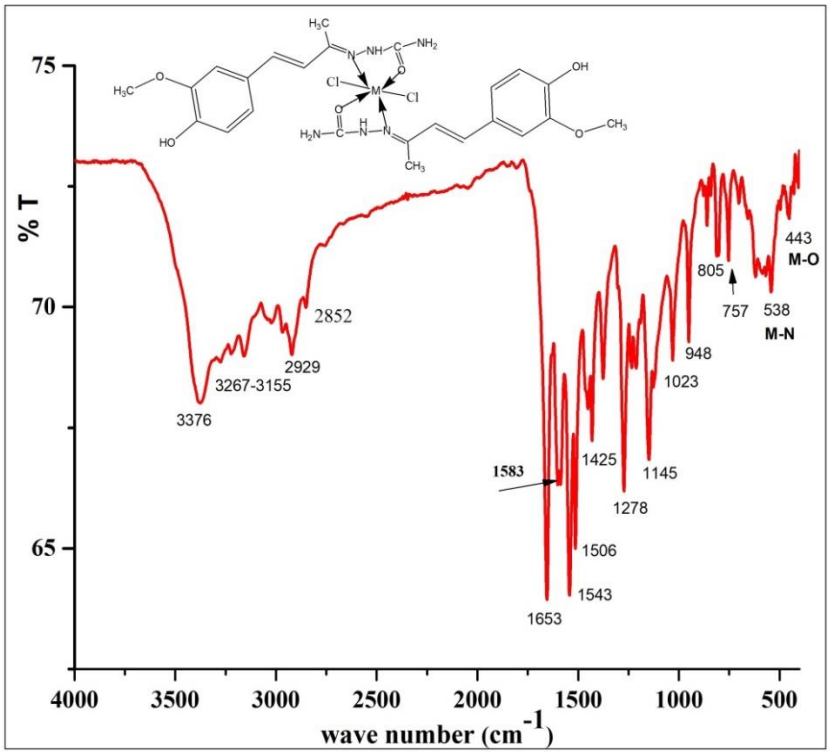

Figure 18. FTIR spectrum of the $[Zn(L1)_2(Cl)_2]$ complex (**1**)

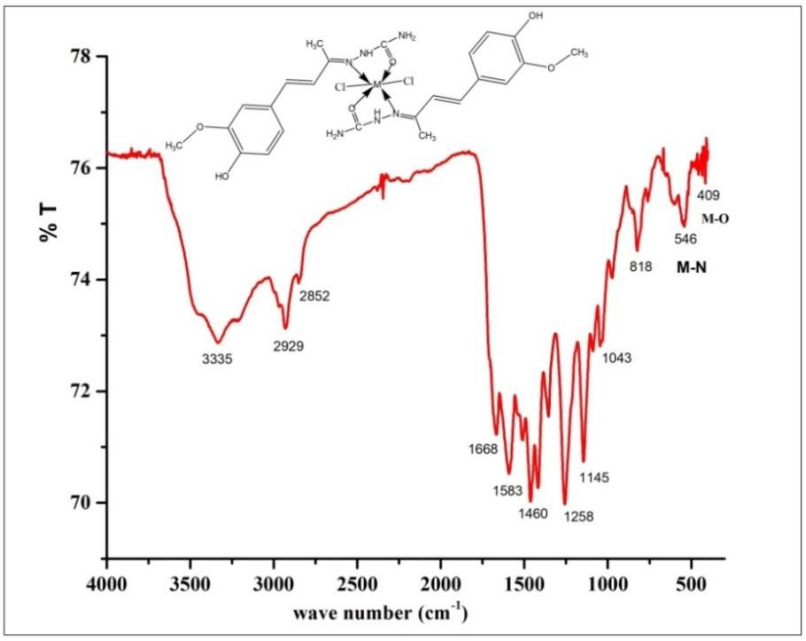

Figure 19. FTIR spectrum of the $[Cu(L1)_2(Cl)_2]$ complex (**2**)

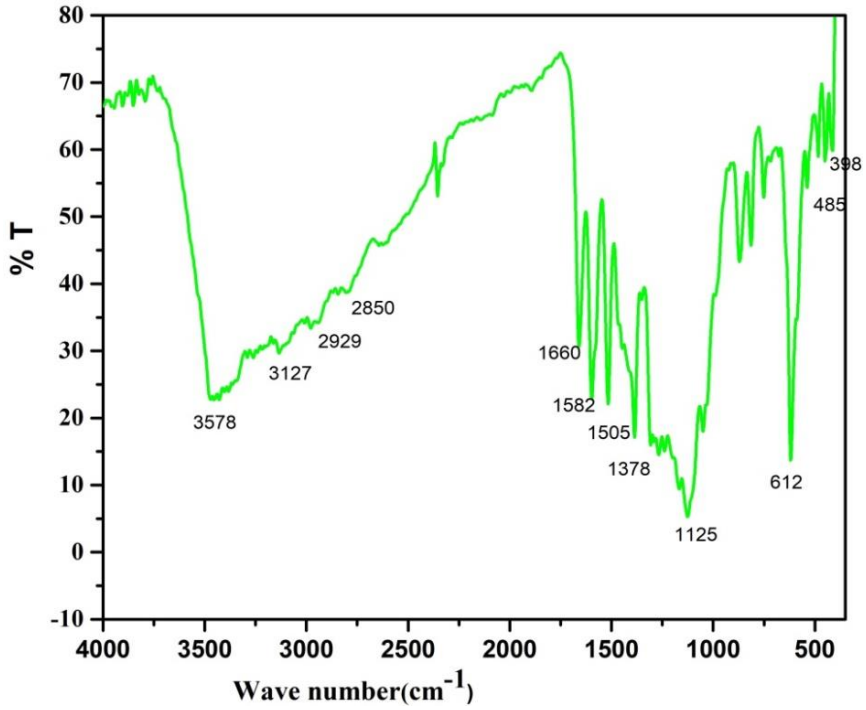

Figure 20. FTIR spectrum of the $[Ni(L_1)_2Cl]$ complex (**3**)

4.2.2.2. FTIR Spectra of L2 and its complexes

The assignments of significant FTIR spectra bands of the [4-(4-hydroxy-3-methoxyphenyl)but-3-en-2-one]thiosemicarbazone (**L2**) were shown in Figure 21. The IR spectral data in Table 3 indicated the bands at 3451 cm^{-1} and 3310 cm^{-1} stretching were assigned for v(O-H) and v(N-H) vibrations respectively (Jirjees et al.; Sajjad H Sumrra &

Chohan, 2012). Aromatic C-H and aliphatic C-H stretching frequencies were observed at 2929 and 2852 cm^{-1} (Ferraro, 2012; Jirjees et al.). The weak peak observed at 1745 cm^{-1} confirms an aromatic ring existence while a strong band at 1611 cm^{-1} was attributed to the ν(C=N), which depicts the formation of the ligand through condensation (Andres et al., 2020). The strong bands detected at 1273 cm^{-1} and 801 cm^{-1} were for the ν(C=S) & ∂(C=S) respectively and aromatic C=C stretching found at 1512 cm^{-1}. The other band at 1435 cm^{-1} was assignable to phenolic O–H bending and the aromatic alkyl ether of characteristic peak of C-O-C stretch was observed at 1016 cm^{-1}.

The FTIR spectra of the complexes (**4** and **5**) were shown on Figures 22 and 23 and the data were summarized in table 3. The spectra of **L2** showed the stretching frequency bond υ(C=N) at 1611 cm^{-1} but this shifts to the lower side by 21 cm^{-1} and 14 cm^{-1} in Cu(II) and Zn(II) complexes, respectively, confirming coordination to metals through the nitrogen atom. The band assigned to ν (C=S) is shifted from 1273 cm^{-1} to 1243 cm^{-1} and 1265 cm^{-1} which was lowered by 8 and 28 cm^{-1} indicating the involvement of sulfur in complexation. These confirmations were more supported by the new bands that appeared around 533 - 566 and 420 - 434 cm^{-1}, which were assignable to ν(M-N) and ν(M-S) vibrations, respectively, indicative of bond formation between M-N and M-S (Tada, Chavda, & Shah, 2011).

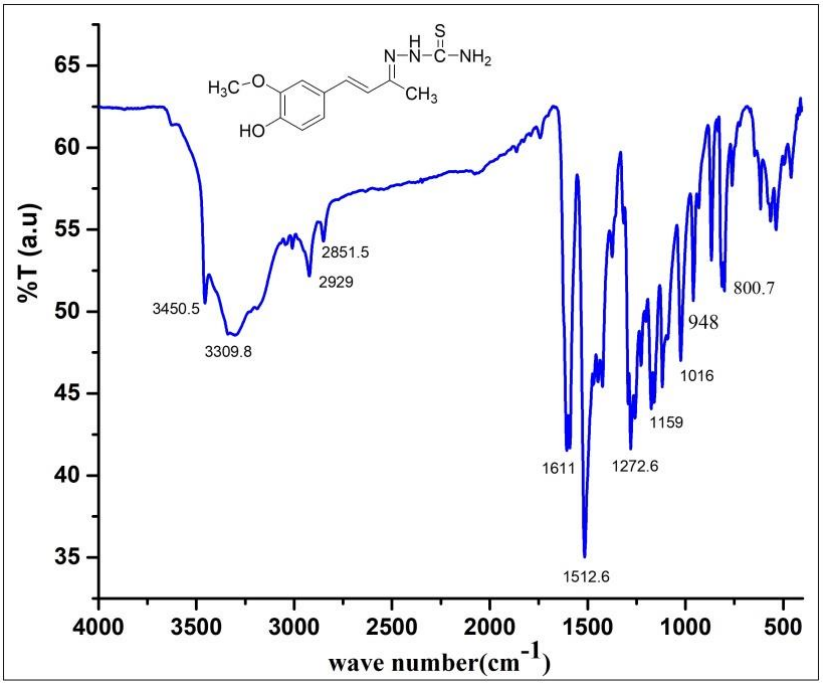

Figure 21. FTIR spectrum of (4-(4-hydroxy-3-methoxyphenyl)but-3-en-2-one) thiosemicarbazone **(L2)**.

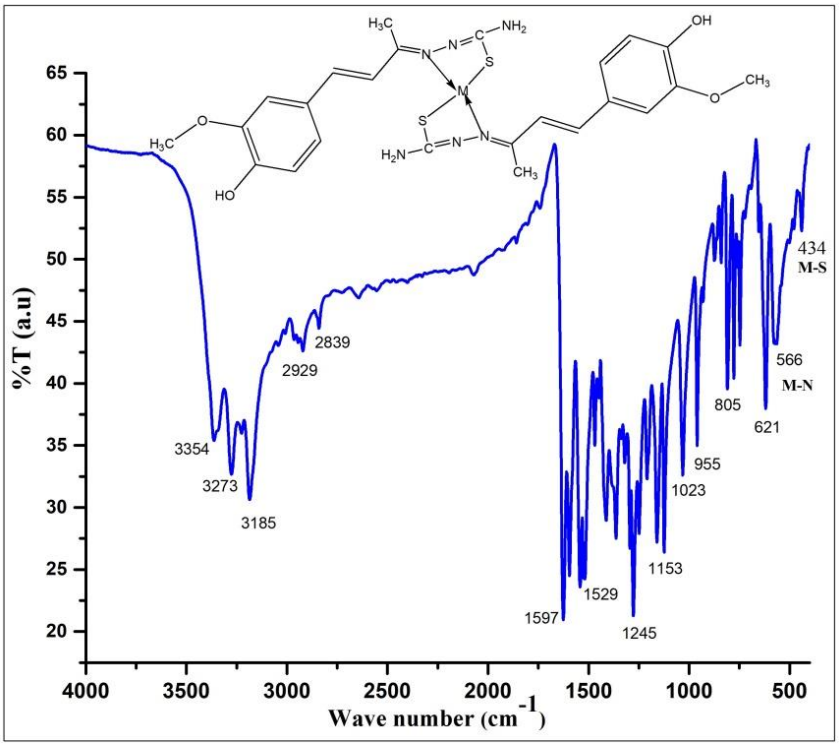

Figure 22. FTIR spectrum of the $[Zn(L2)_2]$ complex (**4)**

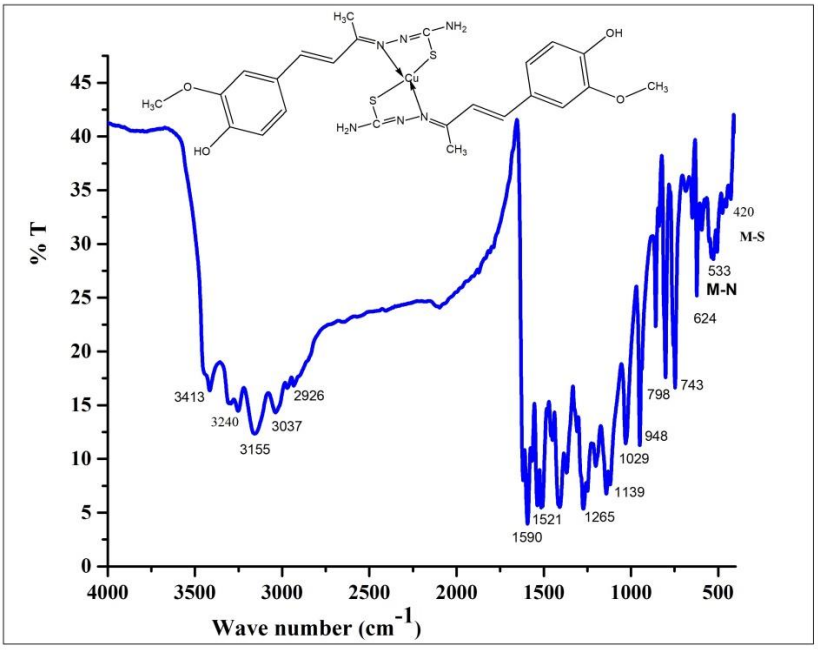

Figure 23. FTIR spectrum of the $[Cu(L2)_2]$ complex **5**

4.2.2.3. FTIR of Spectra of (1E)-1,4-bis(4-hydroxy-3-methoxybenzylidene) semicarbazone ligand (L3) and their homoleptic metal complexes

In the FTIR spectra of the ligand, the diagnostic peaks were found between 3447 - 1270 cm^{-1} (Figure 24). The frequency of the (O-H) band was located at 3447 cm^{-1} (sharp) (Saucedo-Balderas et al., 2015). The frequency band at 3293 and 3069 cm^{-1} were due to (N-H) bond vibration which is attached to the semicarbazone moiety. The other characteristic peaks of the aromatic C-H vibrational band were observed at 2929 cm^{-1} and the aliphatic C-H vibrational band was located at 2852 cm^{-1}. The larger intensity with stronger bands found at 1643 cm^{-1} and 1593 cm^{-1} was for carbonyl (C=O) and imine (C=N) bonds respectively which best confirms the real formation of **L3** ligand. The other stretching frequency observed at 1506 cm^{-1} corresponds to the C=C bond found in the aromatic ring. The phenolic (O-H) bending was indicated at 1431 cm^{-1}.

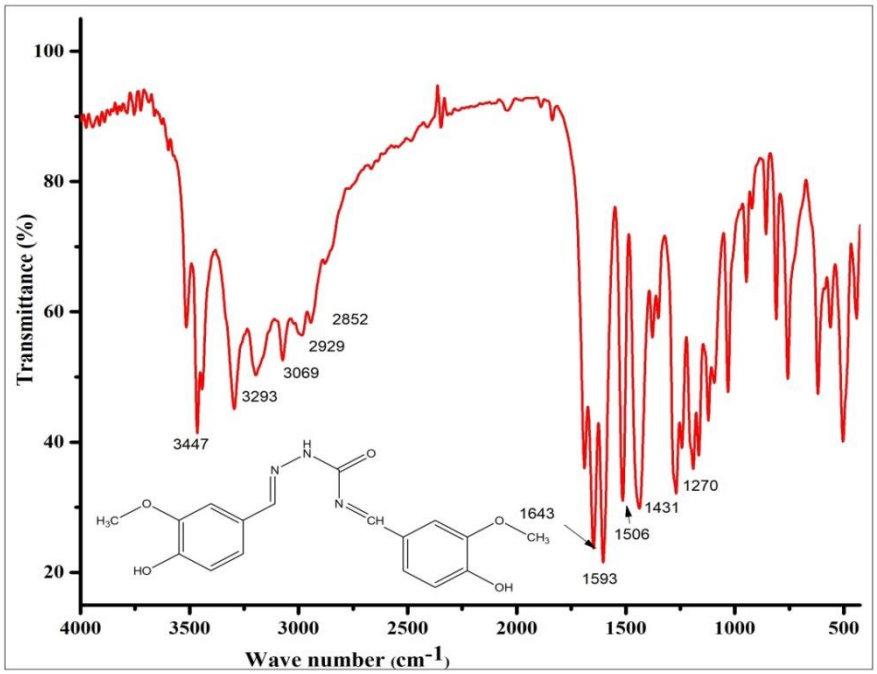

Figure 24. FTIR spectrum of (1E)-1,4-bis(4-hydroxy-3-methoxybenzylidene) semicarbazone ligand (L3)

By comparing the spectra bands of **L3** and the metal complexes, the actual synthesis of the complexes from the ligand was examined. The frequencies of (C=O) and (N-H) bonds were found at 1643 cm^{-1} and 3293 cm^{-1} respectively for the free ligand, but there are complete disappearances (absence) of both bands in the spectra of the Cu(II), Zn(II) and Ni(II) complexes, indicates deprotonation of the amide (N-H) group favoring the neighboring

carbonyl oxygen (C=O) to coordinate to the metals through the donor oxygen atom. Furthermore, the absence of v(C=O) in the Cu(II), Zn(II), and Ni(II) complexes indicates the change from C=O to C-O bond which is observed by an intense peak around 1033, 1036, and 1070 cm^{-1} were due to coordination of **L3** to the metals through an oxygen atom, in which the oxygen atom bind to the metal by a covalent bond to act as an ionic ligand (Jirjees et al.; Ramzan et al., 2017). On the other hand, the frequency of imine (C=N) bond for **L3** found at 1593 cm^{-1} was a shift to 1582 cm^{-1}, which was lowered by 11 cm^{-1} for Cu(II), Zn(II), and Ni(II) complexes. This indicates the coordination of **L3** to the metals through the nitrogen atom as the binding site (Tada et al., 2011). Additionally, the new weak bands appeared between the ranges 526 - 630 cm^{-1} and 456 - 551 cm^{-1} corresponding to v(M-N) and v(M-O) respectively (Figures 25, 26, and 27) (Tada et al., 2011). The FT-IR spectra of copper complexes also showed strong bands between 3155 and 3413 cm^{-1} region for the complexes, suggesting the existence of coordinated water molecules. Also, the new band that appeared between 621.5 and 624.6 cm^{-1} was assignable to a rocking mode of water (F. Ommenya, Nyawade, Andala, & Kinyua, 2020).

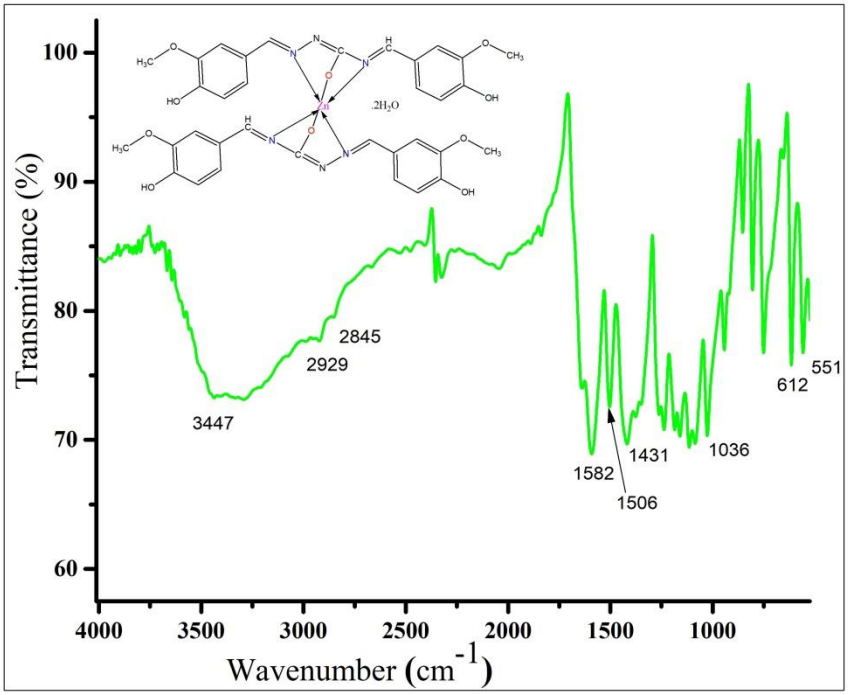

Figure 25. FTIR spectrum of the $[Zn(L3)_2].2H_2O$ complex **6**

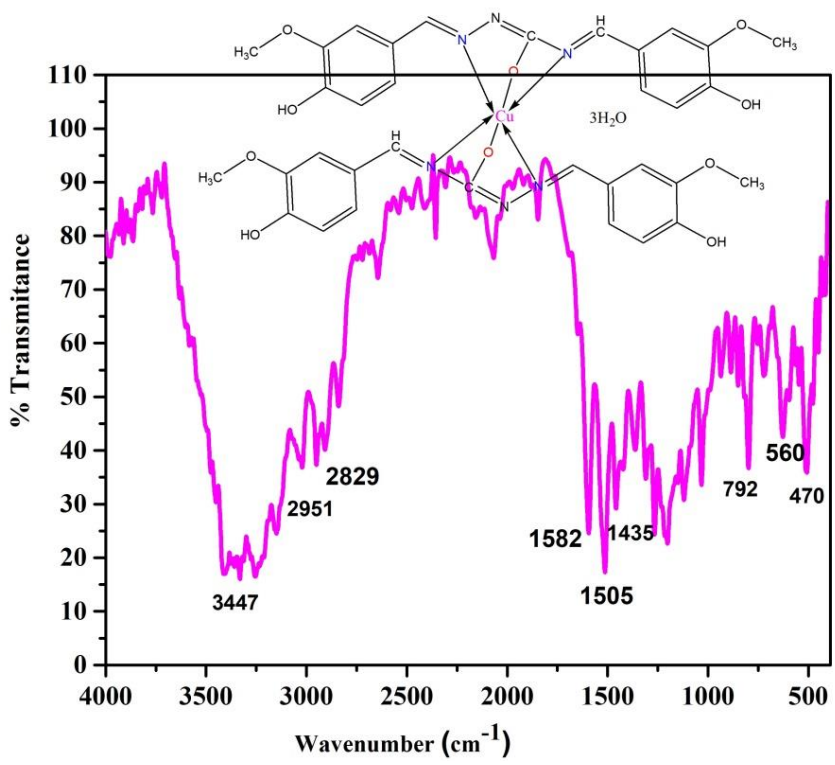

Figure 26. FTIR spectrum of the $[Cu(L3)_2].3H_2O$ complex **7**

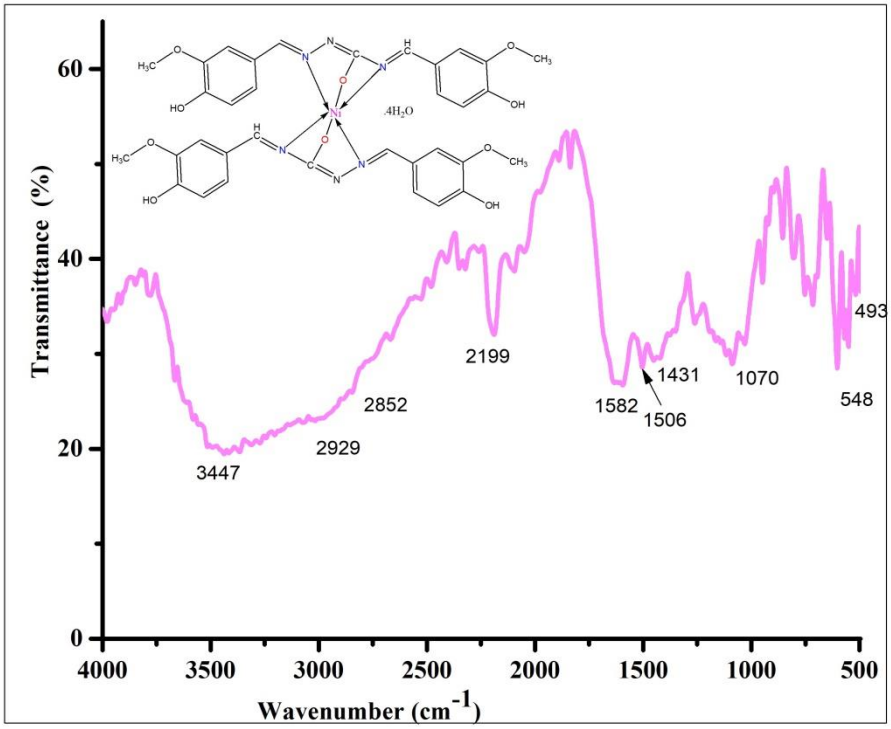

Figure 27. FTIR spectrum of the $[Ni(L3)_2].4H_2O$ complex **8**

Table 3. FTIR spectral data ($\upsilon(cm^{-1})$) for the ligand **L1**, **L2**, and **L3** and their homoleptic complexes

Compound	Main functional groups								Coordination site		
	O-H	N-H	C- H_{ar}	C-$H)_{al}$	C = O	C = S	C = N	C = C	M–N	M–O	M–S
L1	3578	3485/ 3204	2929	2852	1696	---	1592	1521	--	--	--
$[Zn(L1)_2Cl_2]$ (**1**)	3378	3218/ 3155	2929	2852	1653	---	1583	1506	538	443	-
$[Cu(L1)_2(Cl)_2]$ (**2**)	3335	3218/ 3205	2928	2852	1668	----	1583	1505	546	409	
$[Ni(L1)_2Cl]$ (**3**)	3578	3127	2929	2852	1660	----	1582	1505	503	398	--
L2	3451	3310/ 3034	2929	2852	--	1273	1611	1513	--	--	--
$[Zn(L2)_2]$ (**4**)	3354	3273/ 3185	2929	2839	---	1245	1625	1529	566	--	434
$[Cu(L2)_2(H_2O)_2]$ (**5**)	3413	3251/ 3155	2928	2852	--	1265	1590	1513	533	----	420
L3	3447	3293	3069	2929	1643	---	1593	1506	-----	---	--
$[Zn(L3)_2].2H_2O$ (**6**)	3447	-	2929	2853	--	--	1582	1506	612	551	--
$[Cu(L3)_2].3H_2O$ (**7**)	3447	-	3069	2929	--	--	1582	1506	560	470	--
$[Ni(L3)_2].4H_2O$ (**8**)	3447	--	2929	2852	--	---	1582	1506	548	493	--

4.2.2.4. FTIR spectral of ligand L1, L4, and their heteroleptic complexes

The FT-IR spectral information of ligands **L1** and **L4** and their heteroleptic Z(II) and Cu(II) complexes were analyzed to allocate the stretching frequencies of bonding groups that exist in the compounds. The data obtained were summarized in Table 4.

Table 4. FTIR spectral data ($\upsilon(cm^{-1})$) of ligands **L1, L4**, and their heteroleptic complexes.

Compound	Main functional groups							Coordination site	
	O-H	N-H	C- H_{Ar}	C-H_{Al}	C = O	C = N_{im}	C = C	M–N	M–O
L1	3578	3485/ 3204	2929	2852	1695	1592	1509	--	--
L4	---	3372	3055	2921	1689	1583	1505	--	--
[Zn(L1)(L4)] (**9**)	3376	3267/ 3155	2920	2844	1652	1530	1505	538	443
[Cu(L1)(L4)] (**10**)	3404	3267/ 3146	2926	2851	1602	1524	1504	538	448

*Note: - **Ar** = aromatic, **Al** = aliphatic and im = imine*

The formation of complexes from the respective ligands can be confirmed by considering their FTIR spectral data indicated in Figures 28 - 30. The appearance of the imine (C=N)

bond could be a good signal for the formation of ligands. The v(C=N) for the ligands were found at 1592 and 1583 cm^{-1}, while the v(C=N) for the [Cu(L1)(L4)] and [Zn(L1)(L4)] complexes appeared at 1524 cm^{-1} and 1530 cm^{-1}, respectively. This implies a 68 cm^{-1} and 53 cm^{-1} shift in frequency, indicating that both ligands were coordinated through the imine's nitrogen (Alias et al., 2014). Also, L1 and L4 had v(C=O) of 1696 and 1689 cm^{-1}, respectively, but [Cu(L1)(L4)] and [Zn(L1)(L4)] had v(C=O) of 1602 and 1652 cm^{-1}, respectively, decreased by 94 and 87 cm^{-1} in [Cu(L1)(L4)] and 37 and 44 cm^{-1} in [Zn(L1)(L4)] complex. This could be attributed to the coordination of ligands to copper and zinc through their oxygen atoms. The L4 ligand consists of two C=O coordinating sites which are near the amine nitrogen atoms and those near the imine and benzene ring, so relatively there is more electrons density due to $\pi \rightarrow \pi$ electron delocalization from the benzene ring. Hence, they are preferably ligated to the metal centers by undergoing deprotonation (McAuliffe & Perry, 1974). This has been confirmed by the spectra data of the FTIR and elemental analysis data. Additionally, the appearance of new weak bands between 538 - 443 cm^{-1} in both complexes is assigned to vibrational frequencies of metals to nitrogen and oxygen coordination (F. Ommenya et al., 2020) (Figures 28, 29 and 30).

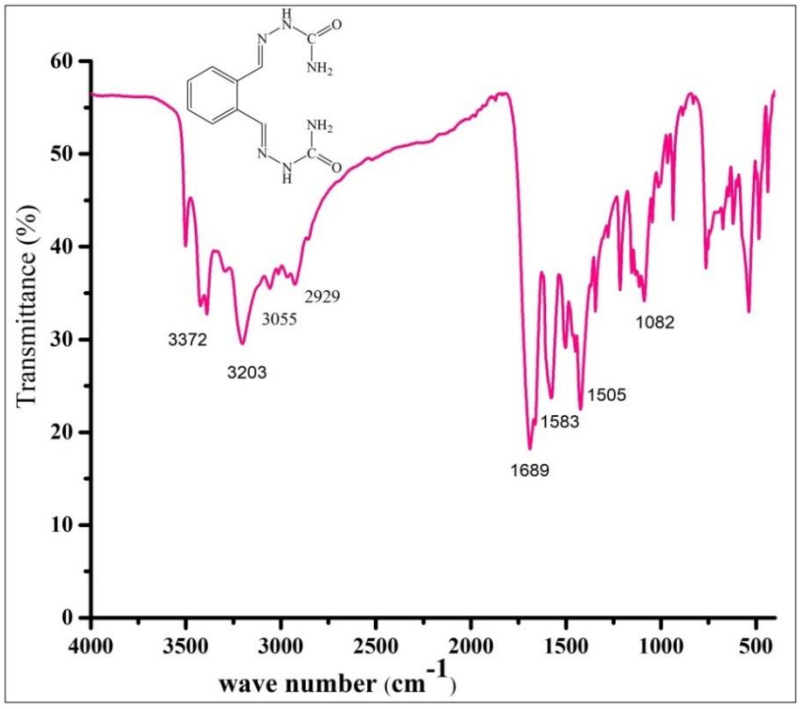

Figure 28. FTIR spectrum of *ortho*-phthalaldehyde disemicarbazone ligand (**L4**)

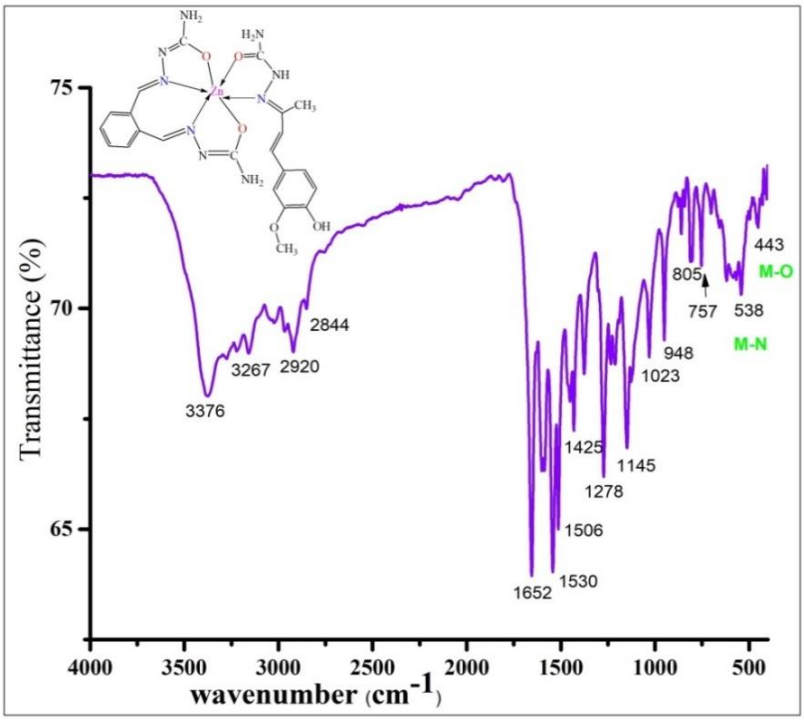

Figure 29. FTIR spectrum of [Zn(L1)(L4)] complex 9

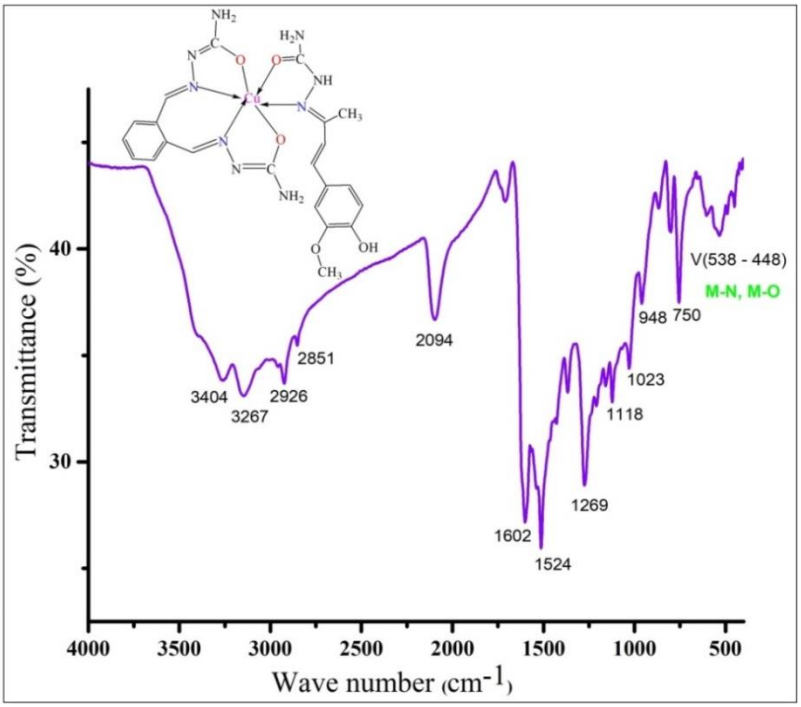

Figure 30. FTIR spectrum of [Cu(L1)(L4)] complex **10**

4.2.3. Electronic spectra analysis

UV-Vis spectra are associated with electronic transitions of the molecules that absorb energy in the form of ultraviolet or visible light going from the ground electronic state into excited states. The UV-Vis spectra of the ligands and their metal complexes were recorded at a wavelength between 200 - 800 nm using 1×10^{-5} M DMSO solution as a solvent of the sample at room temperature and the spectra graphs were shown in Appendix 12-25. The UV-Vis absorption spectra were produced due to the electronic transitions from the highest occupied molecular orbital (HOMO) to the lowest unoccupied molecular orbital (LUMO) (Dejpasand, Saievar-Iranizad, Bayat, Montaghemi, & Ardekani, 2020). The obtained spectra for the prepared compounds showed bands due to ($\pi\rightarrow\pi^*$), ($n\rightarrow\pi^*$) transitions and in addition L→M or M → L charge transition in the metal complexes. But due to dominances of LMCT or MLCT, the d-d transitions were very small band or not visible or observed due to it is a forbidden transition. The n - π* transitions are weaker (less light absorbed) than those due to π - π* transitions (L. L. Li et al., 2012). When the UV-Vis spectra of the ligand were compared with the metal complexes, it undergoes bathochromic (red) and hypsochromic (blue) shifts under metal complexation. The shift of absorption to a longer wavelength (lower frequency) due to some effect is called Bathochromic shift and to shorter wavelength (higher frequency) is called hypsochromic shift. These shifts are indications of the formation of the targeted metal complexes when compared with free ligands.

4.2.3.1. UV-visible spectra of L1, L2, and their homoleptic metal complexes

The UV-Vis spectra of the newly prepared ligands **L1** and **L2** displayed absorption bands in their ultraviolet spectra between 200 – 800 nm. The spectral band of **L1** represented in Appendix 12 shows peaks at 309 nm and 332.6 nm. The peak recorded at 309 nm was for the π→ π* transition in the benzene ring and the peak at 332.6 nm was assignable to n – π∗ transitions of non-bonding electrons on the nitrogen of (-HC=N-) group (F. Ommenya et al., 2020).

The zinc(II) complex (**1**) displayed an absorption band at 234, 266, and 332 nm, which undergo hypsochromic (blue) shift from 308 nm and 332.6 nm of L1 corresponds to π→ π* and n - π∗ transitions (Appendix 13). In addition to these transition bands, the broad band observed at 332 nm, for the complex may be assigned to Metal to Ligand charge transfer (MLCT). This might be due to the dominance of inter-ligand electron transition. These can confirm the ligand might be participated in metal complex formation which is in agreement

with the previously reported studies (F. Ommenya et al., 2020). Similarly, a copper complex of **L1** shows observed absorption peaks at 211 nm and 264 nm which experience hypsochromic (blue) shift corresponding to π→ π* and n – π∗ transitions (Appendix 14). The other absorption band observed at 332 nm was attributable to the transfer of charge from metal to ligand (MLCT) (Mahdi & Karem, 2018).

The nickel(II) complex of **L1** also shows absorption bands at 275 nm and 315 nm corresponding to π→ π* and n – π∗ transitions respectively that occur in the coordinated ligands but undergo bathochromic (red) shifts under metal complexation at 370 nm, which corresponds to the ligand to metal charge transfer (LMCT) (Vogler & Kunkely, 2007) (Appendix 15).

The UV-Vis spectra band of the **L2** ligand also shows absorption bands 350 nm (Appendix 16) corresponding to n – π∗ transitions in the benzene ring and (-HC=N-), of the imine bond.

The UV-Vis spectra revealed that broad bands at 415 nm for the zinc complex (**4**) and for the copper complex (**5**) at 408, 452, and 511 nm, which occurred due to the metal ions have many d –electrons, and they are good in forming MLCT (through back donation) metal to ligand charge transfer (Appendix 17 and 18). Zinc (II) complexes possess a 3d filled orbital with no d-d absorption spectra bands and display metal to ligand charge transfer (MLCT) possibly due to back donation ability of carbonyl carbon. Zinc(II) complexes are usually diamagnetic and commonly tetrahedral geometry (Ekennia, Onwudiwe, Olasunkanmi, Osowole, & Ebenso, 2015). But copper (II) complexes undergo Jahn-Teller distortions possessing complicated spectra bands in the visible region. Copper (II) complexes of regular octahedral geometry usually have single broadband above 10,000 cm^{-1} endorsed to $^2E \rightarrow {}^2T_2$ transition, a tetrahedral geometry usually has single broadband below 10,000 cm^{-1} is endorsed to $^2T_2 \rightarrow {}^2E$ transition (Ekennia et al., 2015). Within this study, the homoleptic copper (II) complexes of L1 showed absorption bands between 211 nm and 511 nm, which are described to the $^2E \rightarrow {}^2T_2$ transitions corresponding to the possible octahedral geometry (O. El-Gammal, 2015; M. Ghosh, Layek, Fleck, Saha, & Bandyopadhyay, 2015).

4.2.3.2. UV-Vis spectra of L3 and its complexes

The electronic emission spectra of the ligand (**L3**) and complexes **6**, **7**, and **8** have been also done in the range of 200 – 800 nm and recorded in DMSO. The UV-Vis spectra band of the ligand (**L3)** showed a peak near 294 nm which was for the ($\pi \rightarrow \pi^*$) transitions in the aromatic ring and the peak near 318 nm was indicated ($n \rightarrow \pi^*$) transitions of non-bonding (lone pair) electrons on the nitrogen of imine (-C=N-) group (F. K. Ommenya, 2021; Tada et al., 2011) (Appendix 19).

The complexes **7** and **8** displayed absorption spectra bands at 330, and 322 nm respectively, which undergo red shift and could be assigned to charge transfer from ligand to metal (M →L) (MLCT) (Alhadi, Shaker, Yehye, Ali, & Abdullah, 2012) (Appendix 20 - 23). The UV-Vis spectra result of Zn(II) complex (**6**) (Appendix 20) showed the $n \rightarrow \pi^*$ transition in the C=N bond of the ligand shifts from 294 nm to 335 nm after coordinating to Zn(II), metals. This shift is because of the back bonding from the metals to the C=O bond in **L3** and subsequently weaken the bond C=O energy (Mahmoud, Deghadi, & Mohamed, 2016). The observed maximum absorbance value of a single spectrum band at 335 nm is related to the transition state corresponding to octahedral geometry around Zn(II) metal(Abd El-Razek, El-Gamasy, Hassan, Abdel-Aziz, & Nasr, 2020).

The brown-colored $[Cu(L3)_2].3H_2O$ complex (**7**) exhibit a broad band at 330 nm (Appendix 21). A distorted octahedral geometry around the Cu(II) ion is confirmed by the occurrence of the broadness of the band that appears, which is explained using the Jahn-Teller distortion theory. Copper complexes usually undergo John-Teller distortions causing unusual spectra bands to occur in the visible region (Rao, Reddy, & Lingaiah, 1988). Furthermore, copper (II) complexes have shown a single broad band above 10,000 cm^{-1} allotted to the $^2E \rightarrow {}^2T_2$ transition which is for a regular octahedral in geometry (Rao et al., 1988). Thus, the copper complex showed absorption at 330 nm allotted to the $^2E \rightarrow 2T_2$ transition correspondence to octahedral in geometry which best fitted the proposed structure of the complex.

The $[Ni(L3)_2].4H_2O$ complex (**8**), displayed two absorbance bands observed at 275 and 306 nm undergo a shift that is assigned to transitions of an octahedral environment (Nagesh, Mahadev, & Mruthyunjayaswamy, 2015). The bands at 275 nm and 306 nm are attributable to the $\pi \rightarrow \pi^*$ and $n \rightarrow \pi^*$ transitions, respectively, (Gobara, 2017) (Appendix 22).

4.2.3.3. UV-Vis spectra of the heteroleptic complexes (9 and 10)

The **L1** spectra band shows two λ_{max} peaks; one observed at 309 nm for π→π* transition of an electron in the aromatic ring (F. Ommenya et al., 2020) and also spectra seen at 332.6 nm for n→π* transition of lone-pair electrons found on nitrogen (-HC=N) atom (Al-Noor, Al-barki, Maihub, & El-ajaily, 2017; Shaker, Nassr, Adam, & Mohamed, 2013). The observed spectra band of L4 represented by Appendix 23 showed λ_{max} peaks at 282 and 314.5 nm. The observed peak at 282.2 nm confirms the π→π∗ transition in the aromatic ring (benzene) and the one observed at 314.5 nm was assignable to n→π∗ transitions of nonbonding electrons on nitrogen (-HC=N-) atom. The Zinc(II) complex (9) showed only one spectra band that underwent a shift in comparison to the ligands (Appendix 24). Copper (II) complex of octahedral structural geometry usually has single broad band above 10,000 cm^{-1} (Li, Shi, Evans, & Findley, 2012). In addition, the broadband has shown around 354 nm for Cu(II) complex allocated to the ligand to metal (L→M) charge transfer (LMCT). These can be a confirmation of the involvement of ligands in the formation of complexes (Mandal, Das, Singh, Shukla, & Bharadwaj, 1997).

4.2.4. EDX-SEM analysis of the metal complexes (1-10)

The compositions of all the synthesized metal complexes were obtained from Energy Dispersive X-ray (EDX) analysis results. The EDX spectra of complexes (**1-10**) revealed distinct qualitative and quantitative indications of carbon, nitrogen, and oxygen compositions with their respective zinc, copper, and nickel metals.

4.2.4.1. EDX analysis of the homoleptic complexes (1-8)

The EDX spectrum of complexes (**1- 3)** showed five characteristic signals peaks which qualitatively correspond to C (carbon), O (oxygen), N (nitrogen), Cl (Chlorine), and metal atoms which indicated the composition of the complexes as CHZnNOCl, CHCuNOCl and CHNiNOCl (Figure 31 - 33). Similarly, the EDX spectrum of complexes (**4** and **5**) showed five characteristic signals which correspond to C (carbon), O (oxygen), N (nitrogen), and S (sulfur) together with Zn (zinc) and Cu (copper) atoms also support formation of CHZnNOS and CHCuNOS complexes (Figures 34 & 35).

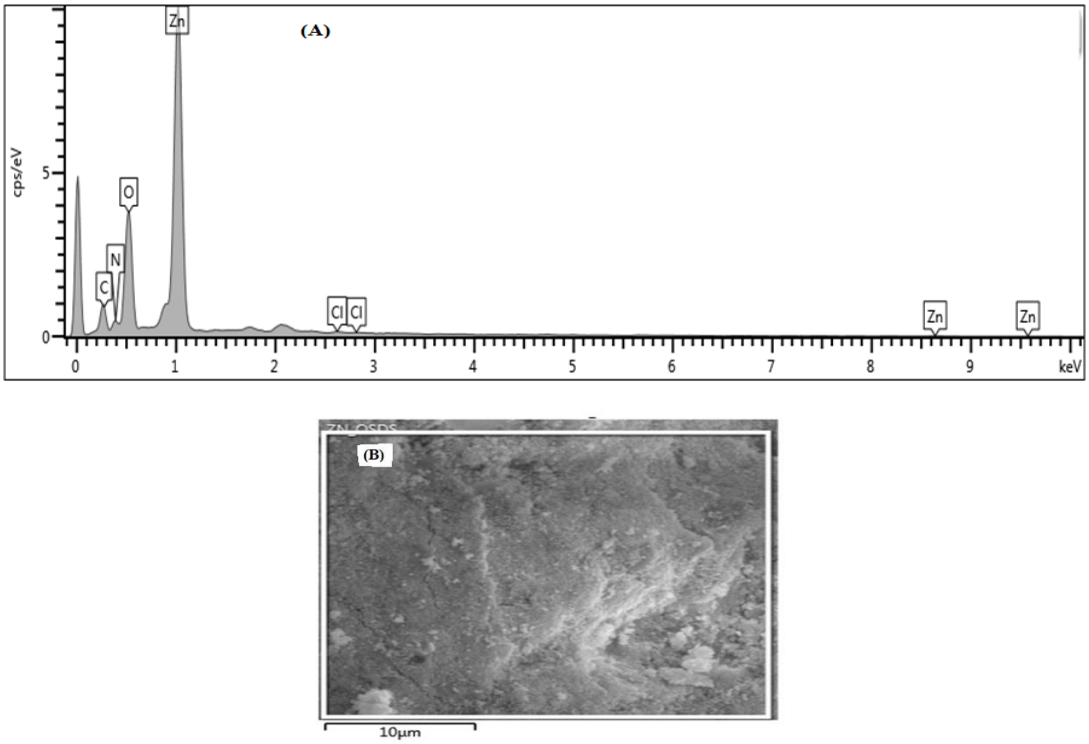

Figure 31. EDX spectrum (A) and SEM image (B) of $[Zn(L1)_2(Cl)_2]$ complex (**1**)

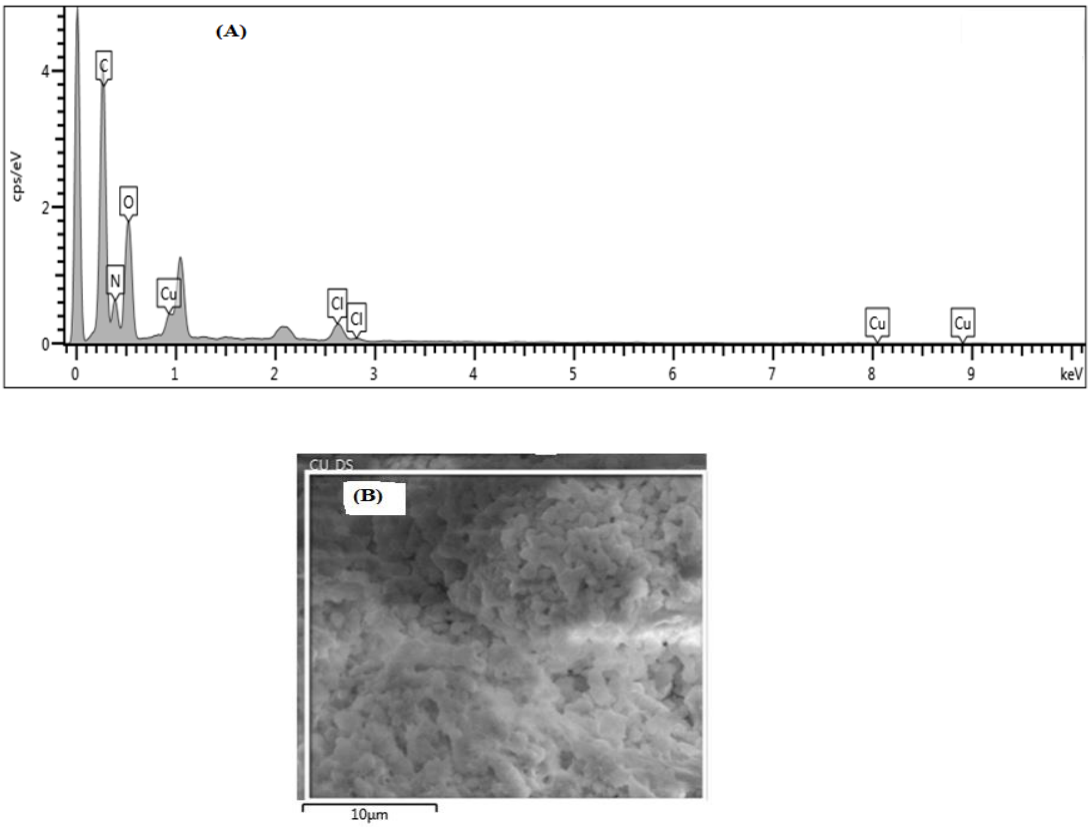

Figure 32. EDX spectrum (A) and SEM image (B) of $[Cu(L1)_2(Cl)_2]$ complex (**2**)

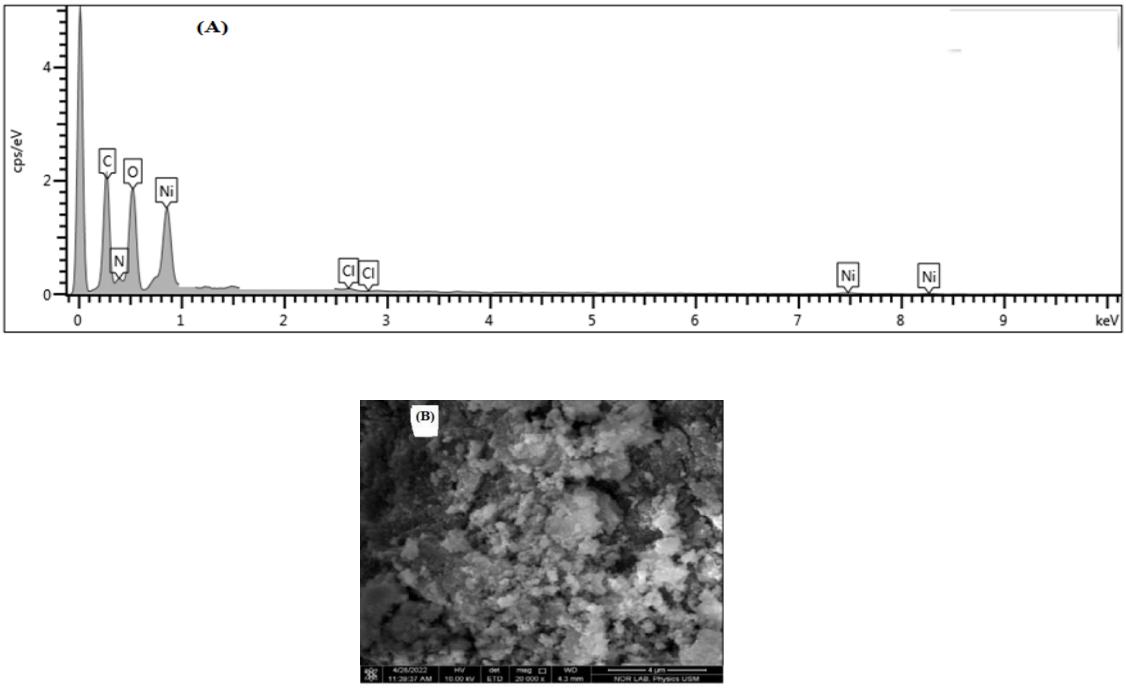

Figure 33. EDX spectrum (A) and SEM image (B) of [Ni[$(L1)_2$(Cl)] complex (**3**)

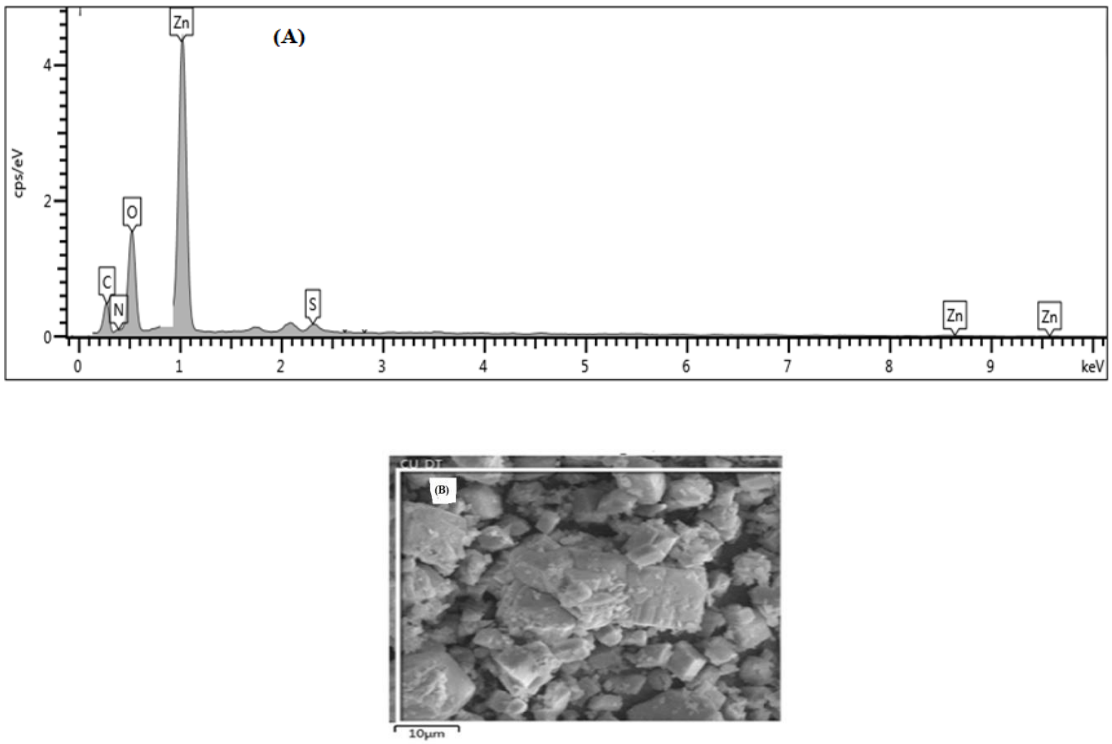

Figure 34. EDX spectrum (A) and SEM image (B) of [Zn$(L2)_2$] complex (**4**)

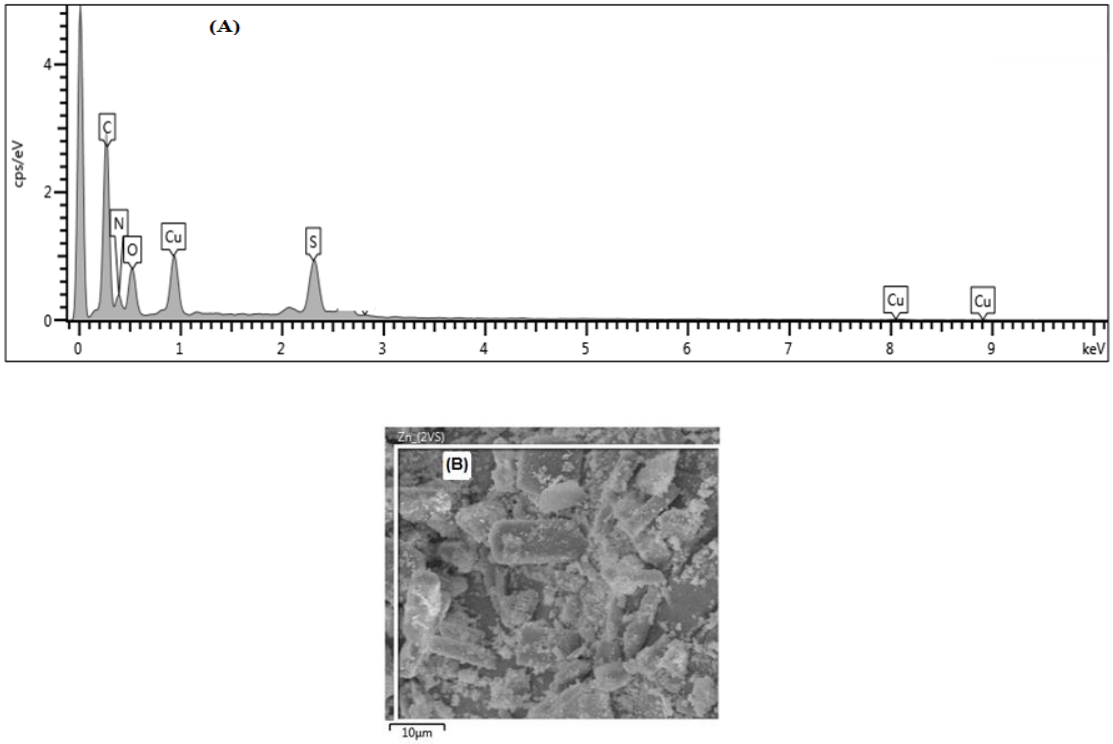

Figure 35. EDX spectrum (A) and SEM image (B) of $[Cu(L2)_2]$ complex (**5**)

The EDX spectrum of complex 6 displayed four characteristic major signals, which indicated the presence of carbon, nitrogen, oxygen, and zinc elements in the compound. This showed the Zn(II) complex with CHZnNO compositions (Figure 36). The EDX spectra of complex **7** similarly showed the characteristic signal confirming the presence of carbon, nitrogen, oxygen, and copper as the constituents of the complex. Therefore, it may be concluded that the complex was pure and contains only CHCuNO as a fundamental component (Figure 37). In the EDX graph of complex 8, the characteristic signals matched the carbon, nitrogen, oxygen, and nickel elements indicating the constituents of the complex as CHNiNO (Figure 38). The elemental analysis data as percentage composition in both experimental and theoretical values were observed to be very close to each other.

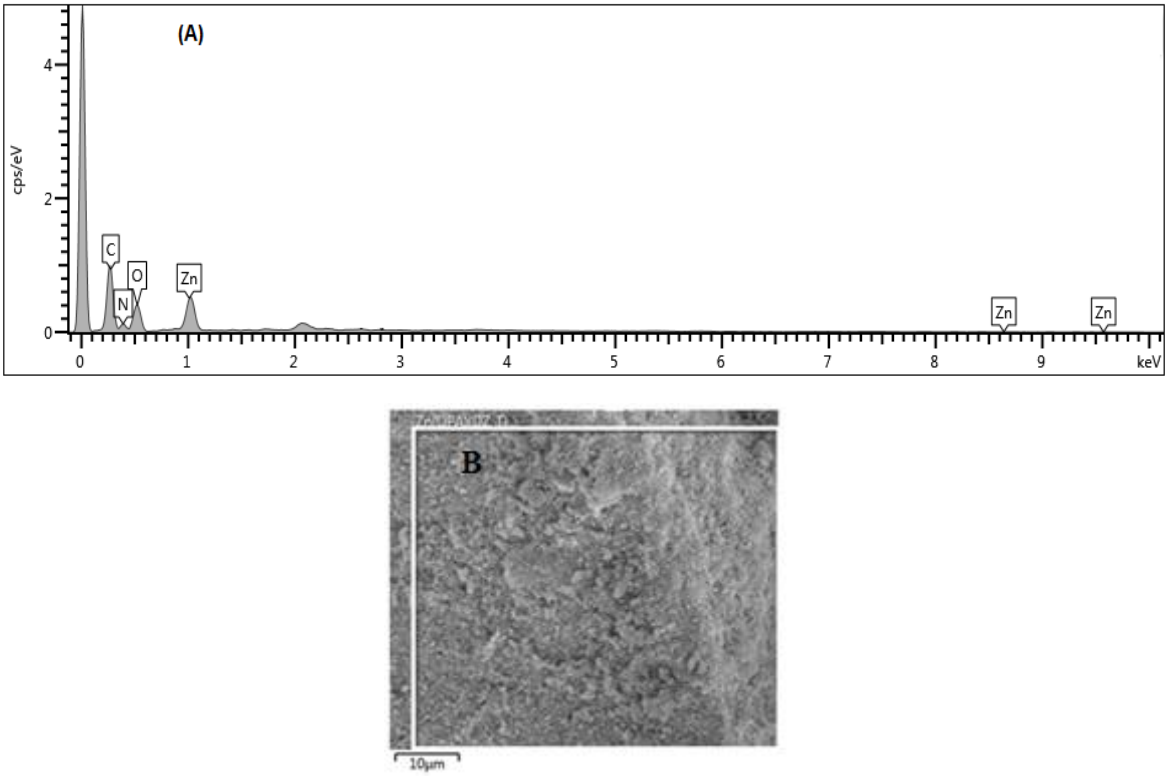

Figure 36. EDX spectrum (A) and SEM image (B) of complex 6

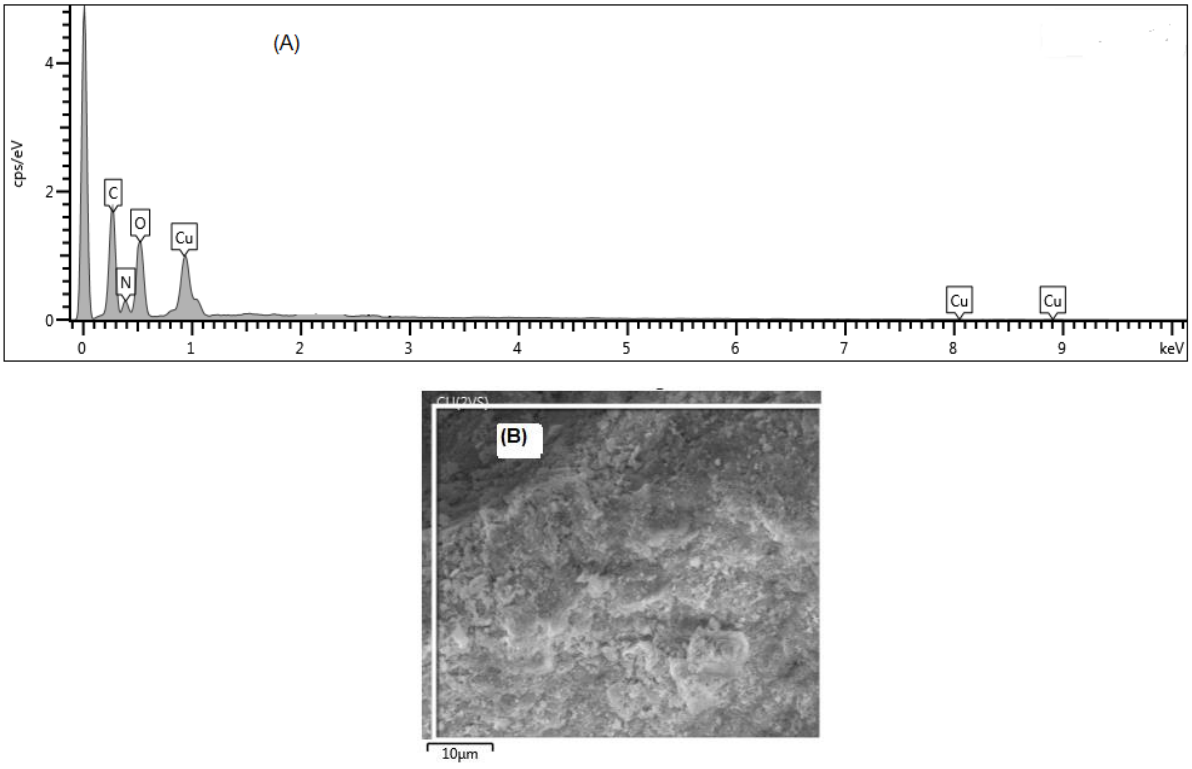

Figure 37. EDX spectrum (A) and SEM image (B) of complex **7**

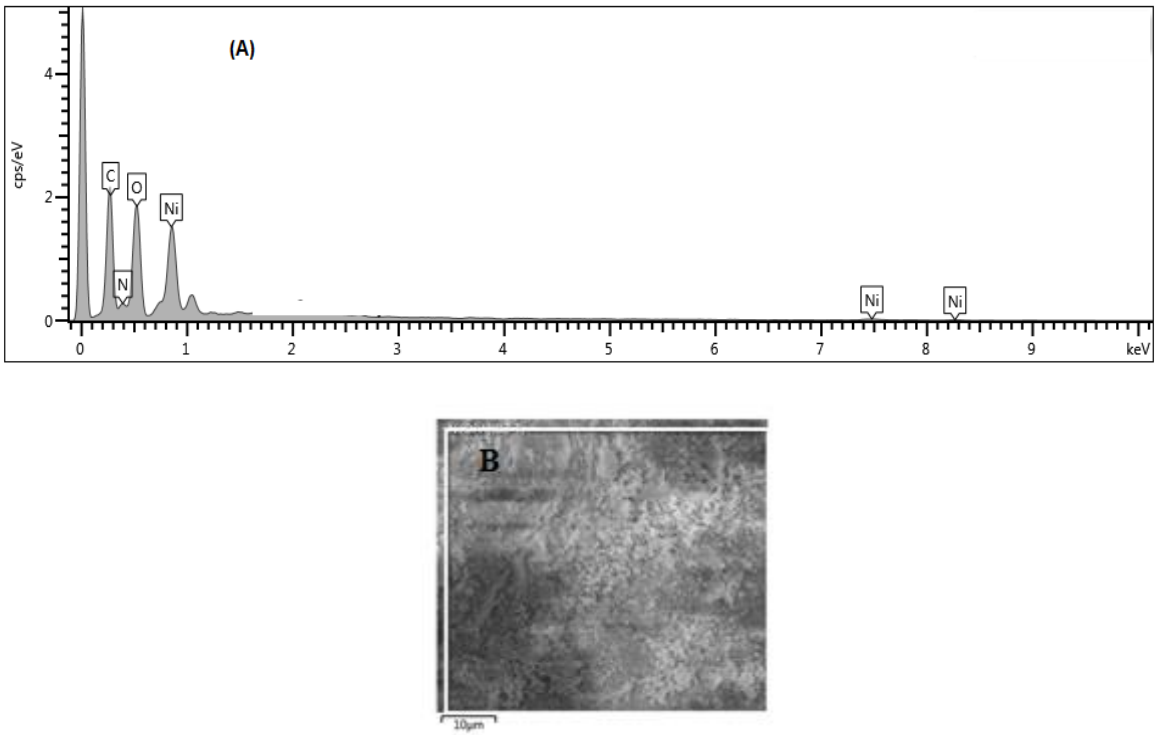

Figure 38. EDX spectrum (A) and SEM image (B) of complex **8**

The EDX spectra of the heteroleptic complexes, [Zn(L1)(L4)] **(9)** and [Cu(L1)(L4)] **(10)** showed distinct qualitative indications of carbon, nitrogen, and oxygen in both complexes as well as zinc and copper metals respectively. Thus, indicating that the complexes are composed of CHZnNO and CHCuNO elemental composition (Figure 39 and 40).

So, the EDX data of complexes showed that the ligands were complex with both copper and zinc metals in the samples (J. H. Lee, Ali, Kim, & Chung, 2017). Calculated and experimental values were found to be in good agreement.

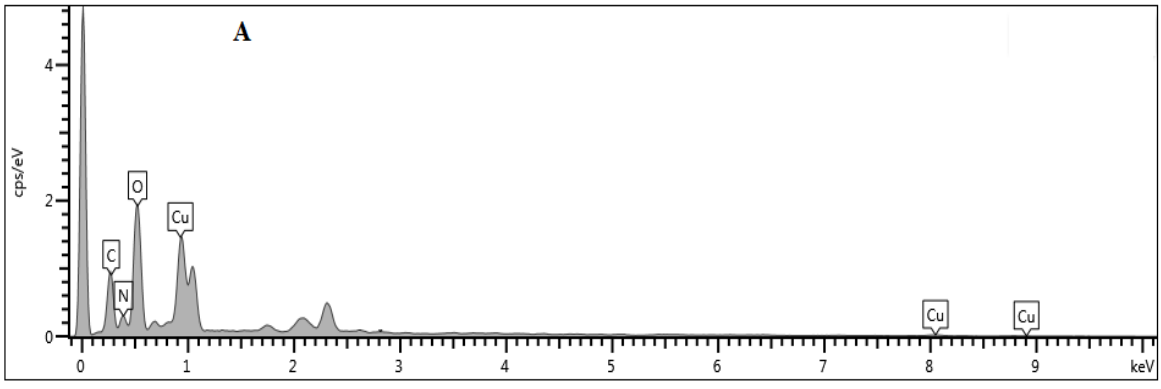

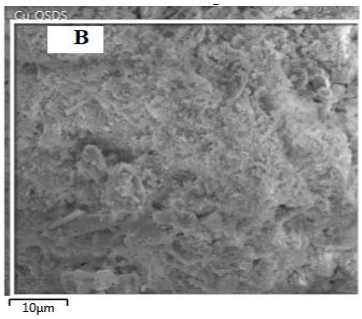

Figure 39. EDX spectra (A) and SEM image (B) of complex **9**

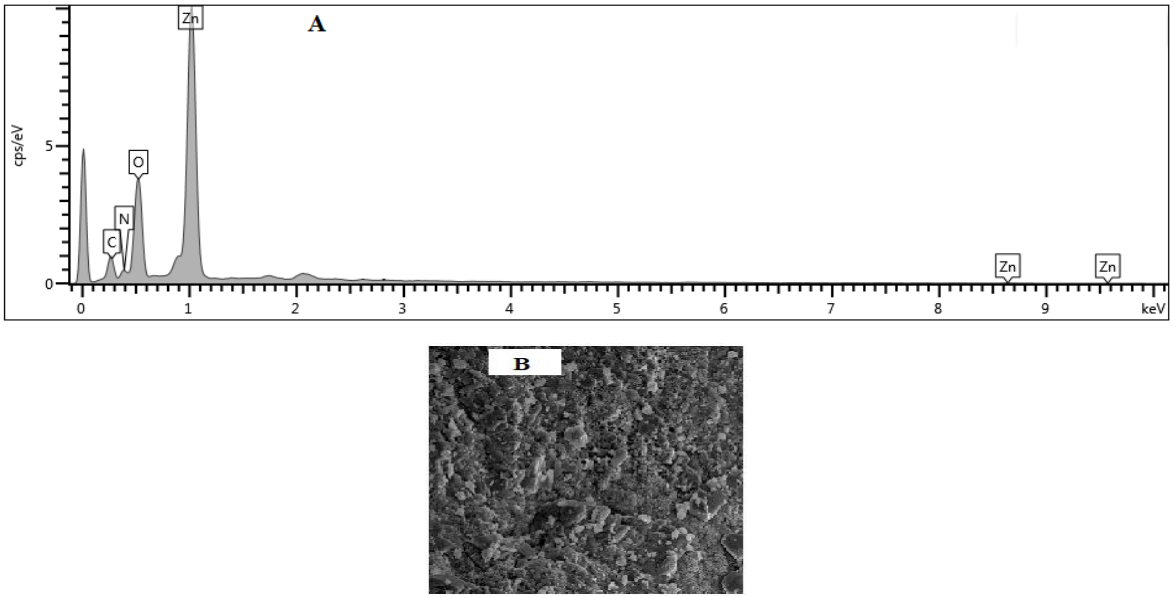

Figure 40. EDX spectra (A) and SEM image (B) of complex **10**

The SEM analyses were carried out to observe the surface morphology of the prepared metal complexes (**1-10**) and the micrographs obtained are given along with their EDX spectra. The micrograph of the complexes (**1-3**) is given in Figure 31(B) – 33(B). The images gave a rock-like appearance with numerous territorial patches. These facts revealed the amorphous nature with small crystal growth. On the other hand, the micrographs of complex 4 (Figures 34B) indicated amorphous like pattern of particles and complex 5 (figure 35B) indicated the presence of well-defined growth of crystals with a shadow of the metal ion on their external surface had a twisted fiber and grass-like morphology. The other complexes from **6 - 10** showed smaller crystals with more amorphous surfaces (Figure 36B – 40B). It is evident from the SEM study that in all the synthesized metal complexes, crystals were found to grow up from just a single molecule to several molecules in an aggregate distribution with particle sizes starting from a few nanometers to several hundred. In addition, different characteristic shapes of semicarbazone and thiosemicarbazone metal complexes were identified by the XRD spectra data, and these SEM images were quite supportive of the XRD data. The overall

SEM images obtained for the complexes exhibited the agglomerated nature of particles of the complex compounds and the powdered XRD graphs agreed with each other to confirm the amorphous nature of the structure for each complex.

4.2.5. Mass spectral analysis

Mass spectrometry (LC-MS) was used to investigate molecular species in solution (Prakash, Singh, Rajour, & Bhojak, 2010). The pattern of the mass spectrum gives an an information about the successive degradation of the target compound with a series of peaks corresponding to the various fragments. The recorded mass spectra of the complexes (**1-10**) and molecular ion peaks have been used to confirm the proposed formulae**.** The obtained mass spectrums at m/z values are similar to the formula weight of the studied complexes. They also showed important molecular fragmentations.

4.2.5.1. Mass spectral analysis of homoleptic metal complexes (1-8)

The mass spectrum of complex **1** shows a parent molecular ion peak at m/z = 634.11 which corresponds to the formula of $[C_{24}H_{30}N_6O_6ZnCl_2]$ (Mwt = 634.95 g/mol) (Appendix 26). The mass spectra of this complex displayed another peak at m/z = 455.10 which corresponds to the formula $[C_{13}H_{18}Cl_2N_6O_4Zn]^{2+}$ ion (Mwt = 456.01 g/mol) and other peaks at m/z = 266.09, and 189.02 assigned to the formula $[C_2H_6Cl_2N_5O_2Zn]^{3+}$ (Mwt = 265.92 g/mol) and $[C_{11}H_{12}NO_2]^{2+}$ (Mwt = 190.09 g/mol) fragmentations respectively.

The complex **2** spectra showed parent molecular ion peaks at m/z = 631.96 which corresponds to the formula of $[C_{24}H_{30}Cl_2N_6O_6Cu]$ (Mwt = 632.98 g/mol) (Appendix 27). It also shows other peaks at m/z = 595.05, 579.53, and 529.41, which corresponds to $[C_{24}H_3OClCuN_6O_6]^+$ (Mwt = 596.12 g/mol), $[C_{24}H_{28}ClCuN_5O_6]^{2+}$ (580.10 g/mol) and $[C_{24}H_{26}CuN_4O_6]^{3+}$ (Mwt = 529.52 g/mol) molecular ion fragmentations respectively.

The mass spectra of complex **3** exhibit a parent molecular ion peak at m/z = 591.14 which corresponds to the formula of the complex $[C_{24}H_{30}ClN_6]$ (Mwt = 592.68 g/mol) (appendix 28). The other peaks were observed at m/z = 561.10 and 542.68 which are assigned to the fragmentation part of the molecule $[C_{23}H_{27}ClN_6NiO_5]^+$ (Mwt = 561.11 g/mol) and $[C_{23}H_{27}ClN_6NiO_4]^{3+}$ (Mwt = 543.18 g/mol), respectively.

Complex 4 exhibit a parent molecular peak at m/z = 598.09 which corresponds to the molecular formula of $[C_{24}H_{28}N_6O_4S_2Zn]$ (Mwt = 596.09 g/mol). The other fragmentation peaks were observed at m/z = 521.21 and 250.12 which are assigned to $[C_{23}H_{26}N_4O_4SZn]^{2+}$ (Mwt. = 521.70 g/mol and $[C_{11}H_{11}N_3O_2S]^{2+}$ (Mwt = 251.05 g/mol) respectively (Appendix 29).

Complex **5** showed a parent molecular ion peak at m/z = 593.11 which corresponds to the exact molecular formula of the complex $[C_{24}H_{28}CuN_6O_4S_2]$ (Mwt = 593.89 g/mol) (Appendix 30). These analyses are in good agreement with the literature-reported studies on how to match with the proposed structure (Indira, Vinoth, Bharathi, & Bharathi, 2019; Tyagi et al., 2015).

Similarly, the mass spectra peaks of the homoleptic metal complexes of **L3** were analyzed, and the mass spectra of complexes $[Zn(L3)_2].2H_2O$ **(6)**, $[Cu(L3)_2].3H_2O$ **(**7**)** and $[Ni(L)_2].4H_2O$ (**8**) exhibit molecular ion peaks observed at m/e- = 783.18, 798.14 and 814.18 g/mol respectively which are similar to their molecular masses (784.17 g/mol, 801.18 g/mol, & 815.41 g/mol). This gives evidence for the exact formation of the complexes by coordination of Zn, Cu, and Ni metals with two moles of the ligand (**L3**) (Appendix 31-33).

The mass spectrum obtained for the $[Zn(L3)_2].2H_2O$ complex (**6**) (Appendix 31) exhibits a parent molecular ion peak at m/e- = 783.141, which is the same as the formula $[C_{34}H_{36}ZnN_6O_{12}]$ (Mwt = 784.17 g/mol). Removal of two (2) moles of lattice water (Mwt = 784.17 g/mole – 36.0012 g/mol = 748.18 g/mol. There are also important peaks showing the other fragmented parts. Fragmentation of $2CH_3O^+$ (Mwt. = 62.0368 g/mol) and the rest part of the compound is $[C_{32}H_{27}N_6O_8Zn]^+$, (Mwt. = 689.12 g/mole), this corresponds to the major ion peak observed at m/e- = 690.16.

The mass fragmentation peak for complex **7** (Appendix 32) exhibits a molecular ion peak at m/e- = 799.13 which is allotted to its molecular weight and is the same as the formula $[C_{34}H_{38}CuN_6O_{13}]$ (Mwt = 801.18 g/mol). The peak shown at m/e- = 764.44 correlates to the formula of the fragmentation ($[C_{34}H_{34}CuN_6O_{11}]$ (Mwt = 765.16 g/mol)], which happens due to loss of lattice water while the peak observed at m/e- = 750.03 was corresponds to the fragmented part of the complex with the molecular formula, $[C_{34}H_{34}CuN_6O_{10}]$ (Mwt = 749.15 g/mol) and the peak observed at m/e- = 739.60 correlates to the fragmented portion with the formula $[C_{33}H_{32}CuN_6O_{10}]^{2+}$ (Mwt = 740.04 g/mol), while the peak at m/e- = 683.54, which agrees to $[C_{30}H_{20}CuN_6O_{10}]^{2+}$ (Mwt = 686.05 g/mol).

The mass spectrum for the $[Ni(L3)_2].4H_2O$ complex **8** (Appendix 33) exhibits a parent molecular ion peak at m/e- = 814.18 g/mol, which is the same as the formula $[C_{35}H_{38}NiN_6O_{13}]$ (Mwt = 815.41 g/mol). The other molecular ion peak observed at m/e- = 590.37, corresponds to $[C_{30}H_{23}NiN_6O_4]^+$ (Mwt = 590.51 g/mol). There is also an important peak at m/e- = 542.68, which corresponds to $[C_{26}H_{24}NiN_4O_6]^{4+}$ (Mwt = 546.10 g/mol). The peak at m/e- = 441.15 corresponds to $[C_{19}H_{18}NiN_4O_5]^{4+}$ (Mwt = 440.063 g/mol). All these existences of fragmented parts of the complex confirm its real formation from the ligand with the proposed structures.

4.2.5.2. Mass spectral analysis of the heteroleptic complexes 9 and 10

The mass spectra of the [Zn(L1)(L4)] complex **9** showed a parent molecular ion peak at m/z = 559.10 corresponds to the formula of the complex $[C_{22}H_{25}N_9O_5Zn]$ (Mwt = 559.13 g/mol). The other molecular ion peak observed at m/z = 417.15 could be assigned to the fragmented mass of the formula $[C_{13}H_{23}ZnN_9O_3]^+$ (Mwt = 417.07 g/mol). The ion peak at m/z = 394.231 corresponds to the formula $[C_{13}H_{15}N_8O_3Zn]^{2+}$ (Mwt = 395.06 g/mol) and the peak at m/z = 353.27 is the same to the molecular formula of $[C_{12}H_{15}N_7O_2Zn]^{2+}$ (Mwt = 353.05 g/mol) (Appendix 34).

The mass spectrum of the [Cu(L1)(L4)] (**10**) complex exhibited a parent molecular ion peak at m/z = 557.0555, which is almost the same as the formula mass of the complex $[C_{22}H_{25}CuN_9O_5]$ (Mwt = 558.1275 g/mol) (Appendix 35). The other molecular ion peak observed at m/z = 529.4103, corresponds to the fragmented part with the formula $[C_{21}H_{24}CuN_9O_4]^+$ (Mwt = 529.11 g/mol). There are also important peaks at m/z = 498.21, which corresponds to $[C_{21}H_{19}CuN_7O_4]^+$ (Mwt = 498.479 g/mol), peak at m/z = 470.21, which relates to $[C_{21}H_{18}CuN_7O_3]^+$ (Mwt = 479.24 g/mol) and peak at m/z = 437.19 corresponds to $[C_{20}H_{17}CuN_6O_2]^+$ (Mwt = 436.071 g/mol).

4.2.6. Thermogravimetric Analysis

The thermal breakdown and stability of complexes were studied by a thermogravimetric analyzer (TGA) and differential thermogravimetric analysis (DTA), which were carried out for the homoleptic and heteroleptic Zn(II), Cu(II), and Ni(II) complexes in ambient condition. The TGA and DTA graph gives useful geometrical information for complex compounds encompassing the coordination sphere.

4.2.6.1. Thermogravimetric analysis of homoleptic metal complexes

The TGA/DTA data for the homoleptic complexes were summarized in Table 5 and the thermogram graphs were shown in Figures 41-50.

Table 5. Thermogravimetric analysis data of homoleptic metal complexes.

Complexes	Temperature of TGA (°C)	Temp of DTA	Weight loss (%)		Assignments
			Calc.	Found	
$[Zn(L1)_2(Cl)_2]$ **(1)**	225 – 280	254	11.2	11	loss of coordinated chlorine
	280 – 449	290	36.6	36.72	loss of $[C_{12}H_{15}N_3O_2]$ moiety
	450 – 730	646	36.7	36.72	release of another L1 species
$[Cu(L1)_2(Cl)_2]$ **(2)**	160 – 252	221	11.2	11	loss of chlorine molecule
	253 – 387	290	36.7	36.71	loss of $(C_{12}H_{15}N_3O_2)$ moiety
	495.5 – 714	604	39.2	39	release of one L1
[Ni(L1)Cl] (**3**)	130 – 256	190	6	5.99	loss of one chlorine
	260 – 760	290	52	51.6	Complete release of ligand (L1)
$[Zn(L_2)_2]$ **(4)**	262- 380	314	32.05	32	loss of part of ligand (DZ)
	634-765	674	56.8	57	loss of DZ with thiol groups
$[Cu(L2)_2]$ **(5)**	230 – 343	242	39.5	39.8	loss of part of L2 ligand
	470 – 736	494.8	39.4	38.6	loss of coordinated L2 moiety
$[Zn(L3)_2].2H_2O$ **(6)**	60 – 120	100	6.72	6.70	Loss of H_2O molecule
	190 – 274	298	3.86	3.81	loss of $C_{17}H_{16}N_3O_4$
	274- 533	467	36.82	36.8	Loss of $C_{16}H_{14}N_3O_3$
$[Cu(L3)_2].3H_2O$ **(7)**	62 – 165	100	6.8	6.7	Loss of 3 x H_2O
	166 – 272	270	3.9	3.87	Loss of CH_3O^+
	273 – 533	491	30.8	30.7	loss of $2(C_7H_7O_2)$ moiety
$[Ni(L3)_2].4H_2O$ **(8)**	56 – 160	262	6.77	6.8	loss of $3xH_2O$
	250 – 347	353	20.95	21	loss of $C_8H_8O_2$ & CH_3O
	347 – 590	482	30.86	30.8	Loss of $2C_7H_7O_2$

The TGA graphs of the complexes showed decomposition stages involving a two or three-step process.

The TGA-DTA graph of complex **1**, $[Zn(L_1)_2(Cl)_2]$, showed that it starts to undergo decomposition from 225 °C, which indicated the absence of both lattice and coordinated water in the complex, which is in agreement with some reported literature reviews (B. Singh et al., 2006) (Figure 41). The TGA curve involves three major decomposition steps. At the initial step decomposition, it showed a mass loss of 11 % (cal. 11.2 %) indicated between the

ranges 225 - 280 ºC is due to the release of coordinated chlorine ion. The second decomposition stage between 280 - 449 ºC showed a higher mass loss of 36.6 % (calc. 36.7 %) was related to the loss of dehydrozingerone-semicarbazone moiety ($C_{12}H_{15}N_3O_2$). The third step decomposition showed another weight loss of 36.67 % (calc. = 36.7 %) attributed to the loss of the ($C_{12}H_{15}N_3O_2$) dehydrozingerone semicarbazone moiety between temperatures, 450 - 730 ^{o}C.

The DTA graph showed small peaks at 254 ºC and 290 ºC related to the release of coordinated chlorine molecules with the other parts of the coordinated ligands. Another broad peak decomposition was observed at 646 ºC and metal residues (zinc oxide residue) was left above 730 ^{o}C (Arshad, Khan, Masud, Arshad, & Ghani, 2000; Mahmoud, Mohamed, & El-Dessouky, 2014) (Figure 41).

The TGA - DTA graph of complex **2,** $[Cu(L1)_2(Cl)_2]$, involves three degradation steps which indicated a mass loss of 11.2 % (cal.11.22%) between 160 - 252 ºC with a DTA peak of 221 ºC observed at the first step decomposition related to the release of a coordinated chlorine molecule, which is in agreement with previous studies of decomposition temperature range of chlorine (Nagesh, Raj, & Mruthyunjayaswamy, 2015; Sharma, Mehta, & Shah, 2013) (Figure 42). The second stage degradation showed mass loss of 36.7 % (36.71 %) between the ranges 253 - 387 ºC corresponding to a release of fragmented part of the ligand ($C_{12}H_{15}N_3O_2$) moiety. The DTA graph exhibited peaks at 290 ºC which could be related to the release of a fragmented part of the ligand. The third step of degradation occurs in the temperature range of 495.5 - 714 ^{o}C (DTA = 604 °C) and is accompanied by a weight loss of 39 % (calc. = 39.2 %) corresponding to the complete loss of one **L1** ($C_{12}H_{15}N_3O_3$) species of the coordinated semicarbazone ligand, while at 604 ºC the sharp intense peak was assigned for complete decomposition (Ambala & Lincoln, 2020; Jirjees et al., 2021) (Figure 42). Then above 725 ^{o}C the complex is left as copper oxide residue (Elsayed, Noufal, & El-Hendawy, 2017).

The TGA-DTA graph of complex **3**, $[Ni(L1)_2Cl]$, indicates two decomposition steps (Figure 43). The first step of degradation was observed due to a mass loss of 6 % (calc. = 5.99 %) related to the elimination of one chlorine atom (Cl) in the temperature ranges of 130 - 256 ^{o}C (Azimi et al., 2021). The second stage degradation of 52 % (calc. = 51.6 %) in the

temperature range of 260 - 760 ^{o}C (DTA_{max} = 290 °C), which corresponds to the elimination of $2C_9H_9O_2^-$ moiety and others left as metal residue (Badwaik, Deshmukh, & Aswar, 2009).

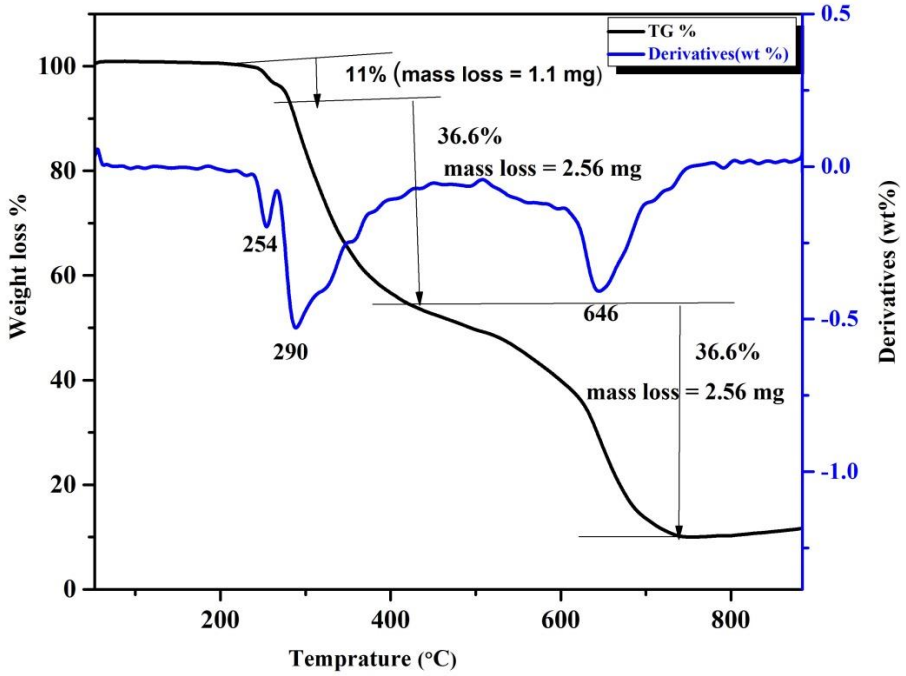

Figure 41. TGA - DTA curves of $[Zn(L1)_2(Cl)_2]$ complex (**1**).

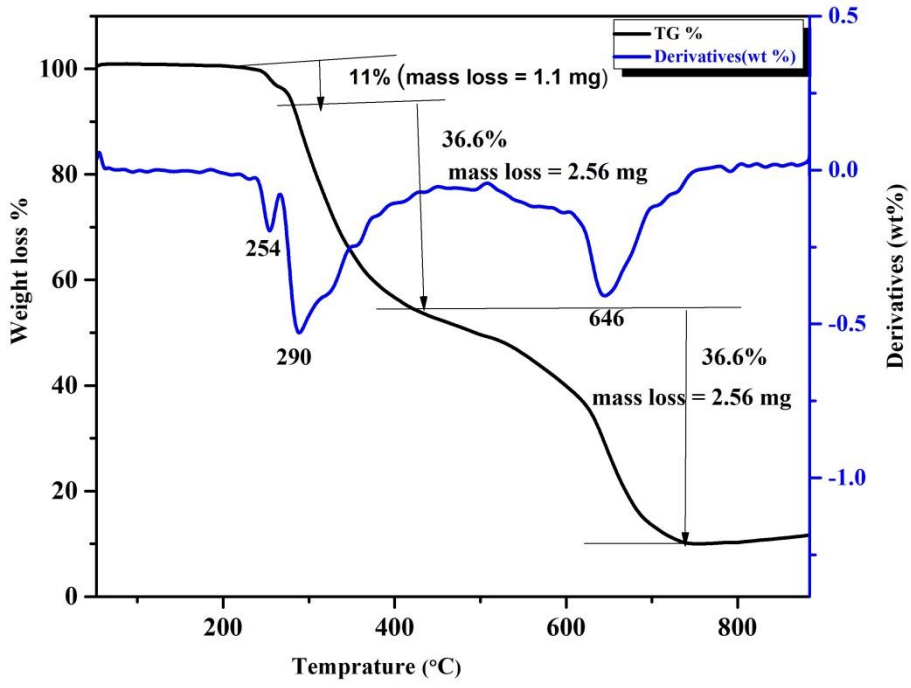

Figure 42. TGA - DTA curves of $[Cu(L1)_2(Cl)_2]$ complex (2).

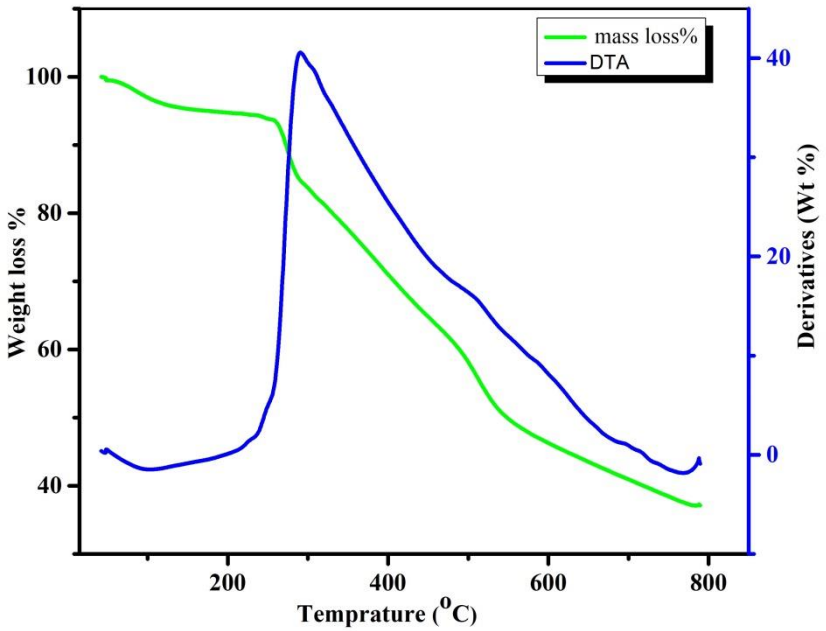

Figure 43. TGA - DTA curves of $[Ni(L1)_2Cl]$ complex (3).

The thermal decomposition of complex **4**, $[Zn(L2)_2]$, indicated a total mass loss of 32.05 % (cal. 32 %) which was observed at the initial stage decomposition between 261.7 - 380 ºC, corresponds to the release of the coordinated part of the ligand (dehydrozingerone). The second stage decomposition indicates mass loss of 57 % (cal. 56.8) between 634 - 764.7 ºC indicating the release of dehydrozingerone with thiol (-$NHCSNH_2$) groups lifting the metal residues (Paul & Hossen, 2020; Zemede, Nithyakalyani, & Kumar, 2015) (Figure 44). The DTA graph showed a large peak at 314 ºC representing a loss of the complex which is dehydrozingerone and a large intense peak located at 676 ºC may be its final decomposition stage (Figure 44). The metal oxide residue left above 750 ^{o}C (Badwaik et al., 2009; Sathis, Gandhi, Mageswari, Karthikeyan, & Sheriff, 2015).

Similarly, the thermal decomposition of complex **5**, $[Cu(L2)_2]$ exhibits two degradation steps (Figure 45). The first step of decomposition occurs in temperature ranges of 230 – 343 ^{o}C, (DTA = 242 °C) which is accompanied by mass loss of 38.6 % (calc. = 39.3 %) corresponding to the loss of coordinated L2 molecule ($C_{12}H_{14}N_3O_2$) (Refat, El-Deen, Anwer, & El-Ghol, 2009). The second decomposition stage between 470 – 736 ºC related to a release of another part of the ligand, which is dehydrozingerone moiety. The DTA graph of the complex showed a peak at 242 ºC followed by 495 ºC for complete decomposition of the complex. The DTA graph, also showed peak at 648 ºC related to the final decomposition

stage and remaining as the metal residues (Figure 45) (Meena, Meena, Kumari, Sharma, & Fahmi, 2023)..

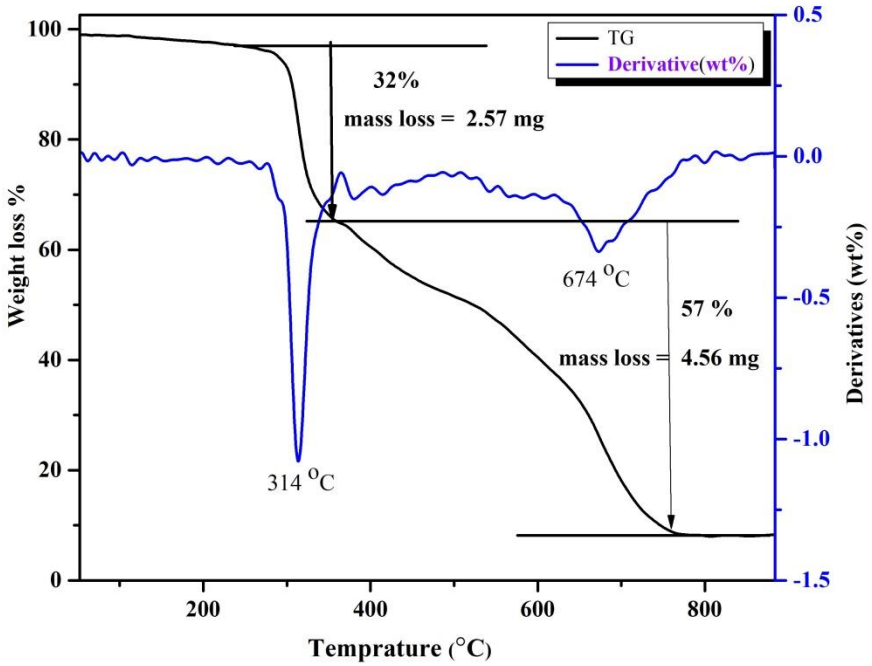

Figure 44. TGA - DTA curves of $[Zn(L2)_2]$ complex (**4**)

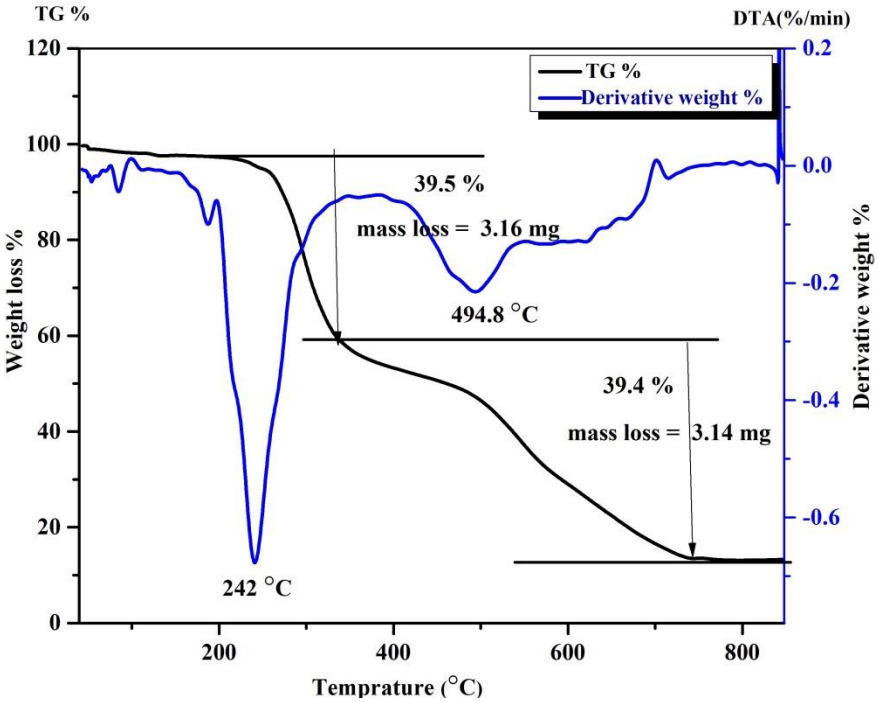

Figure 45. TGA - DTA curves of $[Cu(L2)_2]$ (**5**)

The thermal decomposition and stability of the other homoleptic L3 metal complexes, $[Zn(L3)_2].2H_2O$ **(6)**, $[Cu(L3)_2].3H_2O$ **(7)** and $[NiL3)_2].4H_2O$ **(8)** were also studied and the TGA/DTA graph of the complexes show a starting stage of endothermic decomposition which indicate the release of coordinated or lattice water molecules as presented in Table 5. By TGA the stability ranges, percentage of weight loss, and percentage of the residue obtained after the decomposition process have been studied. The complexes were start to decompose thermally at 60 ^oC, 62 ^oC, and 52 ^oC respectively, confirming that there are lattice water molecules within the complexes, due to the fact that when complexes undergo decomposition below 100 ^oC, it is an indication of the existence of lattice water molecule (Badwaik et al., 2009).

Accordingly, the thermogravimetric analysis (TGA) diagram of complex **6**, $[Zn(L3)_2].2H_2O$, showed mass loss of about 6.7 % (calc. 6.72 %) at the initial stage of decomposition between temperature range 60 - 120 ^oC, confirming the release of lattice water molecules from the complex (Ali, Elasala, Mohamed, & Kolkaila, 2019; K. D. Patel & Patel, 2017). At the second decomposition stage, another mass loss of 3.8 % (calc. 3.82 %) between the temperature range 190 ^oC - 274 ^oC with an endothermic peak of 298.8 ^oC occurred, which corresponds to the loss of the CH_3O group from the complex. In the third step of decomposition, the major mass loss of 36.8 % occurred between temperature ranges of 274 ^oC -533 ^oC. This corresponds to a loss of part of the ligand ($C_{16}H_{14}N_3O_3^-$) moiety. The final stage of decomposition above 533 ^oC remains with the metal residues (Figures 46) (Sangeeta et al., 2018; Sharma et al., 2013).

The TGA thermal decomposition of complex **7**, $[Cu(L3)_2].3H_2O$, exhibits three degradation steps (Figure 47). The first step of decomposition occurs in temperature ranges of 62 – 165 ^oC, (DTA_{max} = 100 °C) which is accompanied by mass loss of 6.8% (calc. = 6.75 %) corresponding to the loss of three lattice water molecules (Nguyen, Pham Thi, Bui, & Nguyen, 2023). The second step of decomposition occurs in between temperature ranges of 165 - 272 ^oC (DTA_{max} = 270 °C), which is accompanied by a mass loss of 3.9 % (calc. = 3.86 %) corresponding to the loss of CH_3O^+ moiety. The third and final step decomposition occurs between temperature ranges of 273 – 533 ^oC (DTA_{max} = 491 °C), which is due to the loss of dehydrozingerone ($2C_7H_7O_2$) ring moiety, which is 30.8% (calc. = 30.7 %). The other

remained as metal residues above 533^{o}C (Chioma & Don-lawson, 2021; Elsayed et al., 2017) (Figure 47).

Similarly, the TGA graph of [Ni(L3)$_2$].4H$_2$O complex **8** showed a mass loss of 6.8 % (calc. 6.77 %) at the first stage of decomposition between 56 - 160 ^{o}C with an endothermic peak of 152 ^{o}C. This mass loss corresponds to the loss of lattice water molecules from the complex. At the second step of decomposition, 21 % (20.95 %) mass loss occurred between the temperatures 250 - 347 ^{o}C, corresponding to the release of two species together ($C_8H_8O_2$ & CH_3O) group. At the third stage, 30.8 % (calc. 30.86 %) mass losses occurred between 347 - 590 ^{o}C. Finally, the complex remained as metal residue above 590 ^{o}C (Elsayed et al., 2017; Omar, Mohamed, & Ibrahim, 2009; Zayed, Mohamed, & Hindy, 2015) (Figures 48). Overall, the fragmented parts obtained for the homoleptic complexes best fit with the formula (structure) proposed by the other characterization techniques**.**

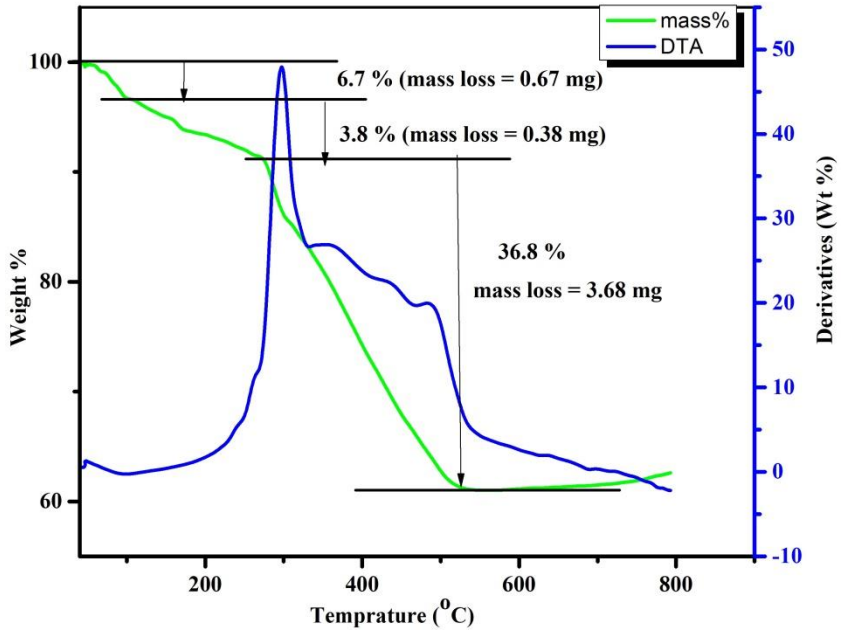

Figure 46. TGA - DTA curves of [Zn(L3)$_2$].2H$_2$O complex (**6**)

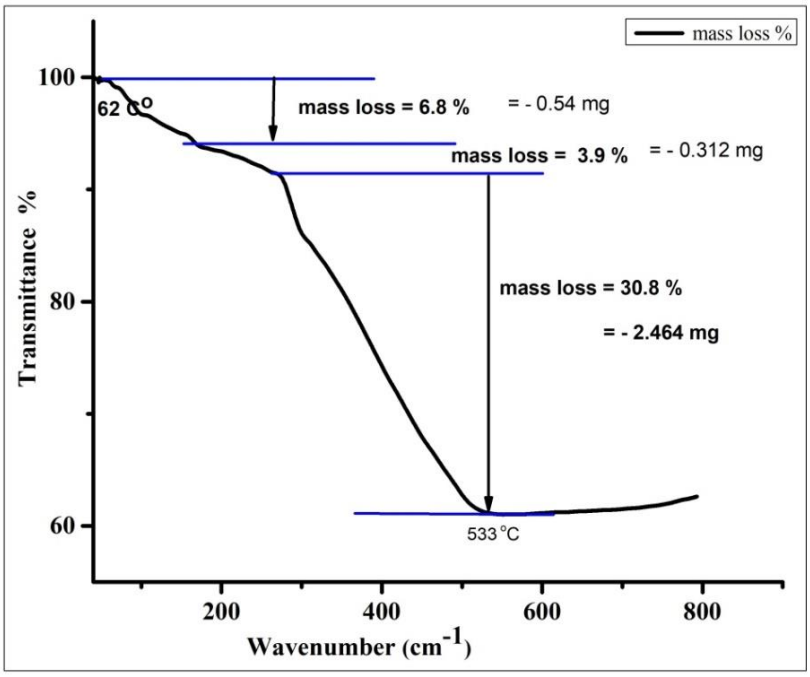

Figure 47. TGA curve of $[Cu(L3)_2].3H_2O$ complex (**7**)

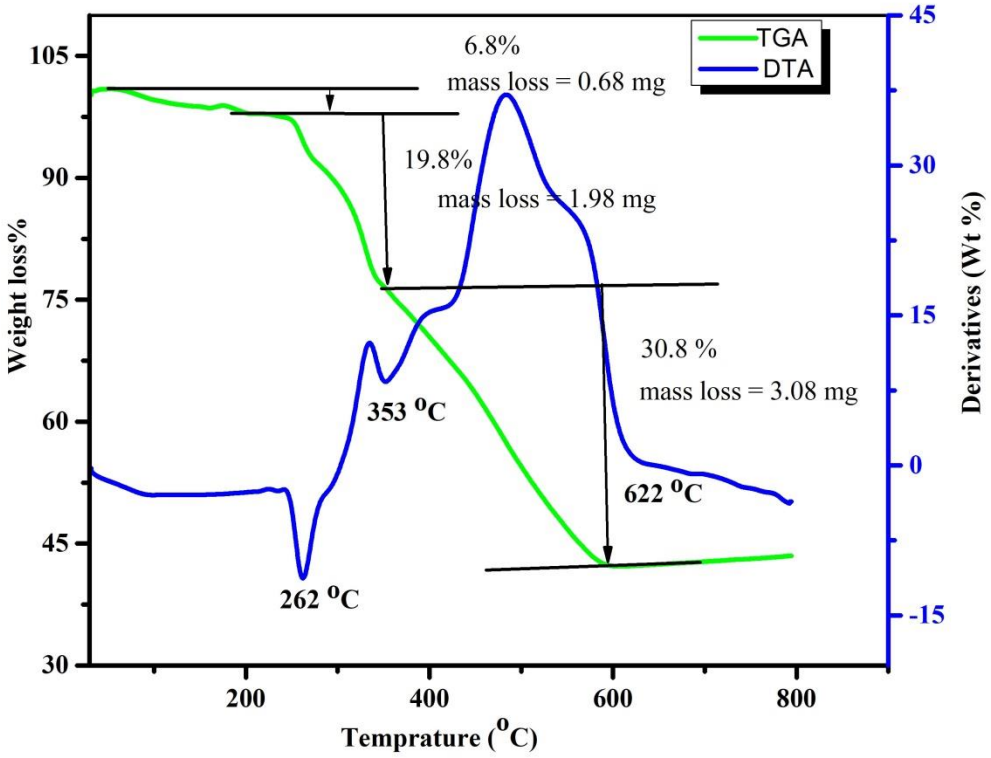

Figure 48. TGA - DTA curves of $[Ni(L3)_2].4H_2O$ complex (**8**)

4.2.6.2. Thermogravimetric analysis of the heteroleptic metal complexes

For the heteroleptic metal complexes, the thermogram curves of Zn(II) complex **(9)** and Cu(II) complex **(10)** shows no mass loss until 207 ^{o}C and 225 ^{o}C respectively, in which they are stable up to those temperatures. This could confirm that there is no possibility of either coordinated or lattice water molecules in the structure of the metal complexes. This is due to the fact that if there are lattice water molecules in the complex, decompositions may occur in temperature ranges of 40 ^{o}C - 120 ^{o}C and for coordinated water molecules until 180 ^{o}C (Deshmukh, Yaul, Bhojane, & Aswar, 2010; Yaul, Dhande, Pethe, & Aswar, 2014). The collected TGA/DTA data were summarized in Table 6, and thermogram curves were shown in Figures 49 - 50.

Table 6. Thermogravimetric analysis data of heteroleptic complexes

Complex	**Temp range of TGA (^{o}C)**	**Temp DTA (Endo)**	**Weight loss (%)**		**Assignments**
			Calc	**Found**	
[Zn(L1)(L4)] (**9**)	207.1 – 394.1	312.3	34.3	34.2	Loss of $C_{14}H_{10}O_3$ moiety
	397.4 – 738.9	559.1	38.8	38.3	loss of fragmented L_1
[Cu(L1)(L4)](**10**)	225.2 – 313.9	291.2	44.4	44.5	loss of ligand L_1
	328.9 – 417.2	396.7	5.5	5.6	loss of NH_2 & CH_3
	497.4 – 586.8	516.2	21.0	21.8	loss of fragmented L4

The thermal decomposition of complex **9**, [Zn(L1)(L4)], exhibits two degradation steps (Figures 49). The graph shows the complex is stable until 207 ^{o}C and starts to decompose in a two-step process. The first stage decomposition showed a mass loss of 34.2 % (cal. 34.3 %) between temperature ranges of 207 - 394 ^{o}C (DTA_{max} = 312 ^{o}C), which corresponds to the loss of the $C_{14}H_{10}O_{3,}$ dehydrozingerone moiety. The second step of decomposition shows mass loss of 38.3 % (cal. 38.8 %) occurred between temperature ranges of 375 - 739 ^{o}C (DTA_{max} = 580 ^{o}C), indicating the release of fragmentation part of the $\mathbf{L_1}$ ligand. The rest is considered as metal residue above 740.5 ^{o}C (Horowitz, Tryon, Christensen, & Perros, 1965; Sharaby, 2007).

Similarly, the TGA curve of complex **10**, [Cu(L1)(L4)], indicates the complex is stable until 225 ^{o}C, after which it starts to decompose through a three-step process (Figure 50). At the initial stage, the graph showed a mass loss of 44.5 % (calc. 44.4 %) between temperature 225.2 - 313.9 ^{o}C with a DTA peak found at 239 ^{o}C and 292 ^{o}C (Figure 50) This

decomposition stage confirms the release of the coordinated **L1** ligand. The remaining succeeding steps at second and third weight losses were 5.6 % and 21.8 %, respectively, totaling up to 27.4 % (cal. 26.5 %) between 329 – 586.4 ºC (DTA_{max} = 396 ^{o}C), confirming the release of NH_2 and CH_3 species and some fragmented part of dehydrozingerone. The rest was metal residue above 586.4 ^{o}C (Figures 50). Therefore, the proposed formulas for this complex agree with the TGA data.

Overall, the thermogravimetric analysis results of the complexes were aligned with the postulated structure of formulae based on the various spectroscopic and analytical data. When comparing the melting points and stability of ligands that have been determined, it is feasible to deduce that metal complexes have a higher level of stability than their constituent ligands. As a result, the versatility of complexes is greater than that of the constituent ligands in terms of biological applications (Soroceanu & Bargan, 2022).

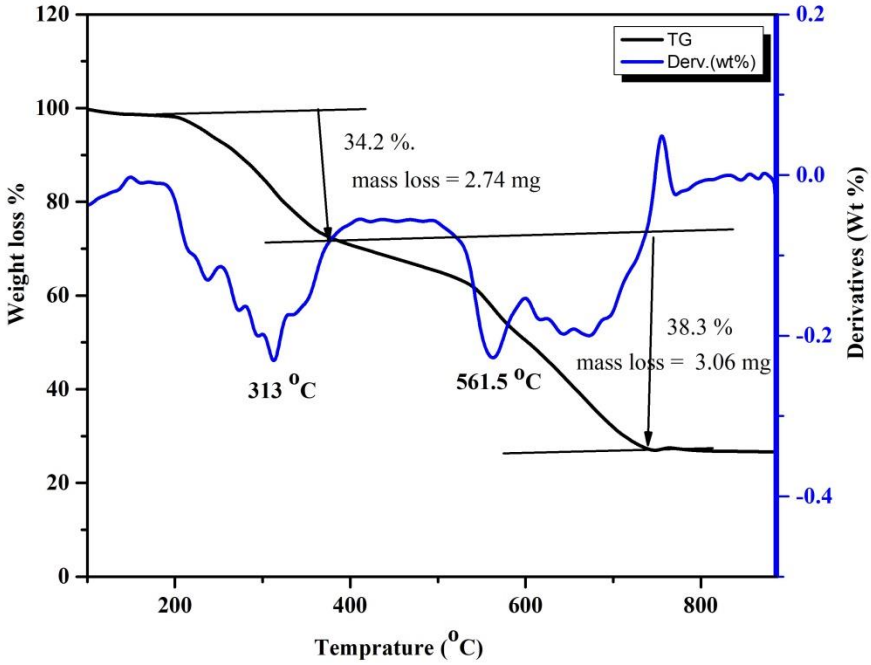

Figure 49.TGA – DTA curves of [Zn[(L1)(L4)] complex (9)

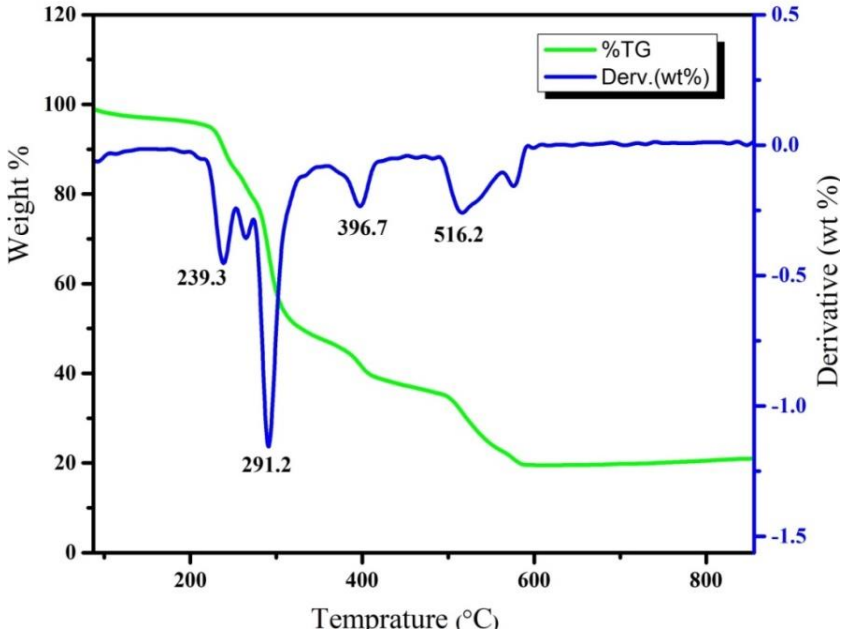

Figure 50. TGA - DTA curves of [Cu(L1)(L4)] complex (**10**)

4.2.7. Molar Conductance

The molar conductivity values of the complexes were measured in 10^{-3} M DMSO in triplicates at room temperature. The molar conductivity values for the prepared complexes (**1 - 10**) were between 4.5 - 18 Ω^{-1} cm^2 mol^{-1}, indicating the complexes are non-electrolyte. Complexes with molar conductance values below 60 $n^{-1}cm^2mol^{-1}$ are non-electrolyte complex (Geary, 1971; Ismael, Abdel-Mawgoud, Rabia, & Abdou, 2020; Mahyavanshi; Natvarlal). From this one can conclude that there were no anions present outside of the coordination sphere of the complexes. The values obtained might be caused by DMSO, which is a coordinating solvent causing the solvolysis process (Šimunková & Malček, 2020). The complexes may be formulated as $[M(Lm)_nX_n(H_2O)_n]$, Where M = Zn, Cu and Ni, Lm = **L1**, **L2**, **L3**, and **L4, n** = number of mole of species exist, while X = Cl^-, since chloride form of metal salts were used.

The conductivities of the prepared complexes were relatively low which is very low to account for their electrolytic behavior. This is mainly due to the fact that the metal cations shared negative charge density electrons from the ligand to make the net charge balance of the complexes to be zero in line with the previously reported studies (Mahmoud, Mohamed, Elsawy, & Radwan, 2018; Vivekanand, Raj, & Mruthyunjayaswamy, 2015; J. Wang et al., 2015). The molar conductance values are also important for the prediction or investigation of the geometrical structures of the complexes (El-Sonbati et al., 2020). According to the non-

electrolytic nature of the metal complexes specifically metal complexes possessing coordinated chlorine ions, the chloride ion is coordinated with the metal ion to satisfy the valence of the coordination sphere. Furthermore, the presence of chloride ions outside the coordination sphere of the specified complexes was confirmed by reaction with silver nitrate ($AgNO_3$) solution. During that time, there was no precipitate formation while conducting the experiment. Therefore, the formed Zn(II), Cu(II), and Ni(II) complexes would be formulated as $[Zn(Lm)_n(H_2O)_n(Cl)_n]$, $[Cu(Lm)_n(H_2O)(Cl)_n]$ and $[Ni(Lm)_n(H_2O)_n(Cl)_n]$ similar with previous literature reports (Ismael et al., 2020).

4.2.8. X-ray Diffraction Analysis of complexes

X-ray Diffraction is a technique employed to determine the underlying crystal structure of a compound; it enables verification of the crystallinity and structure of a sample. The crystalline nature of the complexes was studied by powder X-ray diffractometer (PXRD) with Cu Kα radiation. The data was recorded at 2θ ranging from 10 - 80^o at lambda (λ) value of 1.54 Å. The XRD analysis of complexes (**1 - 5**) was performed and shown in Appendix 36-40 and complexes (**6 - 10**) were shown in Figure 51-55 below. The patterns of complexes **3** and **4** have shown amorphous-like peaks particle nature but complexes (**1**, **2**, **5-10**) have shown polycrystalline nature of peaks due to the appearances of many diffraction peaks (A. El-Sonbati et al., 2019; Jirjees et al.). But complexes **1**, **2,** and **5** showed a little number of peaks of crystallinity nature. A polycrystalline sample should contain several crystallites. Therefore, all possible diffraction peaks should be observed. The average crystal size (Cs) was calculated using the formula developed by Debye Scherer (Nagesh, Raj, et al., 2015) (equation 5).

$$\mathbf{Cs} = \frac{\mathbf{K\lambda}}{\boldsymbol{\beta}\ \mathbf{COS}\ \boldsymbol{\theta}} \quad \ldots\ldots\ldots\ldots\ldots\ldots \quad (5)$$

where k = 0.94 is constant, λ = 0.154 nm (wavelength of XRD machine), β = width at half maxima of all peaks of XRD arrays while θ is Bragg angle (Jirjees et al.; Morgan, El-Sonbati, & Eissa, 2017). Accordingly, the average crystallite sizes of complexes **1, 2, 5, 6, 7, 8, 9,** and **10** are 26.72, 28.94, 24.00, 40.56, 18.40, 46.72, 54.64, and, 62.38 nm, respectively. On the other hand, the XRD pattern for synthesized metal complexes **3** and **4** shows broad peaks in the range of 2θ = 10 – 80^o (Appendix 38 and 39) and is due to the amorphous nature of the complexes which is in agreement with the previous studies (El-Sonbati, Diab, Eldesoky, Morgan, & Salem, 2019; Saikumari, 2021). The XRD patterns of $[Zn(L3)_2].2H_2O$ complex (6) shows diffraction peaks which are characteristic peaks for the monoclinic crystal system

with space group p121/c1 and lattice parameters 9.3510 Å, 8.6310 Å, 9.7630 Å, 90°, 98.580°, 90° for a, b, c, α, β and γ, respectively (Engelhardt, Kniep, R"udiger, Kristallographie, (1999)

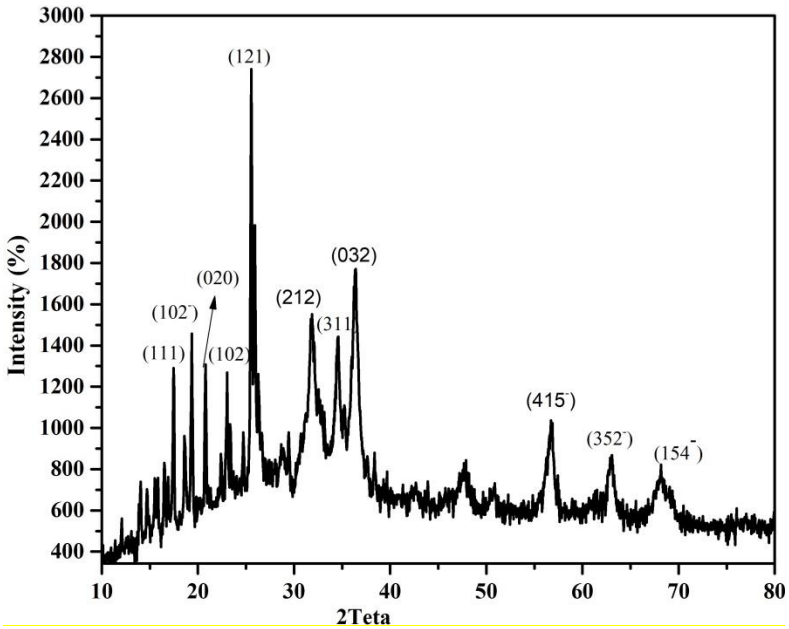

Figure 51. XRD patterns of $[Zn(L3)_2].2H_2O$ complex (**6**)

Similarly, $[Cu(L3)_2].3H_2O$ complex (7) was found to be a monoclinic crystal system with p12/cl space group and lattice parameters , 12.680 Å, 14.916 Å, 18.327 Å, 90°, 97.580°, 90° for a, b, c, α, β and γ respectively (Mueller-Bunz, Schleid, Allgemeine Chemie, (2000).

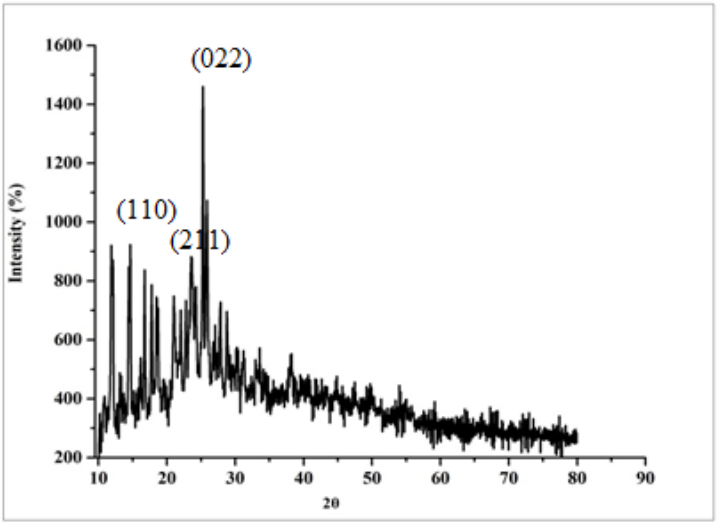

Figure 52. XRD patterns of $[Cu(L3)_2].3H_2O$ complex (**7**)

Complex 8, $[Ni(L3)_2].4H_2O$ was found to be a triclinic crystal system and p-1 space group together with lattice parameters, 8.987 Å, 9.065 Å, 10.723 Å , 84.44°, 70.23°, 71.89° respectively for a, b, c, α, β and γ (Zeitschrift f"ur Kristallographie, 2014) .

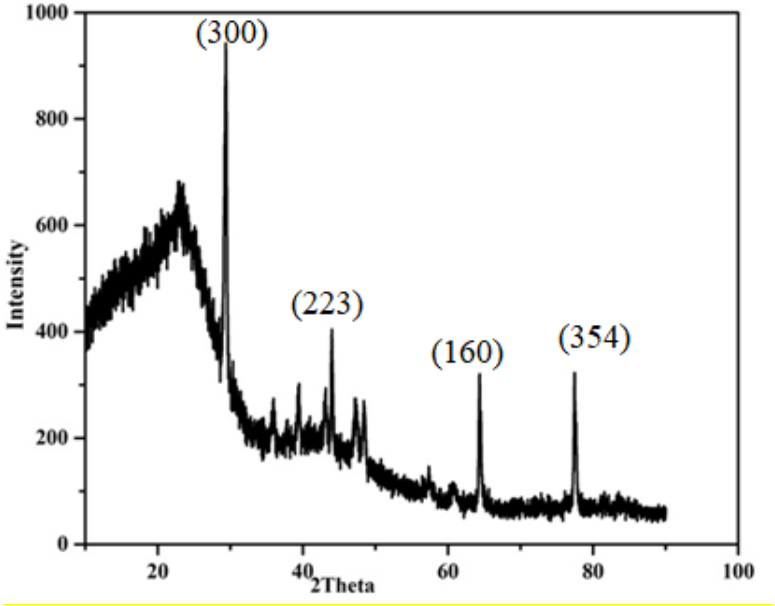

Figure 53. XRD patterns of $[Ni(L3)_2].4H_2O$ complex (**8**)

The [Zn(L1)(L4)] complex (9) was found to be monoclinic crystal system with p121/n1 space group and lattice parameters 7.3406 Å, 11.1655 Å, 10.4062 Å, 90°, 97.280° , 90° respectively for a, b, c, α, β and γ (Mueller-Bunz, H. Schleid, T., Zeitschrift fuer Anorganische und Allgemeine Chemie, 2000).

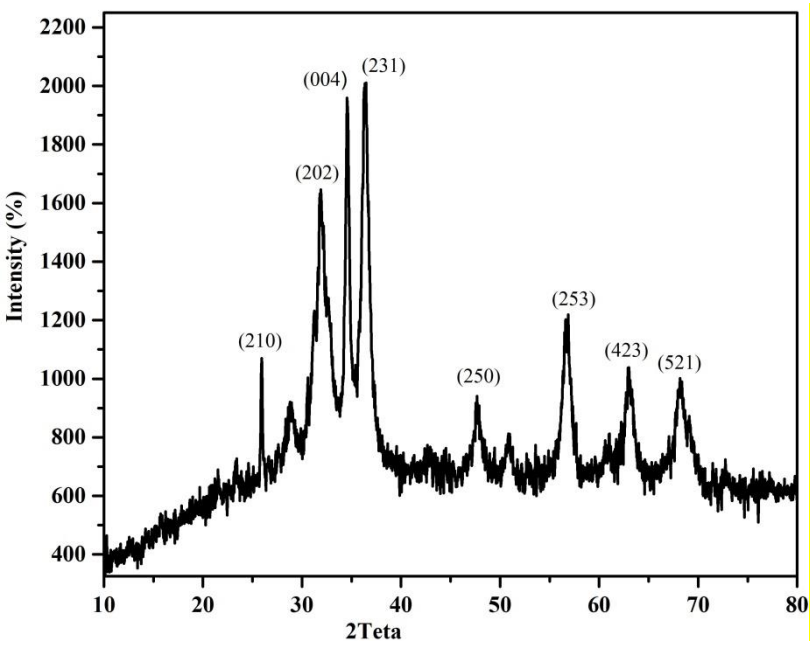

Figure 54. XRD patterns of [Zn(L1)(L4)] complex (**9**)

The XRD patterns of [Cu(L1)(L4)] (10) shows diffraction peaks which are characteristics peaks for the orthorhombic crystal system with space group pnma and lattice parameters 18.005 Å, 7.4970 Å, 11.7960 Å, 90°, 90°, 90° for a, b, c, α, β and γ respectively (Haddad, Amor Boughzala, Habib Jouini, Tahar, Acta Crystallographica Section C, 54 (1998).

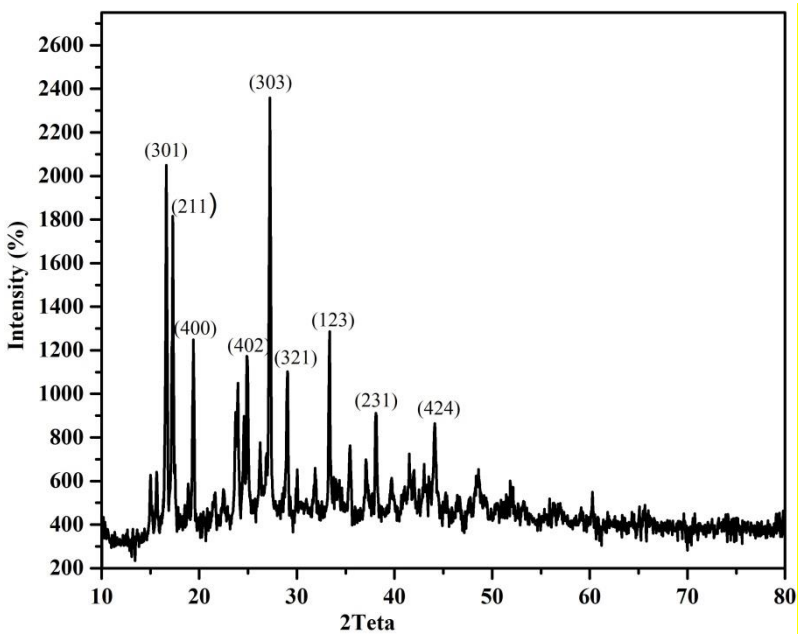

Figure 55. XRD patterns of [Cu(L1)(L4)] complex (**10**)

4.3. Biological applications of Ligands and their homoleptic and heteroleptic metal complexes

4.3.1. Antibacterial Activity studies

Intensive research reports indicate that both Gram-positive and Gram-negative bacteria species endure adaption and resistance towards known multi-drugs. This emergence of multidrug-resistant bacterial strains towards the existing antibiotics is one of the challenges and threats to public health recently. The concept of creating metal complexes with various bioactive organic ligands can be a crucial tactic to boost the effectiveness against developed resistance and, more importantly, to overcome the rising rate of microbial resistance to recognized antibiotics. Thus, in this study, we have synthesized homoleptic and heteroleptic zinc(II), copper(II), and nickel(II) complexes with semicarbazone and thiosemicarbazone derivative ligands of natural product constituent and synthetic products to evaluate their antibacterial activities against four different bacterial pathogens. Semicarbazones and thiosemicarbazones moieties are organic ligands characterized mainly by their bioactive constituent of an imine (–N=CH-) group. The imine group results in different mechanistic

reactions in biological systems. It makes the derivatives of these compounds to be active in a biological system. Thus, to develop more bioactive drug candidates against resistant bacteria pathogens, the newly prepared compounds were evaluated for their antibacterial activities on two Gram-positive (*Staphylococcus aureus* and *Streptococcus pyogenes)* and two-Gram-negative (*Escherichia coli* and *Pseudomonas aeruginosa*) bacteria pathogens. The zone of inhibition values of the studied ligands **L1**, **L2**, and their homoleptic complexes **1-5** have shown potential antimicrobial activity when compared to the standard drug Trimethoprim, and the obtained results were summarized in Table 7 and shown in Figures 56 and 57.

Table 7. Antibacterial activity data of compounds (by mm (mean ± SD of triplicates)

		Gram-negative		Gram-positive	
Compound	**Conc. *(µg/ml)***	***E. Coli***	***P. Aeruginosa***	***S. Aureus***	***S. Pyogenes***
L1	100	4.50 ± 0.24	3.50 ± 0.00	6.34 ± 0.42	6.64 ± 0.74
	200	5.44 ± 0.64	7.33 ± 0.64	8.68 ± 0.32	8.84 ± 0.92
L2	100	5.54 ± 0.34	6.34 ± 0.44	7.68 ± 0.22	8.64 ± 0.42
	200	8.54 ± 0.66	9.63 ± 0.54	8.68 ± 0.42	10.86 ± 0.82
$[Zn(L_1)_2Cl_2]$ **(1)**	100	7.52 ± 0.68	10.46 ± 0.44	9.67 ± 0.86	10.24 ± 0.74
	200	8.12 ± 0.64	10.89 ± 0.73	11.72 ± 0.64	11.67 ± 0.54
$[Cu(L_1)_2Cl_2]$ (**2)**	100	7.44 ± 0.55	8.4 ± 0.63	9.24 ± 0.89	10.12 ± 0.00
	200	8.50 ± 0.67	10.24 ± 0.84	10.66 ± 0.46	11.8 ± 0.63
$[Ni(L1)_2Cl]$ (**3)**	100	6.40 ± 0.52	5.50 ± 0.23	8.50 ± 0.47	8.40 ± 0.28
	200	7.50 ± 0.44	5.80 ± 0.13	10.50 ± 0.57	8.50 ± 0.36
$[Zn(L_2)_2]$ (**4)**	100	10.74 ± 0.46	11.48 ± 0.33	9.84 ± 0.29	11.21 ± 0.26
	200	13.94 ± 0.33	15.44 ± 0.31	12.64 ± 0.46	14.80 ± 0.23
$[Cu(L_2)_2]$ (**5)**	100	9.34 ± 0.73	8.45 ± 0.22	11.28 ± 0.79	12.12 ± 0.43
	200	11.78 ± 0.24	10.43 ± 0.68	13.67 ± 0.88	14.00 ± 0.20
Trimethoprim (standard drug)	100	14.69 ± 0.77	16.64 ± 0.84	13.05 ± 0.64	16.71 ± 0.62
	200	16.48 ± 0.46	18.26 ± 0.16	17.06 ± 0.57	18.34 ± 0.68

L1 = (4-(4-hydroxy-3-methoxyphenyl)but-3-en-2-one)semicarbazone

L2 = (4-(4-hydroxy-3-methoxyphenyl)but-3-en-2-one)thiosemicarbazone

The data in Table 7 revealed that all the prepared compounds had medium to good activity on the four bacterial species. The data also shows the complexes exhibited higher antimicrobial activities than the free ligands for all bacteria species at similar concentrations which is similar to literature reports (Sadeek, El-Attar, & Abd El-Hamid, 2013). Both **L1** and **L2** ligands showed lower activity on *E. coli* and *P. aeruginosa* species (3.50 ± 0.00 - 5.54 ± 0.34 at 100 µg/mL). The **L2** shows higher inhibition zones on *S. pyogenes* (8.54 ± 0.66 at 100 µg/mL to 10.86 ± 0.82 mm at 200 µg/mL). Complexes **1**, **2**, and **3** have low to medium zone of inhibition ranging from 7 ± 0.44 mm to 11.67 ± 0.54 mm diameters at both 100 and 200 μg/mL on the four bacteria species.

Complex **4** and **5** showed an enhanced activity against *S. pyogenes* with a mean inhibition zone of 14.80 ± 0.23 and 14.00 ± 0.2 mm at 200 µg/mL respectively relative to Trimethoprim (18.34 ± 0.68 mm at 200 µg/mL). Similarly, complex **4** exhibited good antibacterial activity against *P. aeruginosa* (15.44 ± 0.31 mm at 200 µg/mL). Complexes **4** and **5** are more active on gram-negative bacteria, which make them to be very important compound than the other. The results concluded that metals coordinated with ligands enhance their activities and induce the potential for inhibition of bacteria growth. The activities of all compounds were directly proportional to their concentration (Figure 56).

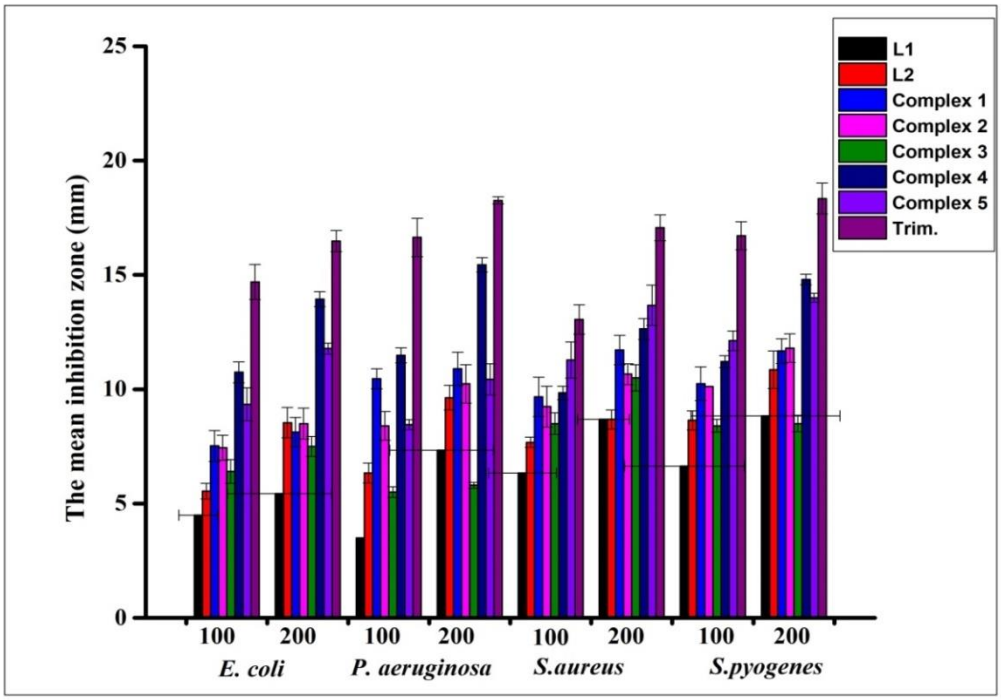

Figure 56. Bacteria growth inhibition potentials of ligands (**L1** and **L2**) and complexes **1-5** in mm (mean ± SD) at 100 µg/mL and 200 µg/mL.

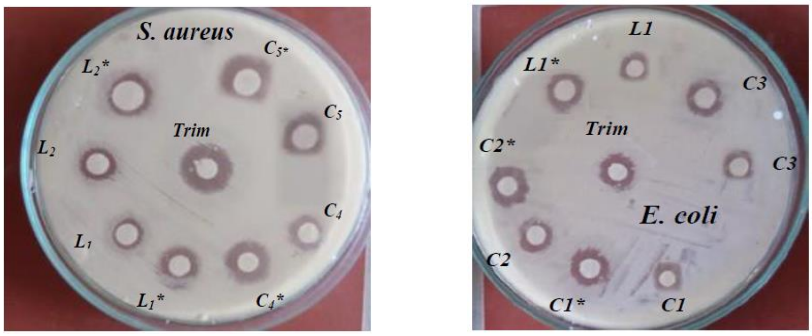

Figure 57. Photos of selected bacteria growth inhibition zone of compounds in mm (mean ± SD) on *S. aureus* and *P. aeruginosa* bacteria species. Where: L & L* = ligand conc. at 100 and 200 µg/ml; C & C* = complex conc. at 100 and 200 µg/ml respectively

Also, the antibacterial activity of ligand (**L3**) and its complexes (**6 - 8**) were also evaluated, and the obtained results were summarized in Table 8 and Figure 58 and the zone of inhibition was shown in Appendix 41.

Table 8. Antibacterial activity data of ligand **L3** and complexes (**6-8**)

Compound	**Gram-negative**		**Gram-positive**		
	Conc. *(µg/mL)*	***E. Coli***	***P. Aeruginosa***	***S. Aureus***	***S. Pyogenes***
L3	100	6.42 ± 0.24	7.50 ± 0.32	10.34 ± 0.40	9.34 ± 0.44
	200	7.38 ± 0.43	8.33 ± 0.22	13.26 ± 0.27	10.17 ± 0.12
$[Zn(L3)2].2H_2O$ **(6)**	100	9.42 ± 0.28	11.54 ± 0.48	12.64 ± 0.40	11.85 ± 0.33
	200	10.16 ± 0.14	14.41 ± 0.38	16.22 ± 0.27	15.66 ± 0.16
$[Cu(L3)_2].3H_2O$ **(7)**	100	10.18 ± 0.28	12.67 ± 0.18	14.84 ± 0.20	13.44 ± 0.18
	200	14.36 ± 0.46	16.84 ± 0.26	18.66 ± 0.34	17.31 ± 0.24
$[Ni(L3)_2].4H_2O$ **(8)**	100	8.46 ± 0.26	10.47 ± 0.24	11.76 ± 0.14	10.28 ± 0.48
	200	9.68 ± 0.48	12.64 ± 0.36	13.28 ± 0.46	12.72 ± 0.38
Trimethoprim (Standard drug)	100	16.70 ± 0.35	17.46 ± 0.31	19.06 ± 0.44	18.24 ± 0.26
	200	18.70 ± 0.47	19.64 ± 0.36	21.48 ± 0.46	19.32 ± 0.48

By mm (mean ± SD of triplicates)

The result in Table 8 showed that the synthesized complexes **(6-8)** possess a higher inhibition zone than the free ligand against the four bacteria species. The ligand (**L3**) showed lower activities on the Gram-negative bacteria species (6.42 ± 0.24 mm at 100 µg/mL on *P. Aeruginosa to* 8.33 ± 0.22 mm at 200 µg/mL on *E. coli)* but showed medium activities on Gram-positive bacterial species (9.34 ± 0.44 mm at 100 µg/mL on *S. Pyogenes* to 13.26 ± 0.27 mm at 200 µg/mL on *S. aureus*).

Complex **6** exhibited higher activity on Gram-negative bacteria species *P. aeruginosa* (14.41 ± 0.38 mm) and among Gram-positive species on *S. aureus* (16.22 ± 0.22 mm at 200 *µg/mL*) than the free ligand (L3). The relative activities were concentration dependent on all the bacteria species. A study by Dutta *et al*. (R. K. Dutta, Nenavathu, Gangishetty, & Reddy, 2012), suggested that Zn(II)-complexes, which can release ROS produced in solutions, may be necessary for zinc complexes to have inhibitory potential. By adhering to bacterial cell walls, damaging those walls, and then attaching to the proteins and nucleic acids of those cells. Zinc complex may be made to adhere by electrostatic forces. This results in cellular deformation and loss of viability (Y. Zhang et al., 2021).

Complex **7**, ([$Cu(L3)_2.3H_2O$]), exhibited more activities than the other synthesized compounds on all bacterial species: *S. aureus* (18.66 ± 0.34 mm), *S. pyogenes* (17.31 ± 0.24 mm) *P. aurigonisa* (16.84 ± 0.26 mm) (Table 8). Copper is an essential bio-metal for the preparation of metal-based drug development due to its better potential for medicinal applications (Čongrádyová et al., 2021; Duncan & White, 2012). The mechanism of action to become cytotoxic on bacteria cell is due to the redox reactions occurring between Cu(II) and Cu(I) oxidation states which results in the formation of reactive radical species (Jomova, Baros, & Valko, 2012). These reactive species under aerobic conditions create high reactive radicals (hydroxyl) which can react with biomolecules including proteins, membrane lipids, and nucleic acids to create dangerous species in the cell of bacteria. These dangerous species can damage the bacteria's DNA (Čongrádyová et al., 2021). The obtained result is also in match with work reported by Duncan and White 2012(R. K. Dutta et al., 2012), which showed that the copper complex of semicarbazones and thiosemicarbazones exhibited higher antibacterial potential against *E. coli* relative to the free ligand. Thus, with a similar fact, here the high inhibition potential of the [$Cu(L3)_2$].$3H_2O$ (**7)** complex on *S. aureus* and *P. aeruginosa* showed it can be a potent antibiotic candidate against the two bacteria species.

The Complex **8**, [$Ni(L3]_2$].$4H_2O$, showed a good inhibitory effect against three bacteria species: *P. aeruginosa* (12.64 ± 0.36 mm), *S. pyogenes* (12.72 ± 0.38 mm), and *S. aureus* (13.28 ± 0.46 mm) at 200 *µg/mL* concentration. Nickel metal is a very important element in medicinal chemistry, due to its antimicrobial activities (R. K. Dutta et al., 2012). This metal has the potential to cross microbial cells and damage the microorganisms by inactivating their enzymes.

The overall antimicrobial potential data confirmed that the complexes show higher activities than the free ligands on the microbial pathogens, which is in agreement with previous studies. Tweedy's chelation theory justifies why the complexes have greater biological activities than the free ligand (Awolope, Ejidike, & Clayton, 2023; R. K. Dutta et al., 2012; Ejidike & Ajibade, 2015; Tweedy, 1964). The metal ion's polarity is lowered to a higher level during chelation because the ligand orbital overlaps and the metal ion's charge is partially shared with the donor atom (Ramesh & Natarajan, 1994; Thangadurai & Natarajan, 2001). Additionally, the chelate sphere promotes the delocalization of π-electrons, increasing the complex's lipophilicity. This enables ability of the complexes, allowing for easier permeability through the cell membrane's lipid layer of the bacteria cell membrane (Alias et

al., 2014). Notably, the nitrogen in azomethine (C=N) may form H- bond with the centers of the active parts of cells, impairing regular cell function and preventing the formation of the cell wall in bacteria cells (Shelke et al., 2012).

On the other hand, the enhancement in the antimicrobial potential of the complex compounds was due to the positive charges that exist on the metals which are crucial in improving the non-polarity property of the ligand causing the solubility mechanism to be improved. This makes the compounds to pass through the bacterial cell membrane, which is impermeable by a number of antibiotic drugs, particularly in the case of gram-negative bacteria pathogens (Bamigboye et al., 2021). The ability of complexes to penetrate the bacterial membrane increases with decreasing polarity, which is attributed to lipophilicity (Al-Amiery, Kadhum, et al., 2012; Beyene, Mihirteu, Ayana, & Yibeltal, 2020).

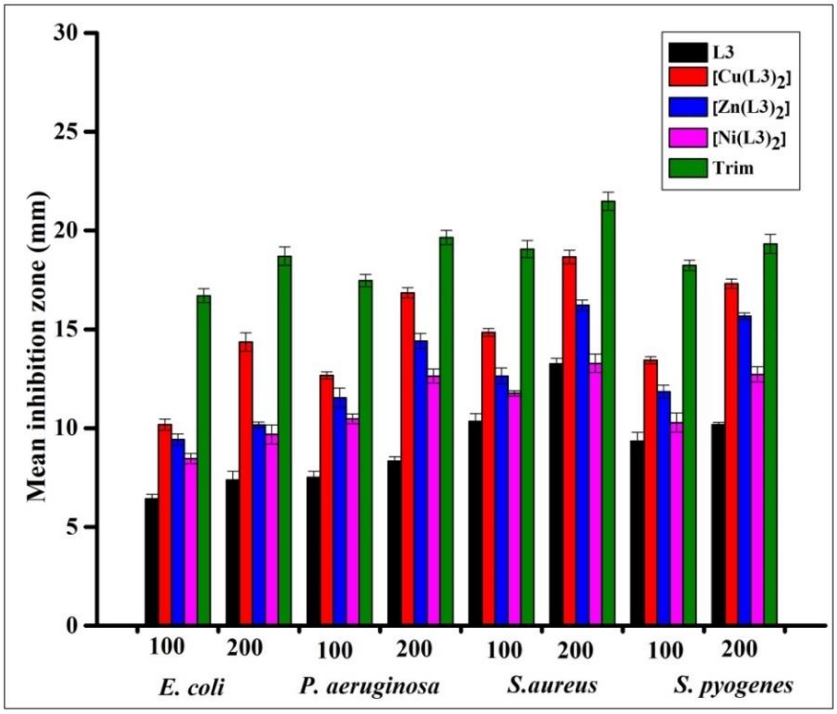

Figure 58. Bacteria growth inhibition vs concentration of **L3** and complexes (**6**-**8**) compounds measured by mm (mean ± SD)

As a result, the metal binds to other molecules of the cell membrane, such as amino acids, amino phospholipids, and cysteine ligands, which are favored. Therefore, these newly synthesized complex compounds may have a significant impact on typical bacteria cell activities and ultimately result in the inhibition of bacterial growth. Furthermore, the results

in Appendix- 43 also revealed the heteroleptic metal complexes (**9** and **10**) showed medium to higher inhibitory activities against all bacteria strains.

The heteroleptic complex **9**, [Zn(L1)(L4)], have shown best activity on *P. Aeruginosa (*14.22 ± 0.33 mm) and Cu(II) complex 10, [Cu(L1)(L4)], exhibited higher antimicrobial activity on *S. Pyogenes* (13.67 ± 0.52 mm at 200 μg/mL) which were comparable to the standard drug Trimethoprim (16.71 ± 0.77 mm) at 200 μg/mL. It was also observed that at similar concentrations, the complexes exhibit higher activity than the constituent ligands for all bacteria strains tested. The obtained data provides evidence that metal complexed with bioactive ligands enhances their activities and induces potential for bacteria growth inhibition. Furthermore, the activities of all compounds were proportional to their concentration, *i.e*., activities were found to increase with increasing sample concentration (doses) (Figure 59 and 70) which is also a similar fact to previous studies (Sadeek et al., 2013).

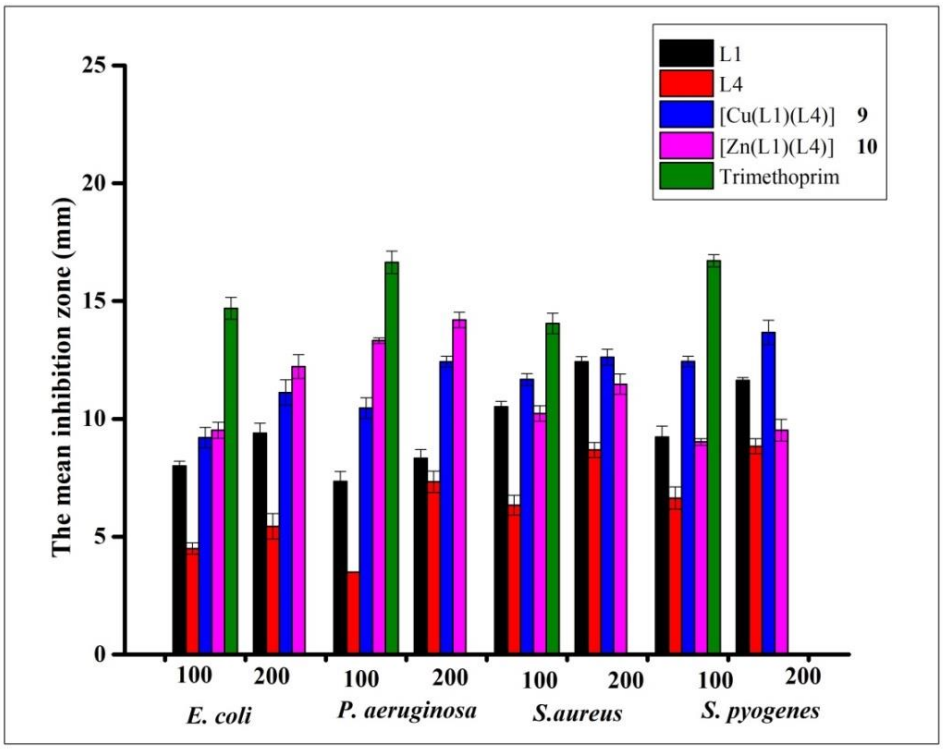

Figure 59. Bacteria growth inhibition against the concentration of **L3** and complexes (**6-8**)

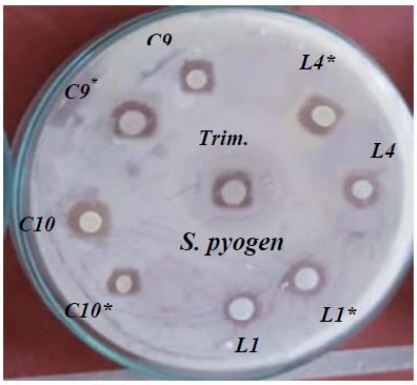

Figure 60. Photo of bacteria growth inhibition zone of the **L1**, **L4**, and complex **9** and **10**, Where: L & L* = ligand conc. at 100 and 200 µg/ml; C & C* = complex (at 100 and 200 µg/ml).

Metal (II) complex compounds exhibiting higher antibacterial activity were selected for minimum inhibitory concentration (MIC) studies (Table 9). The MIC is defined as the lowest or minimum antimicrobial concentration that inhibits visible microbial growth in artificial media after fixed incubation of time. Thus, the minimum inhibitory concentration was determined using the disc diffusion technique following the method described under section 3.7.1 by preparing discs containing, 12.5, 25, and 50 µg/mL of the compounds and applying the protocol. The inhibition zones were shown by Figure 61.

Table 9. Results of minimum inhibitory concentration (µg/mL) of the top five antimicrobial active compounds; complex (**4**), (**5**), (**7**), (**8**), and (**10**) against four bacteria species

Bacteria species	***µg/Ml***	**Selected complex compounds (mm)**				
		4	**5**	**7**	**8**	**10**
E. coli	12.5	NA	NA	NA	NA	NA
	25	0.4	NA	NA	0.6	NA
	50	0.8	0.6	0.5	1.6	NA
P. aeruginosa	12.5	NA	NA	NA	NA	NA
	25	0.5	NA	1.2	0.4	NA
	50	1.5	NA	2.5	1.8	0.5
S. aureus	12.5	NA	NA	NA	NA	NA
	25	NA	1.5	NA	1.5	1.5
	50	0.4	4	2.0	4.0	3.0
S. pyogenes	12.5	NA	NA	NA	NA	NA
	25	NA	0.5	1.0	NA	0.8
	50	0.5	2.5	2.5	NA	3.5

Note: By mm (millimeter), NA = not active or no visible inhibition zone.

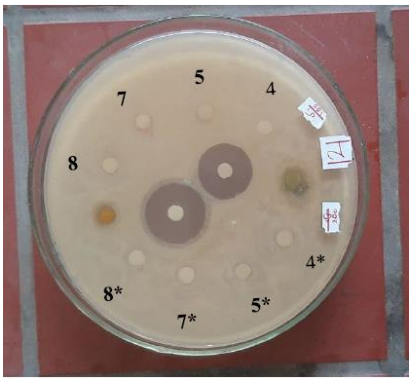

Figure 61. Photos of MIC of selected complexes at 25 and 50 µg/ml concentration

The results of the selected complexes and fractions are displayed in Table 9. The compounds with the best antibacterial activity were chosen and fractions were done by lowering the concentrations. The metal complexes **5**, **8**, and **10** could be identified as the most active compounds with MICs values ranging from 25 - 50 µg/mL with an inhibition zone of 1.5 – 4.0 mm diameter on *S. aureus* bacteria strain. Complex **4** and complex **7** also demonstrated visible inhibition zones against *P. aeruginosa* at 25 µg/mL with an inhibition zone of 0.5 mm and 1.2 mm respectively. All the tested compounds did not show an inhibition zone on any of the four bacteria pathogens at ≤ 12.5 µg/mL concentration, which could be taken as a benchmark of concentration for the antimicrobial activities of the selected complexes.

4.3.2. Antioxidant Activity of the ligands and their metal complexes

Free radicals, which are created during biological processes, may be produced during metabolic activities in our bodies. If the body cannot process and remove free radicals efficiently, oxidative stress can result. This can harm cells and body function. Free radicals are also known as reactive oxygen species (ROS). These include OH^-, O_2^-, and H_2O_2. These ROS are reactive species that could potentially interact with biomolecules like proteins, lipids, and nucleic acids to cause different chronic diseases like cancer, heart disease, aging, and others (Akila, Usharani, & Rajavel, 2013; El Jemli et al., 2016; J. Kumar et al., 2020). Thus, these free radicals can be removed by using potential antioxidant molecules. Antioxidants are substances that can prevent or slow damage to body cells caused by free radicals, reactive (unstable) molecules that the body produces as a reaction during the metabolic process.

Thus, the antioxidant activities of the newly synthesized ligands and their homoleptic and heteroleptic complexes were evaluated based on their capability to donate protons with the help of UV-visible absorbance using the method of DPPH assay. DPPH (2, 2-diphenyl-1-

picrylhydrazyl) is the most common method that is widely used due to its ease, speed, and sensitivity. DPPH is a stable free radical that can abstract hydrogen or electron from a corresponding donor, which causes it to lose the characteristic deep purple color, leading to bleaching of the strong absorption at 517 nm (S. Dutta et al., 2005). Compounds that have antioxidant activity may reduce the absorbance of DPPH at 517 nm, which is resulted in changes in the color of DPPH in the reaction process (S. Dutta et al., 2005). The degree of discoloration indicates the scavenging potential of the antioxidant compounds in terms of hydrogen-donating ability (Benabadji, Wen, Zheng, Dong, & Yuan, 2004; El-Ghorab et al., 2010). The reaction can, therefore, be conveniently used to examine the radical scavenging ability of the prospective molecule.

In this study, the radical scavenging activities of the newly synthesized ligands and their metal complexes (**1-10**) were evaluated and analyzed. The antioxidant potentials of the compounds were evaluated using different concentrations of the semicarbazone and thiosemicarbazone derivative ligands (**L1-L4**) and complexes (**1-10**) with DPPH radical while ascorbic acid (vitamin C) was used as a standard and DMSO as a positive control. The results obtained were expressed in percentage (%) scavenging activities and the data obtained are summarized in Appendix 43 and 44 and the % free radical scavenging potential against a concentration of the samples are shown in Figures 62 and 63.

The data obtained showed that the synthesized compounds, **L1**, **L2**, and **L3** and their homoleptic complexes (**1 - 8**) have shown moderate to high antioxidant potential. The complexes exhibited higher antioxidant potential than the free ligands. This is expected to be due to synergetic effects, hence the complexes have a strong potential to be useful as radical scavengers (O. A. El-Gammal et al., 2021). Among the compounds complex **3**, $[Ni(L1)_2Cl]$, shows the highest percent of free radical scavenging potential (85.76 ± 0.24) comparable to the standard ascorbic acid (89.48 ± 0.74), while the least activity (36.00 % - 41.46 %) was displayed by **L1** (Figure 62). The other complexes **4 - 8,** exhibited good antioxidant potential near ascorbic acid with maximum percentage scavenging activities of 76.78 ± 0.68, 78.55 ± 0.48, 78.55 ± 0.48, 78.45 ± 0.38, and 81.43 ± 0.56 % at 100 μg/mL concentration respectively. Complexes **3**, **6**, **7**, **8,** and **L3** are highly dependent on the change in concentration, but complexex1 and 2 are almost independent of the change in concentration

(Figure 62). All the complexes showed higher antioxidant activities than their respective free ligand.

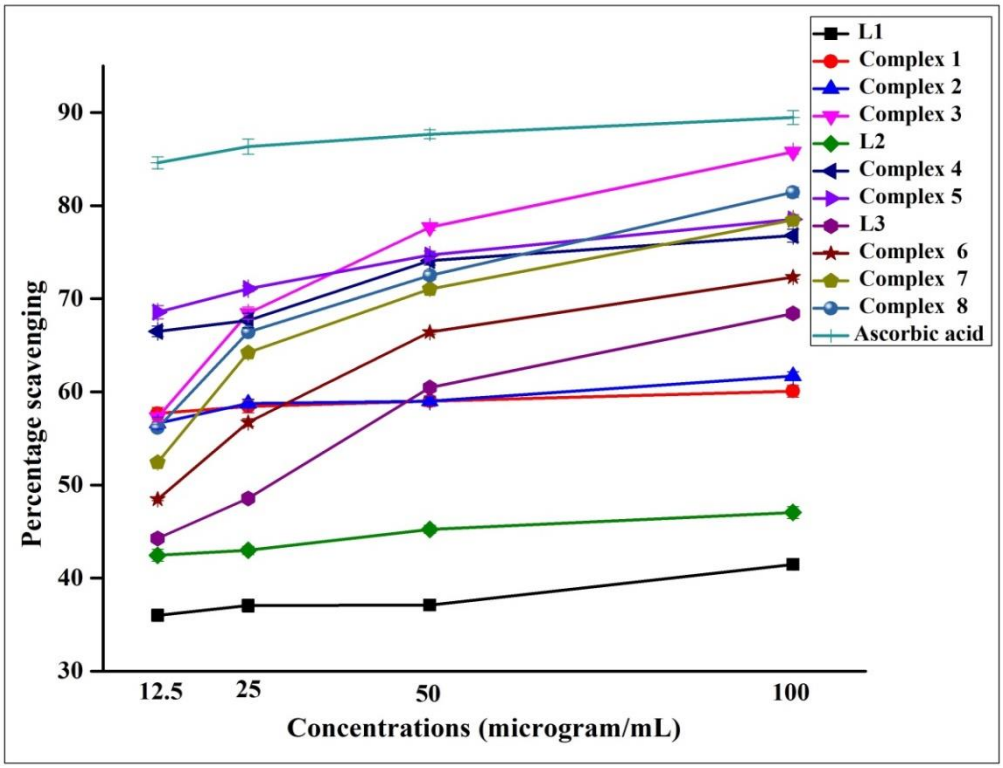

Figure 62. Percentage free radical scavenging (%) of DPPH by the ligands and homoleptic metal complexes (**1 - 8**) compared with ascorbic acid.

Also, the data displayed in Appendix 43 showed that **L3** possesses a relatively higher percentage of free radical scavenging activity value than the other two ligands (**L1** and **L2**). Then, it can be clearly concluded that the metal (II) complexes scavenge DPPH more effectively than the semicarbazone and thiosemicarbazone derivative ligands. The order of antioxidant potential of the compounds at a maximum concentration of 100 µg/mL can be as Ascorbic acid > $[Ni(L1)_2Cl]$ (**3**) > $[Ni(L3)_2].3H_2O$ (**8**) > $[Cu(L2)_2]$ **(5)** > $[Cu(L3)_2].3H_2O$ (**7**) > $[Zn(L2)_2]$ **(4)** > $[Zn(L3)_2].2H_2O$ (**6**) > **L3** > $[Cu(L1)_2Cl_2]$ (**2**) > $[Zn(L1)_2Cl_2]$ (**1**) > **L2** > **L1**. This potential of samples to scavenge free radicals may be associated with the existence and donation ability of hydrogen to stabilize radicals (Hernandez, Jiménez, Mullineaux, & Sevilia, 2000). Hence, the results obtained provide insight toward the use of mostly metal complexes in the treatment of diseases caused due to oxidative strain.

Similarly, the antioxidant activities of the heteroleptic metal complexes (**9** and **10**) were also conducted and findings were summarized in Appendix 44 and the free radical scavenging potential versus concentration of the complexes was shown in Figure 63. All the complexes

showed higher antioxidant activity than the parent ligands. Also as shown appendix 44 shows that the [Cu(L1)(L4)] complex **(10)** has shown the best potential, with maximum scavenging activities (60.4 - 63.7 %) at and the [Zn(L1)(L4)] complex (**9**) also has good activities (56.4 - 59.7 %), while the ligands L1 (32.60 - 40.34 %) and L4 (36.0 - 41.5 %) have the least activities. The scavenging potentials were roughly concentration dependent, meaning that as concentrations increased, so were the activities. Moreover, the data revealed that complexes have better antiradical potential than individual ligands. This could be explained by metals' electron deficient characteristics in comparison to ligands. Thus, the mixed ligand complex **9**, [Zn(L1)(L4)] and complex **10**, [Cu(L1)(L4)] can be the best candidates for free radical scavengers.

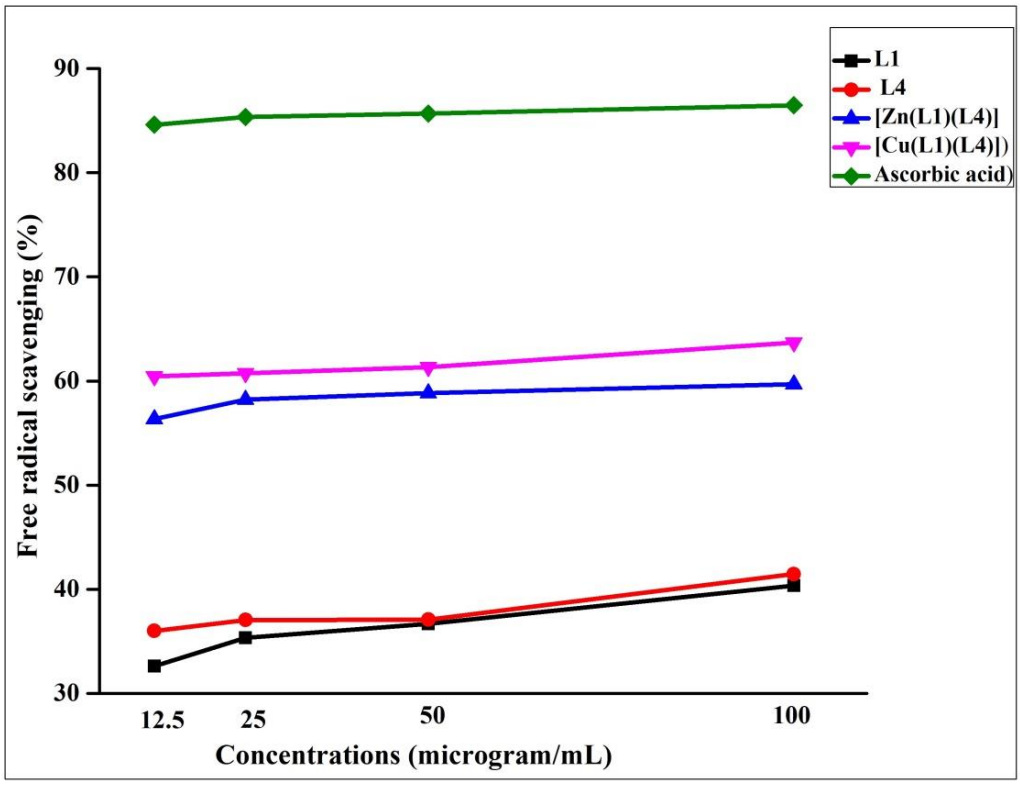

Figure 63. Percentage free radical scavenging potential of ligands and heteroleptic complexes (**9** and **10**)

4.3.3. Antifungal activity of the ligands (L1 - L4)) and their complexes (1-10)

The newly synthesized ligands and their homoleptic and heteroleptic complexes were tested for *in* vitro antifungal activity against two fungi species; - *Aspergillus fumigates* and *Candida albicans* fungi. Amphotericin B was used as a standard fungicide agent. The results of the antifungal potential of free ligands and their complexes were summarized in Table 10 and the inhibition zone is presented in Appendix 45.

Table 10. The antifungal activity of ligands and their complexes

Samples	Fungal inhibition zone (mm) conc. in mg/ml					
	Aspergillus fumigatus			***Candida albicans***		
	25	**50**	**100**	**25**	**50**	**100**
DMSO (Control)	0.0	0.0	0.0	0.0	0.0	0.0
Amphotericin B	18.5	22	22.5	24.5	24	24.5
L1	8.5	10.5	12.5	12	14.	14
L2	12	13.5	18	18	18.4	24
L3	NA	NA	NA	NA	NA	NA
L4	NA	5.4	8.5	6.4	6.5	8
$[Zn(L1)_2 (Cl)_2]$ (**1**)	10.5	13.3	16.4	16	14	18
$[Cu(L1)_2(Cl)_2]$ (**2**)	8.4	8.6	10.4	5.4	5.6	6.5
$[Ni(L1)_2Cl]$ (**3**)	6.3	7.5	15.3	10.6	11.7	14.6
$[Zn(L2)_2]$ (**4**)	20.2	19.3	20.5	24.3	24.5	26..5
$[Cu(L2)_2]$ (**5**)	16	18	22	20.5	22.3	24
$[Zn(L3)_2].2H_2O$ (**6**)	NA	3.4	6.5	NA	4.5	8
$[Cu(L3)_2].3H_2O$ (**7**)	NA	2.5	4.5	1.5	3.0	3.5
$[Ni(L3)_2].4H_2O$ **(8)**	NA	NA	2.0	NA	2.0	3.5
[Cu(L1)(L4)] (**9**)	4.3	4.4	9.5	5.4	6.0	7,5
[Zn(L1)(L4)] (**10**)	4	6	8.4	6	6.8	10.5

Note: NA= not active

The results summarized in Table 10 showed, the free ligands (**L1** and **L2**) were active against both fungi species, and even **L2** shows comparable antifungal activity to the standard drug, Amphotericin B. These results are in line with the previous studies (Jirjees et al.; Kubra et al., 2014), which reported that dehydrozingerone and its derivatives have shown antifungal activity against *Rhizochonial solani species.* The antifungal activity of the dehydrozingerone and its derivatives showed that the carbonyl moiety plays a major role in the antifungal activity (Kubra et al., 2014; V. Kumar, Bala, Dhawan, Singh, & Karpoormath, 2022). The existence of polarized carbon-oxygen double bond of the ketone group probably contributes to their ability to form covalent bonds with DNA and proteins and then interfere with normal metabolism. The **L1** complexes showed the least antifungal activity, especially those of Zn(II), and Cu(II). But Ni(II) shows similar activity to the ligand. The complexes of **L2** ligand, which is Complex **4**, $[Zn(L2)_2]$, showed antifungal activities (26.5 mm) more than the standard against *Candida albicans* fungi. Also, complex **5**, $[Cu(L2)_2]$ showed good activity (24.0 mm) against *Candida albicans.*

The free ligand (**L3**) was not active against both fungi species, and its Zn(II), Cu(II) and Ni(II) complexes showed the least activity compared with the other complexes. The antifungal activity of the heteroleptic Cu(II) and Zn(II) complexes of **L1** together with **L4** showed moderate activity. The higher fungi toxic effect of the complex compared with the free ligand can be understood in terms of the chelation theory which stated that upon complexation the polarity of the metal ion gets decreased which increases the lipophilicity of the metal complex, facilitating them to cross the cell membrane (Kurtoglu, 2009).

This finding or display for the antifungal activity of the free ligand and their metal complexes against the tested species needs further investigation against other fungal species. Although the efficiency of the prepared compounds is high to the best of my knowledge, it may be a solid base for further research on dehydrozingerone derivative ligands and their metal complexes.

4.4. *In Silico* docking *analysis* of ligands and their metal complexes

4.4.1. Molecular docking analysis of synthesized ligands (L1 and L2) and complexes (1 5) docked against *S. aureus Gyrase* (PDB ID 2XCT)

Recently, *in-silico* methods that include molecular docking analysis and online ADMET predictions (SwissADME, Pro-Tox II, and OSIRIS property explorer) are being used to facilitate the process of identifying the potential bioactive molecule (Priyanka Banerjee et al., 2018; Garg et al., 2021; O Trott & Olson, 2009). The evaluation of pharmacological parameters such as drug-likeness, ADME (absorption, distribution, metabolism, and excretion), and toxicity are paramount in identifying lead compounds (DeLano, 2002) for drug development. In general, molecular docking studies are used to examine the binding energy and to confirm further the molecular mechanisms for ligands at the active site of proteins. To understand the binding mode of the ligands, all the synthesized compounds were subjected to molecular docking study against selected proteins viz. *S. aureus Gyrase* (PDB ID 2XCT) using Auto-dock Vina (O Trott & Olson, 2009). The *S. aureus Gyrase*, a bacterial topoisomerase enzyme, regulates the topology of DNA during transcription, replication, and recombination by temporarily rupturing both DNA strands. Hence, the bacterial gyrase is paramount for bacterial survival and therefore necessary to disrupt as an antibacterial drug target (El-Etrawy & Sherbiny, 2021). Therefore, the molecular docking of the ligands (**L1** and **L2**) and complexes (**1 - 5**) were docked against DNA gyrase of *S. aureus Gyrase* (PDB

ID 2XCT) to investigate their mode of action and the results were compared with the *in vitro* antibacterial activity profile data. The molecular interaction between the synthesized ligands and their complexes against the *S. aureus Gyrase* were studied to understand the mechanism of action and the results were compared with standard anti-bacterial agent Trimethoprim.

Table 11. Molecular docking scores and the corresponding prominent residual amino acid interactions of the ligands and their complexes against *S. aureus* (PDB ID: 2XCT), were reported experimentally as a complex with trimethoprim

Compounds	**Binding energy (kcal/mol**	**H-bonding with**	**Residual interactions**	
			π-Sigma/π-Alkyl	van der Waals
L1	−8.0	,Ser-1084, Arg-458, Arg-1122, Glu-477	Arg-458	Gly-1082, DG-12
L2	**−7**.6	Asp-437, DC-12, DT-10, DA-11	Arg-458, DA-11, DG-9 DA-13	Gly-459, Lys-460, DT-8, DA-11
Complex **1**	−8.4	Lys-460, Arg-458, Arg-458, DG-9, DT-	DA-13, Arg-458	Gly-459, Asn-475, Glu-477, Ile-461,
Complex **2**	−8.2	Ser-438, Asp-1083 DG-9, DG-9:	Ala-1120, Met-1121, Arg-1122	Tyr-1087, Glu-1088, Ser-1084, Ala-1118, Gly-1117, Ala-1119,
Complex **3**	−8.5	Arg-458, Arg-458, Arg-1122, Glu-477, Asp-494, Tyr-496,	Arg-1122, Arg-458 DG-9, DA-13, Metal-Acceptor (Ni: O, N)	Ser-1084, Asp-437, Phe-1123, DG-12
Complex **4**	−9.1	Arg-458, Asp-437, DC-12, DG-9, DT-10	Arg-458, DG-9, DA-13, 4 Metal-Acceptor (Zn: O, S, N)	Gly-459, Asn-476, Gln-480
Complex **5**	−7.4	Arg-458, Asp-437, DT-10:, DA-11 -13	Electrostatic-Attractive Charge-Asp-437 Electrostatic-Pi-Cation-DA-13(Dist. 4.27588) Hydrophobic-Pi-Alkyl-	Gly-459, Glu-477, DT-8, DG-9, DC-12
Trimethoprim	**−7.9**	Arg-458, Arg-458, DT-8, DG-9, DC-12	Arg-458, DT-8, DG-9 DA-13	Phe-1123, Gly-459, Asp-437, DT-10

DA = deoxyadenosine; DG = deoxyguanosine; DT = deoxythymidine; DC = Deoxycytidine.

The results in Table 11 showed that the synthesized compounds were found to have minimum binding energy ranging from -7.4 to -9.1 kcal/mol, with the best result achieved by the metal complexes **1**, **2**, **3**, and **4** having binding affinity of -8.4, -8.2, -8.5 and -9.1 kcal/mol respectively. Compared to Trimethoprim (-7.9 kcal/mol), the other synthesized compounds, **L1**, **L2** and complex **5** have shown comparable binding affinity (-8.0, -7.6, -7.4 kcal/mol respectively). Among the metal complexes, complex **4** displayed the best binding energy (-9.1 kcal/mol) compared to the standard drug Trimethoprim (-7.9 kcal/mol) (Table 11). The complexes have shown better docking scores compared to the free ligands. In general, the complexes (**1**, **2**, **3**, and **4**) have higher docking scores than the standard drug Trimethoprim. The *in-vitro* antimicrobial analysis results are matching with the molecular docking analysis docking score.

The ligands (**L1** and **L2**) and the complexes (**1 - 5**) showed the best binding affinities with different amino acid residues through a hydrogen bond, π-Sigma/π-Alkyl, and van der Waals forces. As observed from the 2D binding interaction model, **L1** forms a hydrogen bond with Ser-1084 through its amine (-NH_2) and (-C=O), Arg-1122 through carbonyl (-C=O), and DA-13 through its -O-H functional groups (Appendix 46). Also forms hydrophobic (pi-cation) interactions with Arg-458 and van der Waals interactions with Gly-1082 and DG-12 amino acid residues. The **L2** ligand also forms hydrogen bond interaction with Asp-437, DC-12, DT-10, and DA-11 amino acid residues (Appendix 47).

The complexes achieve good interaction affinities with different amino acid scums (Appendix 48-52). According to the binding model of the best active compound (complex **4**), three hydrogen bonds were observed between residues Arg-458, Asp-437, DC-12, DG-9, DT-10 with amide (NH), amine (NH_2), and oxygen of hydroxyl and methoxy (OCH_3) groups of the complex respectively (Appendix 51). Also, hydrophobic (π-Sigma/π-Alkyl) interactions between the complex and residues Arg-458, DG-9, DA-13, 4 Metal-Acceptor (Zn: O, S, N) were observed. The other potential compound [complex 3) was able to form H- bonds with Arg-458, Arg-458, Arg-1122, Glu-477, Asp-494, Tyr-496, Phe-432 through NH_2 and hydroxyl groups (Appendix 50). The complex was also able to interact with Arg-1122, Arg-458, DG-9, DA-13, and Metal-Acceptor (Ni: O, N) residues through hydrophobic.

4.4.2. Molecular docking analysis of synthesized ligands and complexes (6 - 10) docked against *S. aureus* (PDB: 2w9h)

The molecular docking of the ligands and complexes (**6 - 10**) were docked against DNA gyrase of *S. aureus Gyrase* (PDB: 2w9h) to investigate their mode of action and the results were compared with the *in-vitro* antibacterial activity data. The results obtained were summarized in Table 12.

Table 12. Molecular docking scores and the corresponding prominent residual amino acid interactions of the ligands and their complexes against *S. aureus* (PDB: 2w9h, were reported experimentally as a complex with trimethoprim

Compounds	**Binding energy (kcal/mol)**	**H-bonding with**	**Residual interactions**	
			π-Sigma/π-Alkyl	van der Waals
L1	-8.14	Leu5, Ala7, Asn18,Thr46, Ser49,Phe92	Leu20,Ile50	Val6,Gly93, Gly94,Lys45,
L3	-8.26	Arg61	Asp73,Val76, Cys79, Ala127	Leu36,Thr75, Thr115, Gly126
L4	-7.39	Leu5, Asn18, Asp27	Val6, Leu20, Phe98	Ala7, Gln19, Thr46, Phe92
Complex **6**	-7.03	Lys16, Ser20, Tyr56	Leu36, Arg61, Asp65	Ile35, Ile52, Val53, Gly54
Complex **7**	-7.21	Ser20, Asn49, Tyr56	Leu36, Phe51, Arg61, Asp65	Glu48, Ile52, Val53, Gly54
Complex 8	-6.70	Ser20, Gln24, Ala50, Ile52	Val53	Ala21, Gly54, Asn55, Ala58
Complex 9	-11.01	Ser49, Thr46, Gln95	Leu20, Lys45	Leu5, Val6, Gln19, Leu28
Complex 10	-9.92	Ala7, Ile14, Ser49	Leu20, Leu28, Phe92	Val6, Ile50, Gly93, Thr46
Trimethoprim $C_{14}H_{18}N_4O_3$	-8.30	Leu5, Ala7, Asp27, Ser49	Ile14, Val31, Thr46, Ile50	Val6, Asn18, Gln19, Leu20
	Experimental	Leu5, Asp27, Phe92, Thr111	Ala7, Leu20, Leu28, Val31, Ile50	Val6, Gln19, Ser49, Thr46

DA = deoxyadenosine; DG = deoxyguanosine; DT = deoxythymidine; DC = Deoxycytidine.

The information presented in Table 12 for complexes compounds synthesized is pictorially described by the two-dimensional and three-dimensional binding model on *S. aureus gyrase* bacteria enzyme as represented by (Figure 64 - 72).

The synthesized compounds were found to have minimum binding energy ranging from –6.70 to - 11.01 kcal/mol (Table 12), with the best docking score achieved by the heteroleptic metal complexes 9 and 10 having binding affinity of -11.01 and -9.92 kcal/mol, respectively, compared to Trimethoprim (-8.30 kcal/mol). The ligands **L1** and **L3** were shown similar binding affinity (-8.14 and -8.26 kcal/mol) to the standard Trimethoprim. The other homoleptic metal complex (**6** - **8**) have shown comparable binding affinity (-7.03, -7.21, -6.7 kcal/mol respectively). The *in-vitro* antimicrobial activity results are best agreed with the molecular docking analysis docking scores.

All the ligands and the complexes showed the best interaction affinities with different amino acid residues. As observed from the 2D binding interaction model the ligands and complexes possess high binding affinity and form hydrogen bonds with various amino acid residues through their different parts of the functional group. Among these, the **L1** ligand also forms hydrogen bond interaction with Leu5 through the amine (-HN-N-) group, Asn18, Ala7, and Thr46 through hydroxyl (O-H) group, Ser49 and Phe92 amino acid residues (Figure 64). Also forms π-Sigma bonds with Leu20 and Ile50 amino acid residues. The ligand **L3** forms a hydrogen bond with Arg61 through its carbonyl (C=O) group. The π-sigma/π-alkyl interactions occurred between **L3** and amino acid residues (Asp73, Val76, Crys79, and Ala127) (Figure 65). The **L4** ligand forms hydrogen bond with Asp27 through its amine (-NH_2) group, Leu5 through amide (-N-H) and both Asn18 through hydroxyl (-O-H) group Also forms π-Sigma/π-Alkyl interactions with Val6, Leu20, Phe98 amino acid residues (Figure 66).

Complex **6** has shown three H-bonding interactions with Lys16, Ser20, and Tyr56 by its hydroxyl, and methoxy (-OH and –OCH_3) groups. Also forms several hydrophobic and van der Waals interactions with amino acid residues (Figure 67).

The other compound, complex **7**, forms an H-bonding with Ser20, Asn49, and Tyr56 amino acid scums through its hydroxyl and methoxy (-OH and OCH_3) active sites. Also, it forms

hydrophobic interactions with Leu36, Phe51, Arg61, and Asp65 residues (Figure 68). Among the metal complexes, the heteroleptic Zn(II) and Cu(II) complexes (**9** and **10**) displayed the best binding energy (-9.92 and -11.01 kcal/mol) compared to the standard drug Trimethoprim (-8.30 kcal/mol) (Figure 72) and they achieve good interaction affinities with amino acid scums. According to the binding model of the best active compound (complex **9)**, three hydrogen bonds were observed between residues Ser49, Thr46, and Gln95 with amide (NH), amine (NH_2), and oxygen of hydroxyl and methoxy (OCH_3) groups of the complex respectively (Figure **70**). Also, hydrophobic (π-Sigma/π-Alkyl) interactions between the complex and residues Leu20 and Lys45 were observed. The second potential complex compound (complex **10**) was able to form three H- bonds with Ala7, Ile14, and Ser49 through NH_2 and hydroxyl groups (Figure 71). The complex was also able to interact with Leu20, Leu28, and Phe92 residues hydrophobic interactions.

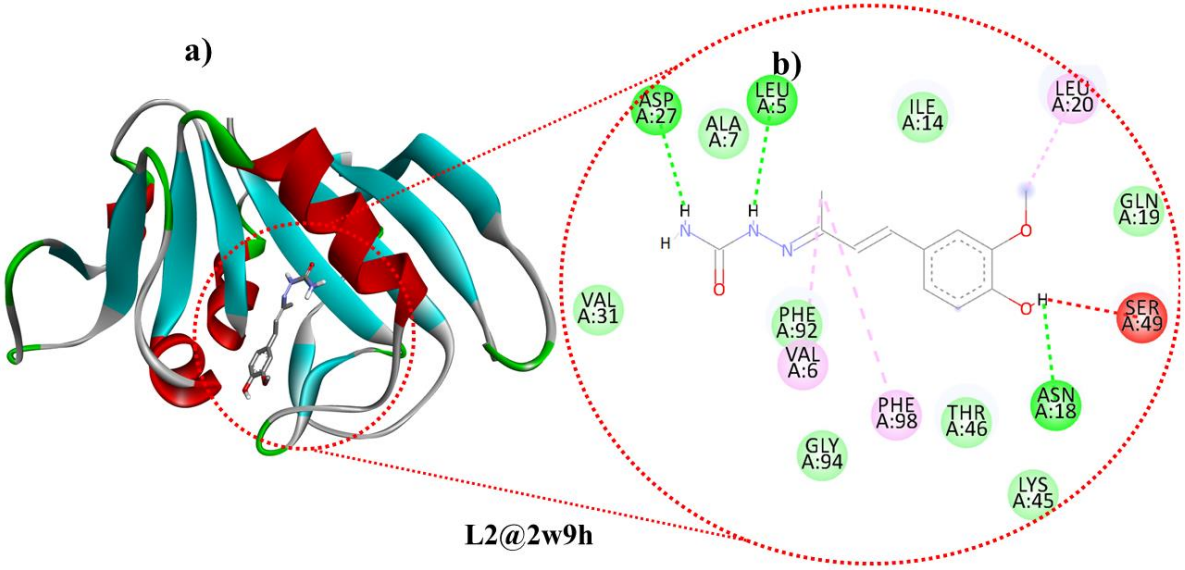

Figure 64. The binding interactions of **L1** against *S. aureus* (PDB: 2w9h, reported experimentally as a complex with trimethoprim); **a)** 3D and **b)** 2D representations.

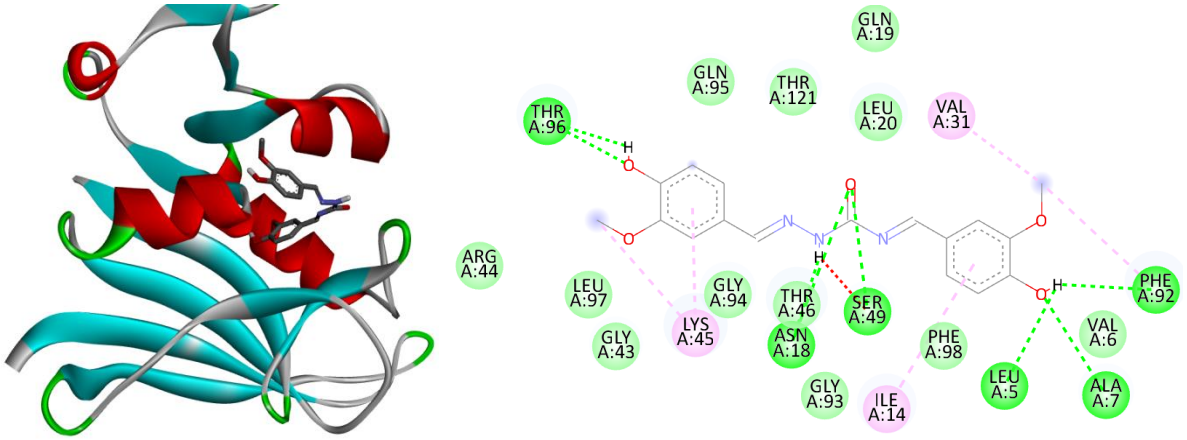

a) **L3@2wgh** b)

Figure 65. The binding interactions of L3 against *S. aureus* (PDB: 2w9h, reported experimentally as a complex with trimethoprim); a) 3D and b) 2D representations

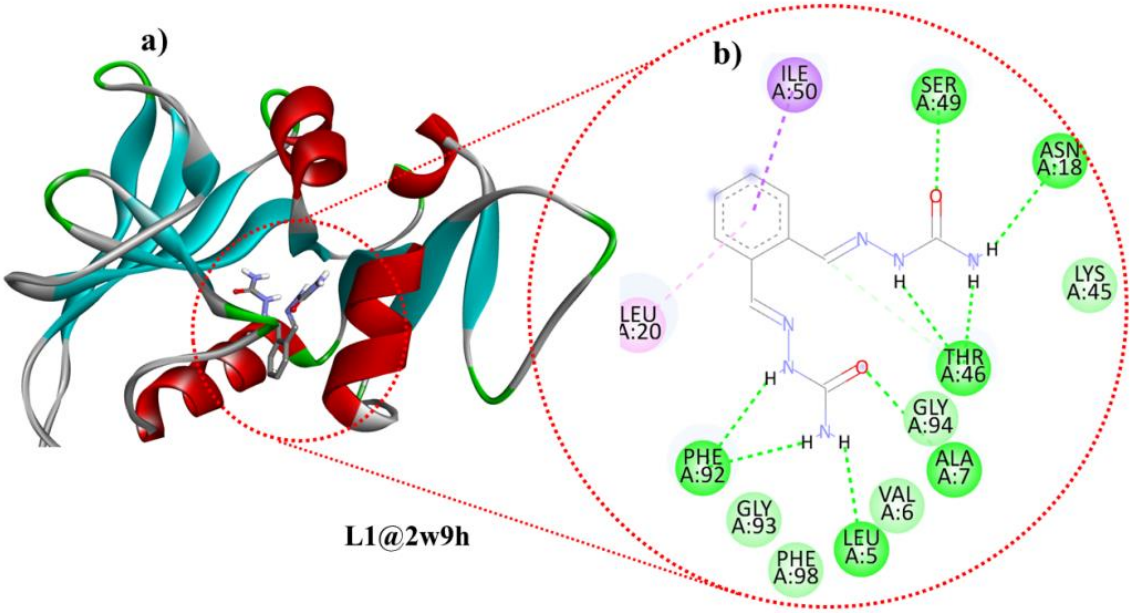

Figure 66. The binding interactions of **L4** against *S. aureus* (PDB: 2w9h, reported experimentally as a complex with trimethoprim); a) 3D and b) 2D representations

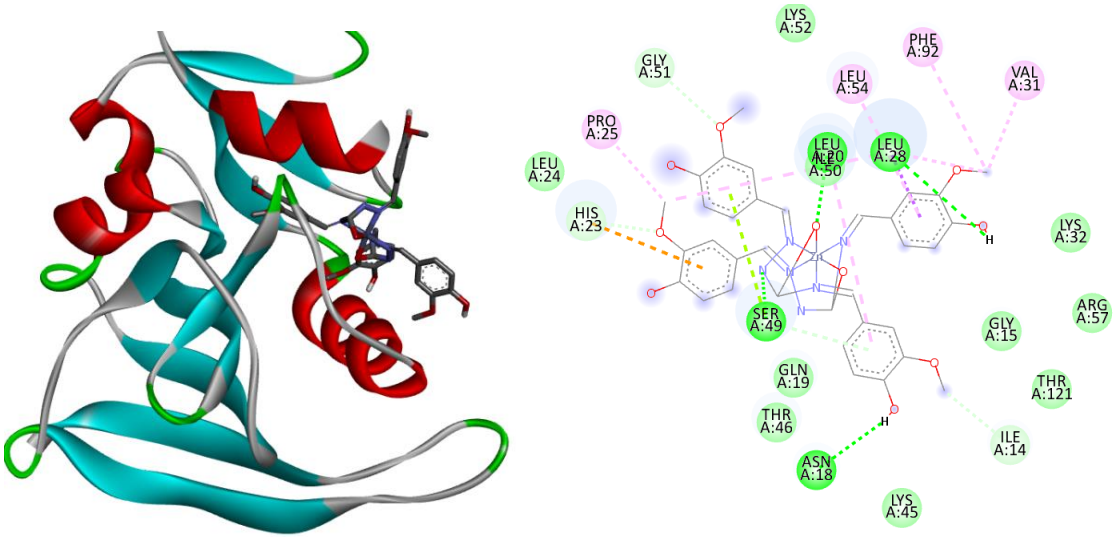

a) **Zn(L3)2@2wgh** b)

Figure 67. The binding interactions of complex **6**, $[Zn(L3)_2].2H_2O$, against *S. aureus* (PDB: 2w9h, reported experimentally as a complex with trimethoprim); a) 3D and b) 2D representations

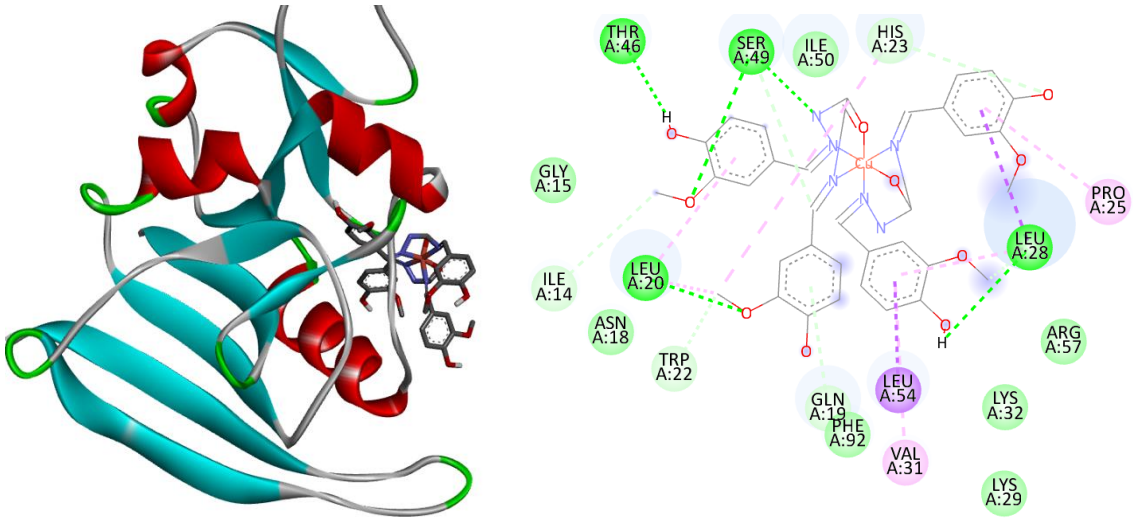

a) **Cu(L2)2@2wgh** b)

Figure 68. The binding interactions of complex **7**, $[Cu(L_2)_2].3H_2O$, against *S. aureus* (PDB: 2w9h, reported experimentally as a complex with trimethoprim); **a**) 3D and **b**) 2D representations.

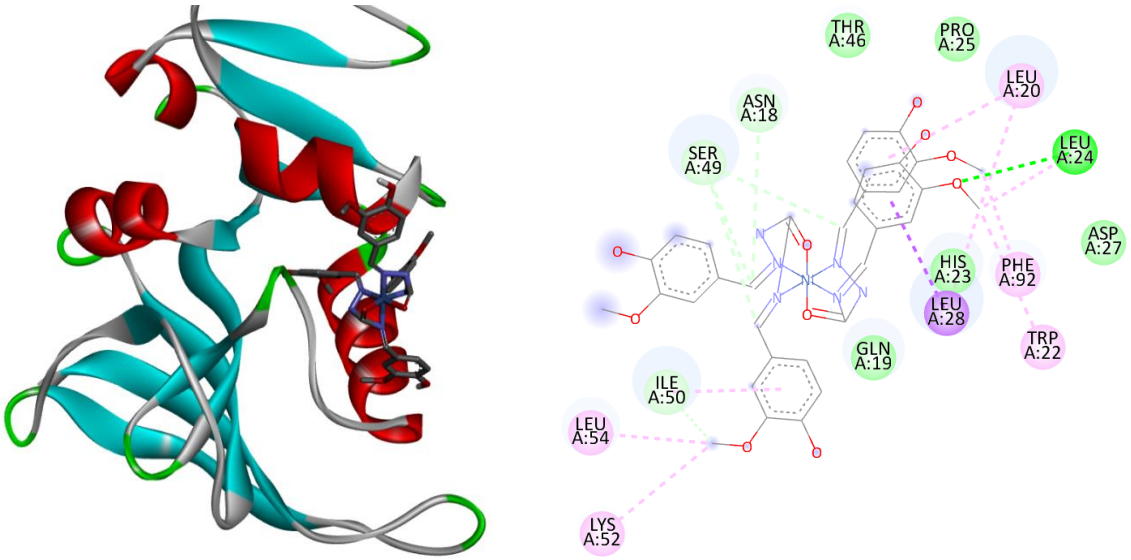

a) **Ni(L3)2@2wgh** **b)**

Figure 69. The binding interactions of complex **8**, $[Ni(L3)_2].4H_2O$, against *S. aureus* (PDB: 2w9h, reported experimentally as a complex with trimethoprim); a) 3D and b) 2D representations

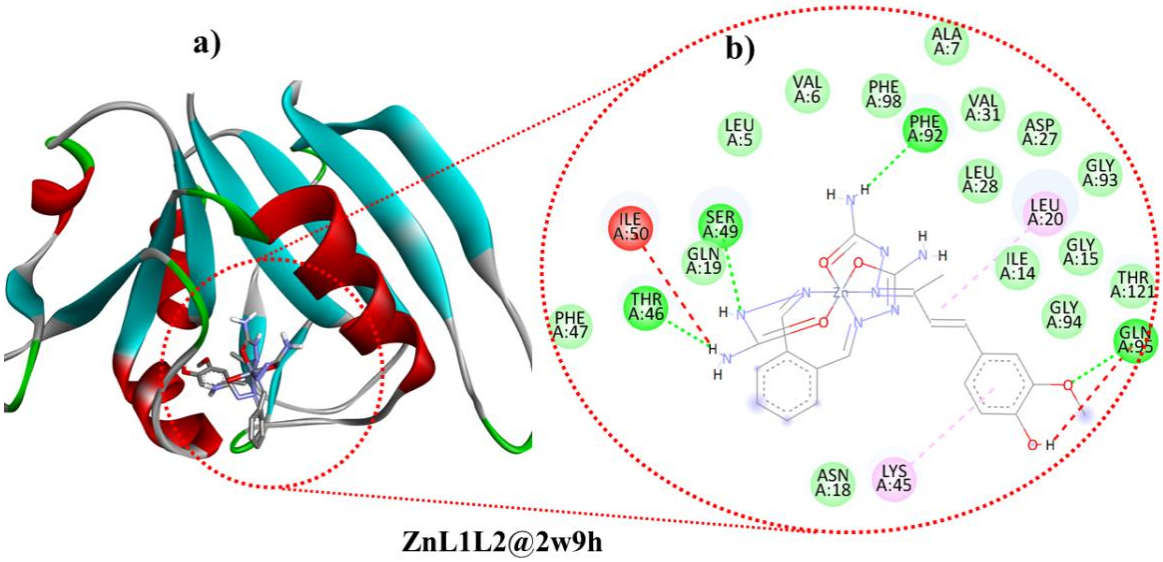

ZnL1L2@2w9h

Figure 70. The binding interactions of complex **9**, [Zn(L1)(L4)], against *S. aureus* (PDB: 2w9h, reported experimentally as a complex with trimethoprim); a) 3D and b) 2D representations

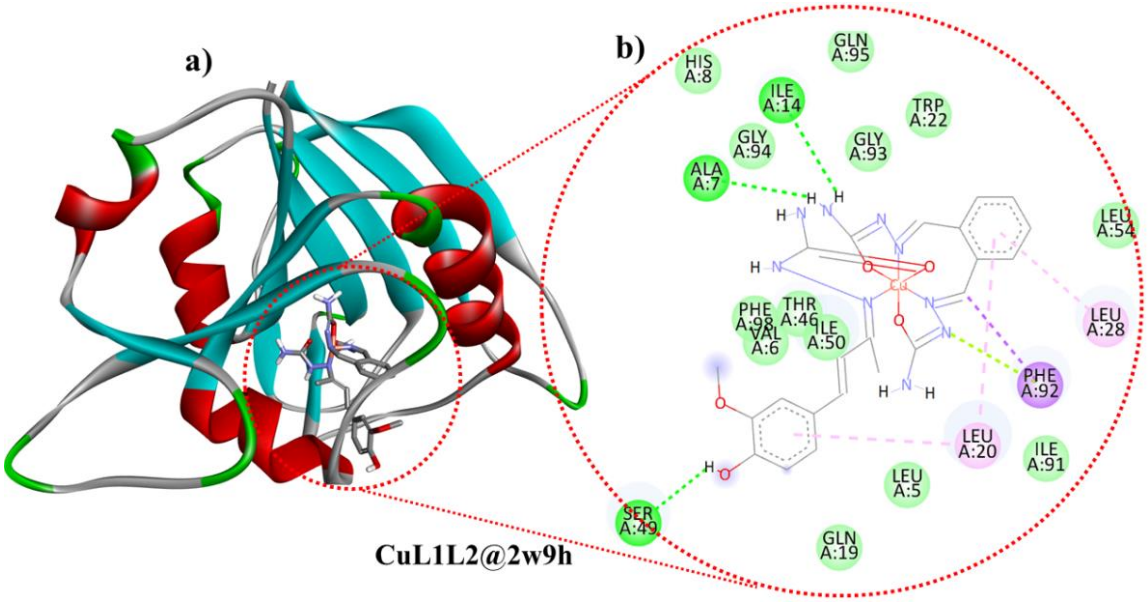

Figure 71. The binding interactions of complex **10**, [Cu(L1)(L4)], against *S. aureus* (PDB: 2w9h, reported experimentally as a complex with trimethoprim); a) 3D and b) 2D representations.

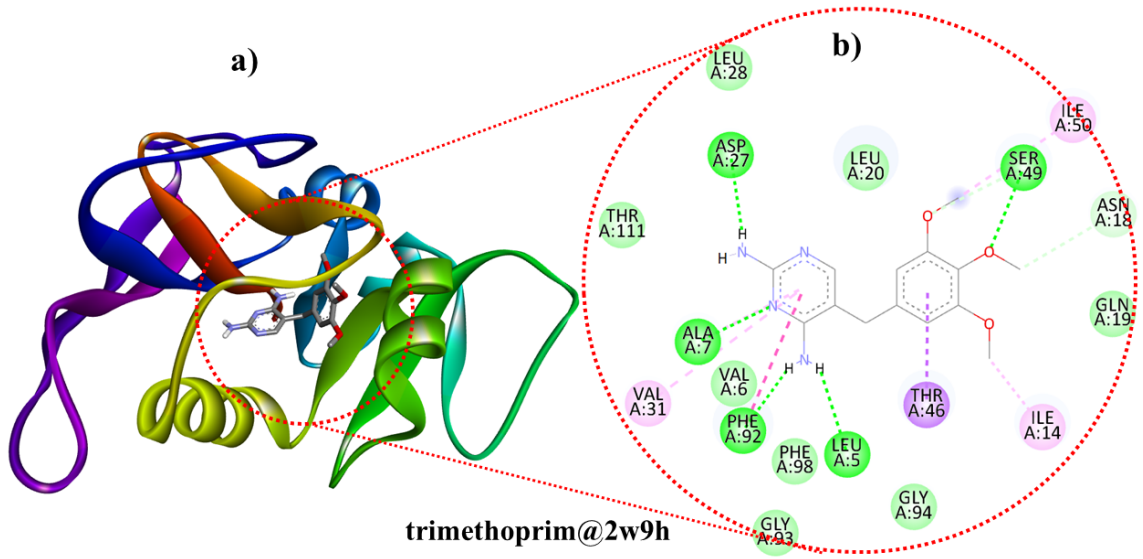

Figure 72. The binding interactions of **trimethoprim** against *S. aureus* (PDB: 2w9h, reported experimentally as a complex with trimethoprim); a) 3D and b) 2D representations

4.4.3. Binding interaction studies of the samples on *P. aeruginosa* (PDB: 2UV0)

Pseudomonas aeruginosa is one type of gram–negative bacteria species widely existing in nature causing various infections. It is one of the multi-drug resistant (MDR) pathogens. Antibiotics with hydrophilic properties can enter cells via non-specifically diffusing across

membrane porin proteins (Tamber & Hancock, 2003). *P. aeruginosa* uses less non-specific porin proteins and more-selective molecules to take in the necessary nutrients, limiting antibiotic entrance as its defense mechanism. This adaptation lowers permeability to toxic substances like drugs. It has grown resistant to commonly used antibiotics like cephalosporins and carbapenems (Hancock & Speert, 2000). However, in this study, the prepared compounds showed higher *in vitro* activity results against the *P. aeruginosa* pathogen. Furthermore, molecular docking tests for the ligand and complexes were conducted as part of these inquiries to assess their interaction and conformation with these bacterium enzymes (Figures 73-77). The obtained docking data were summarized and analyzed relative to Trimethoprim as standard as displayed in Table 13.

Table 13. Molecular docking scores and the corresponding prominent residual amino acid interactions of the ligand (**L3**) and complex (**6-8**) against *P. aeruginosa* (PDB: 2UV0)

Compounds	**Binding energy (kcal/mol)**	**H-bonding with**	**π-Sigma/π-Alkyl**	**van der Waals**
L3	-8.26	Arg61	Asp73,Val76, Cys79,Ala127	Leu36,Thr75, Thr115,Gly126
$[Zn(L3)_2].3H_2O$ (6)	-7.03	Lys16,Ser20, Tyr56	Leu36,Arg61, Asp65	Ile35,Ile52, Val53,Gly54
$[Cu(L3)_2].3H_2O$ (7)	-7.21	Ser20,Asn49, Tyr56	Leu36,Phe51, Arg61,Asp65	Glu48,Ile52, Val53,Gly54
$[Ni(L3)_2].3H_2O$ (8)	-6.70	Ser20,Gln24, Ala50,Ile52	Val53	Ala21,Gly54, Asn55,Ala58
Trimethoprim	-8.27	Arg61,Thr75, Asp73,Tyr93	Leu36,Ile52, Tyr64,Val76	Tyr56,Phe101, Ser129

The information presented in Table 13 showed that the binding energy of the compounds against *P. aeruginosa* (PDB: 2UV0) was observed between -6.70 kcal/mol to -8.26 kcal/mol. The ligand possesses the best binding energy which is -8.26 kcal/mol the same as the reference drug Trimethoprim (-8.27 kcal/mol), while the homoleptic metal (II) complexes showed moderate binding energy between (-6.70 kcal/mol to -7.21 kcal/mol). All the ligands and the complexes showed the best interaction affinities with different amino acid residues.

As observed from the 2D binding interaction model the ligand **L3** forms a hydrogen bond with Arg61 through its carbonyl (C=O) group. The π-sigma/π-alkyl interactions occurred between **L3** and amino acid residues (Asp73, Val76, Crys79, and Ala127) (Figure 73). Complex **6** has shown three H-bonding interactions with Lys16, Ser20, and Tyr56 by its hydroxyl, and methoxy (-OH and $–OCH_3$) groups. Also forms several hydrophobic and van der Waals interactions with amino acid residues (Figure 74). The next and more potent compound having good binding energy is complex **7**, which forms H-bonding with Ser20, Asn49, and Tyr56 amino acid scums through its hydroxyl and methoxy (-OH and OCH_3) active sites. Also, it forms hydrophobic interactions with Leu36, Phe51, Arg61, and Asp65 residues (Figure 75).

Similarly, complex **8** having moderate binding energy (-6.70 kcal/mol) has shown hydrogen binding interaction with Ser20, Gln24, Ala50, and Ile52 through its hydroxyl and methoxy groups. And possess hydrophobic interaction with the amino acid Val53 (Figure 76). The ligand and complexes possess the same hydrophilic interaction with the amino acid residues as that of the reference during Trimethoprim such as L = Val76, complex 6 = Leu36, and complex 7 = Leu36 as shown in Table 13. The synthesized compounds also showed van der Waals interaction with several amino acids similar to the reference drug, Trimethoprim (Table 13). Figures 73 - 77 below was hold information summarized under Table 13.

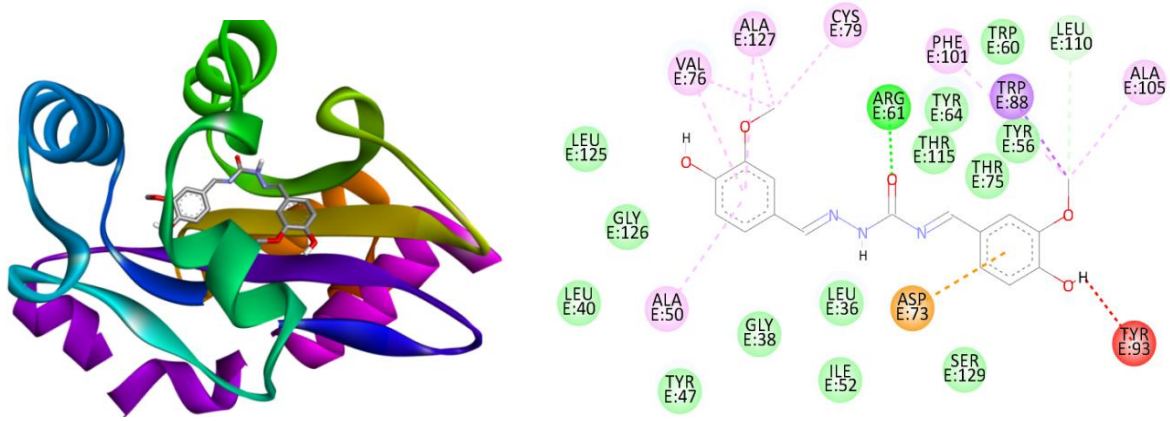

a) **b)**

Figure 73. The binding interactions of **L3** against *P. aeruginosa* (PDB: 2UV0); a) 3D and b) 2D representations

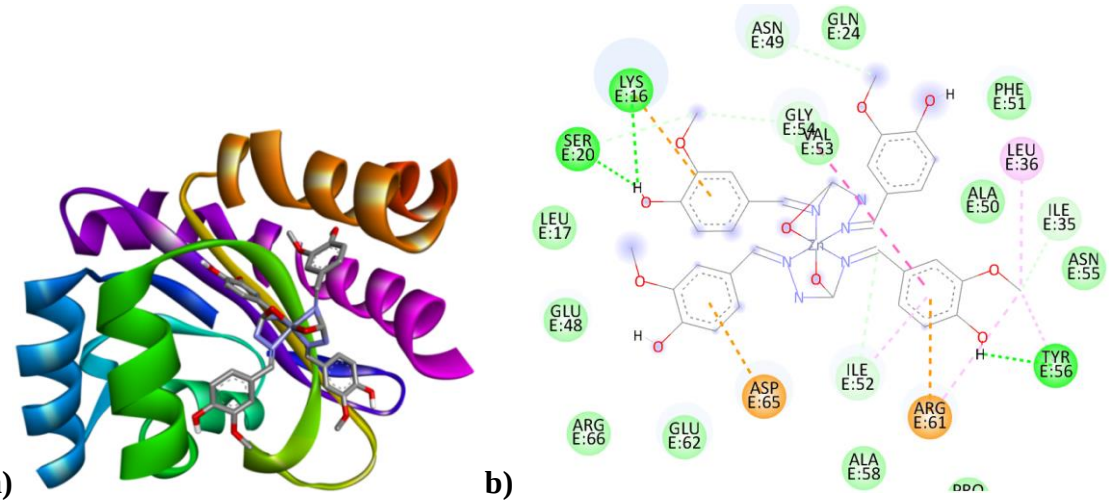

Figure 74. The binding interactions of complex **6** against *P. aeruginosa* (PDB: 2UV0); **a)** 3D and **b)** 2D representations.

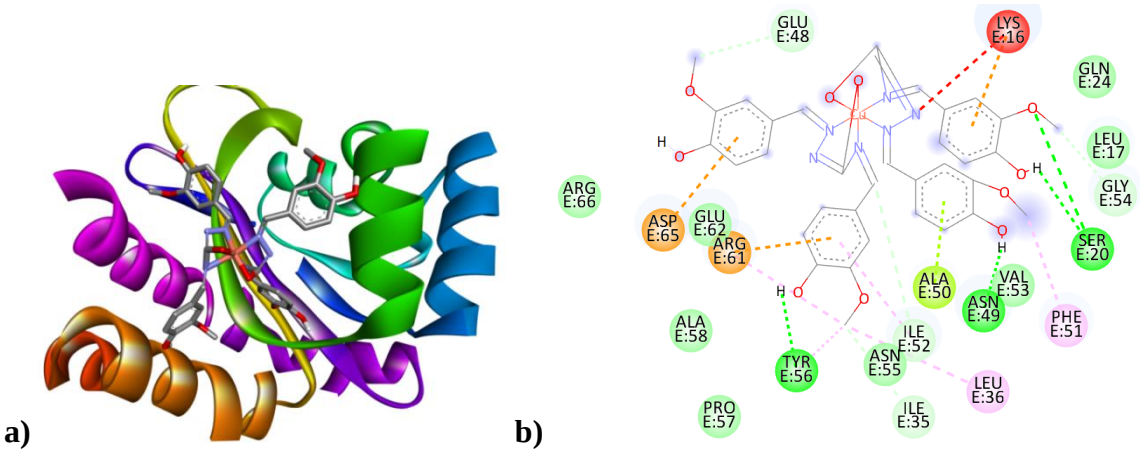

Figure 75. The binding interactions of complex 7 against *P. aeruginosa* (PDB: 2UV0); a) 3D and b) 2D representations

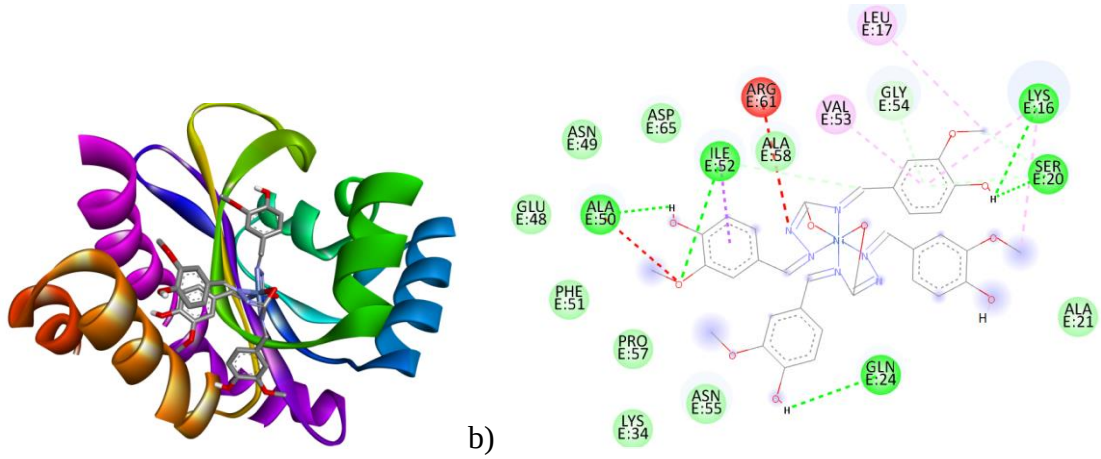

Figure 76. The binding interactions of complex 8 against *P. aeruginosa* (PDB: 2UV0); a) 3D and b) 2D representations

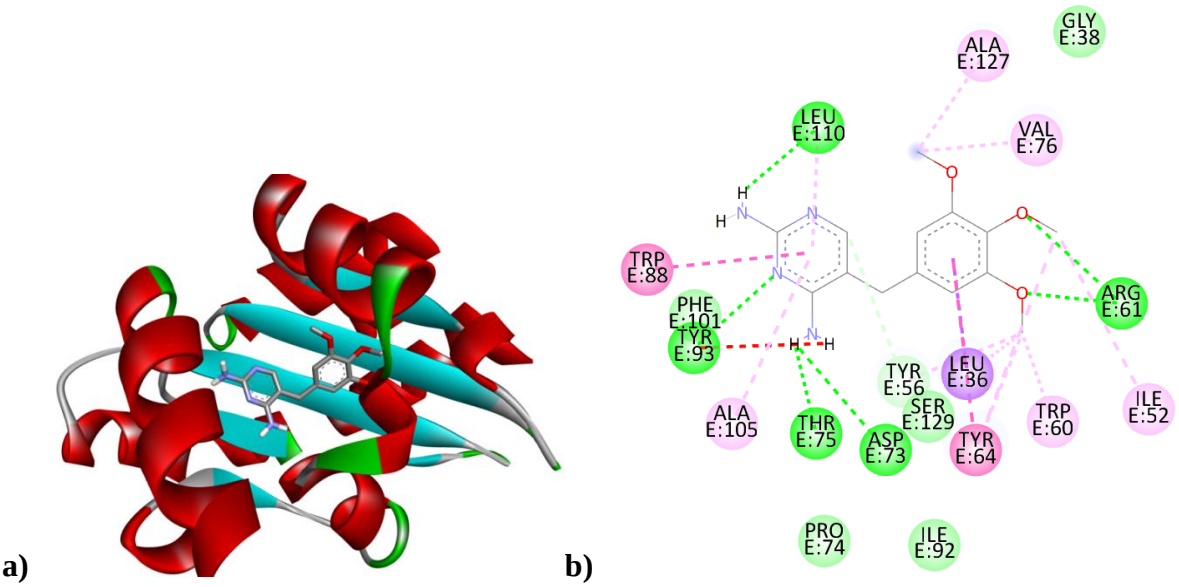

Figure 77. The binding interactions of **trimethoprim** against *P. aeruginosa* (PDB: 2UV0); **a)** 3D and **b)** 2D representations

Also, the molecular docking tests for the ligands (**L1** and **L4**) and their heteroleptic complexes (**9** and **10**) were conducted as part of these inquiries against *P. aeruginosa* (PDB: 2UV0) to assess their interaction and conformation with this bacterium enzymes. The obtained docking results were summarized and analyzed relative to the standard drug Trimethoprim as display in Table 14.

Table 14. Molecular docking scores and the corresponding prominent residual amino acid interactions of the ligands and their heteroleptic complexes against *P. aeruginosa* (PDB: 2UV0)

Compounds	**Binding energy (kcal/mol)**	**H-bonding with**	**π-Sigma/π-Alkyl**	**van der Waals**
L1	-7.36	Leu125	Leu36,Gly38, Tyr64,Val76	Ile52,Trp88, Ser129,Gly126
L4	-7.64	Tyr47,Tyr64, Asp73,Ser129	Val76,Cys79, Leu125,Ala127	Leu36,Leu40, Ile52,Ala70
Complex 9	-6.29	Ser20,Ala50, Gly54,Arg61	Val53	Lys16,Glu48, Phe51,Glu62
Complex 10	-7.64	Tyr47,Asp65	Asp73,Ala70, Val76	Ala50,Ile52, Ala127,Tyr64
Trimethoprim	-8.27	Arg61,Thr75, Asp73,Tyr93	Leu36,Ile52, Tyr64,Val76	Tyr56,Phe101, Ser129

The data in Table 14 presented the minimum binding quantity of energy for the prepared samples against *P. aeruginosa* (PDB: 2UV0) were found to be between -6.29 to -.7.64 kcal/mol. The prepared compounds interacted with the main amino acid residues of *P. aeruginosa* (PDB: 2UV0) through forming H-bonds and π-Sigma/π-Alkyl (hydrophobic) interactions. For instance, complex **9** forms H-bonds with Ser20, Ala50, Gly54, and Arg61 (Figure 80), and complex **10** forms hydrogen bonds with Tyr47 and Asp65 amino acid residues (Figure 81). Also, they form hydrophobic and van der Waals interactions with various amino acid residues at the active sites of the protein. The observed docking scores of the ligands and complexes on *P. aeruginosa* showed moderate and similar binding affinity compared to Trimethoprim (Figure 82). Both **L4** and complex **10** possess good binding energy (-7.64 kcal/mol) relative to the others when compared with Trimethoprim (-8.27 kcal/mol).

On the other hand, the *in vitro* assay results of these complexes against *p. aeruginosa* showed an inhibition zone of 13.32 ± 0.12 mm for complex **9** and 12.43 ± 0.23 mm for complex **10**, which indicated that the docking results obtained agree with the *in vitro* activity data. Hence, the compounds can be considered the best antibacterial drug candidate with few modifications. Figures 78- 82, depict the information displayed under Table 14 by a 2D and, 3D binding model on the *P. aeruginosa* (PDB: 2UV0) bacteria species. The varied bonds that resulted between the sample compounds and amino acid residues of the bacteria were shown by variable colors: H-bonds were represented by green lines, π-Sigma/π-Alkyl interactions by pink colors, and others.

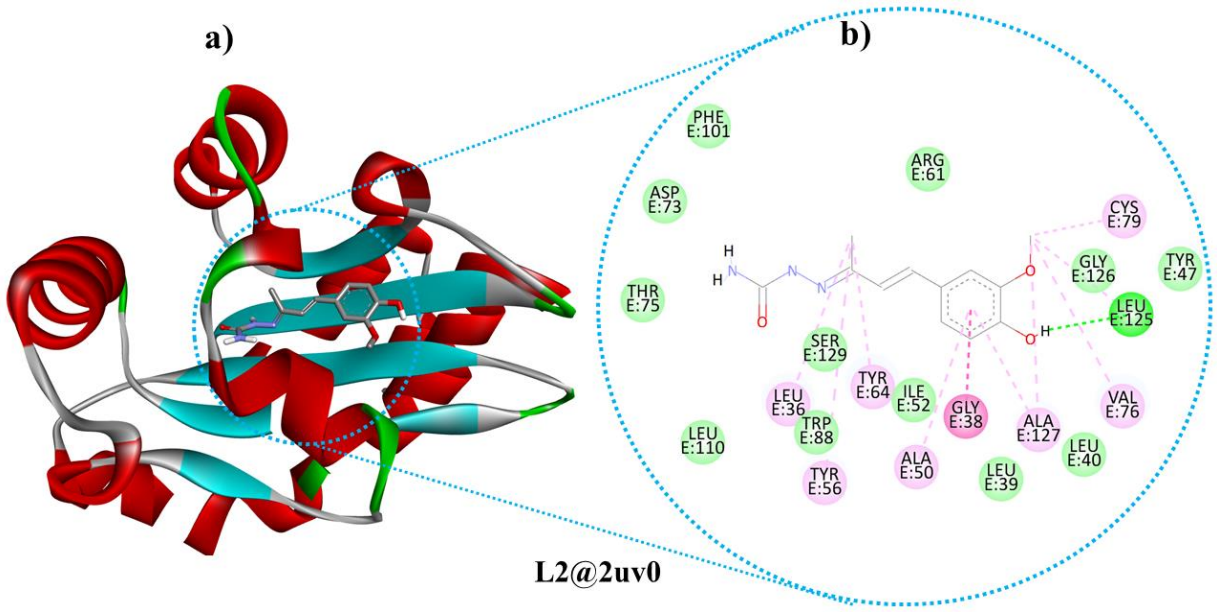

Figure 78. The binding interactions of **L1** against *P. aeruginosa* (PDB: 2UV0); a) 3D and b) 2D representations.

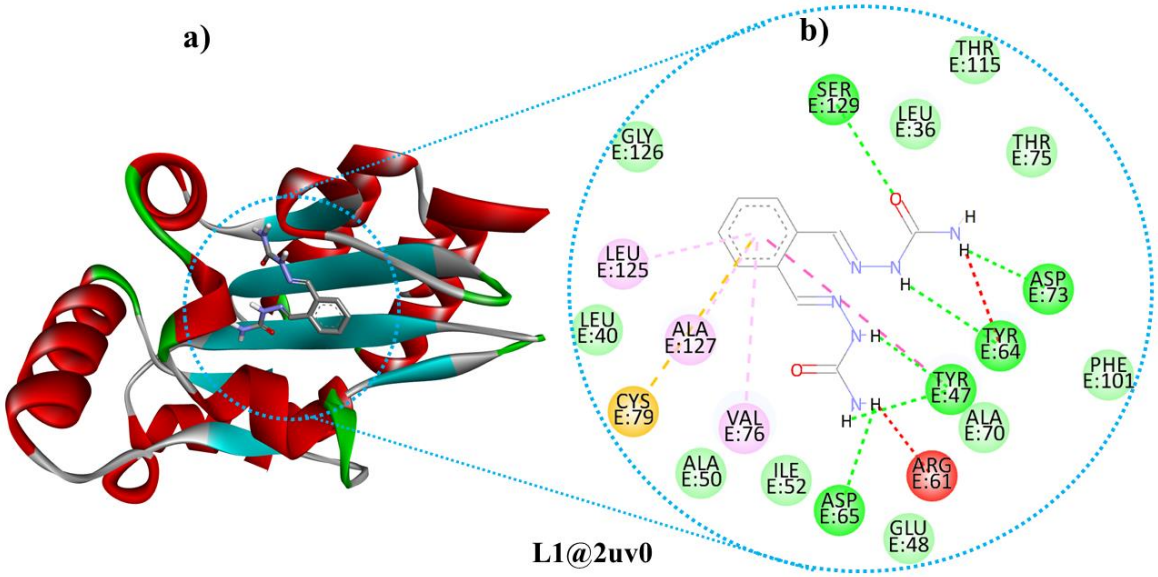

Figure 79. The binding interactions of **L4** against *P. aeruginosa* (PDB: 2UV0); **a)** 3D and **b)** 2D representations

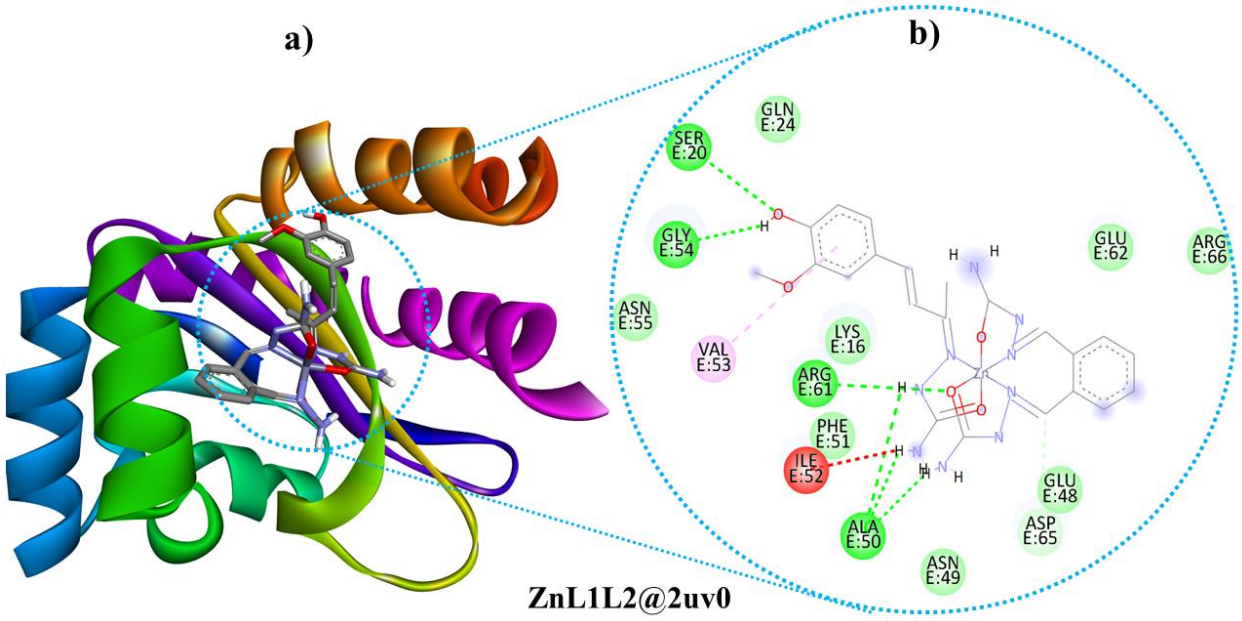

Figure 80. The binding interactions of complex **9** against *P. aeruginosa* (PDB: 2UV0); **a)** 3D and **b)** 2D representations

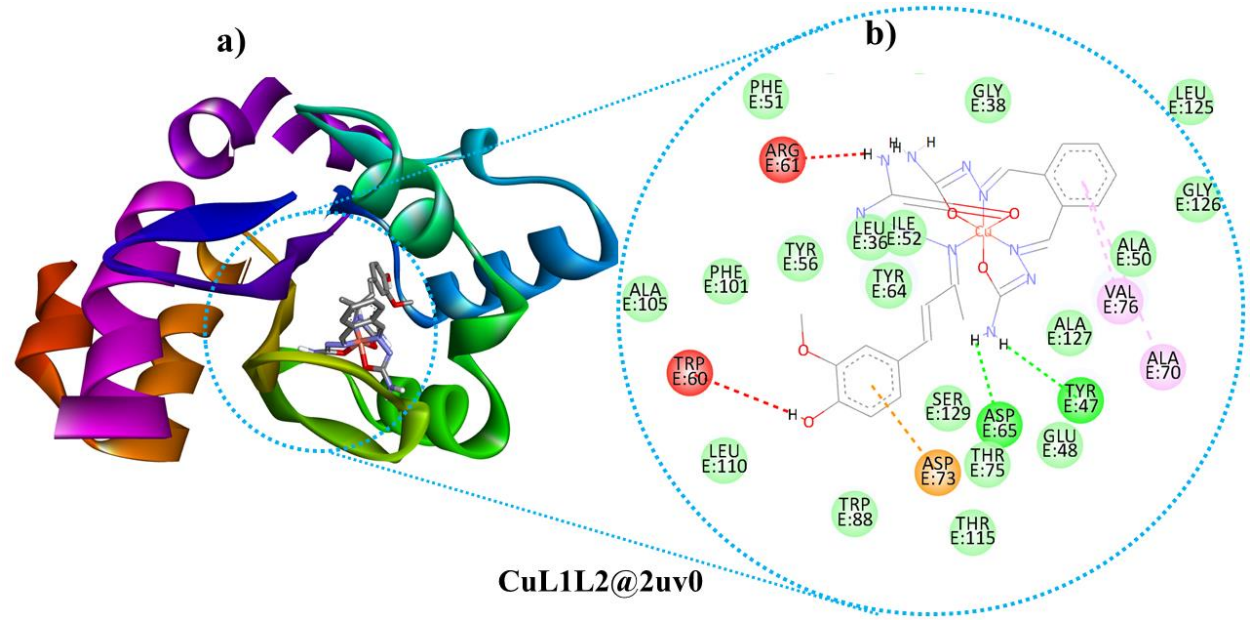

Figure 81. The binding interactions of complex **10** against *P. aeruginosa* (PDB: 2UV0); **a)** 3D and **b)** 2D representations

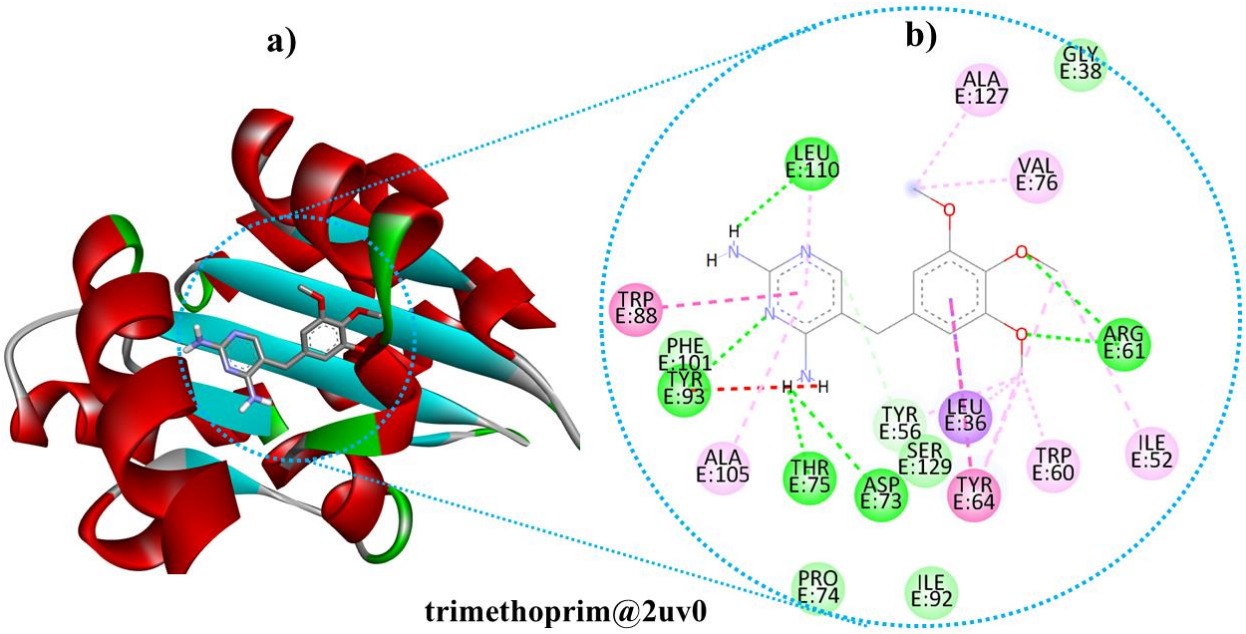

Figure 82. The binding interactions of **trimethoprim** against *P. aeruginosa* (PDB: 2UV0); **a)** 3D and **b)** 2D representations

4.4.4. *In-Silico* Pharmacokinetics (Drug-likeness) and Toxicity analysis of the ligands

The physicochemical, ADME properties and drug likeness of the ligands (**L1 - L4**) are presented in Tables 15 and 16. The synthesized ligands have molecular weights ranging from 243.34 to 265.33 g/mol. The drug likeness of the synthesized ligands (**L1 - L4**) was characterized according to 'Lipinski's rule of five'. As per the Lipinski's rule, the potential molecules should have the following physicochemical properties;(Lipinski, Lombardo, Dominy, & Feeney, 2012; M.-Q. Zhang & Wilkinson, 2007), such as, (i) less than 5 hydrogen-bond donors (HBDs), (ii) less than 10 hydrogen-bond acceptors (HBAs), (iii) a molecular mass less than 500 Da and (iv) log P not greater than 5 and (v) total polar surface area (TPSA) should not be greater than 140 Å. In general Lipinski's rule states that, an orally active drug has no more than one violation of the above criteria.

Table 15. Drug-likeness predictions of ligands, computed by SwissADME

Ligand	Mol.Wt (g/mol)	NHD	NHA	NRB	TPSA ($A^{\circ 2}$)	Log *P* (iLOGP) Lipophilicity	Log *S* (ESOL) Water Solub.	Synthetic Accessibility	Lipinski's rule of five
L1	249.27	3	4	5	96.94	1.42	-1.90	2.80	0
L2	265.33	3	3	5	111.96	2.51	-2.38	2.95	0
L3	343.34	4	5	4	135.84	1.82	-2.34	2.40	0
L4	248.24	4	4	6	134.96	-0.43	-0.78	2.37	0
Trimethoprim	290.32	2	5	5	105.51	2.21	-2.31	2.58	0

NHD = number of hydrogen donors, NHA = number of hydrogen acceptors, NRB = number of rotatable bonds, and TPSA = total polar surface area.

According to the data summarized in Table 15, the iLogP values of the ligands **L1** to **L4** were found to be 1.42, 2.51, 1.82, and -0.43, respectively, compared to the standard drug Trimethoprim (2.21). The low value of iLogP for the ligands indicates good water solubility relative to the control (Balajee, Srinivasadesikan, Sakthivadivel, & Gunasekaran, 2016). Thus, the synthesized ligands have good water solubility values than the standard drug except for ligand **L2** which are in good agreement with the experimental solubility data values. The number of hydrogen bond donors (HBDs) of all the ligands were 3 and 4, which are less than five (<5), whereas the number of hydrogen bond acceptors (HBAs) range from 3 to 5, which are less than ten (≤ 10). Also, the TPSA (topological polar surface area) of the synthesized ligands ranges from 96.94 to 134.96 Å, which are less than 140 Å satisfying Lipinski's rule of five. As per the previously reported studies, compounds with a TPSA value of 140 Å and below would be well absorbed by the intestine. Polar surface area (TPSA) has been a widely used method in molecular descriptors in the study of drug transport properties like as intestinal absorption (Prasanna & Doerksen, 2009). Thus, the TPSA data of the ligands confirm they have good intestinal absorption. Therefore, the SwissADME computed results showed that all the synthesized ligands (**1-4**) in the present study are satisfying Lipinski's rule of five with zero violations (Ahmed & Alkali, 2019). Hence, all the ligands can be a good starting point of view for the synthesis of their metal complexes and might be candidates for antibacterial, antioxidant, and antifungal studies.

A study about the absorption, distribution, metabolism, and excretion (ADME) nature of compounds is also a key parameter in the investigation of bioactive drug agents. The toxicity properties of the synthesized ligands (**L1** – **L4**) depend on ADME properties compared to the reference drugs Trimethoprim are summarized in Table 16.

Table 16. ADME predictions of ligands, computed by SwissADME and PreADMET

Ligands	**SPV (Log *Kp*) cm/s**	**GI Absorption**	**BBBp**	**Inhibitor Interaction**					
				Pgp substrate	**CYP1A2 inhibitor**	**CYP2C19 inhibitor**	**CYP2C9 inhibitor**	**CYP2D6 inhibitor**	**CYP3A4 inhibitor**
L1	-7.15	High	No	No	No	No	No	No	No
L2	-6.82	High	No	No	No	No	No	No	No
L3	-7.50	High	No	No	No	No	No	No	No
L4	-7.82	High	No	No	No	No	No	No	No
Trimethoprim	-7.42	High	No	Yes	No	No	No	No	No

SPV = Skin Permeation Value, *GI = gastrointestinal, BBBP = blood brain barrier pereabilityr, P-gp = P-glycoprotein, and CYP = cytochrome-P*

The compound with a large negative value of logKp confirms incapable to absorb by the skin. Thus, the ligands **L1**, **L3**, and **L4** have shown similar skin absorption (-7.15, -7.50, and -7.82 cm/s respectively) to the standard drug trimethoprim (-7.42 cm/s) while **L2** showed a higher skin absorption value (-6.82 cm/s). Furthermore, the ligands have shown high absorption by GI but all have shown no blood-brain barrier absorptivity.

Acute toxicity predictions result such as LD_{50} values and toxicity class classification [**1** (toxic) to **6** (non-toxic)] reveal that none of the ligands has shown acute toxicity and were found similar to standard drugs. The LD_{50} values and toxicity class classification [1 (toxic) to 6 (non-toxic)] and organ toxicity results were present in Table 17.

Table 17.Toxicity analysis of ligands

Ligands	LD_{50} (mg/kg	Toxicity Class	Organ Toxicity					
			Hepatotoxicity	Carcinogenicity	Immunotoxicity	Mutagenicity	Cytotoxicity	Irritant
L1	3400	4	Active	Active	Active	Active	Inactive	No
L2	3500	5	Active	Active	Active	Inactive	Inactive	No
L3	3600	5	Inactive	Active	Inactive	Inactive	Inactive	No
L4	3200	4	Inactive	Active	Active	Inactive	Inactive	No
Trimethoprm	3500	5	Inactive	Active	Active	Inactive	Inactive	No

LD_{50} = Lethal Dose 50

The result in the table confirms that the ligands did not show severe toxicity properties similar to standard drugs. The **L1** and **L4** have displayed toxicity class classification 4 (unsafe if swallowed), while **L2** and **L3** showed better toxicity class 5. All the synthesized ligands were predicted as non-cytotoxic. Hence, depending on the analyzed data the ligand can be considered the best drug candidate. The toxicological prediction gives results of endpoints such as hepatotoxicity, carcinogenicity, mutagenicity, immunogenicity, and cytotoxicity (Table 17). All the synthesized compounds were predicted to be non-cytotoxic. Hence, based on ADMET prediction analysis, none of the compounds have shown acute toxicity so might be proven as good drug candidates.

5. CONCLUSIONS AND RECOMMENDATIONS

5.1. Conclusions

Semicarbazide and thiosemicarbazide derivatives are important class of organic compounds recently due to their biological activities. Their derivatives have been effective scaffolds to develop enhanced bioactive molecules. They are found to be physiologically and pharmacologically active compounds. The derivatives of these organic compounds can act as special ligands, possessing several heteroatoms serving as donor atoms during coordination with metals. Thus, the increasing microbial resistance to common antibiotics and difficulty of treating microorganism diseases induced the assessment of the biological activities of metal complexes with different transition metals such as zinc(II), Cu(II), and Ni(II). This approach would possibly give compounds with greater biological activity with novel modes of action in pharmacological research.

In the present study, new semicarbazone and thiosemicarbazone forms of natural product-based derivatives of dehydrozingerone, *o*-phthalaldehyde, and vanillin with their novel homoleptic and heteroleptic Zn(II), Cu(II), and Ni(II) complexes were successfully synthesized and characterized using various physical, analytical and spectral techniques. The ligands and their complexes were characterized using ^{1}H-NMR, ^{13}C-NMR, FT-IR, SEM–EDX, XRD, UV-Vis, conductometer, TGA/DTA analysis, and mass spectroscopy techniques. Accordingly, the ligands act as bidentate ON donor atoms (**L1**), bidentate SN donor atoms (**L2**), and tridentate ONN donor atoms (**L3** and **L4**) while forming their respective complex with the metals. The synthesized ligands coordinated with the metals through nitrogen (-C=N-), oxygen (-C=O), and sulfur (-C=S) donor atoms, resulting in their respective stable complexes. According to the electronic spectra information analysis and the other characterization techniques, the geometrical structure of the complexes were proposed to be octahedral (complex **1**, **2**, and **6-10**) and tetrahedral (complex **4** and **5**). Unfortunately, complex **3** showed square planar five-coordinated geometry. Furthermore, the conductivity data of all complexes showed values below 60 $\Omega^{-1}cm^{2}mol^{-1}$, confirmed the complexes formed were neutral with no free anions outside the coordination sphere. The *In vitro* antibacterial, antifungal, and antioxidant activities analysis of the ligands and their metal complexes were studied with the well diffusion method and DPPH methods.

The data obtained showed that most of the complexes displayed an enhanced antibacterial, antifungal as well as antioxidant potential than the free ligands under similar investigational conditions. Among the synthesized ligands, both **L1** and **L2**, which are natural product based-semicarbazone and thiosemicarbazone derivatives showed good antibacterial activities with an inhibition zone of 8.84 ± 0.92 mm and 10.86 ± 0.82 mm respectively against *S. pyogenes* bacteria species. The analysis of the antibacterial activities of the complexes showed that complexes (**1**-**10**) showed medium to highest antimicrobial activities. The best activities were achieved by complex **4** (15.44 ± 0.31 mm) against *P. aeruginosa),* complex **5** (14.00 ± 0.20 mm) against *S. pyogenes*, complex **6** (16.22 ± 0.27 mm) against *S. Aureus,* complex **7** (18.66 ± 0.34 mm) *against S. Aureus* bacteria pathogens compared to trimethoprim with a mean inhibition zone of 18.70 ± 0.47 mm to 21.48 ± 0.46 mm diameter. The antifungal activities data of the compounds also showed that the ligands **L1** and **L2** showed medium inhibition zone while **L4** showed lower activity and **L3** is not active against both tested fungal species (*Aspergillus fumigatus and Candida albicans*)**.** But the metal complexes were active on both fungal species. Among them, complex **1** with an inhibition zone of 10.5 - 18 mm, complex **4** with 20.2 - 26.5 mm, and complex **5** with a 16 – 24 mm diameter were the best active compounds against the two tested fungal species.

The synthesized compounds were also evaluated for their antioxidant properties using the DPPH assay method in which all metal complexes showed higher antioxidant activities than the free ligand. The order of antioxidant potential of the compounds at a maximum concentration of 100 μg/mL was arranged as Ascorbic acid > $[Ni(L1)_2Cl]$ (**3**) > $[Ni(L_3)_2].4H_2O$ (**8**) **>** $[Cu(L2)_2]$ **(5)** > $[Cu(L3)_2].3H_2O$ (**7**) > $[Zn(L2)_2]$ **(4)** > $[Zn(L3)_2].2H_2O$ (**6**) > L3 > $[Cu(L1)_2Cl_2]$ (**2**) > $[Zn(L1)_2Cl_2]$ (**1**) > **L2** > **L1**. Note that the nickel complexes showed the highest free radical scavenging potential. The *in-silico* analysis results of the binding mode of these compounds against *S. aureus (PDB: 2w9h)* and *P. aeruginosa* (PDB: 2UV0) were in good agreement with the *in-vitro* biological activity results. Generally, the ligands and complexes prepared and investigated under this study have shown promising potential as antibacterial, antioxidant, and antifungal activities and can be further optimized to serve as principal drug compounds.

5.2. Recommendations

In this study, a novel concept of coordination chemistry was applied as an important strategy to synthesize both homoleptic and heteroleptic metal complexes from synthesized bioactive organic ligands. The synthesized ligands, metal complexes, characterization techniques, and their antibacterial, antifungal, and antioxidant activities were reported. The results showed that the natural product-based semicarbazone and thiosemicarbazone and their homoleptic metal complexes were effective antibacterial and antioxidant bioactive compounds which were also supported by the *in*-silico studies. Therefore, research and development in the area of antimicrobial metallo-drug discovery is a potential strategy to overcome the global rise of antibiotic resistance. However, there are not many *in-vivo* data available at the moment on metal complexes, which limits further synthesis of such potent compounds. Hence, further investigation of the *in-vivo* antibacterial, antifungal, and antioxidant actions are recommended for future research. Additionally, using natural components of ginger to synthesize bioactive organic ligands may be the promising method for improving metal-based drug development. Therefore, it is also recommended that future studies will give more attention to natural product-based ligands and their metal complexes.

6. REFERENCES

Abbas, M. K., Ahmad, M., Barkat, K., & Aslam, N. (2017). Antifungal, antioxidant and phytochemical screening of Melia azedarach flower extracts by using different solvents. *J. Pharma. Res. Int, 20*, 1-12.

Abd El-Razek, S. E., El-Gamasy, S. M., Hassan, M., Abdel-Aziz, M. S., & Nasr, S. M. (2020). Transition metal complexes of a multidentate Schiff base ligand containing guanidine moiety: Synthesis, characterization, anti-cancer effect, and anti-microbial activity. *Journal of Molecular Structure, 1203*, 127381.

Abuga, H., & Gaobotse, G. (2019). Antibacterial potential of extracts of the roots of Zingiber officinale against bacterial strains commonly associated with nosocomial infections. *Journal of Medicinal Plants Research, 13*(2), 41-46.

Acar, J., & Rostel, B. (2001). Antimicrobial resistance: an overview. *Revue Scientifique et Technique-Office International des Epizooties*, *20*(3), 797-810.

Adhikari, S., Bhattacharjee, T., Butcher, R. J., Porchia, M., De Franco, M., Marzano, C., . . . Tisato, F. (2019). Synthesis and characterization of mixed-ligand Zn (II) and Cu (II) complexes including polyamines and dicyano-dithiolate (2-): In vitro cytotoxic activity of Cu (II) compounds. *Inorganica Chimica Acta, 498*, 119098.

Aghatabay, N. M., Neshat, A., Karabiyik, T., Somer, M., Haciu, D., & Dülger, B. (2007). Synthesis, characterization and antimicrobial activity of Fe (II), Zn (II), Cd (II) and Hg (II) complexes with 2, 6-bis (benzimidazol-2-yl) pyridine ligand. *European journal of medicinal chemistry*, *42*(2), 205-213.

Ahmad, B., Rehman, M. U., Amin, I., Arif, A., Rasool, S., Bhat, S. A., Bilal, S. (2015). A review on pharmacological properties of zingerone (4-(4-Hydroxy-3-methoxyphenyl)-2-butanone). *The Scientific World Journal, 2015*.

Ahmed, A. H., & Alkali, Y. I. (2019). In silico pharmacokinetics and molecular docking studies of lead compounds derived from Diospyros mespiliformis. *PharmaTutor, 7*(3), 31-37.

Akila, E., Usharani, M., & Rajavel, R. (2013). Metal (II) complexes of bioinorganic and medicinal relevance: Antibacterial, Antioxidant and DNA cleavage studies of tetradentate complexes involving O, N-donor environment of 3, 3′-dihydroxybenzidine-based Schiff bases. *International Journal of Pharmacy and Pharmaceutical Sciences, 5*(2), 573-581.

Al-Amiery, A. A., Al-Majedy, Y. K., Ibrahim, H. H., & Al-Tamimi, A. A. (2012). Antioxidant, antimicrobial, and theoretical studies of the thiosemicarbazone derivative Schiff base 2-(2-imino-1-methylimidazolidin-4-ylidene) hydrazinecarbothioamide (IMHC). *Organic and medicinal chemistry letters, 2*, 1-7.

Al-Amiery, A. A., Kadhum, A. A. H., & Mohamad, A. B. (2012). Antifungal and antioxidant activities of pyrrolidone thiosemicarbazone complexes. *Bioinorganic chemistry and applications, 2012*.

Al-Noor, T., Al-barki, N., Maihub, A., & El-ajaily, M. (2017). Synthesis and spectroscopic characterization of some mixed schiff base complexes. *International Journal of Science and Research, 6*(3), 2421-2426.

Alhadi, A. A., Shaker, S. A., Yehye, W. A., Ali, H. M., & Abdullah, M. A. (2012). Synthesis, magnetic and spectroscopic studies of Ni (II), Cu (II), Zn (II) and Cd (II) complexes of a newly Schiff base derived from 5-bromo-2-hydroxybezylidene)-3, 4, 5-trihydroxybenzohydrazide. *Bulletin of the Chemical Society of Ethiopia, 26*(1).

Ali, A. E., Elasala, G. S., Mohamed, E. A., & Kolkaila, S. A. (2019). Spectral, thermal studies and biological activity of pyrazinamide complexes. *Heliyon, 5*(11), e02912.

Alias, M., Kassum, H., & Shakir, C. (2014). Synthesis, physical characterization and biological evaluation of Schiff base M (II) complexes. *Journal of the Association of Arab Universities for Basic and Applied Sciences, 15*(1), 28-34.

Aliyu, H., & Mohammed, A. (2009). Synthesis and characterization of iron (ii) and nickel (ii) schiff base complexes. *Bayero Journal of Pure and Applied Sciences, 2*(1), 132-134.

Ambala, A., & Lincoln, C. A. (2020). Synthesis, characterization, antimicrobial activity and DNA cleavage study of (E)-2-(((2-(P-Tolyloxy) Quinolin-3-Yl) Methylene) Amino) Benzenethiol Schiff base metal complexes. *Chemical Data Collections, 27*, 100372.

Amerikova, M. (2019). Pencheva El-Tibi I, Maslarska V, Bozhanov S, Tachkov K. Antimicrobial activity, mechanism of action, and methods for stabilisation of defensins as new therapeutic agents. *Biotechnol Biotechnol Equip, 33*(1), 671-682.

Amerikova, M., Pencheva El-Tibi, I., Maslarska, V., Bozhanov, S., & Tachkov, K. (2019). Antimicrobial activity, mechanism of action, and methods for stabilisation of defensins as new therapeutic agents. *Biotechnology & Biotechnological Equipment, 33*(1), 671-682.

Andres, S. A., Bajaj, K., Vishnosky, N. S., Peterson, M. A., Mashuta, M. S., Buchanan, R. M., . . . Grapperhaus, C. A. (2020). Synthesis, characterization, and biological activity

of hybrid thiosemicarbazone–alkylthiocarbamate metal complexes. *Inorganic chemistry, 59*(7), 4924-4935.

Arjmand, F., Mohani, B., & Ahmad, S. (2005). Synthesis, antibacterial, antifungal activity and interaction of CT-DNA with a new benzimidazole derived Cu (II) complex. *European journal of medicinal chemistry, 40*(11), 1103-1110.

Arshad, M., Khan, S. A., Masud, K., Arshad, N., & Ghani, A. (2000). A thermal analysis study of 1, 2-dipiperidinoethane complexes of cobalt, nickel, copper, zinc and cadmium by TG–DTG–DTA techniques. *Thermochimica acta, 364*(1-2), 143-153.

Awasthi, A., Lohani, M., Singh, M. K., Singh, A. T., & Jaggi, M. (2014). Pharmacokinetic evaluation of C-3 modified 1, 8-naphthyridine-3-carboxamide derivatives with potent anticancer activity: lead finding. *Journal of enzyme inhibition and medicinal chemistry, 29*(5), 710-721.

Awolope, R. O., Ejidike, I. P., & Clayton, H. S. (2023). Schiff base metal complexes as a dual antioxidant and antimicrobial agents. *Journal of Applied Pharmaceutical Science, 13*(3), 132-140.

Azimi, F., Ghasemi, J. B., Azizian, H., Najafi, M., Faramarzi, M. A., Saghaei, L., . . . Mahdavi, M. (2021). Design and synthesis of novel pyrazole-phenyl semicarbazone derivatives as potential α-glucosidase inhibitor: Kinetics and molecular dynamics simulation study. *International Journal of Biological Macromolecules, 166*, 1082-1095.

Ba, S., At, K., & Mg, A. E.-N. (2018). A therapeutic journey of semicarbazide and thio semicarbazide derivatives and their transition metals complexes: mini review. *Research & Reviews: Journal of Chemistry*.

Babamale, H., Lawal, A., Oloyede, E., & Rajee, O. (2016). Synthesis, Characterization and Biological Studies of Mixed Paracetamol-Ascorbic acid Metal Complexes.

Babamale, H., Lawal, A., Rajee, O., & Oloyede, E. (2016). Synthesis, characterization and biological activity studies of mixed paracetamol-ascorbic acid metal complexes. *Journal of Applied Sciences and Environmental Management, 20*(4), 1157-1161.

Badwaik, V., Deshmukh, R., & Aswar, A. (2009). Transition metal complexes of a Schiff base: synthesis, characterization, and antibacterial studies. *Journal of Coordination Chemistry, 62*(12), 2037-2047.

Baeuerle, P. A., & Baichwal, V. R. (1997). NF-kB as a frequent target for immunosuppressive and anti-inflammatory molecules. *Advances in immunology, 65*, 111-138.

Bahojb Noruzi, E., Shaabani, B., Geremia, S., Hickey, N., Nitti, P., & Kafil, H. S. (2020). Synthesis, crystal structure, and biological activity of a multidentate calix [4] arene ligand doubly functionalized by 2-hydroxybenzeledene-thiosemicarbazone. *Molecules, 25*(2), 370.

Bakir, M., Lawrence, M. A., Ferhat, M., & Conry, R. R. (2017). Spectroscopic, electrochemical and X-ray crystallographic properties of a novel palladium (II) complex of thioamide deprotonated di-2-pyridyl ketone thiosemicarbazone (dpktsc-H)−. *Journal of Coordination Chemistry*, *70*(17), 3048-3064.

Balajee, R., Srinivasadesikan, V., Sakthivadivel, M., & Gunasekaran, P. (2016). In silico screening, alanine mutation, and DFT approaches for identification of NS2B/NS3 protease inhibitors. *Biochemistry Research International, 2016*.

Baliga, M. S., Haniadka, R., Pereira, M. M., Thilakchand, K. R., Rao, S., & Arora, R. (2012). Radioprotective effects of Zingiber officinale Roscoe (ginger): past, present and future. *Food & function, 3*(7), 714-723.

Balouiri, M., Sadiki, M., & Ibnsouda, S. K. (2016). Methods for in vitro evaluating antimicrobial activity: A review. *Journal of pharmaceutical analysis, 6*(2), 71-79.

Bamigboye, M. O., Ejidike, I. P., Awolope, R. O., Obaleye, J. A., & Ejimofor, F. K. (2021). Preparation, characterization, and antimicrobial activities of mixed ibuprofen-salicylic acid metal-drug complexes. *Tanzania Journal of Science, 47*(5), 1835-1843.

Banerjee, P., Eckert, A. O., Schrey, A. K., & Preissner, R. (2018). ProTox-II: a webserver for the prediction of toxicity of chemicals. *Nucleic acids research, 46*(W1), W257-W263.

Banerjee, P., & Eckert, O. (2018). A.; Schrey, AK; Preissner, R. ProTox-II: A webserver for the prediction of toxicity of chemicals. *Nucleic Acids Res, 46*, W257-W263.

Barnett, B., Kretschmar, H., & Hartman, F. (1977). Structural characterization of bis (N-oxopyridine-2-thionato) zinc (II). *Inorganic chemistry, 16*(8), 1834-1838.

Belicchi Ferrari, M., Capacchi, S., & Biscegile, F. (2001). Synthesis and characterization of square planar nickel (II) complexes with p-fluorobenzaldehyde thiosemicarbazone derivatives. *Inorg Chim Acta, 312*, 81-87.

Benabadji, S. H., Wen, R., Zheng, J. B., Dong, X. C., & Yuan, S. G. (2004). Anticarcinogenic and antioxidant activity of diindolylmethane derivatives. *Acta Pharmacologica Sinica, 25*(5), 666-671.

Beyene, B. B., Mihirteu, A. M., Ayana, M. T., & Yibeltal, A. W. (2020). Synthesis, characterization and antibacterial activity of metalloporphyrins: Role of central metal ion. *Results in Chemistry, 2*, 100073.

Bisceglie, F., Bacci, C., Vismarra, A., Barilli, E., Pioli, M., Orsoni, N., & Pelosi, G. (2020). Antibacterial activity of metal complexes based on cinnamaldehyde thiosemicarbazone analogues. *Journal of inorganic biochemistry, 203*, 110888.

Bisceglie, F., Tavone, M., Mussi, F., Azzoni, S., Montalbano, S., Franzoni, S., . . . Pelosi, G. (2018). Effects of polar substituents on the biological activity of thiosemicarbazone metal complexes. *Journal of inorganic biochemistry, 179*, 60-70.

Blasco, F., Perelló, L., Latorre, J., Borrás, J., & Garciá-Granda, S. (1996). Cobalt (II), Nickel (II), and Copper (II) complexes of sulfanilamide derivatives: Synthesis, spectroscopic studies, and antibacterial activity. Crystal structure of [Co (sulfacetamide) 2 (NCS) 2]. *Journal of inorganic biochemistry, 61*(2), 143-154.

Bolhuis, A., & Aldrich-Wright, J. R. (2014). DNA as a target for antimicrobials. *Bioorganic chemistry, 55*, 51-59.

Bondet, V., Brand-Williams, W., & Berset, C. (1997). Kinetics and mechanisms of antioxidant activity using the DPPH. free radical method. *LWT-Food Science and Technology, 30*(6), 609-615.

Bottari, B., Maccari, R., Monforte, F., Ottana, R., Rotondo, E., & Vigorita, M. (2000). Isoniazid-related copper (II) and nickel (II) complexes with antimycobacterial in vitro activity. Part 9. *Bioorganic & medicinal chemistry letters, 10*(7), 657-660.

Brown, E. D., & Wright, G. D. (2016). Antibacterial drug discovery in the resistance era. *Nature, 529*(7586), 336-343.

Buczkowska, M. K. (2011). *Synthesis, characterization, antitumor and antimicrobial activities of heterocyclic transition metal complexes.*

Burmudžija, A. Z., Muškinja, J. M., Kosanić, M. M., Ranković, B. R., Novaković, S. B., Đorđević, S. B., . . . Ratković, Z. R. (2017). Cytotoxic and antimicrobial activity of dehydrozingerone based cyclopropyl derivatives. *Chemistry & Biodiversity, 14*(8), e1700077.

Cabrera-Martinez, R. M., Setlow, B., & Setlow, P. (2002). Studies on the mechanisms of the sporicidal action of ortho-phthalaldehyde. *Journal of applied microbiology, 92*(4), 675-680.

Canpolat, E., & Kaya, M. (2004). Studies on mononuclear chelates derived from substituted Schiff-base ligands (part 2): synthesis and characterization of a new 5-bromosalicyliden-p-aminoacetophenoneoxime and its complexes with Co (II), Ni (II), Cu (II) and Zn (II). *Journal of Coordination Chemistry, 57*(14), 1217-1223.

Chaires, J. B. (2006). A thermodynamic signature for drug–DNA binding mode. *Archives of biochemistry and biophysics, 453*(1), 26-31.

Chandra, S., Raizada, S., & Verma, R. (2012). Synthesis, characterisation and biological activities of copper (II) complexes with semicarbazones and thiosemicarbazones. *Journal of Chemical and Pharmaceutical Research, 4*(3), 1612-1618.

Chandra, S., & Tyagi, M. (2008). Ni (II), Pd (II) and Pt (II) complexes with ligand containing thiosemicarbazone and semicarbazone moiety: synthesis, characterization and biological investigation. *Journal of the Serbian Chemical Society, 73*(7), 727-734.

CHIOMA, F., & DON-LAWSON, C. D. (2021). Synthesis, characterization, antimicrobial, and antioxidant studies of new-fangled M (II) complexes of NO Schiff base Chelator. *Journal of Applied Chemical Science International*, 24-34.

Chohan, Z. H., Sumrra, S. H., Youssoufi, M. H., & Hadda, T. B. (2010). Metal based biologically active compounds: Design, synthesis, and antibacterial/antifungal/cytotoxic properties of triazole-derived Schiff bases and their oxovanadium (IV) complexes. *European journal of medicinal chemistry, 45*(7), 2739-2747.

Choudhary, A., Sharma, R., Nagar, M., Mohsin, M., & Meena, H. S. (2011). Synthesis, characterization and antioxidant activity of some transition metal complexes with terpenoid derivatives. *Journal of the Chilean Chemical Society, 56*(4), 911-917.

Cilliers, J., Hughes, B., & Moyer, J. (2011). African Futures 2050-the next forty years. *Institute for security studies monographs, 2011*(175), 102.

Claudel, M., Schwarte, J. V., & Fromm, K. M. (2020). New antimicrobial strategies based on metal complexes. *Chemistry, 2*(4), 849-899.

Čongrádyová, A., Jomová, K., Kucková, L., Kožíšek, J., Moncoľ, J., & Valko, M. (2021). Antimicrobial activity of copper (II) complexes. *Journal of Microbiology, Biotechnology and Food Sciences, 2021*, 67-70.

Contreras-Guzmán, E. S., & Strong III, F. C. (1982). Determination of tocopherols (vitamin E) by reduction of cupric ion. *Journal of the Association of Official Analytical Chemists, 65*(5), 1215-1221.

Cordes, E., & Jencks, W. (1962a). General acid catalysis of semicarbazone formation. *Journal of the American Chemical Society, 84*(22), 4319-4328.

Cordes, E., & Jencks, W. (1962b). On the mechanism of Schiff base formation and hydrolysis. *Journal of the American Chemical Society, 84*(5), 832-837.

d'Angelo, J., Morgant, G., Ghermani, N. E., Desmaële, D., Fraisse, B., Bonhomme, F., . . . Journaux, Y. (2008). Crystal structures and physico-chemical properties of Zn (II) and Co (II) tetraaqua (3-nitro-4-hydroxybenzoato) complexes: their anticonvulsant activities as well as related (5-nitrosalicylato)–metal complexes. *Polyhedron, 27*(2), 537-546.

Da Silva, C. M., da Silva, D. L., Modolo, L. V., Alves, R. B., de Resende, M. A., Martins, C. V., & de Fátima, Â. (2011). Schiff bases: A short review of their antimicrobial activities. *Journal of Advanced research, 2*(1), 1-8.

Daina, A., Michielin, O., & Zoete, V. (2017). SwissADME: a free web tool to evaluate pharmacokinetics, drug-likeness and medicinal chemistry friendliness of small molecules. *Scientific reports, 7*(1), 42717.

de Kraker, M. E., Stewardson, A. J., & Harbarth, S. (2016). Will 10 million people die a year due to antimicrobial resistance by 2050? *PLoS medicine, 13*(11), e1002184.

Dejpasand, M. T., Saievar-Iranizad, E., Bayat, A., Montaghemi, A., & Ardekani, S. R. (2020). Tuning HOMO and LUMO of three region (UV, Vis and IR) photoluminescent nitrogen doped graphene quantum dots for photodegradation of methylene blue. *Materials Research Bulletin, 128*, 110886.

DeLano, W. L. (2002). Pymol: An open-source molecular graphics tool. *CCP4 Newsl. Protein Crystallogr, 40*(1), 82-92.

Deshmukh, P. S., Yaul, A., Bhojane, J. N., & Aswar, A. (2010). Synthesis, characterization and thermogravimetric studies of some metal complexes with N 2 O 2 Schiff base ligand. *World Appl. Sci. J, 9*, 1301-1305.

Dhabale, R. H., Shah, S., Tiwari, N., & Patani, P. (2022). Review Of Semicarbazone, Thiosemicarbazone, And Their Transition Metal Complexes, And Their Biological Activities. *Journal of Pharmaceutical Negative Results*, 2416-2424.

Di Vaira, M., Bazzicalupi, C., Orioli, P., Messori, L., Bruni, B., & Zatta, P. (2004). Clioquinol, a drug for Alzheimer's disease specifically interfering with brain metal metabolism: structural characterization of its zinc (II) and copper (II) complexes. *Inorganic chemistry, 43*(13), 3795-3797.

Dreyer, D. (1965). Citrus bitter principles—II: Application of NMR to structural and stereochemical problems. *Tetrahedron, 21*(1), 75-87.

DS, M. Copper (II) Complex of Salicylaldehyde Semicarbazone: Synthesis, Characterization and Antibacterial Activity.

Duckworth, H. E., Barber, R. C., & Venkatasubramanian, V. (1986). Mass spectroscopy.

Duncan, C., & White, A. R. (2012). Copper complexes as therapeutic agents. *Metallomics, 4*(2), 127-138.

Dutta, R. K., Nenavathu, B. P., Gangishetty, M. K., & Reddy, A. (2012). Studies on antibacterial activity of ZnO nanoparticles by ROS induced lipid peroxidation. *Colloids and Surfaces B: Biointerfaces, 94*, 143-150.

Dutta, S., Padhye, S., Priyadarsini, K. I., & Newton, C. (2005). Antioxidant and antiproliferative activity of curcumin semicarbazone. *Bioorganic & medicinal chemistry letters, 15*(11), 2738-2744.

Ejidike, I. P., & Ajibade, P. A. (2015). Synthesis, characterization, antioxidant, and antibacterial studies of some metal (II) complexes of tetradentate schiff base ligand:(4E)-4-[(2-(E)-[1-(2, 4-dihydroxyphenyl) ethylidene] aminoethyl) imino] pentan-2-one. *Bioinorganic chemistry and applications, 2015*.

Ejidike, I. P., Bamigboye, M. O., & Clayton, H. S. (2021). Spectral, in vitro antiradical and antimicrobial assessment of copper complexes containing tridentate Schiff base derived from dihydroxybenzene functionality with diaminoethylene bridge. *Spectroscopy Letters, 54*(3), 212-230.

Ejidike, I. P., Bamigboye, M. O., Fadare, D. A., Adetunji, J. B., & Obaleye, J. A. (2022). Antimalarial and Antimicrobial Activities of some Heteroleptic Metal (II) Complexes of Sulfadiazine–Vitamin C: Synthesis and Spectroscopic Studies. *Tanzania Journal of Science, 48*(4), 973-984.

Ekennia, A. C., Onwudiwe, D. C., Olasunkanmi, L. O., Osowole, A. A., & Ebenso, E. E. (2015). Synthesis, DFT calculation, and antimicrobial studies of novel Zn (II), Co (II), Cu (II), and Mn (II) heteroleptic complexes containing benzoylacetone and dithiocarbamate. *Bioinorganic chemistry and applications, 2015*.

El-Etrawy, A.-A. S., & Sherbiny, F. F. (2021). Design, synthesis, biological assessment and molecular docking studies of some new 2-Thioxo-2, 3-dihydropyrimidin-4 (1H)-ones as potential anticancer and antibacterial agents. *Journal of Molecular Structure, 1225*, 129014.

El-Gammal, O. (2015). Mononuclear and binuclear complexes derived from hydrazone Schiff base NON donor ligand: Synthesis, structure, theoretical and biological studies. *Inorganica Chimica Acta*, *435*, 73-81.

El-Gammal, O. A., Mohamed, F. S., Rezk, G. N., & El-Bindary, A. A. (2021). Synthesis, characterization, catalytic, DNA binding and antibacterial activities of Co (II), Ni (II) and Cu (II) complexes with new Schiff base ligand. *Journal of Molecular Liquids, 326*, 115223.

El-Ghorab, A. H., Nauman, M., Anjum, F. M., Hussain, S., & Nadeem, M. (2010). A comparative study on chemical composition and antioxidant activity of ginger (Zingiber officinale) and cumin (Cuminum cyminum). *Journal of agricultural and food chemistry, 58*(14), 8231-8237.

El-Sonbati, A., Diab, M., Morgan, S. M., Abou-Dobara, M., & El-Ghettany, A. (2020). Synthesis, characterization, theoretical and molecular docking studies of mixed-ligand complexes of Cu (II), Ni (II), Co (II), Mn (II), Cr (III), UO2 (II) and Cd (II). *Journal of Molecular Structure, 1200*, 127065.

El-Sonbati, A., Diab, M., Mohamed, G., Saad, M., Morgan, S. M., & El-Sawy, S. (2019). Polymer complexes. LXXVII. Synthesis, characterization, spectroscopic studies and immune response in cattle of quinoline polymer complexes. *Applied Organometallic Chemistry, 33*(8), e4973.

El-Sonbati, A. Z., Diab, M. A., Eldesoky, A. M., Morgan, S. M., & Salem, O. L. (2019). Polymer complexes. LXXVI. Synthesis, characterization, CT-DNA binding, molecular docking and thermal studies of sulfoxine polymer complexes. *Applied Organometallic Chemistry, 33*(5), e4839.

El Jemli, M., Kamal, R., Marmouzi, I., Zerrouki, A., Cherrah, Y., & Alaoui, K. (2016). Radical-scavenging activity and ferric reducing ability of Juniperus thurifera (L.), J. oxycedrus (L.), J. phoenicea (L.) and Tetraclinis articulata (L.). *Advances in pharmacological sciences, 2016*.

Elsayed, S. A., Noufal, A. M., & El-Hendawy, A. M. (2017). Synthesis, structural characterization and antioxidant activity of some vanadium (IV), Mo (VI)/(IV) and

Ru (II) complexes of pyridoxal Schiff base derivatives. *Journal of Molecular Structure, 1144*, 120-128.

Emam, S. M., Bondock, S., & Aldaloa, A. A. (2023). Schiff base coordination compounds including thiosemicarbazide derivative and 4-benzoyl-1, 3-diphenyl-5-pyrazolone: Synthesis, structural spectral characterization and biological activity. *Results in Chemistry, 5*, 100725.

Fang, M., Chen, J.-H., Xu, X.-L., Yang, P.-H., & Hildebrand, H. F. (2006). Antibacterial activities of inorganic agents on six bacteria associated with oral infections by two susceptibility tests. *International journal of antimicrobial agents, 27*(6), 513-517.

Farrell, N. (2012). *Transition metal complexes as drugs and chemotherapeutic agents* (Vol. 11): Springer Science & Business Media.

Fathy, A., Ibrahim, A. B., Abd Elkhalik, S., Meurer, F., Bodensteiner, M., & Abbas, S. (2022). Thiosemicarbazones and Derived Antimony Complexes: Synthesis, Structural Analysis, and In Vitro Evaluation against Bacterial, Fungal, and Cancer Cells. *Inorganics, 10*(10), 172.

Ferraro, J. R. (2012). *Low-frequency vibrations of inorganic and coordination compounds*: Springer Science & Business Media.

Festus, C., Okafor, S. N., & Ekennia, A. C. (2019). Heteroleptic metal complexes of a Pyrimidinyl based Schiff base ligand incorporating 2, 2′-Bipyridine moiety: Synthesis, characterization, and biological studies. *Frontiers in chemistry, 7*, 862.

Francis, S. M., Gas, M.-E., Daugeron, M.-C., Bravo, J., & Seraphin, B. (2012). Rbg1–Tma46 dimer structure reveals new functional domains and their role in polysome recruitment. *Nucleic acids research, 40*(21), 11100-11114.

Frei, A., Zuegg, J., Elliott, A. G., Baker, M., Braese, S., Brown, C., . . . Jung, N. (2020a). Correction: Metal complexes as a promising source for new antibiotics. *Chemical Science, 11*(17), 4531-4531.

Frei, A., Zuegg, J., Elliott, A. G., Baker, M., Braese, S., Brown, C., . . . Jung, N. (2020b). Metal complexes as a promising source for new antibiotics. *Chemical Science, 11*(10), 2627-2639.

Frieri, M., Kumar, K., & Boutin, A. (2017). Antibiotic resistance. *Journal of infection and public health, 10*(4), 369-378.

Garg, A., Tadesse, A., & Eswaramoorthy, R. (2021). A four-component domino reaction: an eco-compatible and highly efficient construction of 1, 8-naphthyridine derivatives,

their in silico molecular docking, drug likeness, ADME, and toxicity studies. *Journal of Chemistry, 2021*, 1-16.

Geary, W. J. (1971). The use of conductivity measurements in organic solvents for the characterisation of coordination compounds. *Coordination Chemistry Reviews, 7*(1), 81-122.

Ghosh, C., Sarkar, P., Issa, R., & Haldar, J. (2019). Alternatives to conventional antibiotics in the era of antimicrobial resistance. *Trends in microbiology, 27*(4), 323-338.

Ghosh, M., Layek, M., Fleck, M., Saha, R., & Bandyopadhyay, D. (2015). Synthesis, crystal structure and antibacterial activities of mixed ligand copper (II) and cobalt (II) complexes of a NNS Schiff base. *Polyhedron, 85*, 312-319.

Gobara, A. G. H. (2017). *Synthesis, Characterization and Biological Activity of Some Thiosemicarbazone Ligands and their Complexes with Some M (II) ions.* University of Gezira,

Goel, S., Chandra, S., & Dwivedi, S. D. (2013). Spectroscopic and biological studies on newly synthesized Cobalt (II) and Nickel (II) complexes with 2-Acetyl coumarone semicarbazone and 2-Acetyl coumarone thiosemicarbazone. *Journal of Chemistry, 2013*.

Goel, S., Chandra, S., & Dwivedi, S. D. (2016). Synthesis, spectral and biological studies of copper (II) and iron (III) complexes derived from 2-acetyl benzofuran semicarbazone and 2-acetyl benzofuran thiosemicarbazone. *Journal of Saudi Chemical Society, 20*(6), 651-660.

Gokhale, N. H., Padhye, S. B., Billington, D. C., Rathbone, D. L., Croft, S. L., Kendrick, H. D., . . . Powell, A. K. (2003). Synthesis and characterization of copper (II) complexes of pyridine-2-carboxamidrazones as potent antimalarial agents. *Inorganica Chimica Acta, 349*, 23-29.

Gopal, N., Hill, C., Ross, P. R., Beresford, T. P., Fenelon, M. A., & Cotter, P. D. (2015). The prevalence and control of Bacillus and related spore-forming bacteria in the dairy industry. *Frontiers in microbiology, 6*, 1418.

Gostin, L. O., & Friedman, E. A. (2019). Imagining global health with justice: transformative ideas for health and well-being while leaving no one behind. *Geo. LJ, 108*, 1535.

Greenfield, T. J., Julve, M., & Doyle, R. P. (2019). Exploring the biological, catalytic, and magnetic properties of transition metal coordination complexes incorporating pyrophosphate. *Coordination Chemistry Reviews, 384*, 37-64.

Guilhelmelli, F., Vilela, N., Albuquerque, P., Derengowski, L. d. S., Silva-Pereira, I., & Kyaw, C. M. (2013). Antibiotic development challenges: the various mechanisms of action of antimicrobial peptides and of bacterial resistance. *Frontiers in microbiology, 4*, 353.

Guillot, C., Ballu, Y., Paigné, J., Lecante, J., Jain, K., Thiry, P., . . . Falicov, L. (1977). Resonant photoemission in nickel metal. *Physical Review Letters, 39*(25), 1632.

Hampannavar, G. A., Karpoormath, R., Palkar, M. B., & Shaikh, M. S. (2016). An appraisal on recent medicinal perspective of curcumin degradant: Dehydrozingerone (DZG). *Bioorganic & medicinal chemistry, 24*(4), 501-520.

Hancock, R. E., & Speert, D. P. (2000). Antibiotic resistance in Pseudomonas aeruginosa: mechanisms and impact on treatment. *Drug resistance updates, 3*(4), 247-255.

Hanif, M., & Chohan, Z. H. (2013). Design, spectral characterization and biological studies of transition metal (II) complexes with triazole Schiff bases. *Spectrochimica Acta Part A: Molecular and Biomolecular Spectroscopy, 104*, 468-476.

Hazra, B., Biswas, S., & Mandal, N. (2008). Antioxidant and free radical scavenging activity of Spondias pinnata. *BMC complementary and Alternative Medicine, 8*(1), 1-10.

Hernandez, J. A., Jiménez, A., Mullineaux, P., & Sevilia, F. (2000). Tolerance of pea (Pisum sativum L.) to long-term salt stress is associated with induction of antioxidant defences. *Plant, cell & environment, 23*(8), 853-862.

Hesamian, G. (2016). One-way ANOVA based on interval information. *International Journal of Systems Science, 47*(11), 2682-2690.

Holm, R., Everett Jr, G., & Chakravorty, A. (1966). Metal complexes of Schiff bases and β-ketoamines. *Progress in Inorganic Chemistry*, 83-214.

Holmes, A. H., Moore, L. S., Sundsfjord, A., Steinbakk, M., Regmi, S., Karkey, A., . . . Piddock, L. J. (2016). Understanding the mechanisms and drivers of antimicrobial resistance. *The Lancet, 387*(10014), 176-187.

Horowitz, E., Tryon, M., Christensen, R. G., & Perros, T. P. (1965). Thermogravimetric study of some new transition metal–schiff base coordination polymers. *Journal of Applied Polymer Science, 9*(7), 2321-2336.

Hossain, M. S., Islam, H. T., & Nuruzzaman, M. A Short Review on Antimicrobial Activity Study on Transition Metal Complexes of Ni Incorporating Schiff Bases.

Hossain, M. S., Zakaria, C., & Kudrat-E-Zahan, M. (2018). Metal complexes as potential antimicrobial agent: a review. *American Journal of Heterocyclic Chemistry, 4*(1), 1.

Hossain, M. S., Zakaria, C., Kudrat-E-Zahan, M., & Zaman, B. (2017). Synthesis, spectral and thermal characterization of Cu (II) complexes with two new Schiff base ligand towards potential biological application. *Der Chemica Sinica, 8*(3), 380-392.

Indira, S., Vinoth, G., Bharathi, M., & Bharathi, K. S. (2019). Synthesis, spectral, electrochemical, in-vitro antimicrobial and antioxidant activities of bisphenolic mannich base and 8-hydroxyquinoline based mixed ligands and their transition metal complexes. *Journal of Molecular Structure, 1198*, 126886.

Ismael, M., Abdel-Mawgoud, A.-M. M., Rabia, M. K., & Abdou, A. (2020). Design and synthesis of three Fe (III) mixed-ligand complexes: Exploration of their biological and phenoxazinone synthase-like activities. *Inorganica Chimica Acta, 505*, 119443.

Jayanthi, K., Meena, R., Chithra, K., Kannan, S., Shanthi, W., Saravanan, R., . . . Satheesh, D. (2017). Synthesis and microbial evaluation of copper (II) complexes of Schiff base ligand derived from 3-methoxysalicylaldehyde with semicarbazide and thiosemicarbazide. *J Pharm Chem Bio Sci, 5*(3), 205-215.

Jesudoss, V. A. S., Santiago, S. V. A., Venkatachalam, K., & Subramanian, P. (2017). Zingerone (ginger extract): antioxidant potential for efficacy in gastrointestinal and liver disease. In *Gastrointestinal tissue* (pp. 289-297): Elsevier.

Jiménez-Garrido, N., Perelló, L., Ortiz, R., Alzuet, G., Gonzalez-Alvarez, M., Canton, E., . . . Pérez-Priede, M. (2005). Antibacterial studies, DNA oxidative cleavage, and crystal structures of Cu (II) and Co (II) complexes with two quinolone family members, ciprofloxacin and enoxacin. *Journal of inorganic biochemistry, 99*(3), 677-689.

Jirjees, V. Y., Al-Hamdani, A. A. S., Wannas, N. M., A. R, F., Dib, A., & Al Zoubi, W. (2021). Spectroscopic characterization for new model from Schiff base and its complexes. *Journal of Physical Organic Chemistry, 34*(4), e4169.

Jomova, K., Baros, S., & Valko, M. (2012). Redox active metal-induced oxidative stress in biological systems. *Transition Metal Chemistry, 37*, 127-134.

Kaczmarek, M. T., Jastrząb, R., Hołderna-Kędzia, E., & Radecka-Paryzek, W. (2009). Self-assembled synthesis, characterization and antimicrobial activity of zinc (II) salicylaldimine complexes. *Inorganica Chimica Acta, 362*(9), 3127-3133.

Kalaichelvan, T., & Maleckid, J. G. Nickel (II) and copper (II) complexes constructed with N2S2 hybrid benzamidine-thiosemicarbazone ligand: Synthesis, X-ray crystal structure, DFT, kinetico-catalytic and in vitro biological applications.

Karaiskos, I., Lagou, S., Pontikis, K., Rapti, V., & Poulakou, G. (2019). The “old” and the “new” antibiotics for MDR gram-negative pathogens: for whom, when, and how. *Frontiers in public health, 7*, 151.

Kargar, H., Adabi Ardakani, A., Munawar, K. S., Ashfaq, M., & Tahir, M. N. (2021). Nickel (II), copper (II) and zinc (II) complexes containing symmetrical Tetradentate Schiff base ligand derived from 3, 5-diiodosalicylaldehyde: Synthesis, characterization, crystal structure and antimicrobial activity. *Journal of the Iranian Chemical Society, 18*, 2493-2503.

Kargar, H., Ardakani, A. A., Tahir, M. N., Ashfaq, M., & Munawar, K. S. (2021). Synthesis, spectral characterization, crystal structure and antibacterial activity of nickel (II), copper (II) and zinc (II) complexes containing ONNO donor Schiff base ligands. *Journal of Molecular Structure, 1233*, 130112.

Kasuga, N. C., Sekino, K., Ishikawa, M., Honda, A., Yokoyama, M., Nakano, S., . . . Nomiya, K. (2003). Synthesis, structural characterization and antimicrobial activities of 12 zinc (II) complexes with four thiosemicarbazone and two semicarbazone ligands. *Journal of inorganic biochemistry, 96*(2-3), 298-310.

Khan, S. U., Ahemad, N., Chuah, L.-H., Naidu, R., & Htar, T. T. (2020). Illustrated step by step protocol to perform molecular docking: Human estrogen receptor complex with 4-hydroxytamoxifen as a case study. *Progress in Drug Discovery & Biomedical Science, 3*(1).

Kizilcikli, İ., Kurt, Y., Akkurt, B., Genel, A., Birteksöz, S., Ötük, G., & Ülküseven, B. (2007). Antimicrobial activity of a series of thiosemicarbazones and their Zn II and Pd II complexes. *Folia microbiologica, 52*, 15-25.

Kovala-Demertzi, D. (2000). Transition metal complexes of diclofenac with potentially interesting anti-inflammatory activity. *Journal of inorganic biochemistry, 79*(1-4), 153-157.

Kremer, E., Facchin, G., Estévez, E., Alborés, P., Baran, E., Ellena, J., & Torre, M. (2006). Copper complexes with heterocyclic sulfonamides: Synthesis, spectroscopic characterization, microbiological and SOD-like activities: Crystal structure of [Cu (sulfisoxazole) 2 (H2O) 4]· 2H2O. *Journal of inorganic biochemistry, 100*(7), 1167-1175.

Kubra, I. R., Bettadaiah, B. K., Murthy, P. S., & Rao, L. J. M. (2014). Structure-function activity of dehydrozingerone and its derivatives as antioxidant and antimicrobial compounds. *Journal of food science and technology, 51*, 245-255.

Kulkarni, N. V., Revankar, V. K., Kirasur, B., & Hugar, M. H. (2012). Transition metal complexes of thiosemicarbazones with quinoxaline hub: an emphasis on antidiabetic property. *Medicinal Chemistry Research, 21*, 663-671.

Kumar, J., Kumar, N., Sati, N., & Hota, P. K. (2020). Antioxidant properties of ethenyl indole: DPPH assay and TDDFT studies. *New Journal of Chemistry, 44*(21), 8960-8970.

Kumar, L. V., & Nath, G. R. (2019). Synthesis, characterization and biological studies of cobalt (II), nickel (II), copper (II) and zinc (II) complexes of vanillin-4-methyl-4-phenyl-3-thiosemicarbazone. *Journal of Chemical Sciences, 131*, 1-13.

Kumar, S., & Trivedi, A. (2016). A review on role of nickel in the biological system. *Int. J. Curr. Microbiol. Appl. Sci, 5*(3), 719-727.

Kumar, V., Bala, R., Dhawan, S., Singh, P., & Karpoormath, R. (2022). The Multi-Biological Targeted Role of Dehydrozingerone and its Analogues. *ChemistrySelect, 7*(35), e202201938.

Kuo, P.-C., Cherng, C.-Y., Jeng, J.-F., Damu, A. G., Teng, C.-M., Lee, E.-J., & Wu, T.-S. (2005). Isolation of a natural antioxidant, dehydrozingerone from Zingiber officinale and synthesis of its analogues for recognition of effective antioxidant and antityrosinase agents. *Archives of pharmacal research, 28*, 518-528.

Kurtoglu, N. (2009). Synthesis, characterization, chelation with transition metal ions, and antibacterial and antifungal studies of the 4-[(E)--phenyldiazenyl]-2-[(E)-(phenylimino) methyl] phenol dye. *Journal of the Serbian Chemical Society, 74*(8-9), 917-926.

Lee, D. K., In, J., & Lee, S. (2015). Standard deviation and standard error of the mean. *Korean journal of anesthesiology, 68*(3), 220-223.

Lee, J. H., Ali, G., Kim, D. H., & Chung, K. Y. (2017). Metal-organic framework cathodes based on a vanadium hexacyanoferrate Prussian blue analogue for high-performance aqueous rechargeable batteries. *Advanced Energy Materials, 7*(2), 1601491.

Li, L., Shi, X., Evans, C. M., & Findley, G. L. (2012). Atomic and Molecular Low-n Rydberg States in Near Critical Point Fluids. *Advanced aspects of spectroscopy*.

Li, L. L., Ji, J., Fei, R., Wang, C. Z., Lu, Q., Zhang, J. R., . . . Zhu, J. J. (2012). A facile microwave avenue to electrochemiluminescent two-color graphene quantum dots. *Advanced Functional Materials, 22*(14), 2971-2979.

Liang, N., & Kitts, D. D. (2014). Antioxidant property of coffee components: assessment of methods that define mechanisms of action. *Molecules, 19*(11), 19180-19208.

Lipinski, C. A., Lombardo, F., Dominy, B. W., & Feeney, P. J. (2012). Experimental and computational approaches to estimate solubility and permeability in drug discovery and development settings. *Advanced drug delivery reviews, 64*, 4-17.

Lobana, T. S., Kaushal, M., Bala, R., Nim, L., Paul, K., Arora, D. S., . . . Jasinski, J. P. (2020). Di-2-pyridylketone-N1-substituted thiosemicarbazone derivatives of copper (II): Biosafe antimicrobial potential and high anticancer activity against immortalized L6 rat skeletal muscle cells. *Journal of inorganic biochemistry, 212*, 111205.

Lobo, V., Patil, A., Phatak, A., & Chandra, N. (2010). Free radicals, antioxidants and functional foods: Impact on human health. *Pharmacognosy reviews, 4*(8), 118.

Lu, T., Liu, Z., Steren, C. A., Fei, F., Cook, T. M., Chen, X.-T., & Xue, Z.-L. (2018). Synthesis, structural characterization and NMR studies of group 10 metal complexes with macrocyclic amine N-heterocyclic carbene ligands. *Dalton Transactions, 47*(12), 4282-4292.

Mahdi, S. H., & Karem, L. A. (2018). Synthesis, spectral and biochemical studies of new complexes of mixed ligand Schiff base and anthranilic acid. *Oriental Journal of Chemistry, 34*(3), 1565-1572.

Mahmoud, W. H., Deghadi, R. G., & Mohamed, G. G. (2016). Novel Schiff base ligand and its metal complexes with some transition elements. Synthesis, spectroscopic, thermal analysis, antimicrobial and in vitro anticancer activity. *Applied Organometallic Chemistry, 30*(4), 221-230.

Mahmoud, W. H., Deghadi, R. G., & Mohamed, G. G. (2018). Metal complexes of novel Schiff base derived from iron sandwiched organometallic and 4-nitro-1, 2-phenylenediamine: Synthesis, characterization, DFT studies, antimicrobial activities and molecular docking. *Applied Organometallic Chemistry, 32*(4), e4289.

Mahmoud, W. H., Mohamed, G. G., & El-Dessouky, M. M. (2014). Synthesis, characterization and in vitro biological activity of mixed transition metal complexes of lornoxicam with 1, 10-phenanthroline. *Int. J. Electrochem. Sci, 9*, 1415-1438.

Mahmoud, W. H., Mohamed, G. G., Elsawy, H. A., & Radwan, M. A. (2018). Metal complexes of novel Schiff base derived from the condensation of 2-quinoline carboxaldehyde and ambroxol drug with some transition metal ions. *Applied Organometallic Chemistry, 32*(7), e4392.

Mahyavanshi, V. N. Synthesis and study of biological activity of some novel thiazolidinones and azetidinones compounds.

Manandhar, S., Luitel, S., & Dahal, R. K. (2019). In vitro antimicrobial activity of some medicinal plants against human pathogenic bacteria. *Journal of tropical medicine, 2019*.

Mandal, S., Das, G., Singh, R., Shukla, R., & Bharadwaj, P. K. (1997). Synthesis and studies of Cu (II)-thiolato complexes: bioinorganic perspectives. *Coordination Chemistry Reviews, 160*, 191-235.

Mandewale, M. C., Kokate, S., Thorat, B., Sawant, S., & Yamgar, R. (2019). Zinc complexes of hydrazone derivatives bearing 3, 4-dihydroquinolin-2 (1H)-one nucleus as new anti-tubercular agents. *Arabian journal of chemistry, 12*(8), 4479-4489.

Mandewale, M. C., Thorat, B., Nivid, Y., Jadhav, R., Nagarsekar, A., & Yamgar, R. (2018). Synthesis, structural studies and antituberculosis evaluation of new hydrazone derivatives of quinoline and their Zn (II) complexes. *Journal of Saudi Chemical Society, 22*(2), 218-228.

Mantsch, H. H., & Chapman, D. (1996). *Infrared spectroscopy of biomolecules*: Wiley-Liss New York.

Markesbery, W. R. (1997). Oxidative stress hypothesis in Alzheimer's disease. *Free Radical Biology and Medicine, 23*(1), 134-147.

Martins, A. F., Facchi, S. P., Follmann, H. D., Pereira, A. G., Rubira, A. F., & Muniz, E. C. (2014). Antimicrobial activity of chitosan derivatives containing N-quaternized moieties in its backbone: a review. *International journal of molecular sciences, 15*(11), 20800-20832.

Matta, C., & Gillespie, R. (2002). Understanding and interpreting molecular electron density distributions. *Journal of Chemical Education, 79*(9), 1141.

McAuliffe, C., & Perry, W. (1974). Transition metal complexes of the zwitterionic amino acid DL-methylsulfoniummethioninate and of the amido acid derived from it by facile amine deprotonation. *Inorganica Chimica Acta, 10*, 215-220.

Medici, S., Peana, M. F., & Zoroddu, M. A. (2018). Noble metals in pharmaceuticals: applications and limitations. *Biomedical Applications of Metals*, 3-48.

Meena, R., Meena, P., Kumari, A., Sharma, N., & Fahmi, N. (2023). Schiff Bases and Their Metal Complexes: Synthesis, Structural Characteristics and Applications.

Meng, X. (2011). Y, Zhang H-X, Mezei M, Cui M. Molecular docking: a powerful approach for structure-based drug discovery. *Curr. Comp. Aided Drug Design, 7*(2), 146-157.

Miroslaw, B. (2020). Homo-and hetero-oligonuclear complexes of platinum group metals (PGM) coordinated by imine Schiff base ligands. *International journal of molecular sciences, 21*(10), 3493.

Mishra, V., Pandeya, S., Pannecouque, C., Witvrouw, M., & De Clercq, E. (2002). Anti-HIV Activity of Thiosemicarbazone and Semicarbazone Derivatives of (±)-3-Menthone. *Archiv der Pharmazie: An International Journal Pharmaceutical and Medicinal Chemistry, 335*(5), 183-186.

Mišković, K., Bujak, M., Baus Lončar, M., & Glavaš-Obrovac, L. (2013). Antineoplastic DNA-binding compounds: Intercalating and minor groove binding drugs. *Arhiv za higijenu rada i toksikologiju, 64*(4), 593-601.

Mittapally, S., Taranum, R., & Parveen, S. (2018). Metal ions as antibacterial agents. *Journal of Drug Delivery and Therapeutics, 8*(6-s), 411-419.

Montelongo-Peralta, L., León-Buitimea, A., Palma-Nicolás, J., Gonzalez-Christen, J., & Morones-Ramírez, J. (2019). Antibacterial Activity of combinatorial treatments composed of transition-metal/antibiotics against Mycobacterium tuberculosis. *Scientific reports, 9*(1), 5471.

More, M., Joshi, P., Mishra, Y., & Khanna, P. (2019a). Mater. Today Chem. 14, 100195 (2019). In.

More, M., Joshi, P., Mishra, Y., & Khanna, P. (2019b). Metal complexes driven from Schiff bases and semicarbazones for biomedical and allied applications: a review. *Materials Today Chemistry, 14*, 100195.

Morgan, S. M., El-Sonbati, A., & Eissa, H. (2017). Geometrical structures, thermal properties and spectroscopic studies of Schiff base complexes: Correlation between ionic radius of metal complexes and DNA binding. *Journal of Molecular Liquids, 240,* 752-776.

Morgant, G., d'Angelo, J., Desmaële, D., Dichi, E., Sghaier, M., Fraisse, B., . . . Tomas, A. (2008). Crystal structures of two (3-hydroxy-4-nitrobenzoato) complexes of

magnesium (II): Ionic entities stabilized by stacking interactions and extensive hydrogen bonding. *Polyhedron, 27*(9-10), 2097-2104.

Mosa, A. I., Ibrahim, M. M., & Aldhlmani, S. A. (2013). Spectroscopic and solution studies of some transition metal complexes of new 4-hydroxy coumarin semi-and thiosemicarbazone complexes. *Journal of Solution Chemistry, 42*, 2364-2383.

Motohashi, N., Yamagami, C., Tokuda, H., Konoshima, T., Okuda, Y., Okuda, M., . . . Saito, Y. (1998). Inhibitory effects of dehydrozingerone and related compounds on 12-O-tetradecanoylphorbol-13-acetate induced Epstein–Barr virus early antigen activation. *Cancer letters, 134*(1), 37-42.

Mukhametzhanova, S., Shtrykova, V., Kuksenok, V. Y., & Filimonov, V. (2014). New approach to semicarbazone, thiosemicarbazone and aminoguanidine synthesis. *Izvestiya Vysshikh Uchebnykh Zavedenii. Seriya Khimiya i Khimicheskaya Tekhnologiya*, *57*(11).

Muleta, F., Desalegn, T., Eswaramoorthy, R., & Garg, A. (2022). Synthesis, characterization, in-silico, and in-vitro biological studies of Cu (II), Zn (II) complexes of semicarbazone, thiosemicarbazone derivatives of dehydrozingerone. *Journal of Molecular Structure, 1268*, 133632.

Nagesh, G., Mahadev, U., & Mruthyunjayaswamy, B. (2015). Mononuclear metal (II) Schiff base complexes derived from thiazole and o-vanillin moieties: Synthesis, characterization, thermal behaviour and biological evaluation. *Int. J. Pharm. Sci. Rev. Res, 31*(1), 190-197.

Nagesh, G., Raj, K. M., & Mruthyunjayaswamy, B. (2015). Synthesis, characterization, thermal study and biological evaluation of Cu (II), Co (II), Ni (II) and Zn (II) complexes of Schiff base ligand containing thiazole moiety. *Journal of Molecular Structure, 1079*, 423-432.

Nair, M. S., Arish, D., & Joseyphus, R. S. (2012). Synthesis, characterization, antifungal, antibacterial and DNA cleavage studies of some heterocyclic Schiff base metal complexes. *Journal of Saudi Chemical Society, 16*(1), 83-88.

Natvarlal, M. V. Synthesis And Study Of Biological Activity Of Some Novel Thiazolidinones And Azetidinones Compounds.

Nguyen, Q. T., Pham Thi, P. N., Bui, Q. D., & Nguyen, V. T. (2023). Synthesis, Spectral Characterization, and Biological Activities of Some Metal Complexes Bearing an Unsymmetrical Salen-Type Ligand,(Z)-1-(((2-((E)-(2-Hydroxy-6-

methoxybenzylidene) amino) phenyl) amino) methylene) Naphthalen-2 (1H)-one. *Heteroatom Chemistry, 2023*.

Nimse, S. B., & Pal, D. (2015). Free radicals, natural antioxidants, and their reaction mechanisms. *RSC advances, 5*(35), 27986-28006.

Noblía, P., Vieites, M., Parajón-Costa, B. S., Baran, E. J., Cerecetto, H., Draper, P., . . . Azqueta, A. (2005). Vanadium (V) complexes with salicylaldehyde semicarbazone derivatives bearing in vitro anti-tumor activity toward kidney tumor cells (TK-10): crystal structure of [VVO2 (5-bromosalicylaldehyde semicarbazone)]. *Journal of inorganic biochemistry, 99*(2), 443-451.

Oladimeji, A. V., & Valan, M. (2020). The potential therapeutic advantage of Abrus precatorius Linn. an alternative to Glycyrrhiza glabra: a review. *J Pharm Res Int, 32*, 79-94.

Omar, M., Mohamed, G. G., & Ibrahim, A. A. (2009). Spectroscopic characterization of metal complexes of novel Schiff base. Synthesis, thermal and biological activity studies. *Spectrochimica Acta Part A: Molecular and Biomolecular Spectroscopy, 73*(2), 358-369.

Ommenya, F., Nyawade, E., Andala, D., & Kinyua, J. (2020). Synthesis, characterization and antibacterial activity of Schiff base, 4-Chloro-2-{(E)-[(4-fluorophenyl) imino] methyl} phenol metal (II) complexes. *Journal of Chemistry, 2020*, 1-8.

Ommenya, F. K. (2021). *2021 Synthesis, Characterization and Antibacterial Activity of Schiff Base, 4-Chloro-2-{(E)-[(4-Fluorophenyl) Imino] Methyl} Phenol and Its Transition Metal (II) Complexes.* JKUAT-IBR,

Osredkar, J., & Sustar, N. (2011). Copper and zinc, biological role and significance of copper/zinc imbalance. *J Clinic Toxicol S, 3*(2161), 0495.

Parmar, S., & Kumar, Y. (2009). Synthesis, spectroscopic, and antimicrobial studies of the bivalent nickel, and copper complexes of thiosemicarbazide. *Chemical and Pharmaceutical Bulletin, 57*(6), 603-606.

Parmar, S., & Kumar, Y. (2010). Synthesis, spectroscopic, and antimicrobial studies of the bivalent cobalt, nickel, and copper complexes of thioacetamide. *Russian Journal of Inorganic Chemistry, 55*(3), 361-367.

Patel, K. D., & Patel, H. S. (2017). Synthesis, spectroscopic characterization and thermal studies of some divalent transition metal complexes of 8-hydroxyquinoline. *Arabian journal of chemistry, 10*, S1328-S1335.

Patel, M., Chhasatia, M., & Parmar, P. (2010). Antibacterial and DNA interaction studies of zinc (II) complexes with quinolone family member, ciprofloxacin. *European journal of medicinal chemistry, 45*(2), 439-446.

Patole, J., Sandbhor, U., Padhye, S., Deobagkar, D. N., Anson, C. E., & Powell, A. (2003). Structural chemistry and in vitro antitubercular activity of acetylpyridine benzoyl hydrazone and its copper complex against Mycobacterium smegmatis. *Bioorganic & medicinal chemistry letters, 13*(1), 51-55.

Paul, T., & Hossen, M. F. (2020). Schiff base metal complexes: Synthesis, characterization, thermal analysis and antibacterial activity. *Asian Journal of Research in Chemistry, 13*(4), 265-274.

Pederson, T., & Aust, S. (1973). The role of superoxide and singlet oxygen in lipid peroxidation promoted by xanthine oxidase. *Biochemical and Biophysical Research Communications, 52*(3), 1071-1078.

Pelosi, G. (2010). Thiosemicarbazone metal complexes: from structure to activity. *The Open Crystallography Journal, 3*(1).

Perkampus, H.-H. (2013). *UV-VIS Spectroscopy and its Applications*: Springer Science & Business Media.

Peters, B. M., Shirtliff, M. E., & Jabra-Rizk, M. A. (2010). Antimicrobial peptides: primeval molecules or future drugs? *PLoS pathogens, 6*(10), e1001067.

Phaniendra, A., Jestadi, D. B., & Periyasamy, L. (2015). Free radicals: properties, sources, targets, and their implication in various diseases. *Indian journal of clinical biochemistry, 30*, 11-26.

Philippe, F., Verdu, I., Morère-Le Paven, M.-C., Limami, A. M., & Planchet, E. (2019). Involvement of Medicago truncatula glutamate receptor-like channels in nitric oxide production under short-term water deficit stress. *Journal of plant physiology, 236*, 1-6.

Piri, Z., Moradi-Shoeili, Z., & Assoud, A. (2017). New copper (II) complex with bioactive 2–acetylpyridine-4N-p-chlorophenylthiosemicarbazone ligand: Synthesis, X-ray structure, and evaluation of antioxidant and antibacterial activity. *Inorganic Chemistry Communications, 84*, 122-126.

Polo-Ceron, D. (2019). Cu (II) and Ni (II) complexes with new tridentate NNS thiosemicarbazones: Synthesis, characterisation, DNA interaction, and antibacterial activity. *Bioinorganic chemistry and applications, 2019*.

Prakash, A., Singh, B. K., Rajour, H. K., & Bhojak, N. (2010). Synthesis, Characterization and Bioactivities of New Schiff Bases with Main Group Metal Ions. *Main Group Metal Chemistry, 33*(4-5), 183-200.

Prasad, S., & Tyagi, A. K. (2015). Ginger and its constituents: role in prevention and treatment of gastrointestinal cancer. *Gastroenterology research and practice, 2015*.

Prasanna, S., & Doerksen, R. (2009). Topological polar surface area: a useful descriptor in 2D-QSAR. *Current medicinal chemistry, 16*(1), 21-41.

Proulx, C., Sabatino, D., Hopewell, R., Spiegel, J., García Ramos, Y., & Lubell, W. D. (2011). Azapeptides and their therapeutic potential. *Future medicinal chemistry, 3*(9), 1139-1164.

Rahman, M., Islam, M., Biswas, M., & Khurshid Alam, A. (2015). In vitro antioxidant and free radical scavenging activity of different parts of Tabebuia pallida growing in Bangladesh. *BMC research notes, 8*(1), 1-9.

Rainsford, K., Brune, K., & Whitehouse, M. (1977). Aspirin and related drugs: Their actions and uses. *Agents and Actions [Suppl 1]. Birkhäuser, Basel Stuttgart*, 7-118.

Ramachandran, E., Raja, D. S., Bhuvanesh, N. S., & Natarajan, K. (2013). Synthesis, characterization and in vitro pharmacological evaluation of new water soluble Ni (II) complexes of 4N-substituted thiosemicarbazones of 2-oxo-1, 2-dihydroquinoline-3-carbaldehyde. *European journal of medicinal chemistry, 64*, 179-189.

Ramesh, R., & Natarajan, K. (1994). Mixed Ligand Complexes of Ruthenium (III) Containing α, β-Unsaturated-β-Ketoamine and Triphenylphosphine/Arsine. *Synthesis and Reactivity in Inorganic and Metal-Organic Chemistry, 24*(10), 1705-1718.

Ramzan, S., Saleem, S., Ali, S., Shahzadi, S., Sharma, S. K., Qunango, K., . . . Ahmed, F. (2017). Synthesis, characterization and thermal studies of transition metal complexes with O-, S-donor ligands. *Journal of Analytical and Pharmaceutical Research, 5*(6), 00160-00173.

Randall, C. P. (2013). *The silver cation (Ag+): antibacterial mode of action and mechanisms of resistance*: University of Leeds.

Rao, T. S., Reddy, K. L., & Lingaiah, P. (1988). *Synthesis and structural studies of complexes of Co (II), Ni (II), Cu (II), Zn (II) and Cd (II) with substituted chalcones.* Paper presented at the Proceedings of the Indian Academy of Sciences-Chemical Sciences.

Reena, T., & Prathapachandra Kurup, M. (2011). Spectral studies and crystal structures of some transition metal complexes of N4-substituted semicarbazones. *Cochin University of Science & Technology*.

Refat, M. S., El-Deen, I. M., Anwer, Z. M., & El-Ghol, S. (2009). Bivalent transition metal complexes of coumarin-3-yl thiosemicarbazone derivatives: Spectroscopic, antibacterial activity and thermogravimetric studies. *Journal of Molecular Structure, 920*(1-3), 149-162.

Refat, M. S., El-Sayed, M. Y., & Adam, A. M. A. (2013). Cu (II), Co (II) and Ni (II) complexes of new Schiff base ligand: Synthesis, thermal and spectroscopic characterizations. *Journal of Molecular Structure, 1038*, 62-72.

Rehman, R., & Gohar, M. (2022). Evaluation of Microbial Contamination in Meat and its Control Using Preservatives. *Int. J. Innov. Sci. Technol. Eval, 4*(2), 404-415.

Rizzotto, M. (2012a). Metal complexes as antimicrobial agents. *A search for antibacterial agents*, 73-88.

Rizzotto, M. (2012b). Metal Complexes as Antimicrobial Agents: A Search for Antibacterial Agents. *InTech, Rijeka*.

Rodríguez-Argüelles, M. C., López-Silva, E. C., Sanmartín, J., Pelagatti, P., & Zani, F. (2005). Copper complexes of imidazole-2-, pyrrole-2-and indol-3-carbaldehyde thiosemicarbazones: inhibitory activity against fungi and bacteria. *Journal of inorganic biochemistry, 99*(11), 2231-2239.

Rosu, T., Pahontu, E., Pasculescu, S., Georgescu, R., Stanica, N., Curaj, A., . . . Leabu, M. (2010). Synthesis, characterization antibacterial and antiproliferative activity of novel Cu (II) and Pd (II) complexes with 2-hydroxy-8-R-tricyclo [7.3. 1.0. 2, 7] tridecane-13-one thiosemicarbazone. *European journal of medicinal chemistry, 45*(4), 1627-1634.

Russell, A. (2003). Bacterial outer membrane and cell wall penetration and cell destruction by polluting chemical agents and physical conditions. *Science progress, 86*(4), 283-312.

Sadeek, S., El-Attar, M., & Abd El-Hamid, S. (2013). Preparation and characterization of new tetradentate Schiff base metal complexes and biological activity evaluation. *Journal of Molecular Structure, 1051*, 30-40.

Saga, T., & Yamaguchi, K. (2009). History of antimicrobial agents and resistant bacteria. *Jmaj, 52*(2), 103-108.

Saikumari, N. (2021). Synthesis and characterization of amino acid Schiff base and its copper (II) complex and its antimicrobial studies. *Materials Today: Proceedings, 47*, 1777-1781.

Sakeena, M., Bennett, A. A., Carter, S. J., & McLachlan, A. J. (2019). A comparative study regarding antibiotic consumption and knowledge of antimicrobial resistance among pharmacy students in Australia and Sri Lanka. *PLoS One*, *14*(3), e0213520.

Sakurai, H., Kojima, Y., Yoshikawa, Y., Kawabe, K., & Yasui, H. (2002). Antidiabetic vanadium (IV) and zinc (II) complexes. *Coordination Chemistry Reviews*, *226*(1-2), 187-198.

Sánchez-Moreno, C. (2002). Methods used to evaluate the free radical scavenging activity in foods and biological systems. *Food science and technology international*, *8*(3), 121-137.

Sangeeta, S., Ahmad, K., Noorussabah, N., Bharti, S., Mishra, M., Sharma, S., & Choudhary, M. (2018). Synthesis, crystal structures, molecular docking and urease inhibition studies of Ni (II) and Cu (II) Schiff base complexes. *Journal of Molecular Structure*, *1156*, 1-11.

Sankar, A., Jose, S., Nithya, P., & Meeran, M. N. Synthesis, Characterization and Antimicrobial Activity of Substituted Acetophenone Based Semicarbazones.

Sanmartín, J., Novio, F., García-Deibe, A. M., Fondo, M., Ocampo, N., & Bermejo, M. R. (2006). Dinuclear neutral complexes of a symmetric N2+ N2-donor diimine ligand. *Polyhedron*, *25*(8), 1714-1722.

Santos-Sánchez, N. F., Salas-Coronado, R., Villanueva-Cañongo, C., & Hernández-Carlos, B. (2019). Antioxidant compounds and their antioxidant mechanism. *Antioxidants*, *10*, 1-29.

Sarker, D., Hossen, M., Haque, M., Zamir, R., & Asraf, M. (2020). Synthesis, characterization, thermal analysis and antibacterial activity of Cu (II) and Ni (II) complexes with thiosemicarbazone derived from thiophene-2-aldehyde. *Journal of Materials Science Research and Reviews*, *5*(2), 15-25.

SATHIS, D., GANDHI, S. R., MAGESWARI, A., KARTHIKEYAN, S., & SHERIFF, A. I. (2015). Mononuclear Transition Metal Complexes Containing Quadridentate Schiff Bases as N2O2 Donors: Synthesis, Spectral Characterization Properties and Antibacterial Activity. *Asian Journal of Chemistry*, *27*(12), 0000-0000.

Saucedo-Balderas, M. M., Delgado-Alfaro, R. A., Martínez-Martínez, F. J., Ortegón-Reyna, D., Bernabé-Pineda, M., Zúñiga-Lemus, O., & González-González, J. S. (2015). Synthesis, Molecular Structure of Diethyl Phenylenebis (Methylene) Dicarbamates and FTIR Spectroscopy Molecular Recognition Study with Benzenediols. *Journal of the Brazilian Chemical Society, 26*, 396-402.

Sen, S., & Chakraborty, R. (2011). The role of antioxidants in human health. In *Oxidative stress: diagnostics, prevention, and therapy* (pp. 1-37): ACS Publications.

Shaker, A. M., Nassr, L. A., Adam, M. S., & Mohamed, I. M. (2013). Hydrophilicity and acid hydrolysis of water-soluble antibacterial iron (II) Schiff base complexes in binary aqueous solvents. *Russian Journal of General Chemistry, 83*, 2460-2464.

Shakir, M., Hanif, S., Alam, M. F., & Younus, H. (2016). Molecular hybridization approach of bio-potent CuII/ZnII complexes derived from N, O donor bidentate imine scaffolds: Synthesis, spectral, human serum albumin binding, antioxidant and antibacterial studies. *Journal of Photochemistry and Photobiology B: Biology, 165*, 96-114.

Sharaby, C. M. (2007). Synthesis, spectroscopic, thermal and antimicrobial studies of some novel metal complexes of Schiff base derived from [N1-(4-methoxy-1, 2, 5-thiadiazol-3-yl) sulfanilamide] and 2-thiophene carboxaldehyde. *Spectrochimica Acta Part A: Molecular and Biomolecular Spectroscopy, 66*(4-5), 1271-1278.

Sharma, A., Mehta, T., & Shah, M. K. (2013). Synthesis and spectral studies of transition metal complexes supported by NO-bidentate Schiff-Base ligand. *Pelagia Research Library: Der Chemica Sinica, 4*(1), 141-146.

Shelke, V., Jadhav, S., Patharkar, V., Shankarwar, S., Munde, A., & Chondhekar, T. (2012). Synthesis, spectroscopic characterization and thermal studies of some rare earth metal complexes of unsymmetrical tetradentate Schiff base ligand. *Arabian journal of chemistry, 5*(4), 501-507.

SHIRODE, P., AGRAWAL, R., JAIN, A., & YEOLE, P. (2015). Synthesis and Structural Studies of Mixed Ligand Complexes of Transition Metals with Pyruvic Acid Semicarbazone and Acetone Semicarbazone. *Chemical Science, 4*(1), 275-281.

Shirode, P., & Yeole, P. (2014). Synthesis and Characterization of Mixed Ligand Complexes of Transition Metals with Schiff's Bases. *Chemical Science Transactions, 3*(3), 1186-1192.

Siji, V., Kumar, M. S., Suma, S., & Kurup, M. P. (2010). Synthesis, characterization and physiochemical information, along with antimicrobial studies of some metal complexes derived from an ON donor semicarbazone ligand. *Spectrochimica Acta Part A: Molecular and Biomolecular Spectroscopy, 76*(1), 22-28.

Simões, M., Simões, L. C., Cleto, S., Machado, I., Pereira, M. O., & Vieira, M. J. (2007). Antimicrobial mechanisms of ortho-phthalaldehyde action. *Journal of basic microbiology, 47*(3), 230-242.

Simons, C., Walsh, S. E., Maillard, J. Y., & Russell, A. (2000). A note: ortho-phthalaldehyde: proposed mechanism of action of a new antimicrobial agent. *Letters in Applied Microbiology, 31*(4), 299-302.

Šimunková, M., & Malček, M. (2020). Dimethyl sulfoxide as a strongly coordinating solvent: 3′, 4′-dihydroxyflavone-Cu (II)-DMSO system case study. *Acta Chimica Slovaca, 13*(2), 38-48.

Singh, B., Sharma, R., & Garg, B. (2006). Kinetics and molecular modeling of biologically active glutathione complexes with lead (II) ions. *Journal of thermal analysis and calorimetry, 84*(3), 593-600.

Singh, M., Singh, S. K., Gangwar, M., Nath, G., & Singh, S. K. (2016). Design, synthesis and mode of action of novel 2-(4-aminophenyl) benzothiazole derivatives bearing semicarbazone and thiosemicarbazone moiety as potent antimicrobial agents. *Medicinal Chemistry Research, 25,* 263-282.

Singhal, M., Paul, A., Singh, H. P., Dubey, S. K., & Songara, R. K. (2011). Synthesis and evaluation of antioxidant activity of semicarbazone derivatives. *Int J Pharmaceut Sci Drug Res, 3,* 150-154.

Sinha, N., & Dixit, D. (2022). In vitro antioxidant and antimicrobial activities of herbal combinations of Rosemarinus officinalis (rosemary) and Mentha piperita (peppermint). *Indian Journal of Agricultural Biochemistry, 35*(2), 148-154.

SOME, S. M. L. C. O., & Benzothiazole, A. International Journal of Pharmacy.

Soroceanu, A., & Bargan, A. (2022). Advanced and biomedical applications of Schiff-base ligands and their metal complexes: A review. *Crystals, 12*(10), 1436.

Sridhar, N., Duggirala, S. L., & Puchchakayala, G. (2014). Antimicrobial activity of ethanolic extracts of Justicia neesii. ||| *Bangladesh Journal of Pharmacology, 9*(4), 624-627.

Stanić, V., Dimitrijević, S., Antić-Stanković, J., Mitrić, M., Jokić, B., Plećaš, I. B., & Raičević, S. (2010). Synthesis, characterization and antimicrobial activity of copper

and zinc-doped hydroxyapatite nanopowders. *Applied Surface Science, 256*(20), 6083-6089.

Suksrichavalit, T., Prachayasittikul, S., Nantasenamat, C., Isarankura-Na-Ayudhya, C., & Prachayasittikul, V. (2009). Copper complexes of pyridine derivatives with superoxide scavenging and antimicrobial activities. *European journal of medicinal chemistry, 44*(8), 3259-3265.

Süleymanoğlu, N., Kubaşık, P., & Direkel, Ş. (2021). DFT study and antiparasitic activity of some azo dyes containing uracil. *Journal of Chemistry, 2021*, 1-11.

Sumalatha, V., Daravath, S., Rambabu, A., & Ramesh, G. (2021). Antioxidant, antimicrobial, DNA binding and cleavage studies of novel Co (II), Ni (II) and Cu (II) complexes of N, O donor Schiff bases: Synthesis and spectral characterization. *Journal of Molecular Structure, 1229*, 129606.

Sumrra, S. H., & Chohan, Z. H. (2012). Metal based new triazoles: their synthesis, characterization and antibacterial/antifungal activities. *Spectrochimica Acta Part A: Molecular and Biomolecular Spectroscopy, 98*, 53-61.

Sumrra, S. H., Ibrahim, M., Ambreen, S., Imran, M., Danish, M., & Rehmani, F. S. (2014). Synthesis, spectral characterization, and biological evaluation of transition metal complexes of bidentate N, O donor Schiff bases. *Bioinorganic chemistry and applications, 2014*.

Surati, K. R., & Sathe, P. A. (2016). Schiff base pyrazolone complexes of iron (III): synthesis, characterization, antimicrobial and antioxidant activity. *Medicinal Chemistry Research, 25*, 2742-2751.

Tada, R., Chavda, N., & Shah, M. K. (2011). Synthesis and characterization of some new thiosemicarbazide derivatives and their transition metal complexes. *Journal of Chemical and Pharmaceutical Research, 3*(2), 290-297.

Takatsuka, M., Goto, S., Kobayashi, K., Otsuka, Y., & Shimada, Y. (2021). Leading individual features of antioxidant systematically classified by the ORAC assay and its single electron transfer and hydrogen atom transfer reactivities; analyzing ALS therapeutic drug Edaravone. *BBA Advances, 1*, 100030.

Tamber, S., & Hancock, R. (2003). On the mechanism of solute uptake in Pseudomonas. *Front Biosci, 8*, s472-s483.

Tanwar, J., Das, S., Fatima, Z., & Hameed, S. (2014). Multidrug resistance: an emerging crisis. *Interdisciplinary perspectives on infectious diseases, 2014*.

Tavman, A., Boz, I., Seher Birteksöz, A., & Cinarli, A. (2010). Spectral characterization and antimicrobial activity of Cu (II) and Fe (III) complexes of 2-(5-Cl/NO2-1 H-benzimidazol-2-yl)-4-Br/NO2-phenols. *Journal of Coordination Chemistry, 63*(8), 1398-1410.

Teles, A. M., dos Santos, B. A., Ferreira, C. G., Mouchreck, A. N., da Silva Calabrese, K., Abreu-Silva, A. L., & Almeida-Souza, F. (2019). Ginger (Zingiber officinale) antimicrobial potential: a review. *Ginger Cultivation and Its Antimicrobial and Pharmacological Potentials*.

Thangadurai, T. D., & Natarajan, K. (2001). Mixed ligand complexes of ruthenium (II) containing α, β-unsaturated-β-ketoaminesand their antibacterial activity. *Transition Metal Chemistry, 26*(4-5), 500-504.

Trott, O., & Olson, A. (2009). Software news and update AutoDock Vina: Improving the speed and accuracy of docking with a new scoring function. *Effic. Optim. Multithreading, 31*, 455-461.

Trott, O., & Olson, A. J. (2010). AutoDock Vina: improving the speed and accuracy of docking with a new scoring function, efficient optimization, and multithreading. *Journal of computational chemistry, 31*(2), 455-461.

Tweedy, B. (1964). *Possible mechanism for reduction of elemental sulfur by monilinia fructicola.* Paper presented at the Phytopathology.

Tyagi, P., Chandra, S., Saraswat, B., & Yadav, D. (2015). Design, spectral characterization, thermal, DFT studies and anticancer cell line activities of Co (II), Ni (II) and Cu (II) complexes of Schiff bases derived from 4-amino-5-(pyridin-4-yl)-4H-1, 2, 4-triazole-3-thiol. *Spectrochimica Acta Part A: Molecular and Biomolecular Spectroscopy, 145*, 155-164.

Uddin, E., Islam, R., Bitu, N. A., Hossain, S., Uddin, N., Ali, M., . . . Haque, M. (2020). Biological applications of isoniazid derived Schiff base complexes: an overview. *Asian Journal of Research in Biochemistry, 6*(3), 17-31.

Udoisang, K., Johnson, A., & Efiong, N. (2019). *Synthesis and Characterisation of Zinc (II) and Nickel (II) Complexes with 3-Hydroxy-4-(2-Hydroxy Phenyl) Amino Cyclobut-3-Ene-1, 2-Dione.* Paper presented at the ABSTRACTS OF PAPERS OF THE AMERICAN CHEMICAL SOCIETY.

Valko, M., Rhodes, C., Moncol, J., Izakovic, M., & Mazur, M. (2006). Free radicals, metals and antioxidants in oxidative stress-induced cancer. *Chemico-biological interactions, 160*(1), 1-40.

Viganor, L., Howe, O., McCarron, P., McCann, M., & Devereux, M. (2017). The antibacterial activity of metal complexes containing 1, 10-phenanthroline: potential as alternative therapeutics in the era of antibiotic resistance. *Current topics in medicinal chemistry, 17*(11), 1280-1302.

Vijayan, P., Viswanathamurthi, P., Velmurugan, K., Nandhakumar, R., Balakumaran, M. D., Kalaichelvan, P. T., & Malecki, J. G. (2015). Nickel (ii) and copper (ii) complexes constructed with N 2 S 2 hybrid benzamidine–thiosemicarbazone ligand: synthesis, X-ray crystal structure, DFT, kinetico-catalytic and in vitro biological applications. *RSC advances, 5*(125), 103321-103342.

Vivekanand, B., Raj, K. M., & Mruthyunjayaswamy, B. (2015). Synthesis, characterization, antimicrobial, DNA-cleavage and antioxidant activities of 3-((5-chloro-2-phenyl-1H-indol-3-ylimino) methyl) quinoline-2 (1H)-thione and its metal complexes. *Journal of Molecular Structure, 1079*, 214-224.

Vogler, A., & Kunkely, H. (2007). Ligand-to-ligand and intraligand charge transfer and their relation to charge transfer interactions in organic zwitterions. *Coordination Chemistry Reviews, 251*(3-4), 577-583.

Wang, G. (2014). Human antimicrobial peptides and proteins. *Pharmaceuticals, 7*(5), 545-594.

Wang, J., Cui, C., Gao, G., Zhou, X., Wu, J., Yang, H., . . . Wu, G. (2015). A new method to prepare vanadium oxide nano-urchins as a cathode for lithium ion batteries. *RSC advances, 5*(59), 47522-47528.

Weckesser, J., & Jügrens, U. J. (1988). [15] Cell walls and external layers. In *Methods in Enzymology* (Vol. 167, pp. 173-188): Elsevier.

Yamano, S., Tsukuda, Y., Mizuhara, N., Yamaguchi, Y., Ogita, A., & Fujita, K. (2023). Dehydrozingerone enhances the fungicidal activity of glabridin against Saccharomyces cerevisiae and Candida albicans. *Letters in Applied Microbiology*, ovad040.

Yamgar, R. S., Nivid, Y., Nalawade, S., Mandewale, M., Atram, R., & Sawant, S. S. (2014). Novel zinc (II) complexes of heterocyclic ligands as antimicrobial agents: synthesis,

characterisation, and antimicrobial studies. *Bioinorganic chemistry and applications, 2014*.

Yaul, A. R., Dhande, V. V., Pethe, G. B., & Aswar, A. S. (2014). Synthesis, characterization, biological and electrical conductivity studies of some Schiff base metal complexes. *Bulletin of the Chemical Society of Ethiopia*, *28*(2), 255-264.

Yogosawa, S., Yamada, Y., Yasuda, S., Sun, Q., Takizawa, K., & Sakai, T. (2012). Dehydrozingerone, a structural analogue of curcumin, induces cell-cycle arrest at the G2/M phase and accumulates intracellular ROS in HT-29 human colon cancer cells. *Journal of natural products, 75*(12), 2088-2093.

Yust, A. E., & Smyth, D. S. (2020). Simulating bacterial growth, competition, and resistance with agent-based models and laboratory experiments. *An introduction to undergraduate research in computational and mathematical biology: From birdsongs to viscosities*, 217-271.

Zayed, E. M., Mohamed, G. G., & Hindy, A. M. (2015). Transition metal complexes of novel Schiff base: Synthesis, spectroscopic characterization, and in vitro antimicrobial activity of complexes. *Journal of thermal analysis and calorimetry*, *120*, 893-903.

Zemede, Y. B., Nithyakalyani, D., & Kumar, S. A. (2015). Synthesis, Characterization and Antimicrobial Properties of Some Transition Metal Complexes with NS-Chelating Schiff Base Ligand Incorporating Thiophene and Sulfonamide Moieties. *Asian Journal of Chemistry, 27*(3), 941.

Zhang, M.-Q., & Wilkinson, B. (2007). Drug discovery beyond the 'rule-of-five'. *Current opinion in biotechnology, 18*(6), 478-488.

Zhang, S.-X., Zhou, Y.-M., Xu, W., Tian, L.-G., Chen, J.-X., Chen, S.-H., . . . Serrano, E. (2016). Impact of co-infections with enteric pathogens on children suffering from acute diarrhea in southwest China. *Infectious Diseases of Poverty, 5*(1), 1-13.

Zhang, Y., Li, X., Li, J., Khan, M., Hossain, Z., Ma, F., & Liu, X. (2021). A novel zinc complex with antibacterial and antioxidant activity. *BMC chemistry, 15*(1), 1-12.

APPENDIXES

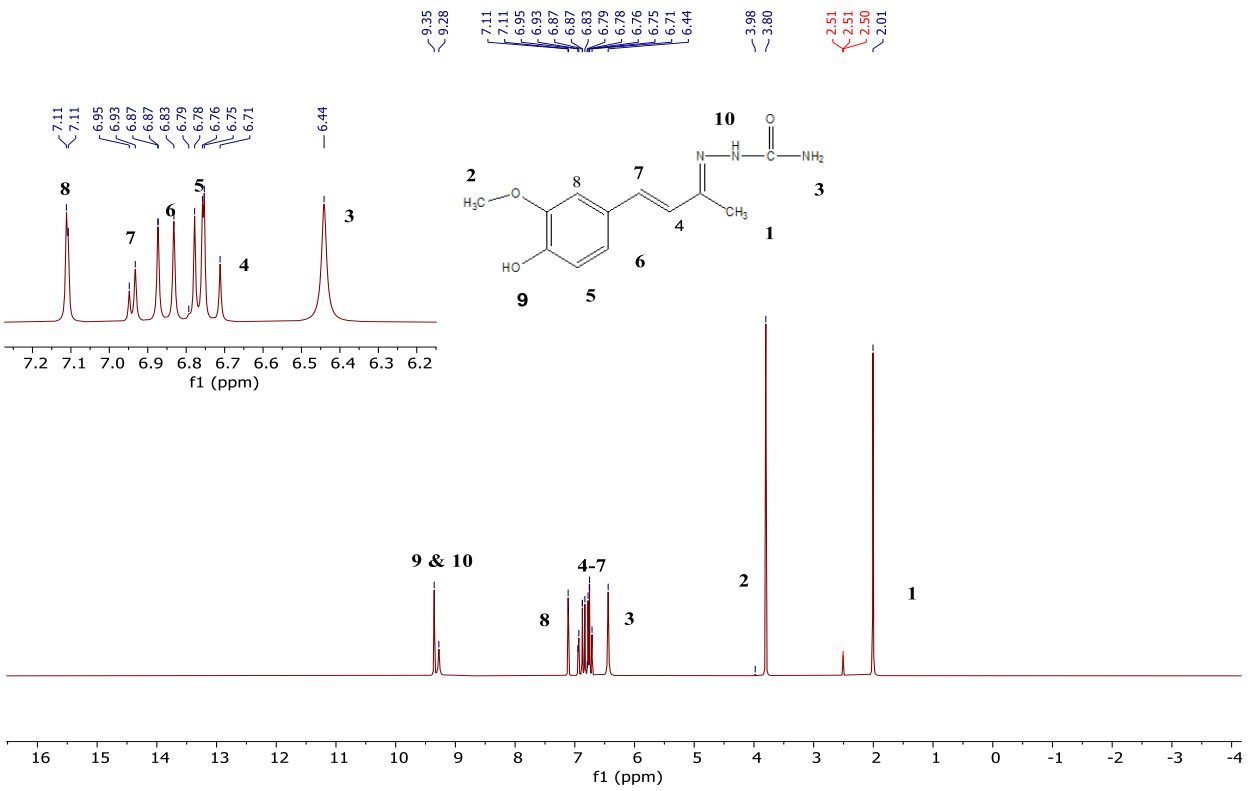

Appendix 1. ^{1}H NMR spectra of ligand (**L1**)

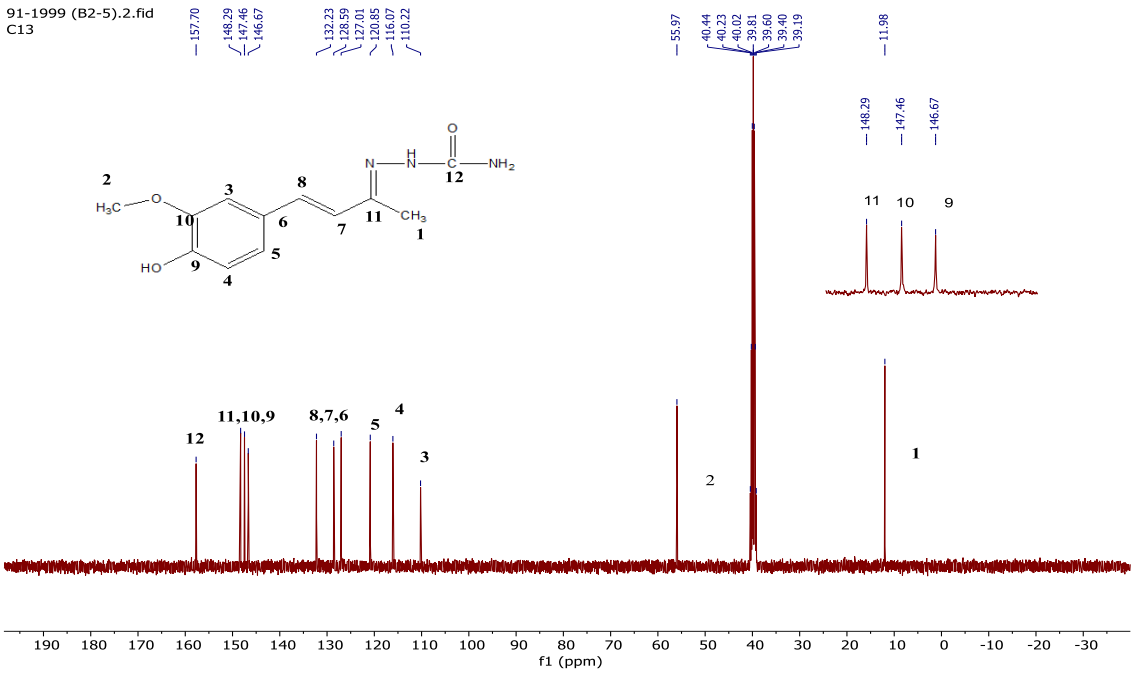

Appendix 2. ^{13}C-NMR spectra of ligand (L1)

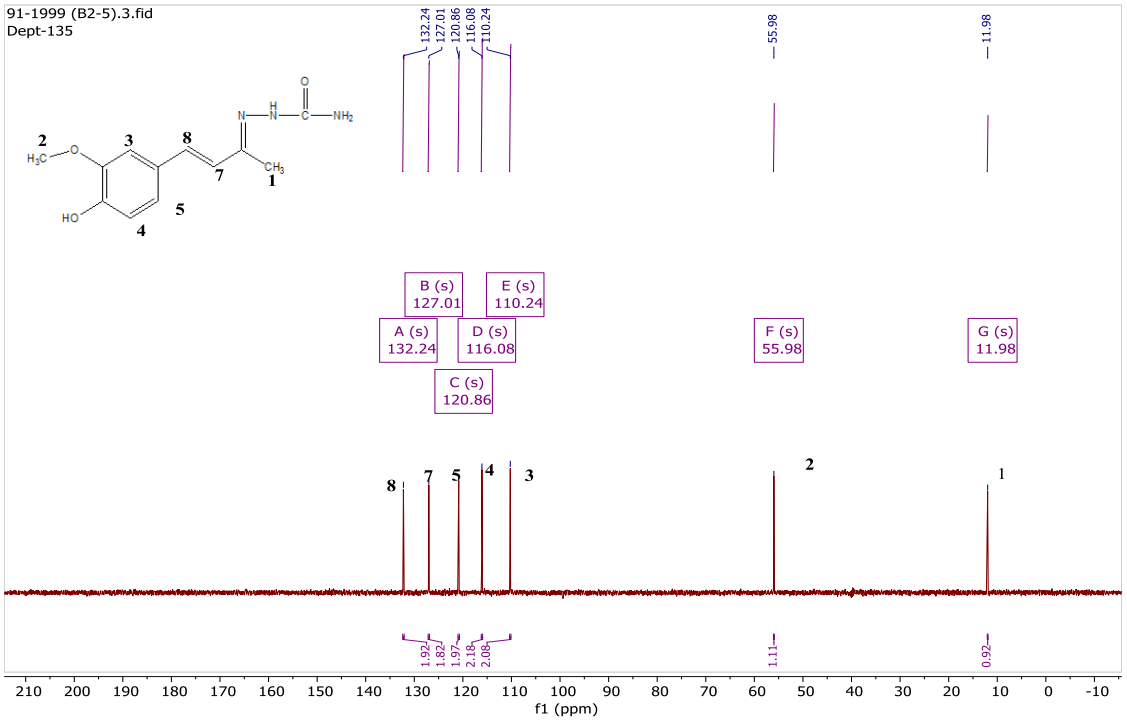

Appendix 3. ^{13}C- Dept spectra of ligand (L1)

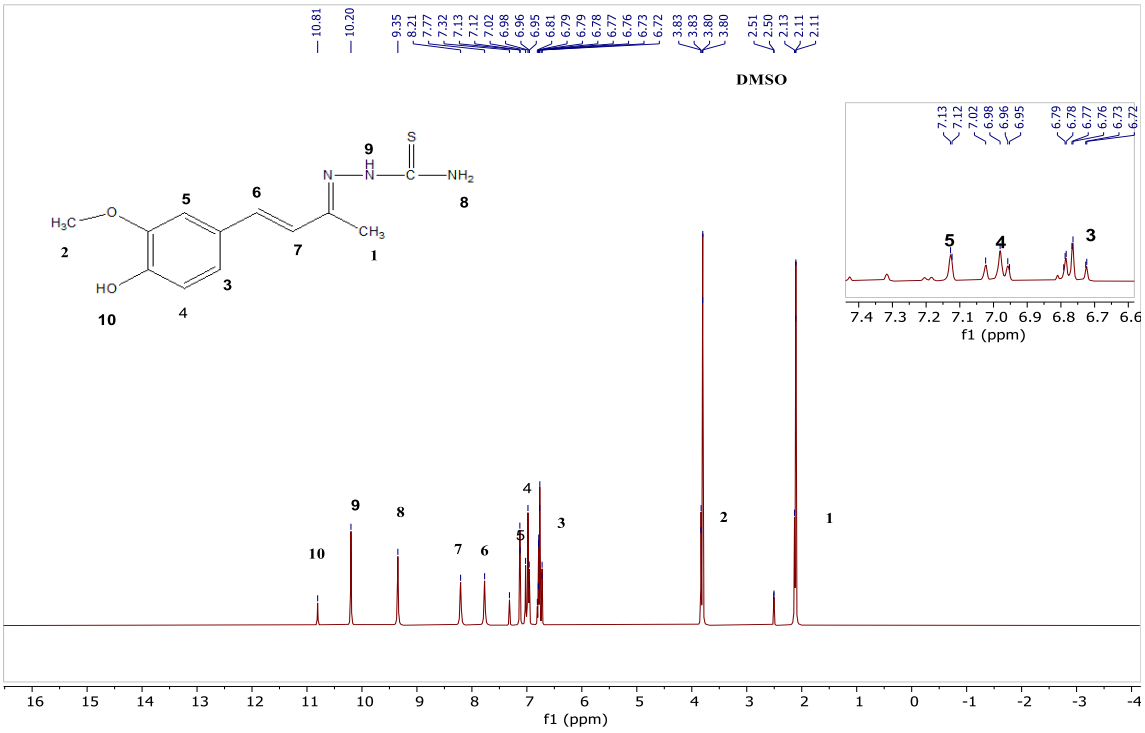

Appendix 4. ^{1}H NMR spectra of ligand (**L2**)

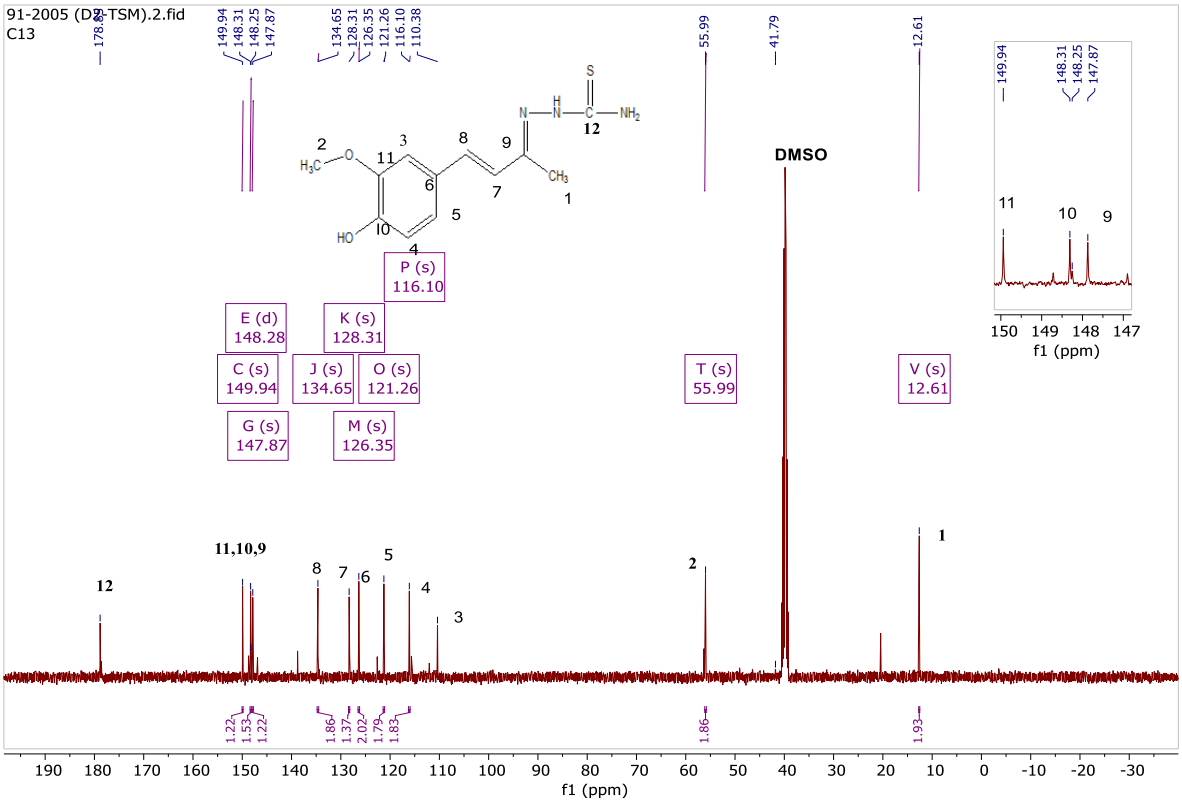

Appendix 5. ^{13}C-NMR spectra of ligand (**L2**)

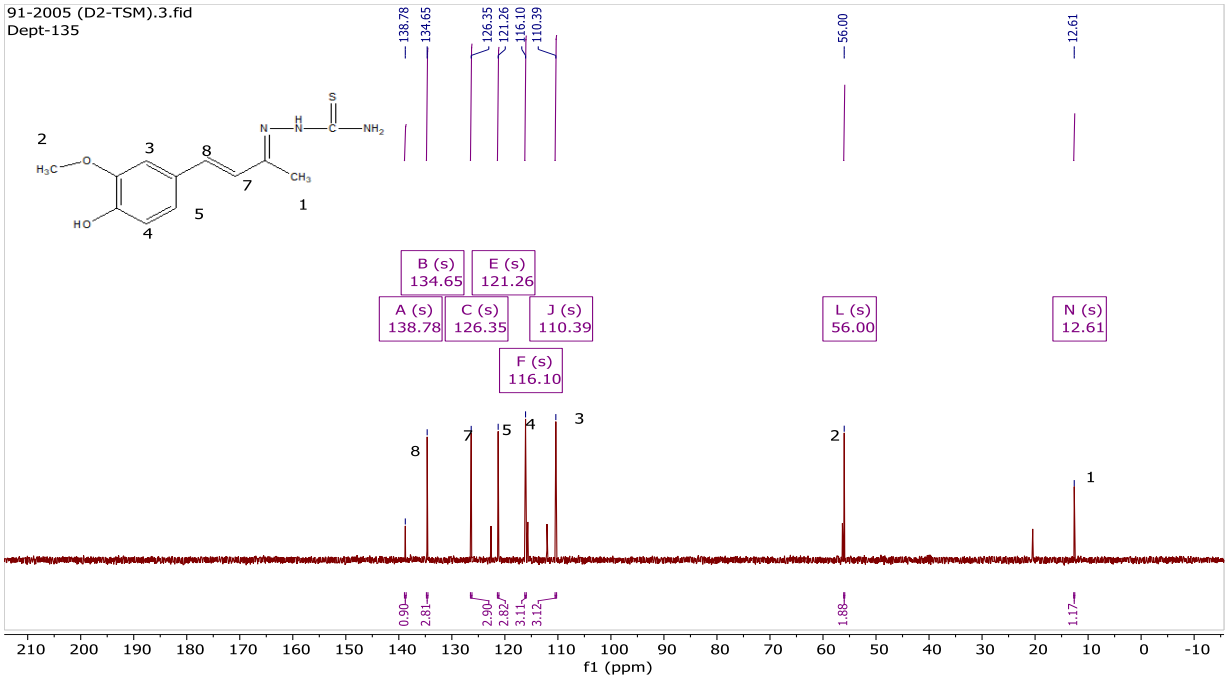

Appendix 6. ^{13}C-Dept spectra of ligand (**L2**)

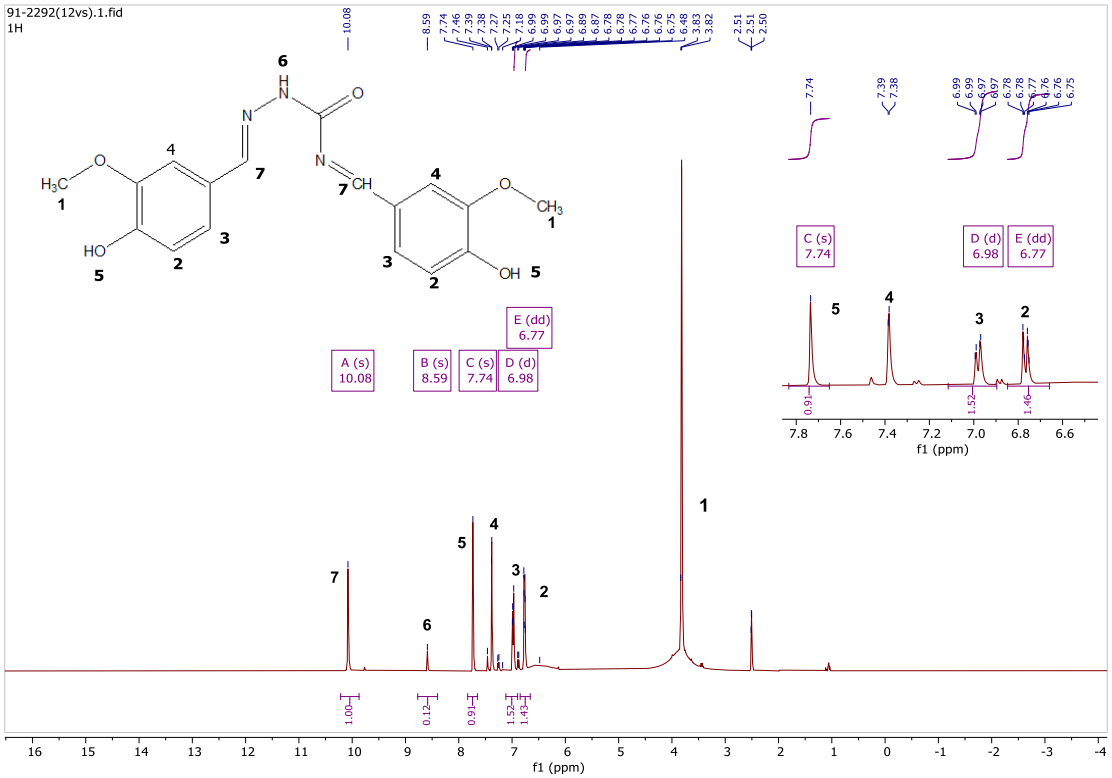

Appendix 7. ^{1}H NMR spectra of (1E)-1,4-bis(4-hydroxy-3-methoxybenzylidene) **semicarbazone (L3)**

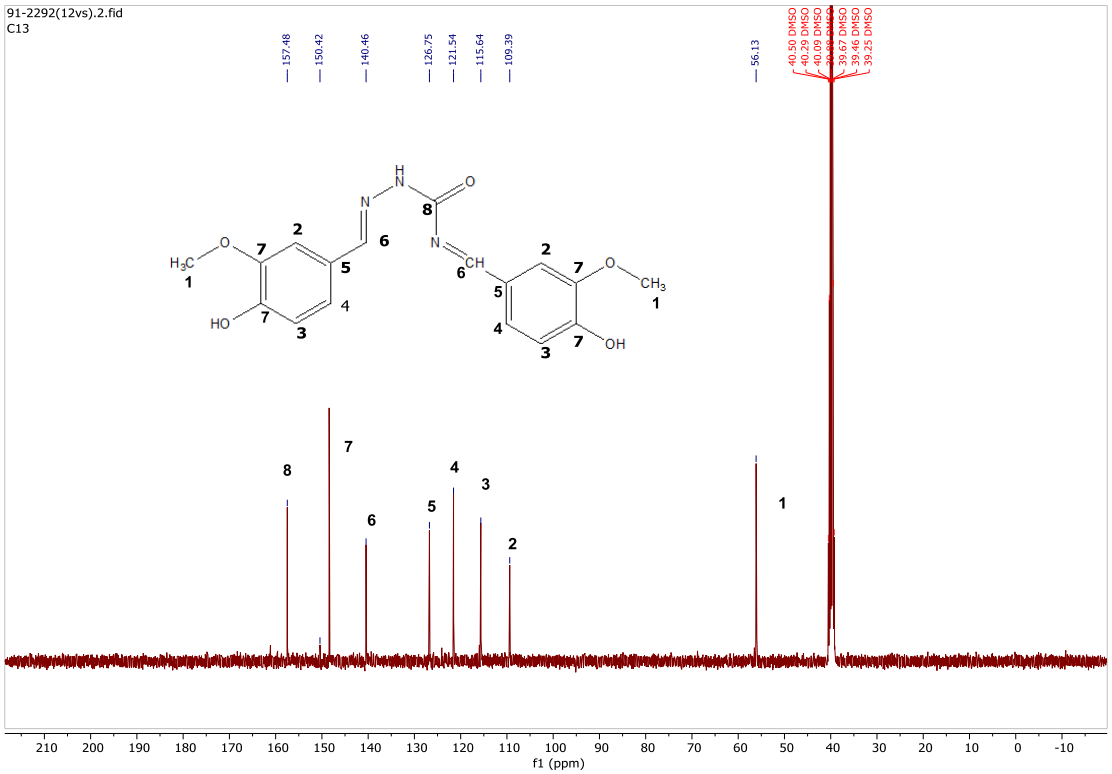

Appendix 8. ^{13}C-NMR spectra of ligand (**L3**)

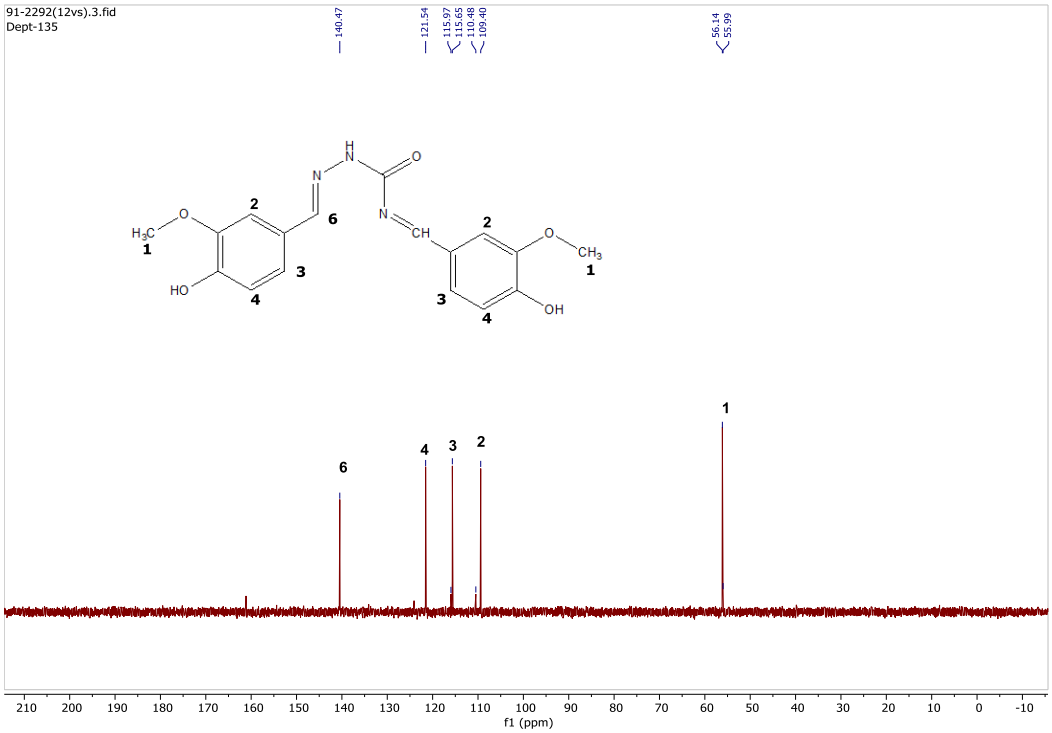

Appendix 9. ^{13}C - Dept spectra of ligand (**L3**)

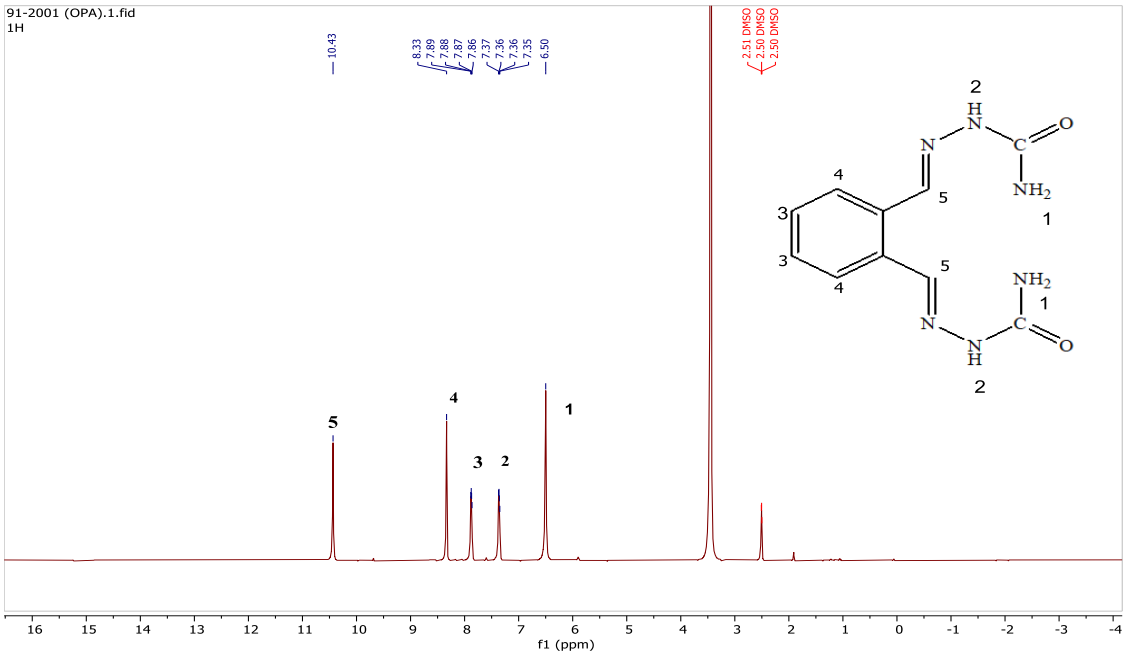

Appendix 10. ^{1}H-NMR spectra of ortho-phthalaldehyde disemicarbazone (**L4**)

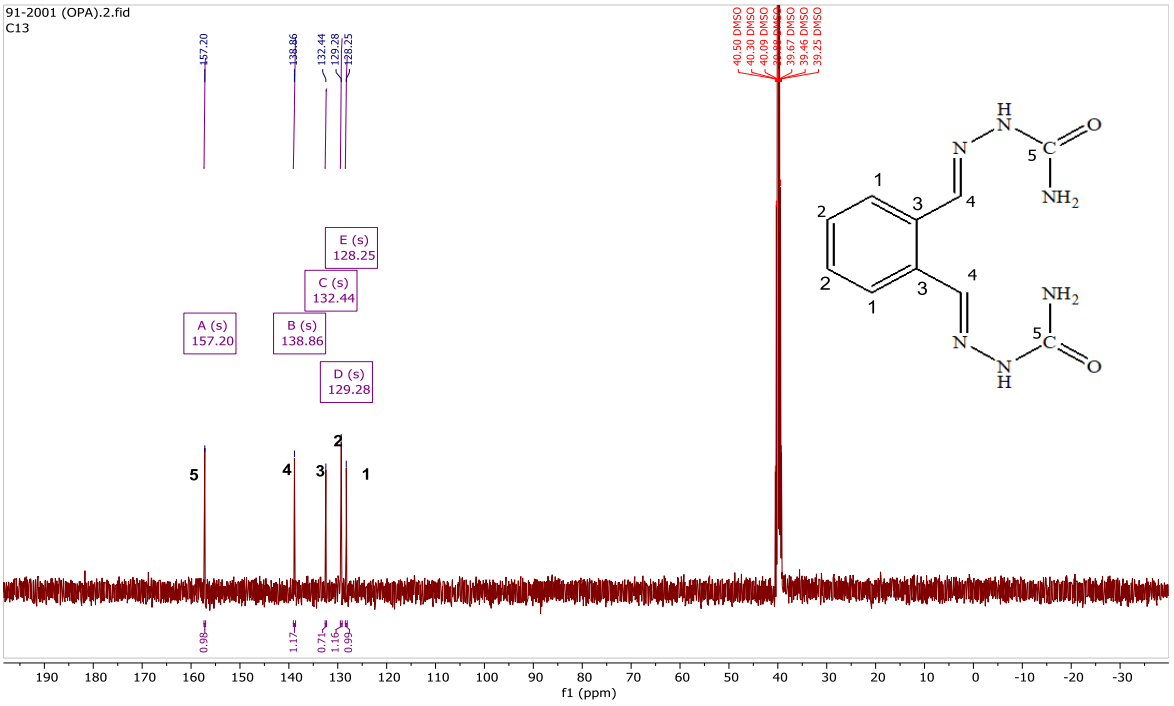

Appendix 11. ^{13}C- NMR spectra of ligand (**L4**)

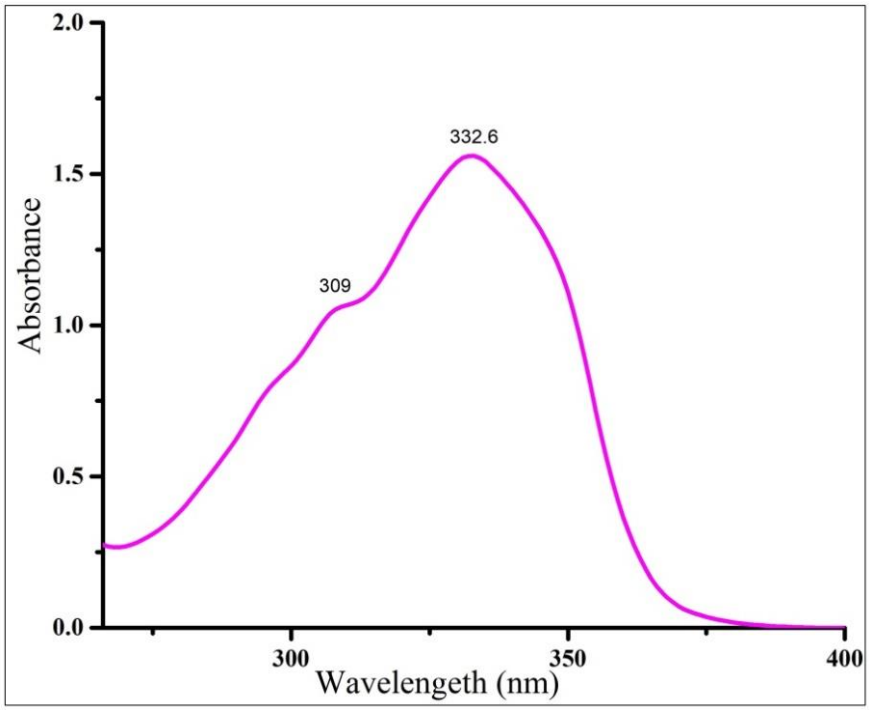

Appendix 12. UV-Vis spectrum of **L1**

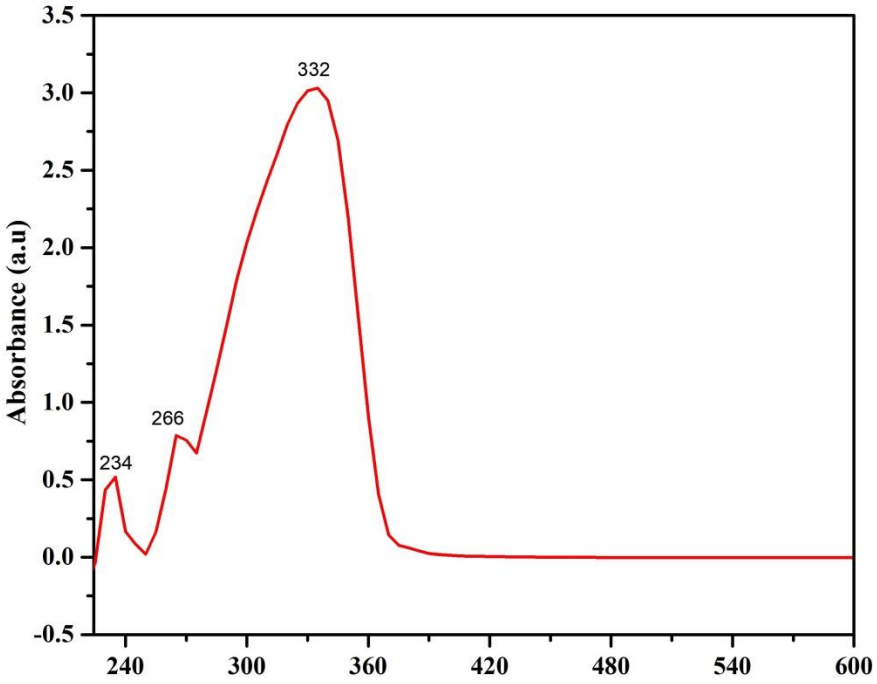

Appendix 13. UV-Vis spectrum of $[Zn(L1)_2(Cl)_2]$ complex (**1**)

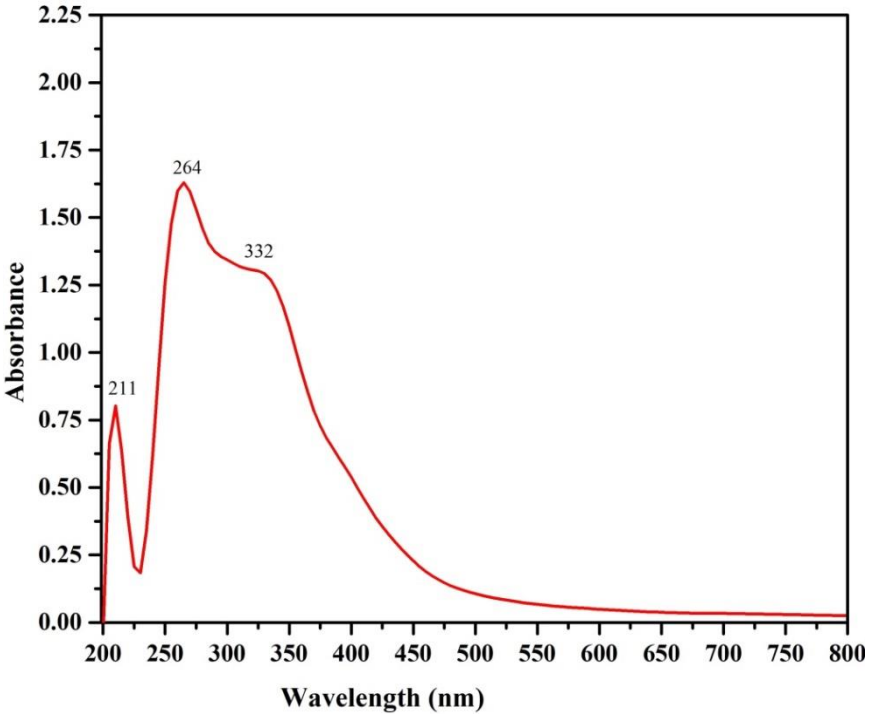

Appendix 14. UV-Vis spectrum of $[Cu(L1)_2(Cl)_2]$ complex (**2**)

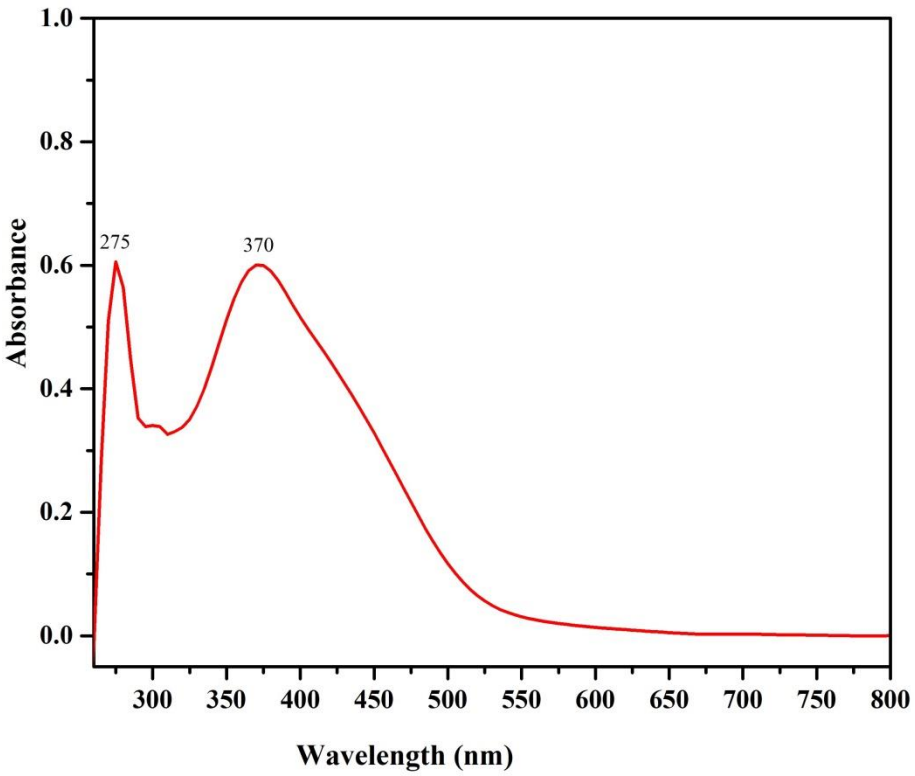

Appendix 15. UV-Vis spectrum of $[Ni(L1)_2Cl]$ complex (**3**)

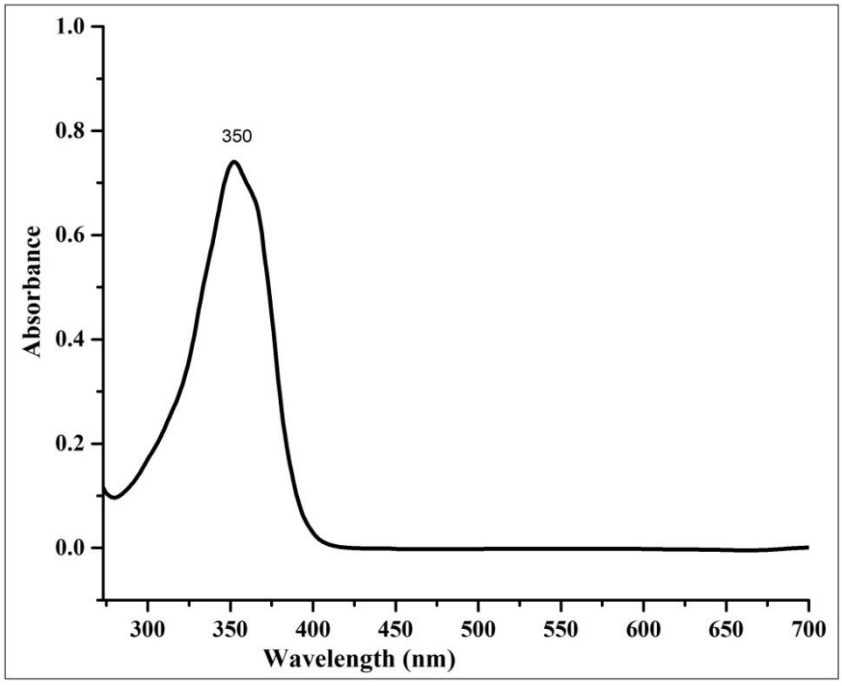

Appendix 16. UV-Vis spectrum of $[Cu(L2)_2(Cl)_2]$ complex **L2**

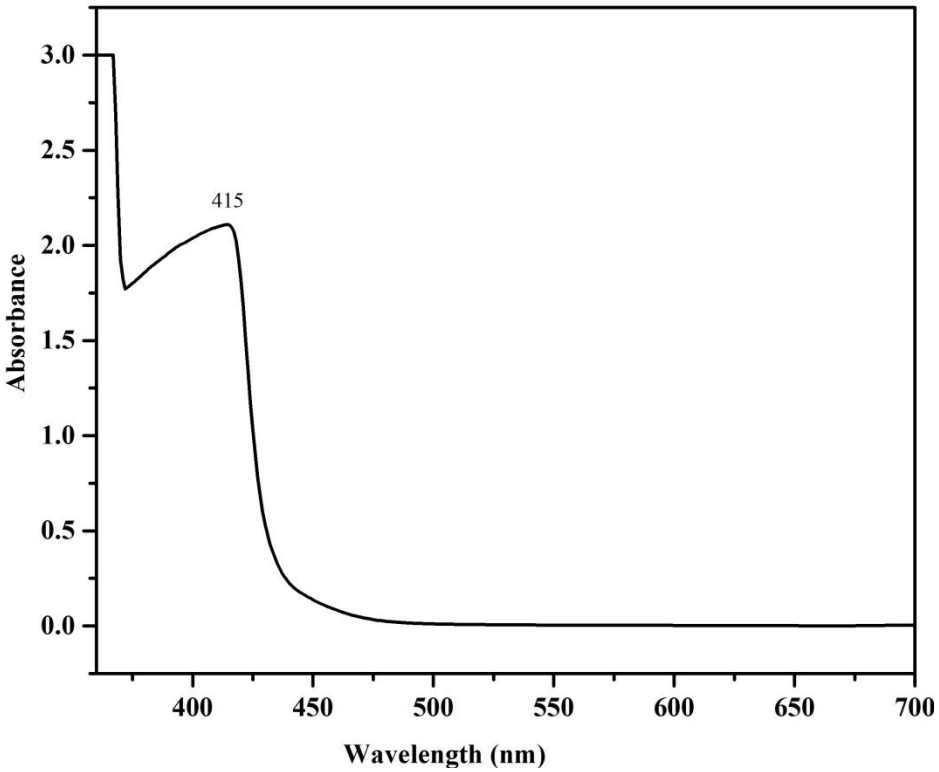

Appendix 17. UV-Vis spectrum of $[Zn(L_2)_2]$ complex (**4**)

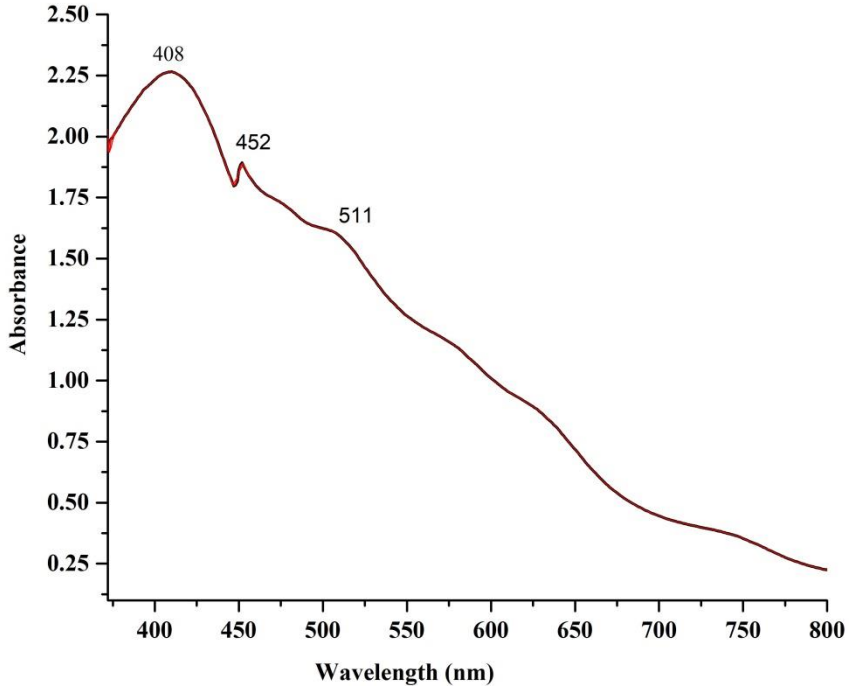

Appendix 18. UV-Vis spectrum of $[Cu(L2)_2Cl_2]$ complexes (5)

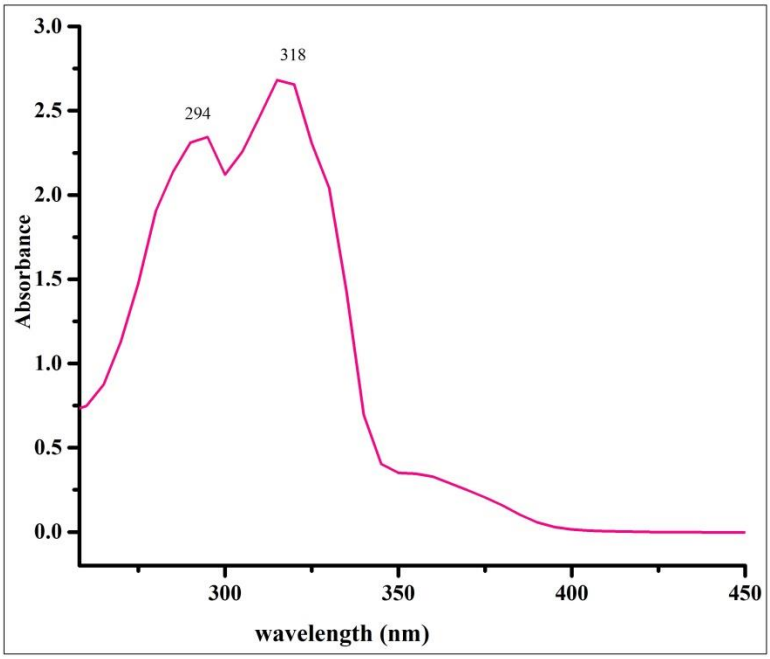

Appendix 19. UV-Vis spectrum of [((1E)-1,4-bis(4-hydroxy-3-methoxybenzylidene) semicarbazone (L3)

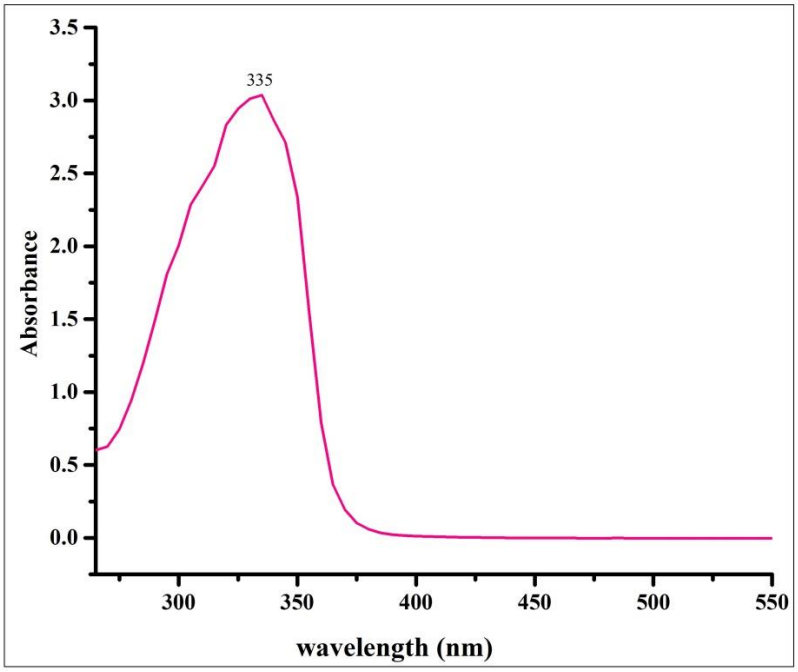

Appendix 20. UV-Vis spectrum of $[Zn(L3)_2].2H_2O$ complex (**6**)

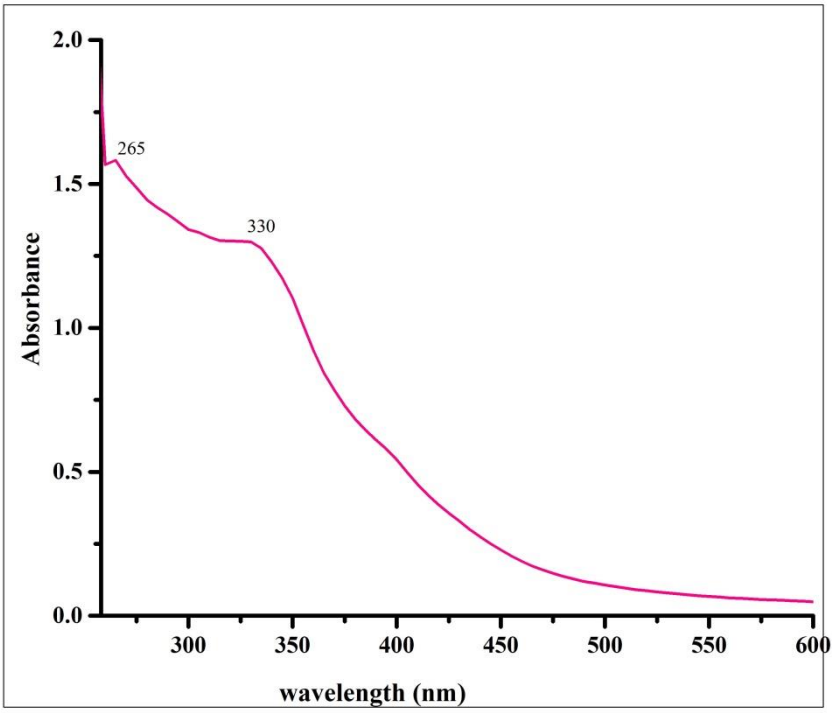

Appendix 21. UV-Vis spectrum of $[Cu(L3)_2].3H_2O$ complex (**7**)

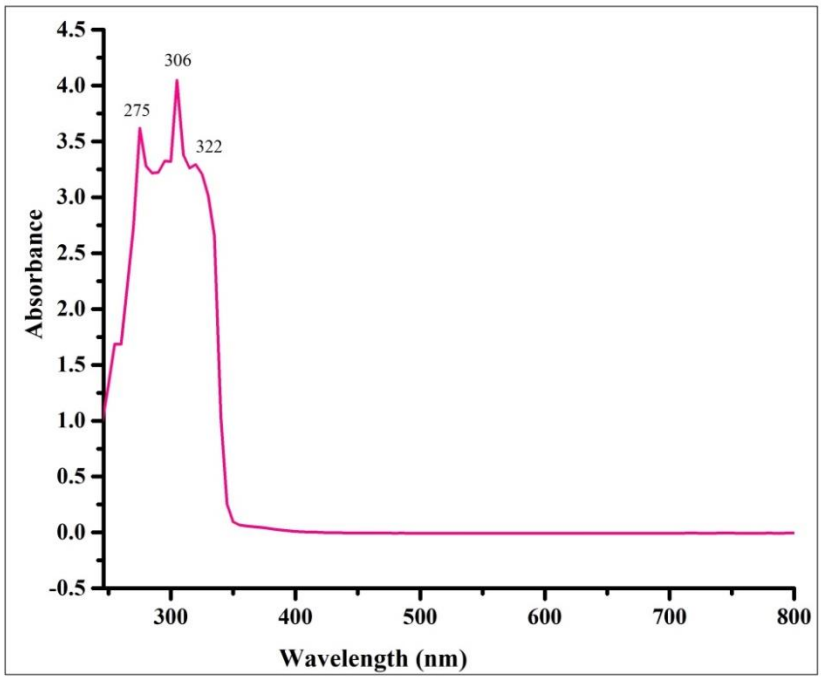

Appendix 22. UV-Vis spectrum of $[Ni(L3)_2].4H_2O$ complex (**8**)

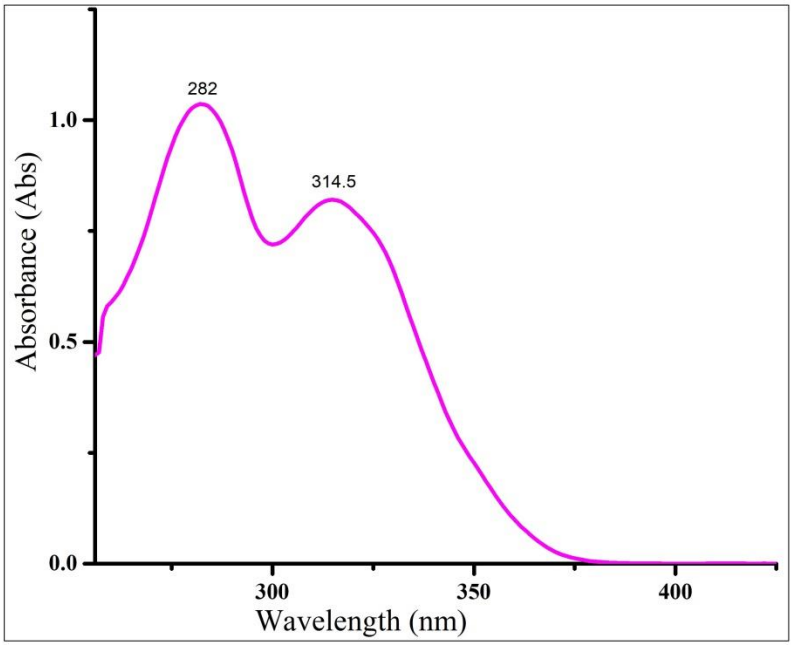

Appendix 23. UV-Vis spectrum of ortho-phthalaldehyde disemicarbazone ligand (**L4**)

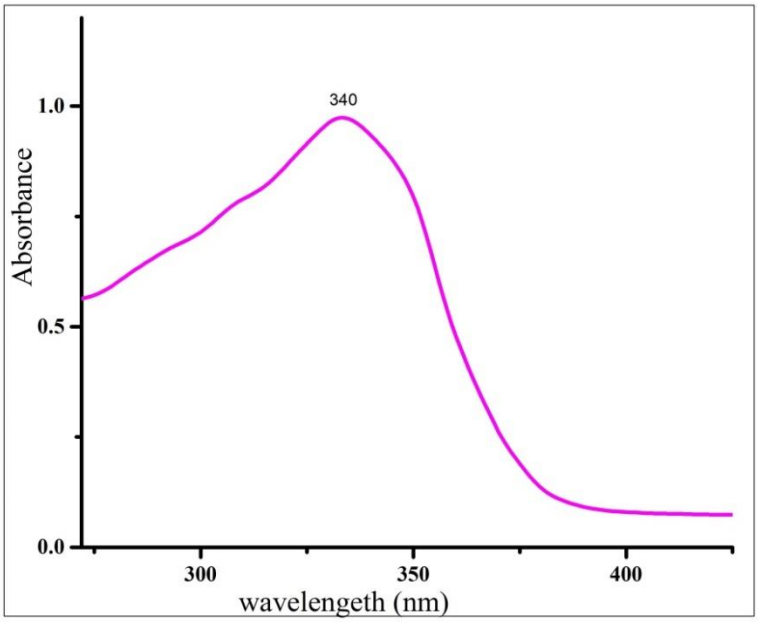

Appendix 24. UV-Vis spectrum of [Zn(L1)(L4)] complex (**9**)

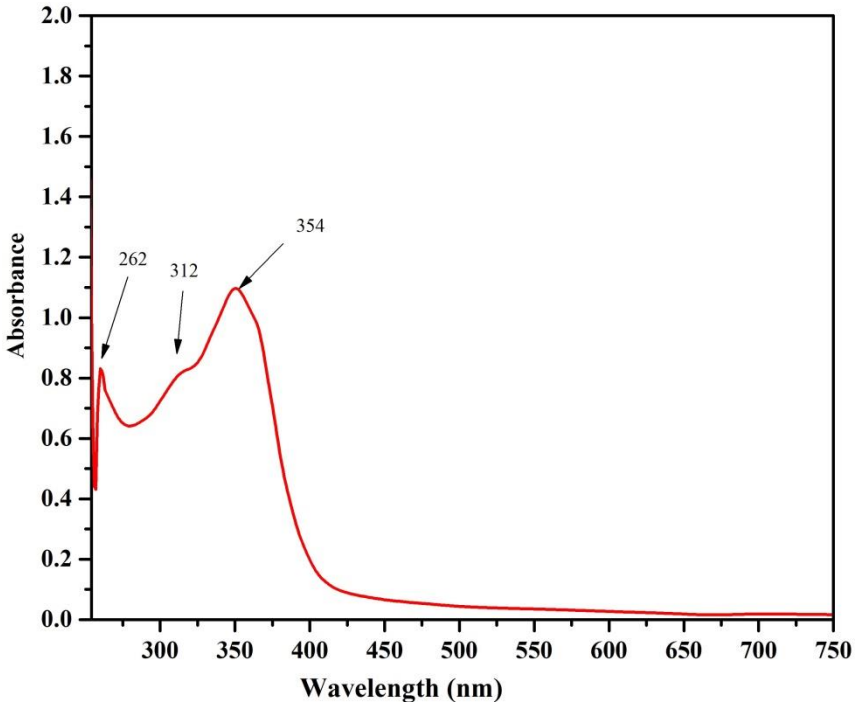

Appendix 25. UV-Vis spectrum of [Cu(L1)(L4)] complex (**10**)

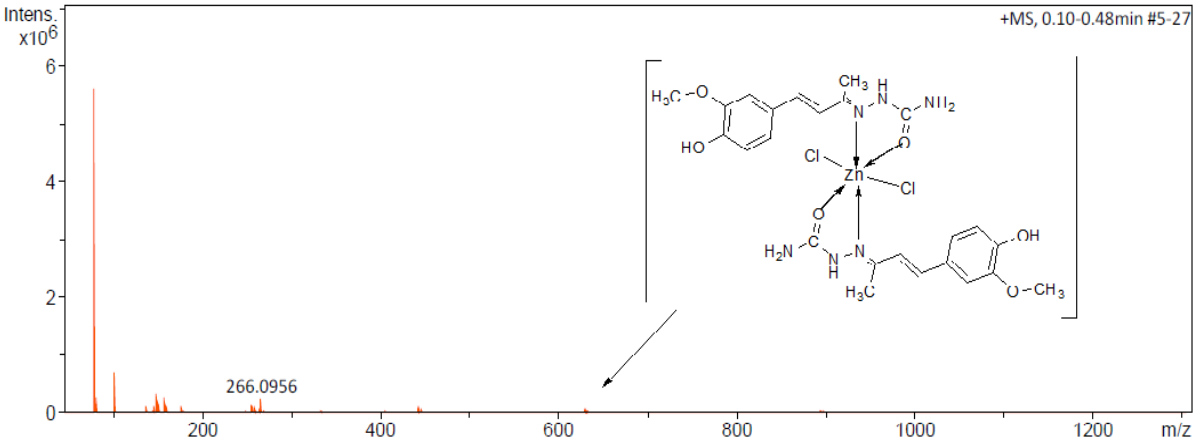

Appendix 26. Mass spectra of $[Zn(L1)_2(Cl)_2]$ complex (**1**)

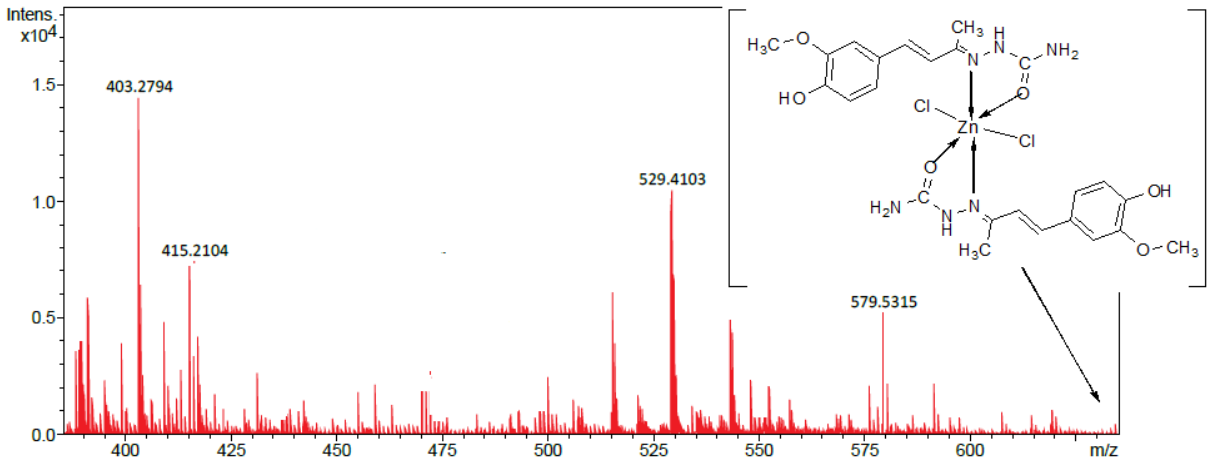

Appendix 27. Mass spectra of $[Cu(L1)_2(Cl)_2]$ complex **2**

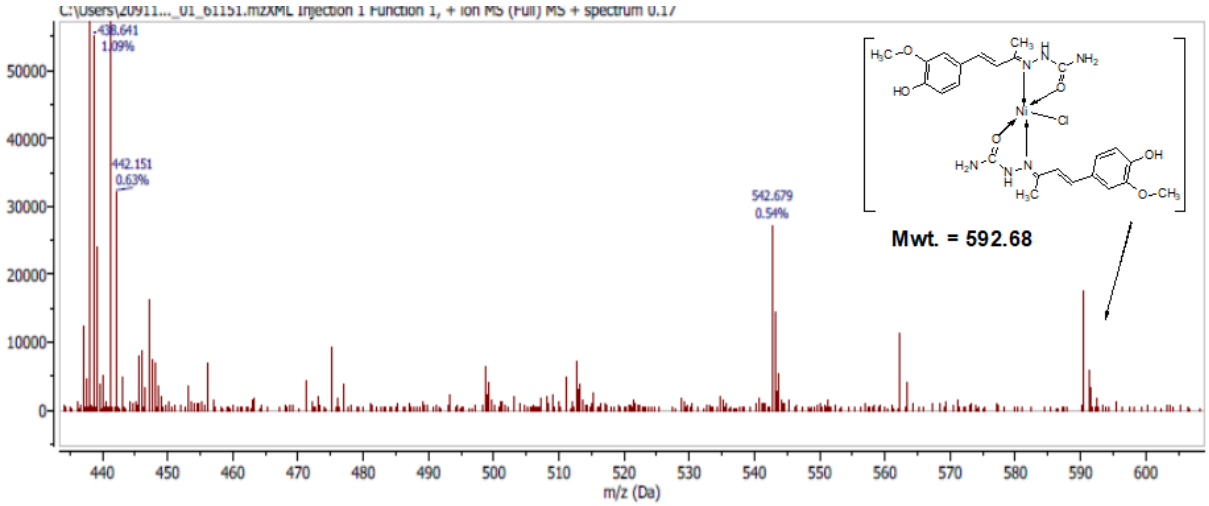

Appendix 28. Mass spectra of $[Ni(L2)_2Cl]$ complexes **3**

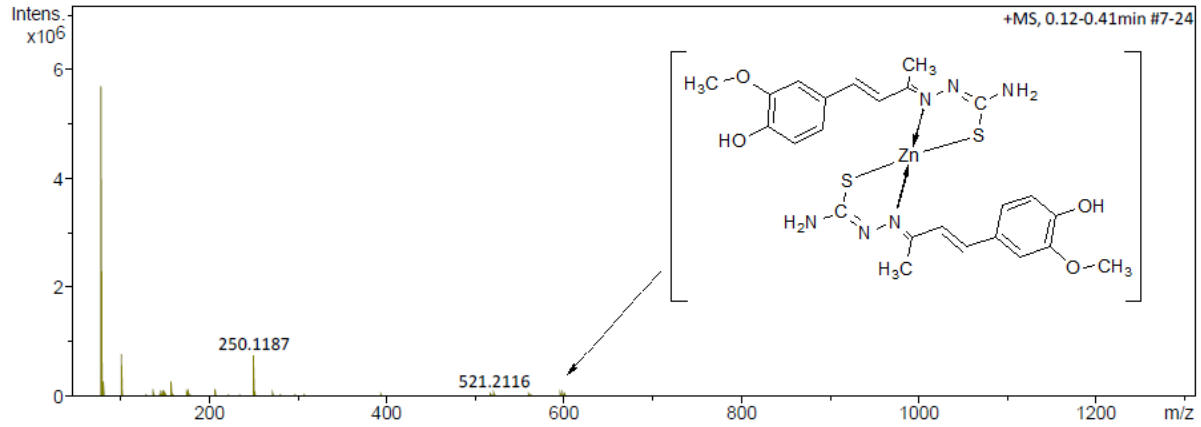

Appendix 29. Mass spectra of $[Zn(L2)_2]$ complex **4**

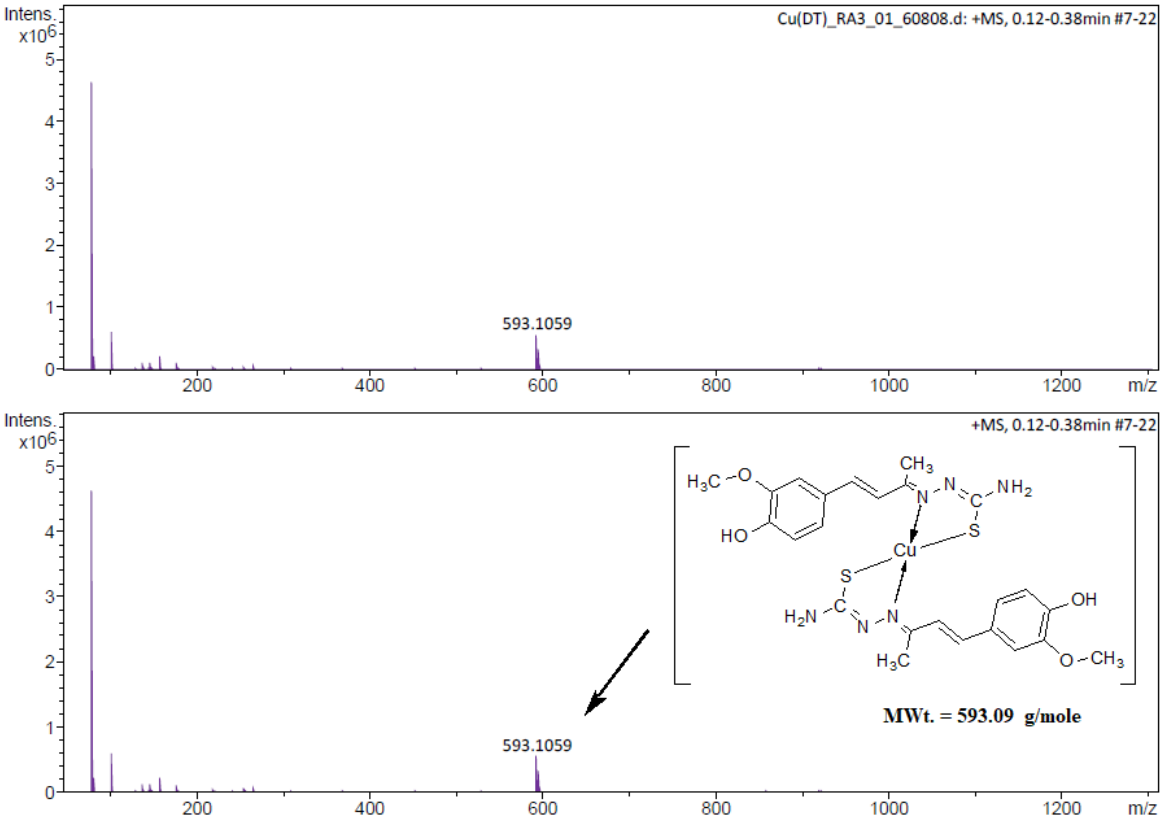

Appendix 30. Mass spectra of $[Cu(L2)_2]$ complex **5**

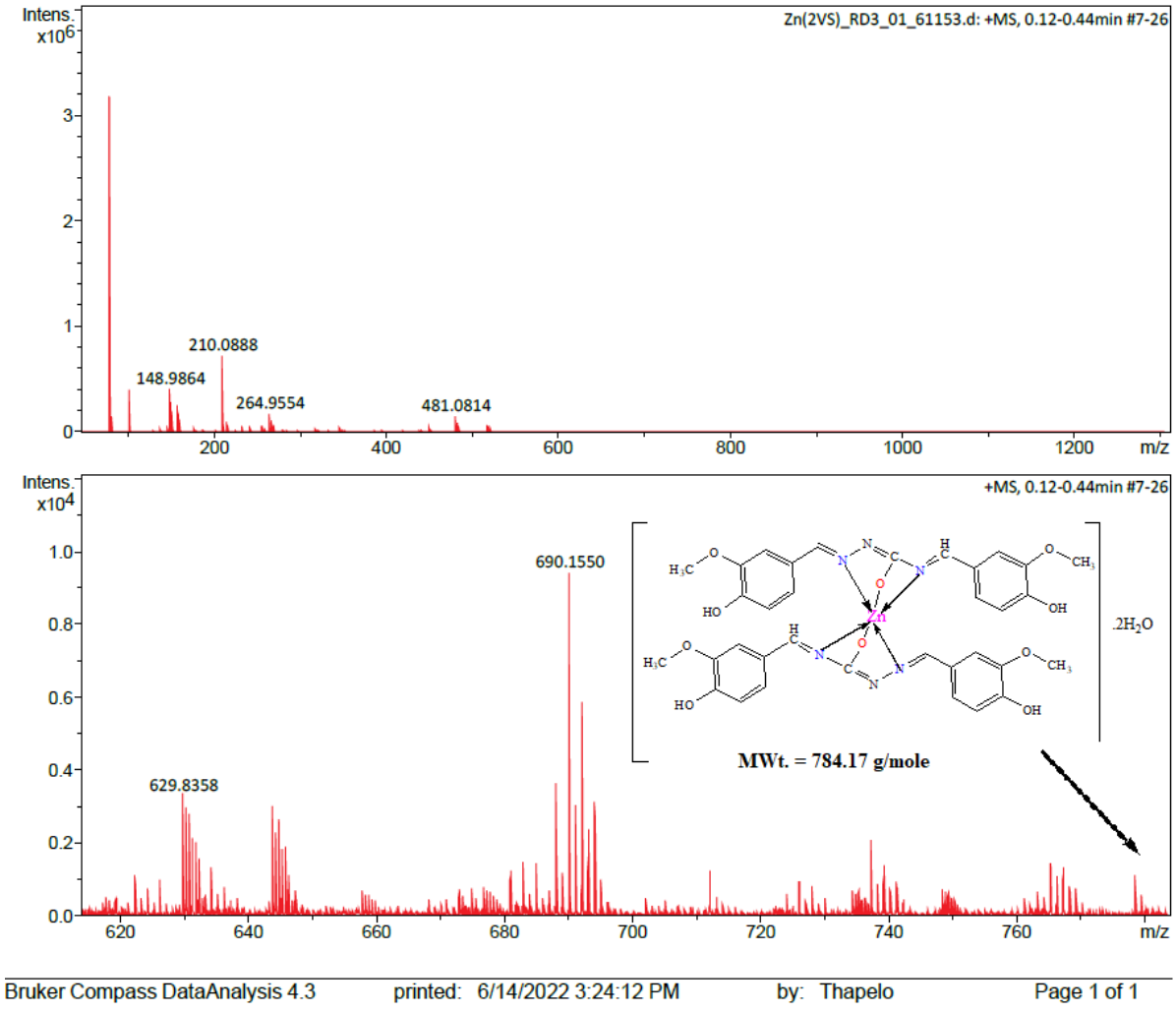

Appendix 31. Mass spectra of $[Zn(L3)_2].2H_2O$ complex (**6**)

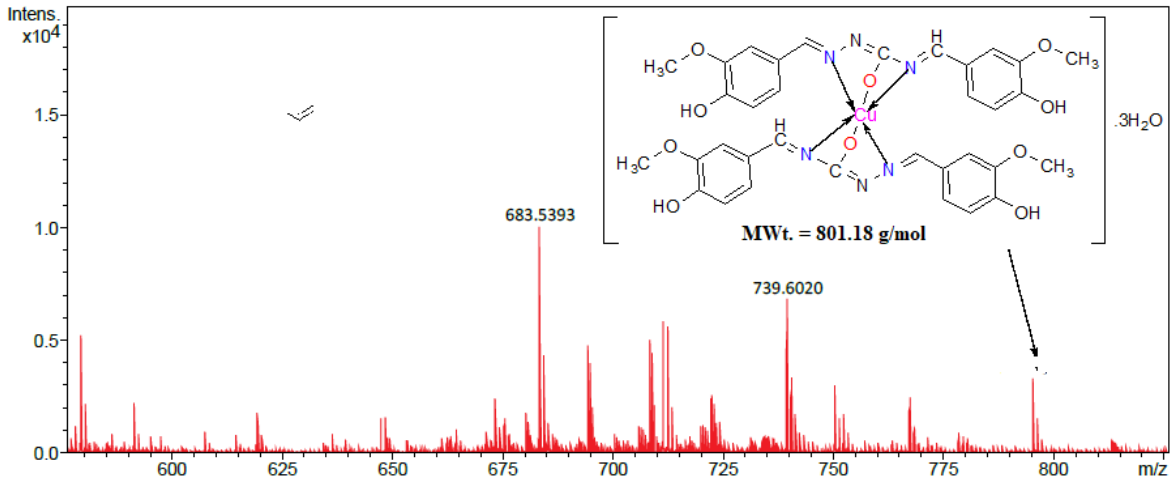

Appendix 32. Mass spectra of $[Cu(L3)_2].3H_2O$ complex (**7**)

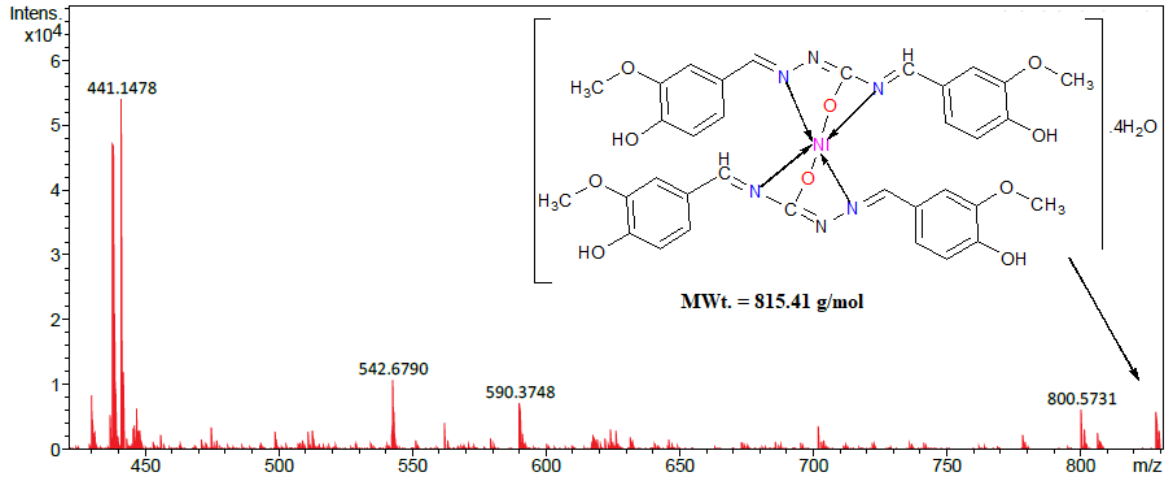

Appendix 33. Mass spectra of $[Ni(L3)_2].4H_2O$ complex **(8)**

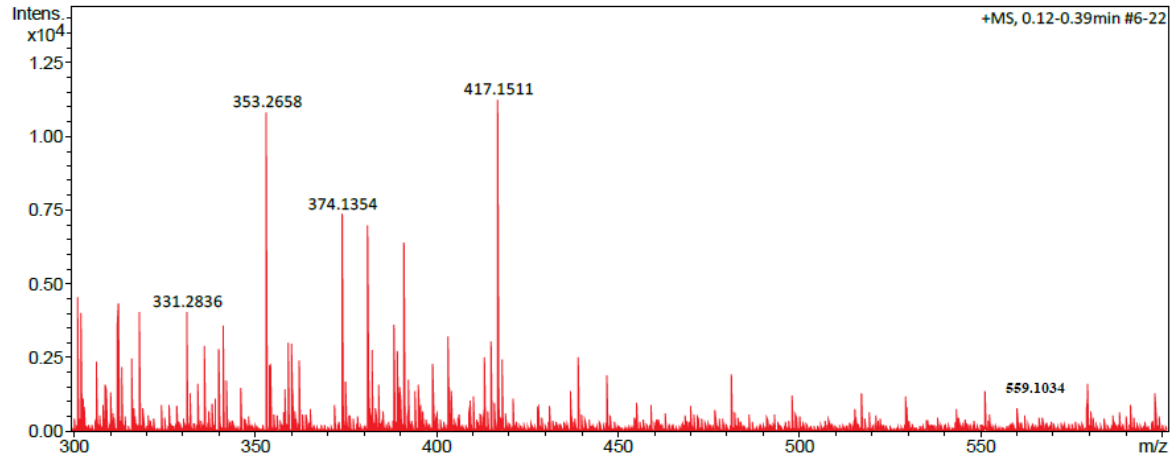

Appendix 34. Mass spectra of [Zn(L1)(L4)] complex **(9)**

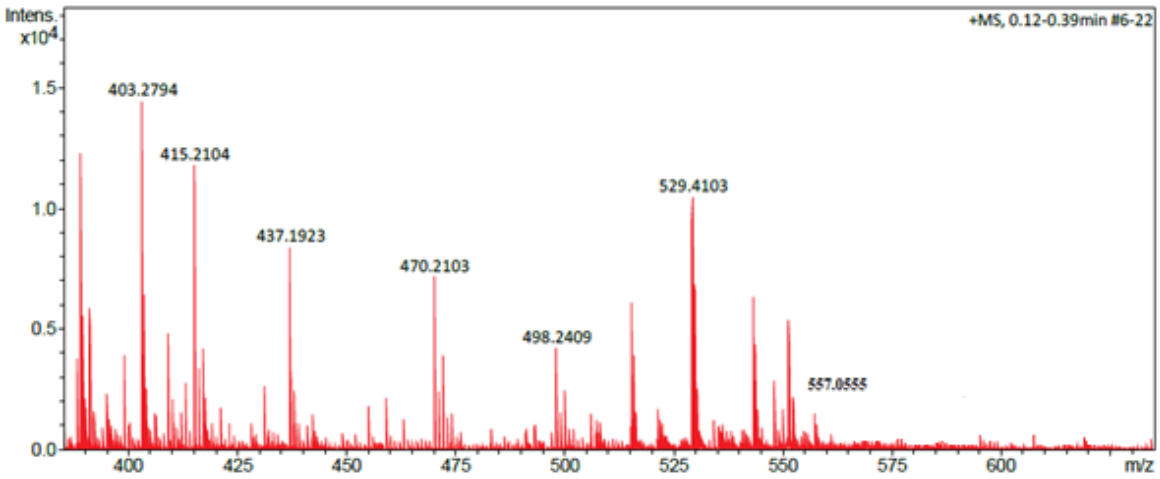

Appendix 35. Mass spectra of [Cu(L1)(L4)] complex **(10)**

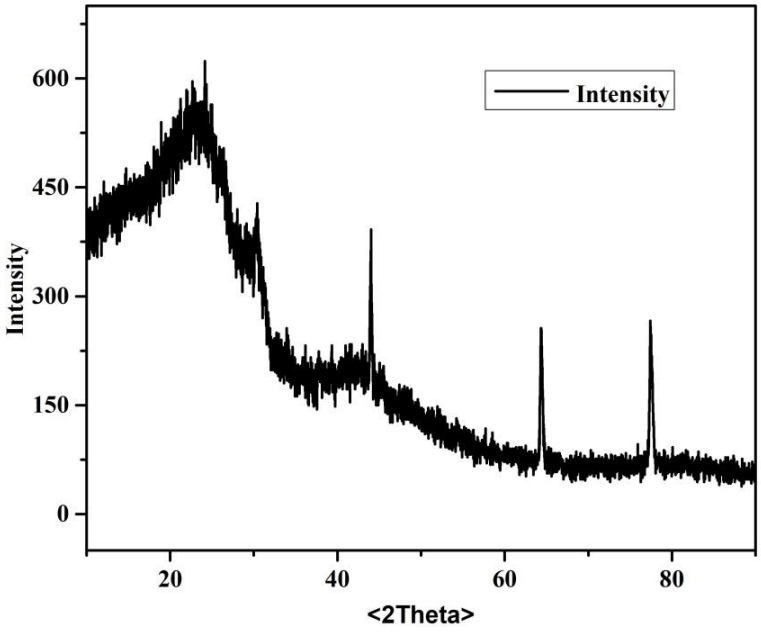

Appendix 36. XRD patterns for $[Zn(L1)_2(Cl)_2]$ complex **1**

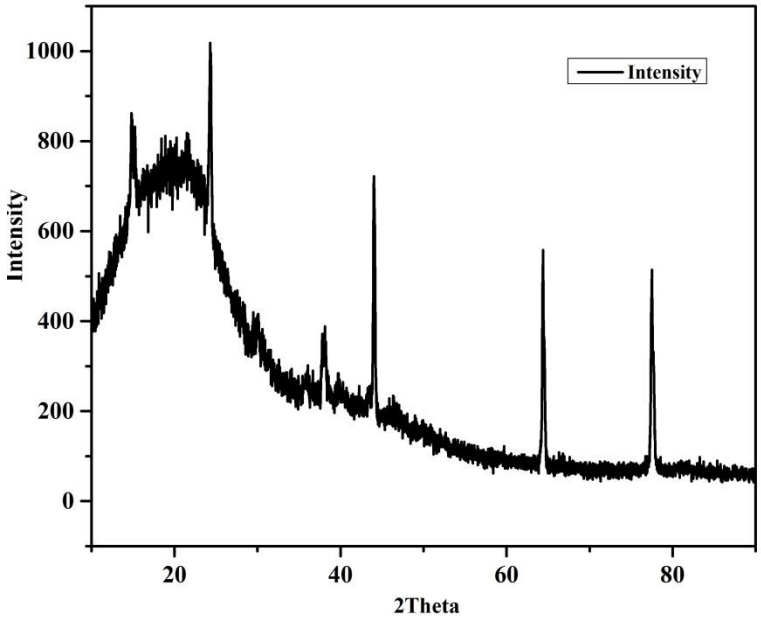

Appendix 37. XRD patterns for $[Cu(L1)_2(Cl)_2]$ complex **2**

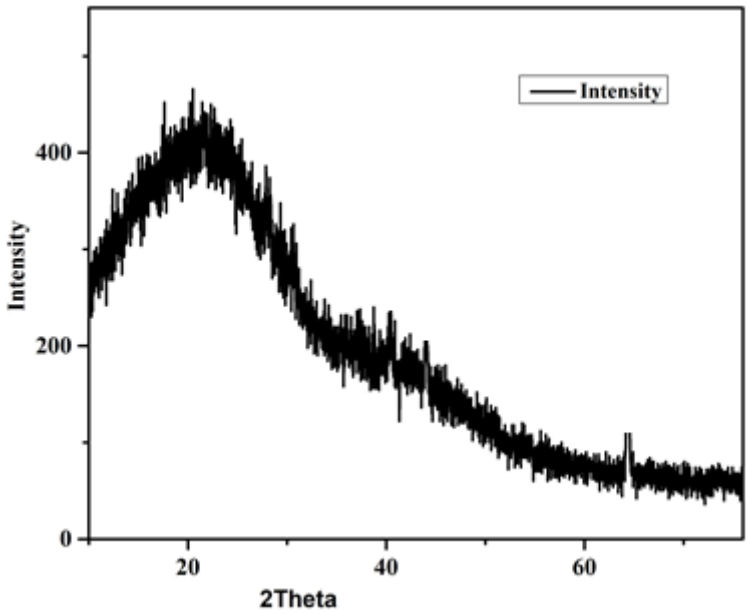

Appendix 38. XRD patterns for [Ni(L2)$_2$Cl] complex **3**

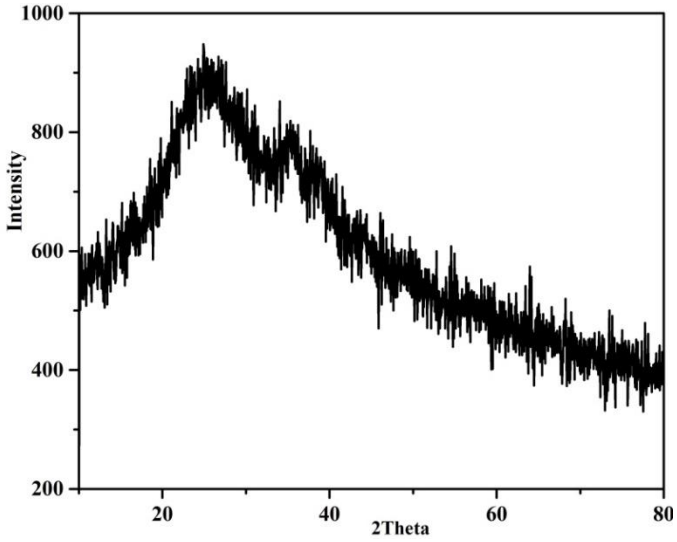

Appendix 39. XRD patterns for [Zn(L2)$_2$] complex **4**

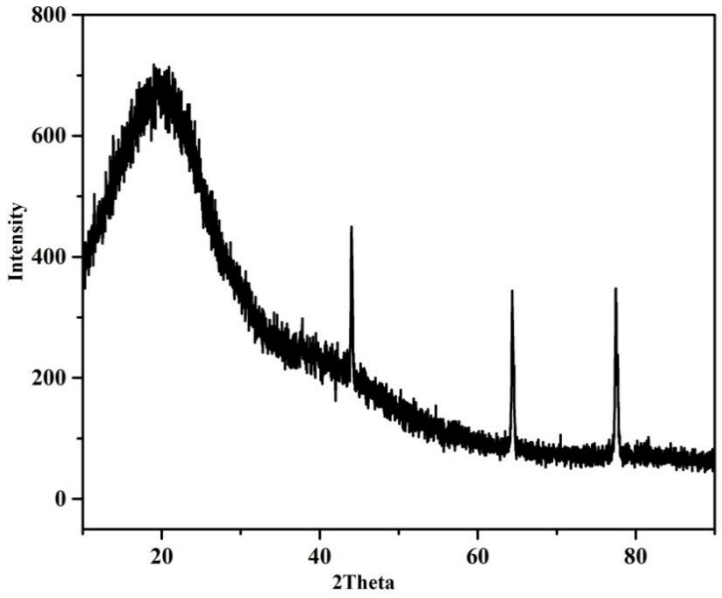

Appendix 40. XRD patterns for $[Cu(L1)_2Cl]$ complex (**5**)

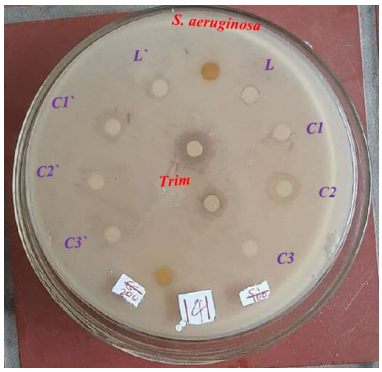

Appendix 41. Selected photos of the distance of inhibition by samples on *S. aureus* bacteria species, *Where: L & L`; ligand conc. of 100 and 200 µg/mL; C & C` = complex conc. (at 100 and 200 µg/mL.*

Appendix 42. Antibacterial activity of heteroleptic complexes **9 and 10**

Compound	Conc. *(µg/mL)*	Gram-negative		Gram-positive	
		E. Coli	***P. Aeruginosa***	***S. Aureus***	***S. Pyogenes***
L1	100	8.00 ± 0.21	7.35 ± 0.42	10.52 ± 0.22	9.23 ± 0.46
	200	9.40 ± 0.42	8.33 ± 0.37	12.42 ± 0.23	11.64 ± 0.12
L4	100	4.50 ± 0.24	3.50 ± 0.00	6.34 ± 0.42	6.64 ± 0.47
	200	5.44 ± 0.54	7.33 ± 0.46	8.68 ± 0.32	8.84 ± 0.32
[Zn(L1)(L4)] **(9)**	100	9.52 ± 0.34	13.32 ± 0.12	10.23 ± 0.33	9.02 ± 0.14
	200	12.22 ± 0.50	14.22 ± 0.33	11.47 ± 0.43	9.52 ± 0.46
[Cu(L1)(L4)] (**10**)	100	9.20 ± 0.44	10.46 ± 0.44	11.67 ± 0.25	12.44 ± 0.22
	200	11.12 ± 0.54	12.43 ± 0.23	12.62 ± 0.34	13.67 ± 0.52
Trimethoprim (standard drug)	100	14.69 ± 0.47	16.64 ± 0.48	14.05 ± 0.44	16.71 ± 0.26

By mm (mean ± SD of triplicates)

Appendix 43. Percentage free radical scavenging activities of the ligands and their homoleptic complexes (1 –8) (mean ± SD)

Compounds	Concentrations in µg/ml			
	12.5	25	50	100
L_1	36.00 ± 0.65	37.04 ± 0.68	37.08 ± 0.45	41.46 ± 0.57
$[Zn(L1)_2Cl_2]$ (1)	57.68 ± 0.64	58.45 ± 0.68	59.01 ± 0.56	60.08 ± 0.64
$[Cu(L1)_2Cl_2]$ (2)	56.64 ± 0.61	58.74 ± 0.48	59.00 ± 0.47	61.7 ± 0.46
$[Ni(L1)_2Cl]$ (3)	57.28 ± 0.48	68.46 ± 0.65	77.68 ± 0.34	85.76 ± 0.24
L2	42.44 ± 0.64	42.98 ± 0.44	45.24 ± 0.45	47.04 ± 0.64
$[Zn(L2)_2]$ (4)	66.48 ± 0.57	67.66 ± 0.78	74.09 ± 0.47	76.78 ± 0.68
$[Cu(L2)_2]$ (5)	68.56 ± 0.71	71.08 ± 0.33	74.68 ± 0.46	78.55 ± 0.48
L3	44.26 ± 0.34	48.56 ± 0.21	60.46 ± 0.45	68.42 ± 0.18
$[Zn(L3)_2].3H_2O$ (6)	48.46 ± 0.16	56.72 ± 0.40	66.42 ± 0.24	72.32 ± 0.20
$[Cu(L3)_2].3H_2O$ (7)	52.42 ± 0.27	64.22 ± 0.14	71.05 ± 0.23	78.45 ± 0.38
$[Ni(L3)].3H_2O$ (8)	56.13 ± 0.36	66.41 ± 0.37	72.50 ± 0.46	81.43 ± 0.56
Ascorbic acid	84.6 ± 0.64	86.34 ± 0.82	87.67 ± 0.48	89.48 ± 0.74

Appendix 44. Percent free radical scavenging activities of ligand 1, ligand 2 and their heteroleptic ZnL1L4 and CuL1L4 complexes**.**

Compounds	Concentrations in *µg/ Ml*			
	12.5	25	50	100
L1	32.60	35.34	36.67	40.34
L4	36.00	37.04	37.08	41.46
[Zn(L1)(L4)] **(9)**	56.36	58.20	58.84	59.68
[Cu(L1)(L4)] **(10)**	60.44	60.74	61.32	63.7
Ascorbic acid	84.6	85.34	85.67	86.48

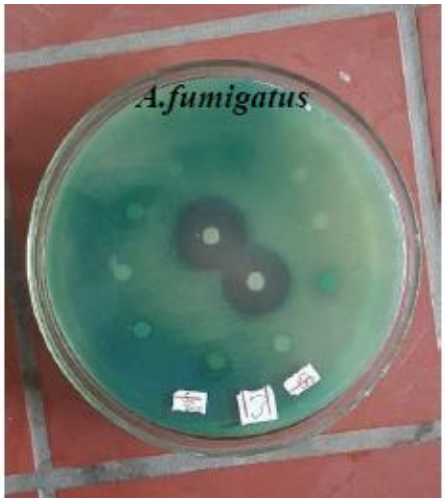

Appendix 45. Selected images showing zone of inhibition against *A. Fumigatus* fungus species

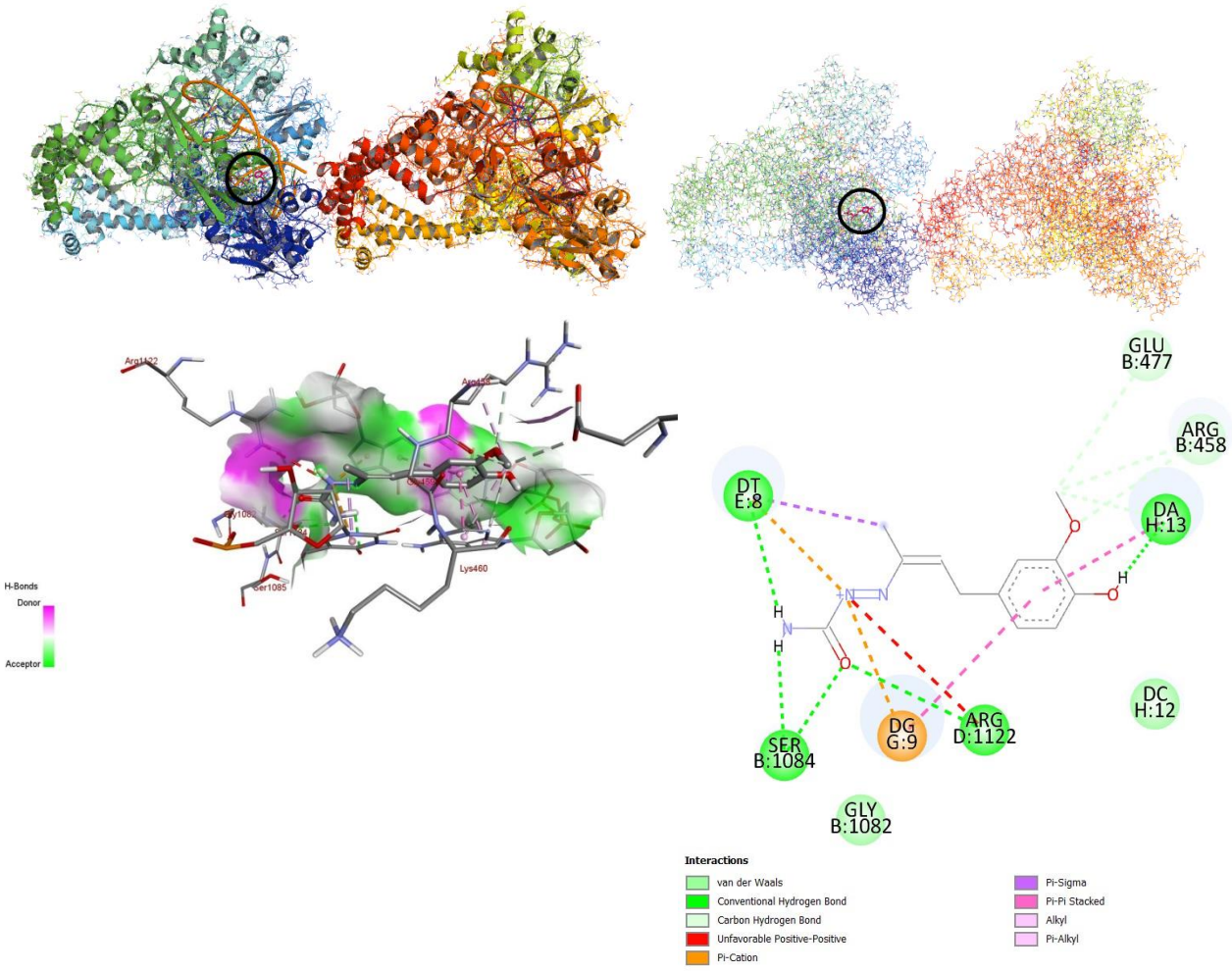

Appendix 46. The 2D and 3D binding interactions of ligand (L1) against *S. aureus* Gyrase (PDB ID: 2XCT).

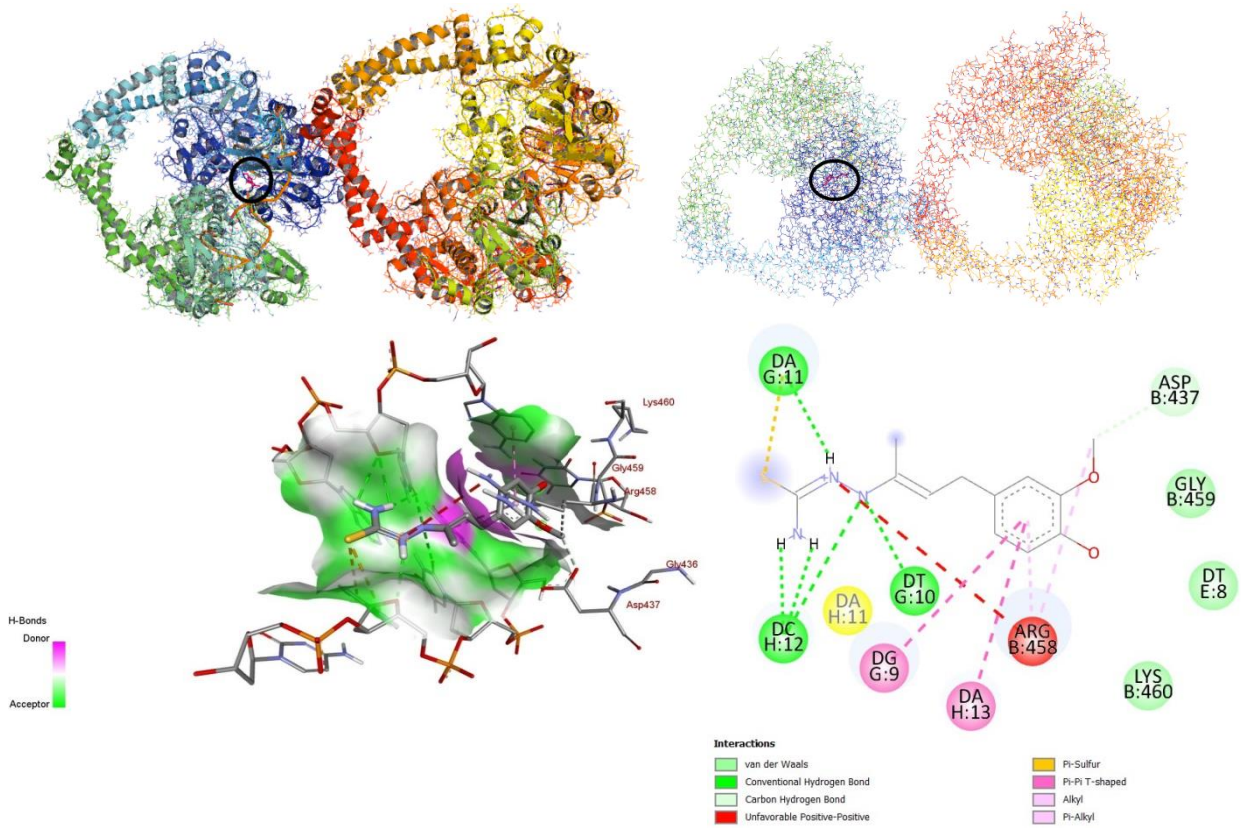

Appendix 47. The 2D and 3D binding interactions of ligand (**L2**) against *S. aureus* Gyrase (PDB ID: 2XCT).

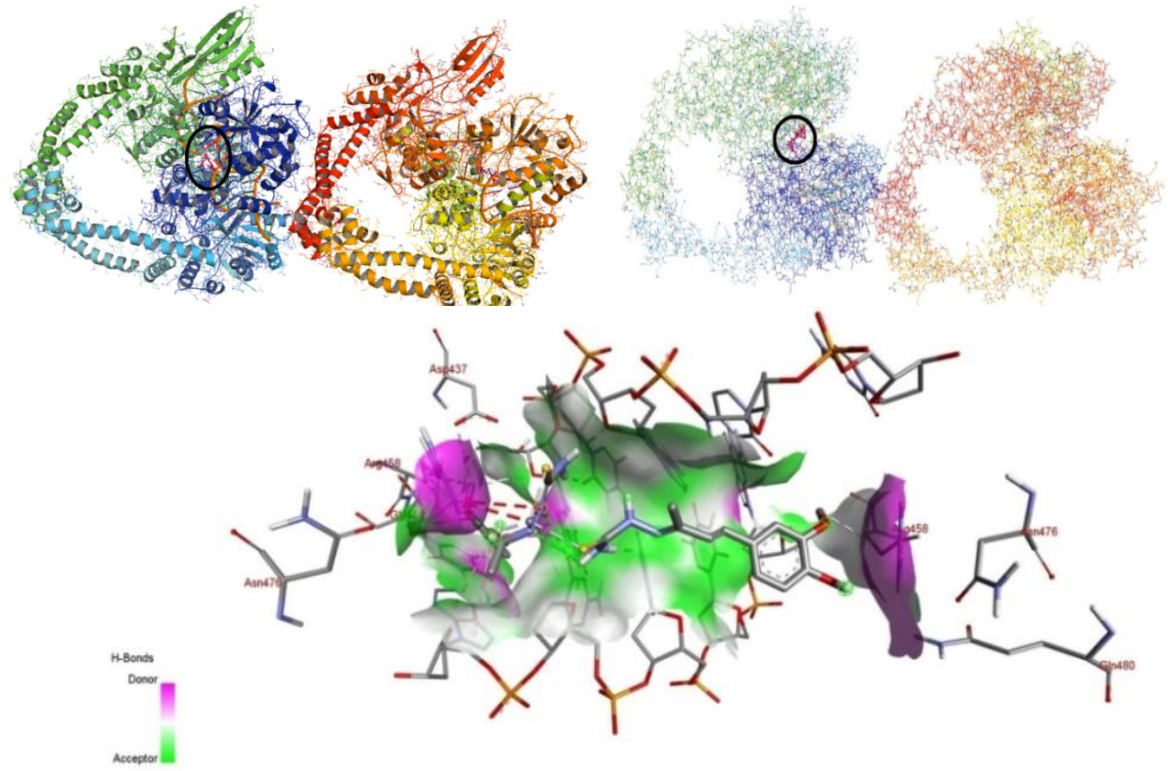

Appendix 48. The 3D binding interactions of complex **1**, $[Zn(L1)_2(Cl)_2]$ against *S. aureus* Gyrase (PDB ID: 2XCT).

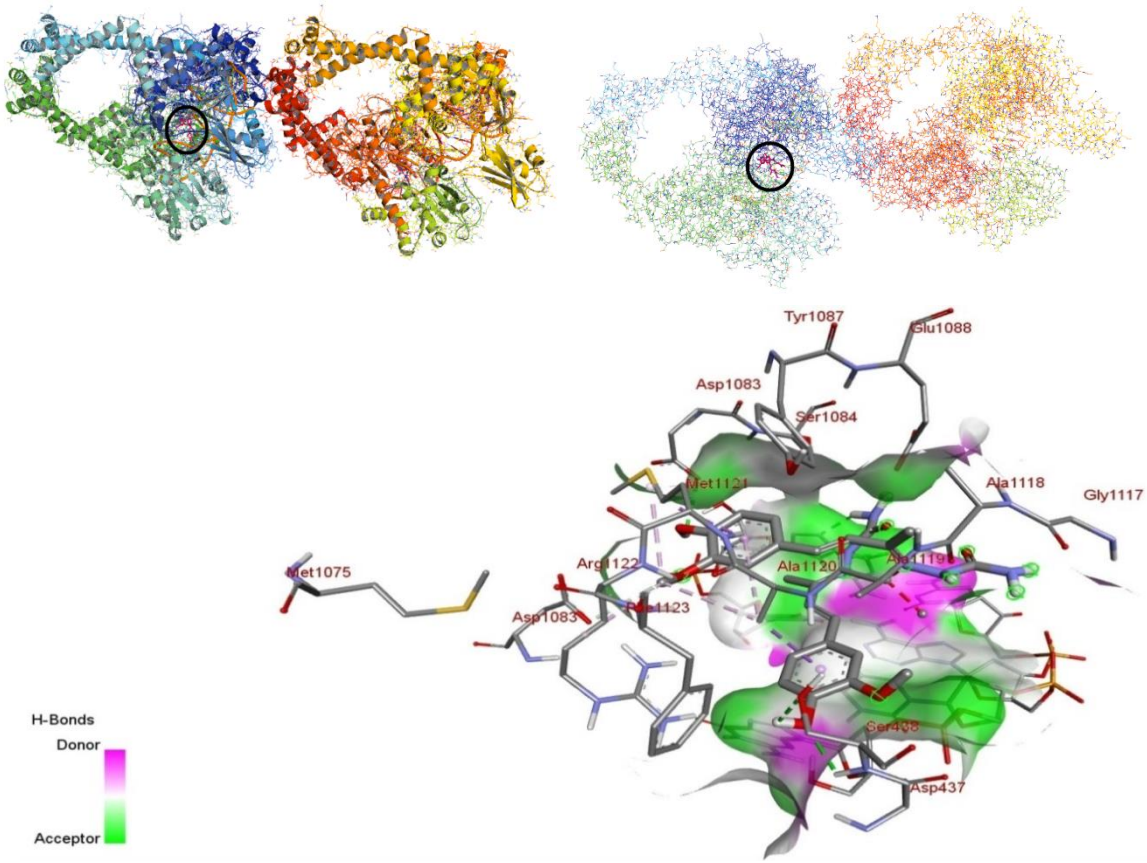

Appendix 49. The 3D binding interactions of complex **2**, $[Cu(L1)_2(Cl)_2]$ against *S. aureus* Gyrase (PDB ID: 2XCT

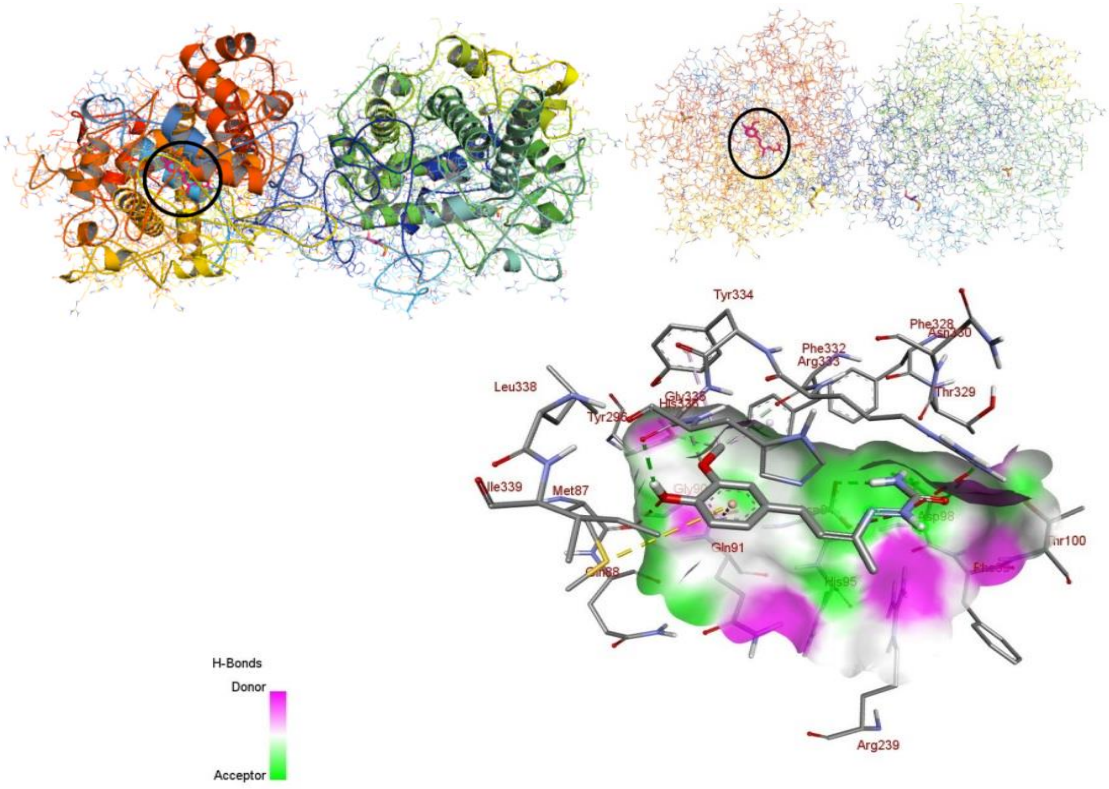

Appendix 50. The 3D binding interactions of compound **3**, $[Ni(L1)_2(Cl)]$ against *S. aureus* Gyrase (PDB ID: 2XCT).

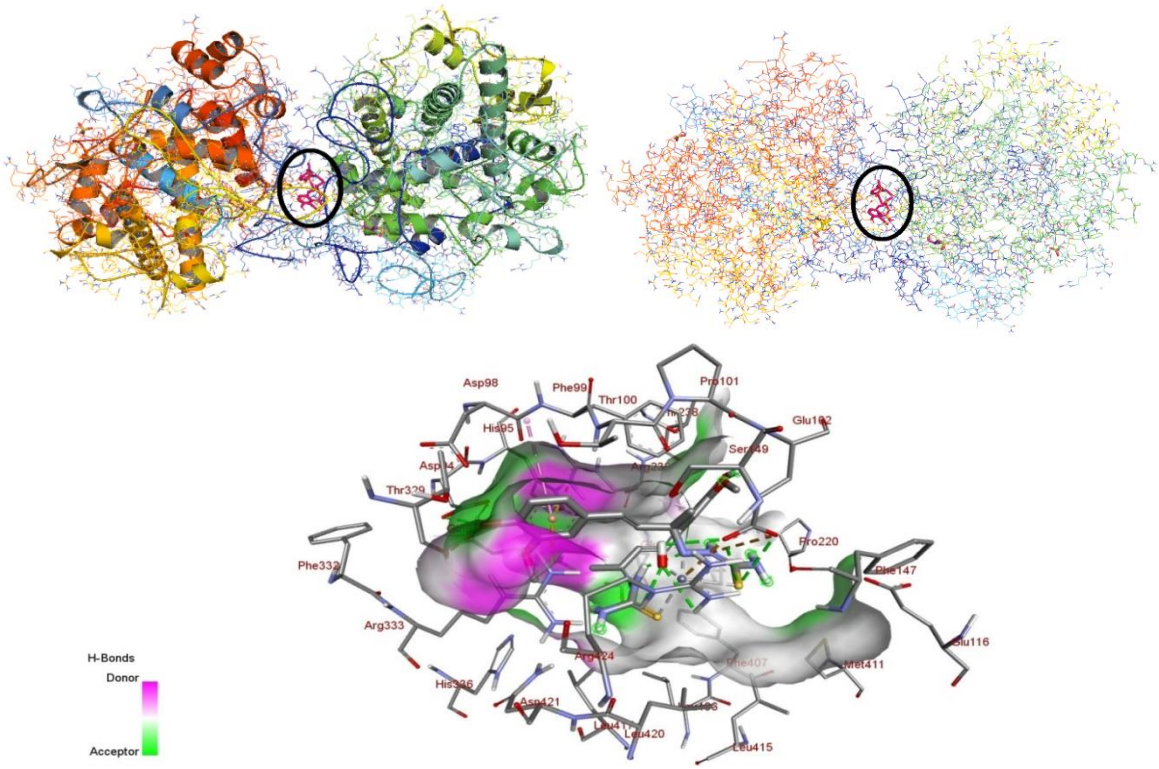

Appendix 51. The 3D binding interactions of compound **4,** $[Zn(L2)_2(Cl)_2]$ against *S. aureus* Gyrase (PDB ID: 2XCT)).

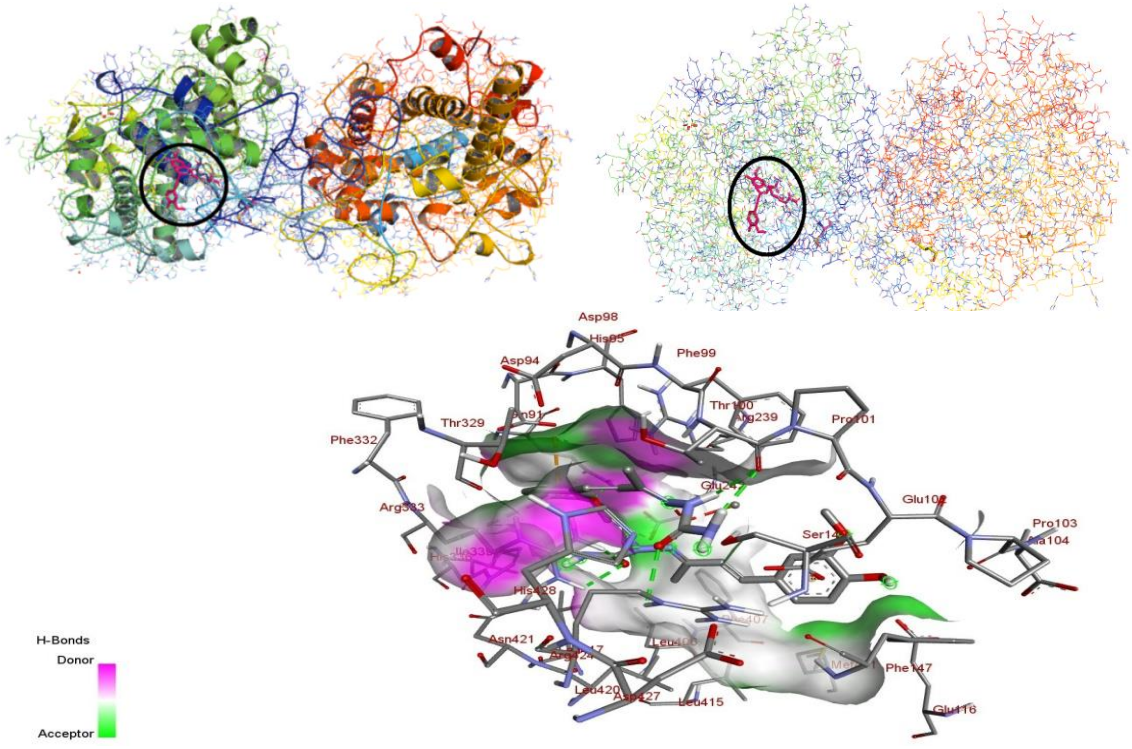

Appendix 52. The 3D binding interactions of compound 5, $[Cu(L2)_2Cl_2]$ against *S. aureus* Gyrase (PDB ID: 2XCT)).

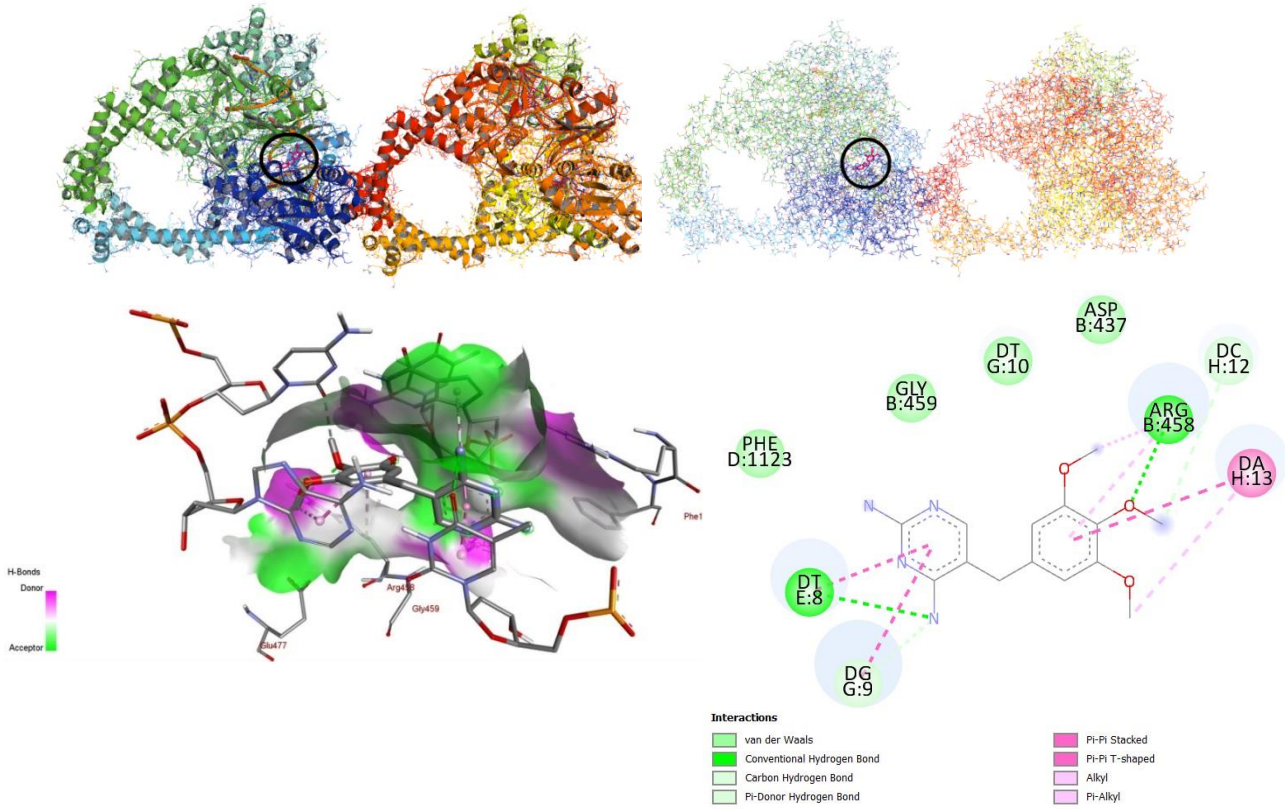

Appendix 53. The 2D and 3D binding interactions of reference drug Trimethoprim against *S. aureus* Gyrase (PDB ID: 2XCT).

Appendix 54. Percentage free radical scavenging activities of the ligands and their homoleptic complexes (1 –8) (mean ± SD)

Compounds	**Concentrations in µg/ml**			
	12.5	**25**	**50**	**100**
L1	36.00 ± 0.65	37.04 ± 0.68	37.08 ± 0.45	41.46 ± 0.57
$[Zn(L1)_2Cl_2]$ (1)	57.68 ± 0.64	58.45 ± 0.68	59.01 ± 0.56	60.08 ± 0.64
$[Cu(L1)_2Cl_2]$ (2)	56.64 ± 0.61	58.74 ± 0.48	59.00 ± 0.47	61.7 ± 0.46
$[Ni(L1)_2Cl]$ (3)	57.28 ± 0.48	68.46 ± 0.65	77.68 ± 0.34	85.76 ± 0.24
L2	42.44 ± 0.64	42.98 ± 0.44	45.24 ± 0.45	47.04 ± 0.64
$[Zn(L2)_2]$ (4)	66.48 ± 0.57	67.66 ± 0.78	74.09 ± 0.47	76.78 ± 0.68
$[Cu(L2)_2]$ (5)	68.56 ± 0.71	71.08 ± 0.33	74.68 ± 0.46	78.55 ± 0.48
L3	44.26 ± 0.34	48.56 ± 0.21	60.46 ± 0.45	68.42 ± 0.18
$[Zn(L3)_2].3H_2O$ (6)	48.46 ± 0.16	56.72 ± 0.40	66.42 ± 0.24	72.32 ± 0.20
$[Cu(L3)_2].3H_2O$ (7)	52.42 ± 0.27	64.22 ± 0.14	71.05 ± 0.23	78.45 ± 0.38
$[Ni(L3)].3H_2O$ (8)	56.13 ± 0.36	66.41 ± 0.37	72.50 ± 0.46	81.43 ± 0.56
Ascorbic acid	84.6 ± 0.64	86.34 ± 0.82	87.67 ± 0.48	89.48 ± 0.74

Appendix 55. Percent free radical scavenging potentials of heteroleptic metal complexes (**9 and 10)**

Compounds	**Concentrations in *µg/ Ml***			
	12.5	**25**	**50**	**100**
L1	32.60	35.34	36.67	40.34
L4	36.00	37.04	37.08	41.46
[Zn(L1)(L4)] **(9)**	56.36	58.20	58.84	59.68
[Cu(L1) (L4)] **(10)**	60.44	60.74	61.32	63.7
Ascorbic acid	84.6	85.34	85.67	86.48

LIST OF PUBLICATIONS

1. **Fekadu Muleta**, Tegene Desalegn, Rajalakshmanan Eswaramoorthy, Ankita Garg; Synthesis, characterization, *in-silico*, and *in-vitro* biological studies of Cu(II), Zn(II) complexes of semicarbazone, thiosemicarbazone derivatives of dehydrozingerone. *Journal of Molecular Structure* 1268 (**2022**) 133632. https://doi.org/10.1016/j.molstruc.2022.133632

2. **Fekadu Muleta**, Tegene Desalegn, Taye B. Demissie, Rajalakshmanan Eswaramoorthy H.C. Ananda Murthy, Kah-Yoong Chan, Bianca L. Davids, Kennedy J. Ngwira; Synthesis, molecular docking, and biological studies of novel heteroleptic Cu(II) and Zn(II) complexes of natural product-based semicarbazone derivatives. *Journal of Molecular Structure* 1274 (**2023**) 134405. https://doi.org/10.1016/j.molstruc.2022.134405.

3. **Fekadu Muleta** and Tegene Desalegn; Synthesis, *In-Silico*, and Biological Applications of Novel Heteroleptic Copper (II) Complex of Natural Product-Based Semicarbazone Ligands. Journal of Chemistry, Volume **2022**, Article ID 1497117. https://doi.org/10.1155/2022/1497117.

4. **Fekadu Muleta**, Tegene Desalegn, Taye B. Demissie, H.C. Ananda Murthy, Benedict Wen-Cheun Au, Zi-Neng Ng, Bianca L. Davids, Kennedy J. Ngwira; Novel Homoleptic Zn(II) and Ni(II) Complexes of Semicarbazone Derivatives: Synthesis, Characterization, Molecular Docking and Biological Applications. *Under review on Journal of Chemistry* (**2023**).